

**SOUTHERN AFRICAN PALAEOCLIMATES AND  
VARIABILITY: THE STORY FROM  
STALAGMITES, POLLEN AND CORAL**

By  
Lisa Frost Ramsay

Submitted in fulfillment of the academic requirements for the  
degree of Master of Science, School of Environmental Sciences,  
University of KwaZulu-Natal

Durban  
2005

## ABSTRACT

Compared to extensive study in the northern hemisphere, very little is known of southern African palaeoclimates. This study aimed to extend understanding of the nature of and controls on southern African palaeoclimates of the last 40 000 years. Through a study of the approximately 20 000 year long Makapansgat and Wonderkrater palaeoclimatic records, and an extensive literature review of southern African palaeoclimatic studies, a number of common rainfall and temperature fluctuations were detected across the summer rainfall region. Based on these trends, general models of rainfall and temperature changes over time were developed for the region. The analysis of a coral core, derived from a *Porites lutea* head from Sodwana Bay, covering the last 116 years, indicated higher frequency climatic fluctuations over the last century. Climatic variability on the long- and short-term could then be related to known atmospheric processes through application of the Tyson (1986) model for southern Africa atmospheric circulation. North-south shifts in mean circulation dominate climatic variability in the region but there are also regular disturbances to this mean, such as in the form of the El Niño – Southern Oscillation.

The fluctuations seen in present and palaeoclimatic records are the result of a complex interaction between internal and external mechanisms of climate change. Wavelet analyses of recorded and proxy climatic datasets highlighted the cycles which dominate southern African climatic variability on timescales from years to millennia. The causes of these cycles were then assessed in the context of established solar, atmospheric and oceanic models. Wavelet analyses also provided an indication of frequency changes over time and were therefore useful for detecting climate change. An analysis of proxy and recorded climatic datasets for southern African rainfall over the last 100 years indicated a frequency modulation of the 18 year rainfall cycle, which was first described by Tyson (1971). This variation may be related to anthropogenic climate change.

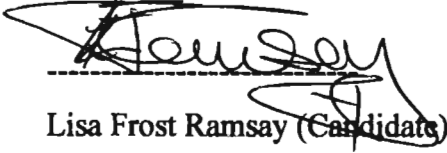
It became apparent from this study that there is a need for increased scientific interest in the palaeoclimatic trends of the region. The number of continuous, high-resolution datasets needs to be increased to allow for comparison and confirmation of various trends with records from sites across the globe. An understanding of the nature of regional and global teleconnections is essential before reliable climate change models can be established. There is also a need for further understanding of short-term southern African climate

variability on inter-annual timescales. It is only once we have an understanding of the natural climatic variability of the region, and its inherent cyclicality, that we can begin to distinguish the impact of anthropogenic activities on climate.

## PREFACE

The work in this thesis was carried out in the School of Environmental Sciences, University of KwaZulu-Natal, Howard College Campus, from January 2004 to September 2005, under the supervision of Professor Fred Ellery.

The study comprises original work by the author. Where use was made of the work of other authors, it has been duly acknowledged in the text. The study has not been submitted previously in any form to another university.

A handwritten signature in black ink, appearing to read 'Lisa Frost Ramsay', written over a horizontal dashed line.

Lisa Frost Ramsay (Candidate)  
September 2005

-----  
Professor Fred Ellery (Supervisor)

## TABLE OF CONTENTS

<b>1. INTRODUCTION</b> .....	1
1.1 MOTIVATION .....	1
1.2 AIMS AND OBJECTIVES .....	2
<b>2. DATA AND PRELIMINARY ANALYSIS</b> .....	4
2.1 INTRODUCTION .....	4
2.2 PALAEOCLIMATIC DATA SOURCES .....	4
2.2.1 Glaciological .....	4
2.2.2 Geological .....	5
2.2.2.1 Marine .....	5
2.2.2.2 Terrestrial .....	5
2.2.3 Biological .....	8
2.2.3.1 Corals .....	8
2.2.3.2 Tree-rings .....	9
2.2.3.3 Micromammals .....	10
2.2.3.4 Pollen .....	10
2.2.4 Historical .....	11
2.3 DATA SOURCES SELECTED FOR THIS STUDY .....	11
2.3.1 Coral Data.....	12
2.3.1.1 Description.....	12
2.3.1.2 Previous Studies.....	15
2.3.1.3 Analysis .....	16
2.3.2 Stalagmite Data .....	18
2.3.3 Pollen Data .....	18

2.3.4	Recorded Data .....	19
2.3.4.1	Southern Oscillation Index .....	19
2.4	SUMMARY.....	21
3.	<b>SOUTHERN AFRICAN PALAEOCLIMATES: A REVIEW .....</b>	<b>22</b>
3.1	INTRODUCTION .....	22
3.2	CASE STUDIES.....	23
3.2.1	Tree-ring Studies .....	25
3.2.2	Verlorenvlei.....	28
3.2.3	Wonderkrater.....	32
3.2.4	Cold Air Cave.....	36
3.2.5	Cango II Cave.....	39
3.2.6	Border Cave.....	41
3.2.7	Lobatse II Cave .....	42
3.2.8	Boomplaas Cave.....	45
3.2.9	Tswaing Crater (Pretoria Saltpan).....	46
3.3	SYNTHESIS: THE CLIMATIC TIMELINE.....	49
3.3.1	40 000 – 30 000 BP .....	50
3.3.2	30 000 – 25 000 BP .....	51
3.3.2.1	Temperature .....	51
3.3.2.2	Rainfall.....	51
3.3.3	25 000 – 21 000 BP .....	51
3.3.3.1	Temperature .....	51
3.3.3.2	Rainfall.....	52
3.3.4	21 000 – 17 000 BP .....	52
3.3.4.1	Temperature .....	52
3.3.4.2	Rainfall.....	53
3.3.5	17 000 - 12 000 BP.....	54
3.3.5.1	Temperature .....	54

3.3.5.2	Rainfall.....	54
3.3.6	12 000 – 10 000 BP .....	55
3.3.6.1	Temperature .....	55
3.3.6.2	Rainfall.....	56
3.3.7	10 000 – 4000 BP .....	56
3.3.7.1	Temperature .....	56
3.3.7.2	Rainfall.....	57
3.3.8	4000 BP – Present .....	59
3.4	TELECONNECTIONS .....	61
3.4.1	Southern Africa .....	61
3.4.2	Africa.....	64
3.4.3	Global .....	64
3.5	SUMMARY.....	66
4.	<b>PALAEOCLIMATIC ANALYSIS: THE GENERAL MODELS AND COMPARISONS.....</b>	<b>67</b>
4.1	INTRODUCTION .....	67
4.2	METHODOLOGY .....	67
4.2.1	Regional Rainfall and Temperature Models .....	67
4.2.2	Back-projection of Climatic Variables for Sodwana Bay and Makapansgat.....	68
4.2.3	Principal Component Analysis of Wonderkrater Pollen Data.....	68
4.3	RESULTS AND DISCUSSION.....	69
4.3.1	General Models of Southern African Climate Change .....	69
4.3.1.1	Temperature .....	69
4.3.1.2	Rainfall.....	72
4.3.2	A Climatic Record for the Last 116 Years from Sodwana Bay .....	74
4.3.2.1	Calcification and Temperature.....	75

4.3.2.2	Length and Rainfall .....	81
4.3.3	A Climatic Record for the Last 6600 Years from Makapansgat.....	83
4.3.3.1	<sup>18</sup> O and Temperature.....	83
4.3.3.2	<sup>13</sup> C and Rainfall .....	85
4.3.4	A Climatic Record for the Last 10 000 Years from Wonderkrater.....	88
4.3.4.1	PC1 and Temperature .....	90
4.3.4.2	PC2 and Rainfall.....	91
4.4	SUMMARY.....	92
5.	<b>ATMOSPHERIC CIRCULATION: PAST AND PRESENT .....</b>	<b>93</b>
5.1	INTRODUCTION .....	93
5.2	THEORIES OF ATMOSPHERIC CIRCULATION.....	93
5.2.1	Mean Atmospheric Circulation Models .....	93
5.2.2	The El Niño Model.....	98
5.3	PRESENT CONDITIONS.....	102
5.3.1	Mean Circulation and Travelling Disturbances.....	102
5.3.2	Rainfall .....	106
5.3.3	Disruptions to the Mean Circulation: El Niño.....	107
5.4	APPLICABILITY OF MODELS TO PALAEOCLIMATES .....	108
5.5	APPLICATION OF MODELS TO PALAEOCLIMATES.....	111
5.5.1	20 000 to 12 000 BP .....	112
5.5.1.1	Mean Atmospheric Conditions .....	112
5.5.1.2	Disturbances to the Mean: El Niño.....	113
5.5.2	12 000 to 10 000.....	114
5.5.2.1	Mean Circulation .....	114
5.5.2.2	Disturbances to the Mean: El Niño.....	115
5.5.3	10 000 to 4000 BP .....	115



5.5.3.1	Mean Circulation .....	115
5.5.3.2	Disturbances to the Mean: El Niño.....	116
5.5.4	4000 BP – Present .....	117
5.5.4.1	Mean Circulation .....	117
5.5.4.2	Disturbances to the Mean: El Niño.....	117
5.6	SUMMARY.....	117
6.	<b>SOUTHERN AFRICAN CLIMATIC VARIABILITY .....</b>	<b>120</b>
6.1	INTRODUCTION .....	120
6.1.1	External Mechanisms of Climate Change .....	121
6.1.2	Internal Mechanisms of Climate Change .....	124
6.2	CLIMATIC CYCLICITY.....	133
6.2.1	Cycles on a Milankovitch Scale .....	134
6.2.2	Cycles on a Millennial Scale.....	135
6.3	METHODOLOGY: WAVELET ANALYSIS .....	136
6.4	RESULTS AND DISCUSSION.....	142
6.4.1	The Sodwana Bay Coral Record .....	142
6.4.1.1	The 22 Year Cycle .....	142
6.4.1.2	The 80 Year Cycle .....	144
6.4.1.3	The Annual Cycle .....	146
6.4.1.4	The 2 – 3 Year Quasi-Biennial and the 4 – 8 Year El Niño Cycles	146
6.4.1.5	The 18 Year Cycle .....	148
6.4.1.6	The 45 Year Cycle .....	149
6.4.2	The Makapansgat Stalagmite Record.....	150
6.4.2.1	The 3000 Year Cycle .....	151
6.4.2.2	The 2000 - 2500 Year Cycle.....	152
6.4.2.3	The 1500 Year Cycle .....	152
6.4.2.4	The 1000 Year Cycle .....	153

6.4.2.5	The 450 Year Cycle .....	156
6.4.2.6	The 120 – 200 Year Cycle .....	156
6.4.2.7	The 80 Year Cycle .....	156
6.4.3	The Wonderkrater Pollen Record.....	156
6.5	RECENT CLIMATE CHANGE DETECTION USING WAVELET ANALYSIS.....	159
6.6	SUMMARY .....	163
7.	CONCLUSION.....	164
7.1	RECOMMENDATIONS.....	166
	<b>REFERENCES.....</b>	<b>168</b>
	<b>APPENDIX 1 - MATLAB SCRIPT FOR MEASURING PIXAL DISTANCE.....</b>	<b>215</b>
	<b>APPENDIX 2 - MATLAB SCRIPTS FOR WAVELET ANALYSIS .....</b>	<b>216</b>
	<b>APPENDIX 3 – CORAL DATA .....</b>	<b>218</b>
	<b>APPENDIX 4 – STALAGMITE DATA.....</b>	<b>222</b>
	<b>APPENDIX 5 – POLLEN DATA .....</b>	<b>235</b>

## LIST OF FIGURES

Figure 2.1	Map of Sodwana Bay showing position of Two-mile Reef (Celliers and Schleyer, 20 138) .....	13
Figure 2.2	Computerised Tomographical coral images showing axis of measurement.... .....	17
Figure 3.1	Deuterium isotope index of the Vostok ice core (Jouzal <i>et al.</i> , 1987 in Tyson, 1999b) .....	24
Figure 3.2	Map indicating main study sites.....	25
Figure 3.3	Tree-ring record from Hall (1976, 699) with annual growth increments in millimetres .....	27
Figure 3.4	Summary of Quaternary vegetation changes at Verlorenvlei (Baxter, 1997 in Meadows, 2001, 49).....	29
Figure 3.5	Holocene sea-level curves from Jeradino (1995), Miller <i>et al.</i> (1993) and Baxter and Meadows (1999) (Baxter and Meadows, 2001, 77) .....	31
Figure 3.6	Wonderkrater boreholes 3 and 4 (Scott <i>et al.</i> , 2003, 484) .....	33
Figure 3.7	Temperature and moisture indices for Wonderkrater (Scott <i>et al.</i> , 2003, 487) .....	34
Figure 3.8	Comparison of Wonderkrater temperature index and Vostok deuterium isotope ratio records (Tyson, 1999b, 339) .....	35
Figure 3.9	Comparison between Wonderkrater (Scott <i>et al.</i> , 2003, 487) and Makapansgat (Holmgren <i>et al.</i> , 2003) temperature and rainfall indices with $\delta^{18}\text{O}$ and $\delta^{13}\text{C}$ expressed relative to the Pedee belemnite (PDB) standard	

	.....	37
Figure 3.10	Temperature record from Cango II Cave (Talma and Vogel, 1992) in Tyson (1999b, 337). Ages in $^{14}\text{C}$ BP except for those less than 5000 BP which are in calendar years BP.....	40
Figure 3.11	Palaeoclimatic record from Border Cave (Butzer <i>et al.</i> , 1984a, 240).....	42
Figure 3.12	Temperature index for Boomplaas, with dots indicating assemblages dated by carbon isotope assays on charcoal samples and crosses indicating assemblage of uncertain age (Thackeray, 1987, 298) .....	46
Figure 3.13	Correlation between Pretoria rainfall and January insolation over 200 000 years (Partridge <i>et al.</i> , 1997, 1128).....	48
Figure 3.14	Generalised temperature conditions of the last 2000 years for southern Africa relative to current mean temperature at 0 (Tyson, 1999b, 342).....	60
Figure 3.15	Comparison of Makapansgat $\delta^{18}\text{O}$ (expressed relative to the Pedee belemnite, PDB, standard) curve and Cango II Cave palaeotemperature curve, with MW = Medieval Warming (Tyson, 1999b, 345) .....	63
Figure 3.16	Southward advance of Holocene Altithermal (Scott, 1993 in Tyson, 1999b, 341) .....	63
Figure 4.1	General model of southern African annual mean temperature for the last 40 000 years .....	70
Figure 4.2	Southern Africa regional corroboration of major events in general model of southern African annual mean temperature for the last 40 000 years .....	71
Figure 4.3	Southern African regional corroboration of major events in the Makapansgat $\delta^{18}\text{O}$ record for the last 3000 years (Tyson, 1999b, 344) .....	72

Figure 4.4	General model of southern African annual mean rainfall for the last 40 000 years .....	73
Figure 4.5	Temperature curves, $\delta^{18}\text{O}$ and PC1, and moisture curves, $\delta^{13}\text{C}$ and PC2, for Makapansgat and Wonderkrater respectively. Younger Dryas and Last Glacial Maximum (LGM) are labelled. Note that temperatures increase between the LGM and the Younger Dryas, while moisture levels decrease in the Makapansgat record and remain similar in the Wonderkrater record (adapted from Scott <i>et al.</i> , 2003, 487).....	74
Figure 4.6	Comparison of sea-surface temperatures (SST) back-projected from coral calcification and modelled sea-surface temperatures (SST) (NOAA-CIRES, 2000) .....	76
Figure 4.7	Comparison of sea-surface temperature (SST) anomalies back-projected from coral calcification and Southern Oscillation Index (SOI) anomalies (NCAR, 2005).....	77
Figure 4.8	Correlation between calcification values and air temperature running means with a peak at a 5 year running mean.....	78
Figure 4.9	Comparison of back-projected air temperatures from coral calcification and recorded air temperatures (SAWS, 2005).....	79
Figure 4.10	Decadal southern hemisphere combined land-sea temperatures compared with South African regional maximum annual air temperature and borehole-derived surface rock temperature anomalies (Tyson and Preston-Whyte, 2000, 324) .....	80
Figure 4.11	Comparison of back-projected rainfall from coral length and recorded rainfall (SAWS, 2005) .....	82
Figure 4.12	Back-projection of the deviation from present annual mean maximum daily temperatures (0) over 6600 years for Makapansgat.....	84

Figure 4.13	Comparison of the back-projected record of deviation from present annual mean of maximum daily temperature (0) for Makapansgat and the general model of southern African annual mean temperature.....	85
Figure 4.14	Back-projection of deviation from present mean January rainfall (0) over 6600 years for Makapansgat .....	87
Figure 4.15	Comparison of the back-projected record of deviation from present mean January rainfall (0) for Makapansgat and the general model of southern African annual mean rainfall.....	87
Figure 4.16	Variance explained by principal components with line of cumulative variance .....	88
Figure 4.17	Principal component weightings of 15 selected pollen taxa.....	89
Figure 4.18	First two principal components with PC1 representing a temperature index and PC2 representing a moisture index for Wonderkrater.....	90
Figure 4.19	Comparison of the Wonderkrater PC1 temperature index and the general model of southern African annual mean temperature.....	90
Figure 4.20	Comparison of the Wonderkrater PC2 moisture index and the general model of southern African annual mean rainfall .....	91
Figure 5.1	Model of zonal wind component anomalies over southern Africa during wet spells (Tyson and Preston-Whyte, 2000, 332).....	94
Figure 5.2	Model of zonal wind component anomalies over southern Africa during dry spells (Tyson and Preston-Whyte, 2000, 332).....	94
Figure 5.3	Model of anomalous meridional circulations during wet spells with positions of upper-tropospheric Atlantic wave, cloud formation zones, surface	

	expressions of South Atlantic High and location of storm tracks. ITCZ = Inter-Tropical Convergence Zone (Tyson and Preston-Whyte, 2000, 333) .....	95
Figure 5.4	Model of anomalous meridional circulations during dry spells with positions of upper-tropospheric Atlantic wave, cloud formation zones, surface expressions of South Atlantic High, and location of storm tracks. ITCZ = Inter-Tropical Convergence Zone (Tyson and Preston-Whyte, 2000, 333) .....	96
Figure 5.5	Conceptual model illustrating changing circulation controls, sea-surface temperatures, moisture-transport conveyors and loci of tropical convection during wet spells (Tyson and Preston-Whyte, 2000, 335) .....	97
Figure 5.6	Conceptual model illustrating changing circulation controls, sea-surface temperatures, moisture-transport conveyors and loci of tropical convection during dry spells (Tyson and Preston-Whyte, 2000, 335) .....	97
Figure 5.7	(a) La Niña, (b) Normal and (c) El Niño conditions (NOAA, 2005) .....	99
Figure 5.8	Monthly mean winds, contours of the 850 and 500 hPa surfaces (gpm) (Tyson and Preston-Whyte, 2000, 177) .....	103
Figure 5.9	Important features of the surface atmospheric circulation over southern Africa (Tyson and Preston-Whyte, 2000, 179) .....	104
Figure 5.10	Present day distribution of summer and winter rainfall regions in southern Africa with isolines indicating percentage annual rainfall received in summer (Cockcroft <i>et al.</i> , 1987) .....	106
Figure 5.11	Distribution of winter and summer rainfall regions at the Last Glacial Maximum (at approximately 18 000 BP) .....	113

Figure 5.12	Model of El Niño–Southern Oscillation power over time (Tudhope <i>et al.</i> , 2001, 1157) .....	114
Figure 5.13	Distribution of summer and winter rainfall regions 12 000 – 1000 BP .....	115
Figure 5.14	The dominance of summer rainfall at the Holocene Altithermal (at approximately 6000 BP) .....	116
Figure 6.1	The geosphere-hydrosphere-cryosphere-atmosphere system (Bradley, 1999, 16) .....	120
Figure 6.2	The Milankovitch cycles showing (a) eccentricity of the orbit, (b) obliquity of the orbit and (c) precession of the equinoxes (Tyson and Preston-Whyte, 2000, 55) .....	122
Figure 6.3	Pretoria rainfall and January insolation at 30° S (Partridge <i>et al.</i> , 1997) ..	122
Figure 6.4	Idealised thermohaline circulations in the Atlantic Ocean (Tyson and Preston-Whyte, 200, 226) .....	128
Figure 6.5	Broecker’s concept of the deep-ocean thermohaline conveyor belt (Tyson and Preston-Whyte, 2000, 227).....	128
Figure 6.6	A comparison of the GRIP ice core oxygen-isotope record and the relative abundance of polar foraminifera in the North Atlantic sediment core V23-81. YD denotes Younger Dryas, D deglaciation, LGM Last Glacial Maximum, IT3 Interstadial 3 and HL Heinrich layer (Tyson and Preston-Whyte, 2000, 337) .....	130
Figure 6.7	A section through the Atlantic Ocean to show the mechanisms likely to affect thermohaline circulation on various timescales (Tyson and Preston-Whyte, 2000, 338).....	130



Figure 6.8	Precession of the equinoxes (Tyson and Preston-Whyte, 2000, 311) with (a) austral summer perihelion and (b) boreal summer perihelion .....	135
Figure 6.9	Comparison of the (a) Fourier analysis and (b) wavelet analysis of the same hypothetical dataset, with positive values of the wavelet indicated by solid lines and negative values indicated by dotted lines .....	138
Figure 6.10	Morlet(x) = $\exp(-x^2 / 2) * \cos(5x)$ (MATLAB, 2005) .....	139
Figure 6.11	Wavelet analysis of 116 year coral density record from Sodwana Bay using the Morlet wavelet, with positive values of the wavelet indicated by solid lines and negative values indicated by dotted lines .....	142
Figure 6.12	Fourier analysis of 116 year coral density record from Sodwana Bay .....	143
Figure 6.13	Wavelet analysis of 116 year coral length record from Sodwana Bay using the Morlet wavelet, with positive values of the wavelet indicated by solid lines and negative values indicated by dotted lines .....	145
Figure 6.14	Fourier analysis of 116 year coral length record from Sodwana Bay .....	145
Figure 6.15	Annual shifts in the Inter-Tropical Convergence Zone (ITCZ) (Engle, 2005) .....	146
Figure 6.16	Modulation of the El Niño-Southern Oscillation (ENSO) in the region of southern Africa by the Quasi-Biennial Oscillation (QBO) in its (a) westerly and (b) easterly phase (Tyson and Preston-Whyte, 2000, 235) .....	147
Figure 6.17	Wavelet analysis of 10 000 year Makapansgat T8 stalagmite $\delta^{18}\text{O}$ record using the Morlet wavelet, with positive values of the wavelet indicated by solid lines and negative values indicated by dotted lines.....	150
Figure 6.18	Fourier analysis of 10 000 year Makapansgat T8 stalagmite $\delta^{18}\text{O}$ record.....	151

Figure 6.19	Wavelet analysis of 10 000 year Makapansgat T8 stalagmite $\delta^{13}\text{C}$ record using the Morlet wavelet, with positive values of the wavelet indicated by solid lines and negative values indicated by dotted lines .....	153
Figure 6.20	Wavelet analysis of 10 000 year Makapansgat T8 stalagmite $\delta^{18}\text{O}$ record using the Morlet wavelet showing higher frequency cycles, with positive values of the wavelet indicated by solid lines and negative values indicated by dotted lines .....	155
Figure 6.21	Wavelet analysis of 10 000 year Makapansgat T8 stalagmite $\delta^{13}\text{C}$ record using the Morlet wavelet showing higher frequency cycles, with positive values of the wavelet indicated by solid lines and negative values indicated by dotted lines .....	155
Figure 6.22	Wavelet analysis of PC1 of 10 000 year Wonderkrater pollen record using the Morlet wavelet, with positive values of the wavelet indicated by solid lines and negative values indicated by dotted lines .....	157
Figure 6.23	Fourier analysis of PC1 of 10 000 year Wonderkrater pollen record .....	157
Figure 6.24	Wavelet analysis of PC2 of 10 000 year Wonderkrater pollen record using the Morlet wavelet, with positive values of the wavelet indicated by solid lines and negative values indicated by dotted lines .....	158
Figure 6.25	Fourier analysis of PC2 of 10 000 year Wonderkrater pollen record .....	158
Figure 6.26	Wavelet analysis of 50 year Lake St Lucia salinity record using Morlet wavelet, with positive values of the wavelet indicated by solid lines and negative values indicated by dotted lines.....	159
Figure 6.27	Wavelet analysis of 45 year Cape St Lucia rainfall record using Morlet wavelet, with positive values of the wavelet indicated by solid lines and negative values indicated by dotted lines.....	160

Figure 6.28	Wavelet analysis of 80 year Vryheid rainfall record using Morlet wavelet with positive values of the wavelet indicated by solid lines and negative values indicated by dotted lines .....	161
Figure 6.29	Wavelet analysis of 116 year coral length record from Sodwana Bay using Morlet wavelet, with positive values of the wavelet indicated by solid lines and negative values indicated by dotted lines.....	162

## LIST OF TABLES

Table 2.1	Recorded and modelled datasets used in this study .....	20
Table 4.1	Statistics of the correlation between calcification and sea-surface temperature .....	75
Table 4.2	Statistics of the correlation between calcification and air temperature .....	78
Table 4.3	Statistics of the correlation between length and rainfall .....	81
Table 4.4	Statistics of the correlation between $^{18}\text{O}$ and mean daily maximum air temperature.....	83
Table 4.5	Statistics of the correlation between $^{13}\text{C}$ and mean January rainfall.....	86
Table 5.1	Summary of atmospheric and oceanic features of La Niña, Normal and El Niño states (adapted from Philander, 1990; Mason, 2001; Cane, 2005) ..	100

## ACKNOWLEDGEMENTS

My thanks are extended to:

Professor Fred Ellery, a humble leader, who has inspired me with his enthusiasm and scientific integrity

Professor Karin Holmgren, Stockholm University, and Professor Louis Scott, University of the Free State, who generously provided their data

The Marine Geoscience Unit, University of KwaZulu-Natal, for the loan of the coral core

Dr Anne Cohen, Woods Hole Oceanographic Institution, for answering my coral questions

Professor Gordon Cooper, University of the Witwatersrand, for tirelessly answering my wavelet questions

Lake, Smit and Partners for performing the Computerised Tomographical scans of the coral core at no cost

Brett for his patience and support, and the many hours formatting data and checking references

Mnr and Mev Winterbach for their generosity, care and encouragement, and Wynand for his mathematical and programming expertise

My parents for proofreading this document

Mrs Spangehl for her scanning skills and Mr Spangehl for accessing the Makopane data

Tombaloms for keeping me strong with tea and rusks

The Ernst and Ethel Eriksen Trust and the National Research Foundation for their financial support during the course of my research

# 1. INTRODUCTION

For over three billion years climate change has been the primary environmental factor determining conditions for life. The focus of palaeoclimatic research is to establish the processes driving climate change during the Quaternary, approximating the last 2 million years of Earth's history, so as to contextualise the current climatic situation. The collection of extended chronologies from various sources, including isotope records from stalagmites, pollen and micromammalian records from sediments, and growth records from trees and coral, has been an essential step towards a better understanding of past environments. These records offer an archive against which the nature, causal factors, frequency and magnitude of contemporary environmental dynamics can be measured.

## 1.1 MOTIVATION

Climate is intricately connected to oceanic circulation through changing salinity and temperature gradients, which yield a thermohaline conveyor, transporting North Atlantic deep waters to the southern oceans (Meadows, 2001). Since it is more oceanic than the northern hemisphere, the southern hemisphere plays a dominant role in the redistribution of solar energy through this thermohaline system (Meadows, 2001). Significant changes in southern African palaeoclimates may indicate simultaneous changes across the globe due to these oceanic and atmospheric teleconnections. Southern African datasets can provide important clues to the nature of these climate perturbations that may not be present in records from the northern hemisphere.

Isolated palaeoclimatic studies were conducted in the region during the 1970s and early 1980s (such as Butzer *et al.*, 1973; 1978a; Hall, 1976; Van Zinderen Bakker, 1982). In the 1980s, when the impacts of anthropogenic global warming became an environmental reality, interest in natural climate change was aroused. Researchers aimed to distinguish natural climate fluctuations from those related to human activities and this required an analysis of climate trends from the period before the industrial revolution and back into the Quaternary history. The number of palaeoclimatic studies increased and researchers became aware of the need to compare their climatic sequences in search of common trends which would allow for the development and validation of palaeoclimatic models. This led

to numerous attempts at synthesis based on the available evidence (such as Meadows, 1988; Partridge *et al.*, 1990; Partridge, 1993; Marker, 1998; Tyson, 1999b) and the publication of an extensive review (Deacon and Lancaster, 1988).

Yet despite increased interest, the number of collected and studied palaeoclimatic records of the northern hemisphere continued to outweigh that of the southern hemisphere, and the number of Quaternary sequences from southern Africa remained small in relation to the geographical area of the subcontinent (Meadows, 2001). This was most likely due to the capital, expertise and equipment required for the identification, collection and analysis of palaeoclimatic records. Over the last decade, however, with improvements in technology and methods, and an increase in foreign interest, a number of reliable records with good continuity have become available (such as Partridge *et al.*, 1997; Holmgren *et al.*, 2003; Scott *et al.*, 2003). Many of these records, such as that of Holmgren *et al.* (2003) from a cave in the Makapansgat Valley, have the added advantage of high resolution. Analyses of these datasets resulted in breakthroughs in palaeoclimatic understanding, including an increased awareness of the effects of orbital precession on rainfall in the region, and of the nature of oceanic and atmospheric teleconnections on various scales.

Thus the time has arrived for an updated synthesis of southern African palaeoclimatic knowledge. An extensive literature review, particularly of work conducted over the last ten years, will provide the information required to extract regional climate trends for the last 40 000 years of the Quaternary and this, in turn, will allow for the generation of general models of temperature and rainfall changes. Climate fluctuations can then be discussed in the context of established models of internal and external forcing mechanisms. In this way, it may be possible to distinguish natural climatic cycles from changes caused by anthropogenic activities.

## **1.2 AIMS AND OBJECTIVES**

The purpose of climate change research is to identify variability and trends in the climate system and to ascribe these changes to specific factors (Dethloff *et al.*, 2003). The aim of this study is to produce a synthesis of the knowledge of Late Quaternary palaeoclimatology of Southern Africa, to identify an atmospheric model that can be applied to the conditions

experienced during various periods of climate history, and to examine variability in the context of this model.

The synthesis of palaeoclimatic knowledge will be achieved through the fulfilment of the following objectives:

- A literature review of palaeoclimatic studies in southern Africa and beyond
- Extraction of southern African climatic trends, with reference to any obvious anomalies
- Development of generalised rainfall and temperature models for the last 40 000 years

An assessment of the accuracy of these models will be achieved through the fulfilment of the following objectives:

- Determination of the correlation between palaeoclimatic proxy records and measured records of the presumed environmental driver
- In the case of a significant correlation over the overlapping period, back-projection of the measured variable over the period of the proxy record
- Comparison of these back-projections with the general models

The application of established atmospheric models to account for palaeoclimatic fluctuations will be achieved through the fulfilment of the following objectives:

- Review of existing atmospheric models for present southern African climates
- Comparison of current conditions with those of the last 40 000 years
- Suggestion of possible atmospheric fluctuations that could account for the palaeoclimatic trends of the last 40 000 years

The interpretation of any persistent cyclicity in southern African present and palaeoclimates will be achieved through the fulfilment of the following objectives:

- Resolution of present and palaeoclimatic datasets into component parts using wavelet transform analysis
- Comparison of the detected cycles with those identified by other authors
- Establishment of whether present variability modes have ancient antecedents
- Comparison of datasets to determine whether common cycles are in phase
- Investigation of potential internal and external forcing mechanisms



## **2. DATA AND PRELIMINARY ANALYSIS**

### **2.1 INTRODUCTION**

This chapter will provide a description of potential data sources for palaeoclimatic study and a discussion of the three main datasets selected for this particular study, namely the Sodwana coral, Makapansgat stalagmite and Wonderkrater pollen records. The coral core (Appendix 3) was analysed and dated by this author. The pollen (Appendix 4) and stalagmite (Appendix 5) data were collected and analysed by Scott *et al.* (2003) and Holmgren *et al.* (2003) respectively and required no dating or calibration.

### **2.2 PALAEOCLIMATIC DATA SOURCES**

There are many potential data sources for the reconstruction of palaeoclimates and no single source is ideal (Farrera *et al.*, 1999). Specific data sources may prove to be more viable and accurate in certain regions. Factors that increase the value of a data source include a wide spatial resolution, potential for accurate dating, direct climatic controls, and the potential to yield quantitative climatic data (Farrera *et al.*, 1999). The four main types of palaeoclimatic data are glaciological, geological, biological and historical.

#### **2.2.1 Glaciological**

Glaciological data is collected in geochemical studies of major ions and isotopes of oxygen and hydrogen, in the study of the gas content of air bubbles, trace elements and microparticle element concentrations, and in an analysis of the physical properties of ice, such as the ice fabric (Bradley, 1999). When snow falls on ice, such as at the poles, there are air gaps between the snowflakes. As more snow falls, layers are compressed to form solid ice, but some air remains trapped in the ice structure. Since snow tends to be laid down in regular annual layers, it is possible to determine the age of an ice layer by counting the layers from the surface (Gribben, 1989). Detailed physical and chemical analyses of ice and fern, which is ice that has survived the summer ablation season, may provide climate data for periods on the scale of hundreds of thousands of years (Bradley,

1999). Isotope measurements and studies of particulates and ice structure provide information of precipitation, air temperature, atmospheric composition, the occurrence of explosive volcanic eruptions, and variations in solar activity over time (Bradley, 1999).

## **2.2.2 Geological**

Geological sources can be divided into marine and terrestrial sources. Marine sources include biogenic sediments, such as planktonic and benthic fossils, and clastic sediments, such as terrestrial dust and ice-rafted debris. Terrestrial sources include glacial deposits and features of glacial erosion, shoreline features, aeolian deposits, lacustrine sediments, speleothems and pedological features of relict soils (Bradley, 1999).

### *2.2.2.1 Marine*

The oceans occupy more than 70% of the Earth's surface and are thus an important source of palaeoclimatic information (Bradley, 1999). Sediments in ocean basins offer an archive of climatic conditions near the ocean surface and on the adjacent continents. Sediments are composed of biogenic and geological materials. The biogenic sediments offer an indication of past atmospheric and oceanic circulation in records of salinity, dissolved oxygen in deep water, and nutrient and trace element concentrations. The oxygen isotope composition of biological sediments is a function of water temperature, and it has been discovered that there is a consistent stable isotope signal in marine sediments from around the globe such that distinct isotope stages can be defined (Imbrie *et al.*, 1984). Clastic sediments mainly provide a record of humidity–aridity variations on the continents, or the intensity and direction of winds or other sediment transporting processes, including fluvial erosion, ice-rafting and turbidity currents (Bradley, 1999).

### *2.2.2.2 Terrestrial*

The range of non-marine geological studies that provide information on palaeoclimates is vast and one could argue that virtually all sedimentary deposits convey a climatic signal to some degree (Bradley, 1999). Aeolian, lacustrine and fluvial deposits are a function of climate although it may be difficult to identify the particular combination of climatic

factors that led to their formation (Bradley, 1999). Three important terrestrial sources are speleothems, lake deposits and snowlines, and a discussion of these sources follows.

Speleothems, which include stalactites, stalagmites and dripstones, are secondary calcium carbonate deposits that are precipitated in caves. Speleothem growth occurs when there is adequate precipitation to produce seepage water and when the ground surface is vegetated so that this water is carbonated. Growth is restricted by extreme cold, intense aridity, or when the cave is flooded by water. The  $\delta^{18}\text{O}$  variation in speleothems is controlled by the  $\delta^{18}\text{O}$  composition of the feeding water and the feeding water is, in turn, controlled by the isotope content of precipitation and by the temperature dependent fractionation between the water and the carbonate (Schwarcz, 1986; Lauritzen, 1995; Holmgren, 1996; Holmgren *et al.*, 2003). The assertion that enrichment in speleothem  $^{18}\text{O}$  can be interpreted as a change to cooler conditions (Ford and Williams, 1989) is empirically based on the results of numerous studies across the globe. If the  $\delta^{18}\text{O}$  of palaeoprecipitation can be measured, for example in old groundwater, the  $\delta^{18}\text{O}$  in the speleothem carbonate can be used to estimate cave temperature at the time of formation and growth (Hendy, 1971; Schwarcz, 1986). Cave temperatures are generally stable, approximating to the mean annual ground temperature of the region (Holmgren *et al.*, 1995).

The stable carbon isotopic content in speleothems,  $\delta^{13}\text{C}$ , indicates changes in vegetation if the bedrock conditions are assumed to be constant over the growth period of the speleothem. C3 plants dominate in high latitude regions where night temperatures are low, winter precipitation is high and there is limited water stress, while C4 plants occur more frequently in low latitude areas of high temperatures and summer rainfall (Vogel *et al.*, 1978).

Previously, most speleothem records were seen as providing estimates of relative changes in various climatic parameters based on an assumed correlation between growth rates and climate (Shaw and Cooke, 1986; Brook *et al.*, 1997). Some studies provided an analysis of isotopic deviations, assuming that they reflect single climatic parameters, or a deconvolution of the temperature and precipitation signals using data from other sources (Holmgren *et al.*, 1995; Bar-Matthews *et al.*, 1997; Burney *et al.*, 1997). Speleothems can be precisely dated with uranium methods (Schwarcz, 1986; Li *et al.*, 1989) and dated stable isotope studies of speleothems are useful for the development of

palaeoenvironmental data series, as demonstrated by Hendy (1971), Gascoyne (1979; 1992), Goede and Vogel (1991), Dorale *et al.* (1992), Talma and Vogel (1988; 1992), Railsback *et al.* (1994) and Holmgren *et al.* (1995; 2003). A lack of independent information of the  $\delta^{18}\text{O}$  composition of fossil cave seepage water limited quantitative interpretation of southern African speleothem records until the study of the Congo Cave by Talma and Vogel (1992).

Lakes offer another important terrestrial source of data. Although lakes usually only provide qualitative records of climate change, several characteristics make them useful for reconstructing palaeoclimatic records. The climatic controls on lake water balances are well known (Street-Perrott and Harrison, 1985; Cheddadi *et al.*, 1996) and lake records are widely distributed, with records of dried lakes common in arid areas. Lake-bottom and marginal sediments represent a quasi-continuous record of long-term changes, and offer material suitable for  $^{14}\text{C}$  dating (Bradley, 1999).

Water-level changes in lakes can occur on a variety of timescales from intra-annual to geological. Changes in water depth influence the physical and biological characteristics of the lake and can be detected in the sedimentary or biostratigraphic records in the lake deposits (Street-Perrott and Harrison, 1985; Harrison and Digerfeldt, 1993). Changes in water depth are usually related to local factors such as the damming of an outlet, geomorphic changes which alter inflows, changes in land use of the catchment, or tectonism (Dearing and Foster, 1986). Generally, these factors affect only individual lakes. Regionally synchronous changes, on the other hand, reflect changes in the hydrological balance, which are driven by changes in climate.

To infer climate changes from lake records, the lake water balance must be understood. Overflowing lakes approach equilibrium such that the sum of runoff from the catchment and the water balance over the lake surface is balanced by discharge (Szestay, 1974; Street-Perrott and Harrison, 1985; Mason *et al.*, 1994). Discharge is a function of lake volume and depends on the form of the lake and its outlet (Henderson-Sellers, 1984). As such, lake area and depth can be interpreted as a function of the difference between precipitation and evaporation (Cheddadi *et al.*, 1996) and reconstructed changes in lake form can be used to develop a palaeomoisture index.

High mountain environments are sensitive to climatic change and snowlines, which offer another valuable terrestrial source of information, can be considered a manifestation of a complex climatic equilibrium (Hastenrath, 1972). In regions of permanent snow, it is usually possible to recognise the seasonal snow zone from an upper region of permanent snow. The actual boundary of the snowline will vary in elevation depending on the weather experienced during the seasons of accumulation and ablation (Bradley, 1999). On a glacier, this would be equivalent to the equilibrium line altitude (ELA). Observations of modern glaciers indicate that the ELA approximates the height at which the accumulation area of the glacier occupies 70% of its total area (Bradley, 1999). Thus, to estimate palaeosnowlines, the common practice is to map the former glacier area, identified from the moraine position, and then determine the position of the ELA based on an accumulation area ratio of approximately 0.7. Mapping the difference between modern and palaeo-ELAs can provide useful insights into past climates.

### **2.2.3 Biological**

The study of biological material as a proxy of climate spans a wide range of sub-disciplines. Biological sources include tree-rings, pollen, plant macrofossils, micromammalian remains, insects, corals, and diatoms in lake and marine sediments. Each source requires a specific form of collection and analysis.

#### *2.2.3.1 Corals*

Most reef-building corals live in the upper 40 m of the ocean where there is sufficient light for the photosynthetic activity of the coral's endosymbiotic zooxanthellae, and are restricted to regions of warm water temperatures (Bessat and Buiges, 2001). Most corals are located equatorward of 23° latitude in regions where mean annual temperatures are not below 24 °C and mean winter minimum temperatures are not below 18 °C (Bessat and Buiges, 2001). However, ocean currents may transport warmer waters to higher latitudes and coral growth can occur at some mid-latitude locations (Felis and Pätzold, 2003).

Corals are sensitive to small changes in ocean temperature and salinity, which register as physical and chemical patterns in the calcium carbonate skeleton (Bessat and Buiges, 2001; Felis and Pätzold, 2003). Advanced techniques have been developed to obtain

information that is stored in the form of changes in skeletal chemistry, for example the oxygen (O) and carbon (C) isotope ratios, and in trace element composition (Mg/Ca, Sr/Ca ratios) with the precision necessary to calculate temperatures to a few tenths of a degree (Cleveland *et al.*, 2004). Growth variables such as density and length also correlate well with measured records of sea-surface temperature and salinity. Dating is achieved by layer counting or isotopic dating methods (Felis and Pätzold, 2003).

Living corals cover the past centuries while fossil corals reveal climate variability during various periods of the Holocene (Felis and Pätzold, 2003). Evidence can be found for long-term climate changes and catastrophic events such as hurricanes and floods. The abundance of large coral colonies, their continuous growth and their longevity (a single colony may live as long as 1000 years) allow for the reconstruction of multi-century records with seasonal, and sometimes weekly, resolution (Felis and Pätzold, 2003). These records improve climate predictability and provide a better understanding of the dominant modes of the global climate system, such as the El Niño-Southern Oscillation (ENSO), and the mechanisms of decadal climate variability (Felis and Pätzold, 2003). Furthermore, coral records offer an historical perspective to assess disruptions to natural environmental cycles caused by anthropogenic influences (Bessat and Buiges, 2001).

#### 2.2.3.2 *Tree-rings*

Dendroclimatology has been defined by Fritts (1971, 420) as ‘dendrochronological studies that use climatic information in dated growth layers to study variability in present and past climate’. Tree-rings are usually annual, especially if there is marked seasonality in rainfall (Dunwiddie and LaMarche, 1980). Liebig’s (1840) ‘Law of Limiting Factors’ states that biological processes cannot occur faster than supported by the most limiting factor and the initial step in a dendroclimatological study is to establish the principal limiting factor. Hall (1976) suggested that this is likely to be precipitation in most regions of southern Africa. As such, growth measurements can provide a proxy rainfall record in most cases.

Few dendrochronological studies have been undertaken in southern Africa despite the potential for the development of tree-ring chronologies extending over hundreds of years (Dunwiddie and LaMarche, 1980). The studies that have taken place (such as Storry, 1975; Hall, 1976; Lilly, 1977) have consisted primarily of ring counts to estimate ages. There is a

need to extend southern African dendroclimatological studies through isotopic dating and more advanced techniques of climate interpretation.

#### 2.2.3.3 *Micromammals*

Micromammalian studies involve the collection of micromammalian remains from sediments followed by species identification, which usually relies on the examination of mandibles and maxillae. Once sample layers have been dated, it is possible to interpret an environmental history (Avery, 1982a; 2003) from micromammalian variations over time. For a meaningful interpretation of past climates, these studies often determine the minimum number of species and minimum number of individuals in sediment layers. The Shannon-Wiener index may be applied, which takes into account the number of species and the extent to which they are evenly represented in the samples. One can interpret vegetation types from the micromammalian content and climatic conditions according to the specific range of the same species at present. A valuable southern African micromammalian study was conducted at Border Cave, on the border of KwaZulu-Natal and Swaziland, by Avery (1982b).

#### 2.2.3.4 *Pollen*

Palaeoclimatic reconstruction from pollen distribution is possible because pollen grains have morphological characteristics that are specific to a particular genus or species (Jackson *et al.*, 1997), and therefore indicator species, which have a distribution strongly affected by climate, can be identified. Pollen is produced in vast quantities and distributed widely from its source. Pollen may be collected from various sedimentary environments, such as sediments from a lake bottom or margin, or from *Neotoma* and *Hyrax* middens in arid environments (Van Deventer *et al.*, 1987), and these can be dated by various techniques, but most commonly by radiocarbon methods. In this way a detailed chronological vegetation history can be derived from the source.

Plant taxa and biome distributions are sensitive to the atmospheric environment – particularly to factors such as the mean temperature of the coldest month, total growing-season warmth, which is defined as the number of days above a threshold temperature for growth, and plant-available moisture, which is the availability of soil moisture to satisfy

the demand for evapotranspiration (Woodward, 1987; Ellery *et al.*, 1991; Prentice *et al.*, 1992). Changes in pollen assemblages usually give an indication of changes in more than one climatic variable (Farrera *et al.*, 1999) and techniques have been developed to infer changes in specific variables. These include qualitative comparisons of identified species with their modern distributions, or quantitative estimates of minimum changes required to produce a biome shift (Guiot, 1991; Bartlein and Whitlock, 1993). In mountainous regions, comparisons of palaeopollen samples with current vegetation from different elevations have been used to estimate shifts in forest belts or the tree line (Farrera *et al.*, 1999).

Despite differences in the production and dispersal of pollen from different plant taxa, pollen assemblages from sediments have been successfully interpreted as quantitative vegetation records (Prentice, 1998). Dominant taxa tend to be well-represented and less common taxa supply the information that is required to assign pollen assemblages correctly to biomes (Prentice *et al.*, 1996). Procedures to assign biomes and to make palaeoclimate inferences can be calibrated using the large sets of pollen data that have been assembled for many sites across the globe, such as in the work of Guiot (1990); Cheddadi *et al.* (1996); Jolly *et al.* (1998) and Yu *et al.* (1998).

#### **2.2.4 Historical**

Historical documentary records are usually accurately dated and deal with high-frequency climatic fluctuations during the most recent past. A great deal can be learnt about the probability of extreme events by reference to historical records. However, these do not usually extend as far back as glaciological, geological or biological sources, and are often subjective observations.

### **2.3 DATA SOURCES SELECTED FOR THIS STUDY**

The collection, dating and processing of palaeoclimatic sources is complicated and costly, and often requires specialised equipment and expertise. For this reason, established datasets were requested from southern African palaeoclimatic experts. Professor Louis Scott of the University of the Free State provided the Wonderkrater pollen data that was used in the study by Scott *et al.* (2003), and Professor Karin Holmgren of Stockholm



University provided the stalagmite dataset that was used in the study by Holmgren *et al.* (2003). A coral core from Sodwana Bay was provided by the Marine Geoscience Unit at the University of KwaZulu-Natal. The study of the core is an original analysis and interpretation.

Biological, geological and historical records are used in this study. The Sodwana Bay coral and the Wonderkrater palynological datasets fall into the biological category, while the Makapansgat stalagmite record comprises geological data. The records of measured air temperature, sea-surface temperature, rainfall and salinity are historical records but have been recorded using scientific equipment rather than by human observation

Individual sources respond differently to various aspects of climate variability. Therefore more than one data source should be utilised to interpret palaeoclimatic conditions accurately. Sampling, processing and analytical errors may also occur during scientific studies and the use of multiple data sources makes it possible to check whether sources are consistent and thus trustworthy (Farrera *et al.*, 1999). The Makapansgat and Wonderkrater datasets were collected from proximate locations and cover a similar time period, which allows for comparison. The Sodwana Bay coral core record extends over the last 116 years and therefore overlaps with the historical record.

### **2.3.1 Coral Data**

#### *2.3.1.1 Description*

The coral sample utilised in this study was sawed from a 4 cm diameter core drilled by Dr. Peter Ramsay in May 1994 into a *Porites lutea* coral head, in 16 m water depth at Two-Mile Reef, Sodwana Bay, South Africa (27° 31' S 32° 41' E), shown in Figure 2.1. The core was made available by the Marine Geoscience Unit of the University of KwaZulu-Natal, courtesy of the Geological Survey of South Africa.

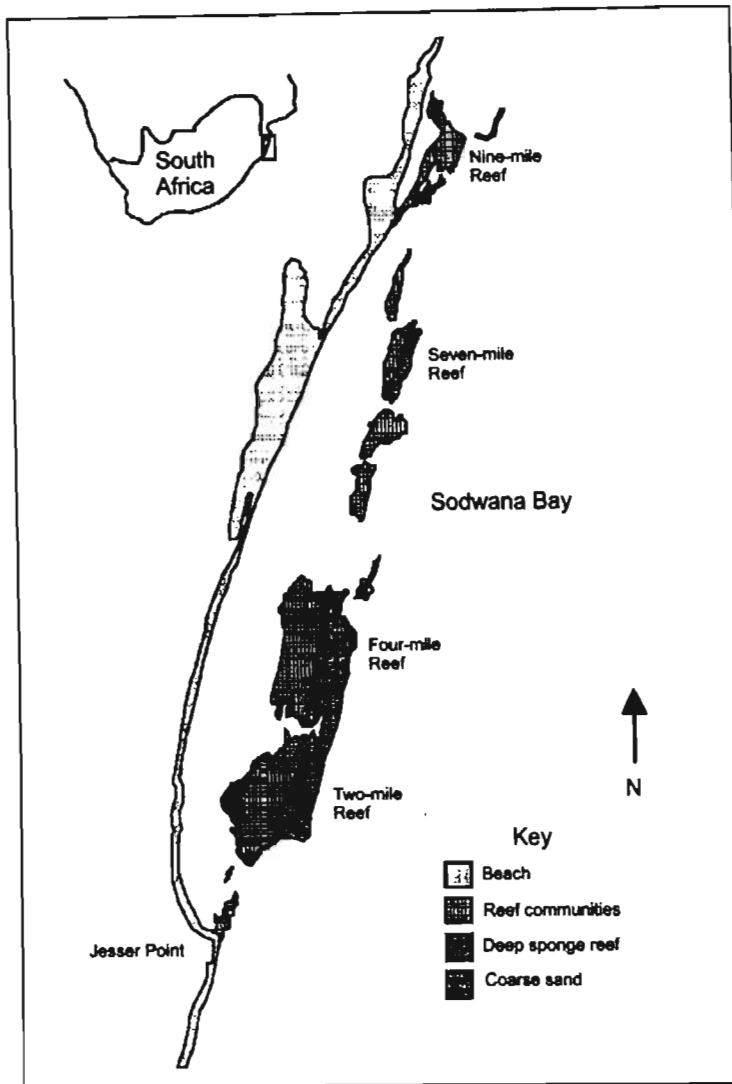


Figure 2.1 – Map of Sodwana Bay showing position of Two-mile Reef (Celliers and Schleyer, 2002, 1381).

Along the Maputaland coastline, coral communities exist on the Pleistocene submerged dune and beachrock systems to a latitude of  $27^{\circ} 50' S$  (Ramsay and Mason, 1990; Ramsay, 1994; Riegl *et al.*, 1995; Riegl, 1996). The substratum is flat, does not reach the surface, and no typical reef morphology is developed (Ramsay, 1990). The main ecological differentiation is along gradients of sedimentation due to resuspension of autochthonous sediment in gullies, and along a depth gradient due to decreasing irradiance, leading to a replacement of coral by sponges (Riegl, 2001). A gradient of diminishing wave stress also exists that leads to an increase in branching corals with depth (Riegl *et al.*, 1995; Riegl and Riegl, 1996).

The total core length covered 116 years of continuous growth, with well delineated growth banding that was evident using X-radiography. At collection, only the top few millimetres

of the coral was alive and below this, the skeleton was intact but tissueless. As corals grow, new skeleton is produced within the living tissue layer, which remains as a thin band of several millimetres width at the surface of the colony (Fischer *et al.*, 2003).

Density variations are caused by changes in the thickness of the vertical and horizontal skeletal elements, and resulting changes in the size of the pore spaces (Dodge *et al.*, 1992; Cohen *et al.*, 2004). The density data are affected by regional climate, local climate, geographical environment, and biological and physiological processes (Lough and Barnes, 1997; 2000; Priess, 1997; Bessat and Buiges, 2001). Density fluctuations along the growth axis therefore reflect the seasonal cycle of temperature, light and salinity (Wellington and Glynn, 1983; Felis and Pätzold, 2003). In general, coral skeletons reveal a pattern of alternating bands of high and low density, with a year being represented by a pair of such bands. An age model of a coral chronology is usually based on counting these annual density-band pairs (Cleveland *et al.*, 2004).

At Sodwana Bay, the low density bands are formed during late austral summer and the high density bands over the rest of the year (Ramsay, 1994). Coral in the region experiences increased growth when sea-surface temperatures are highest, extending rapidly and producing low density tissue. Various studies have shown that the high frequency annual banding is superimposed upon low frequency changes that correspond with interannual and decadal scale variability (Draschba *et al.*, 2000; Cohen *et al.*, 2004; Lough and Barnes, 1997; 2000).

Measurement of skeletal density as a climatic proxy has several advantages over conventional geochemical methods. Skeletal density can be five times more sensitive to changes in ocean temperature than skeletal isotope or elemental ratios and this is especially important at the mid-latitudes where interannual variability is usually 1 °C or less (Cohen *et al.*, 2004). Furthermore, image analysis is faster and cheaper than chemical analyses (Cleveland *et al.*, 2004) and this was an important consideration in this study as funding was limited. Furthermore, it was advised that a future analysis of a second core from the site should be undertaken to validate results (A. Cohen, 2005, pers. comm.), and the replication of chemical analyses would have proven too expensive.

### 2.3.1.2 Previous Studies

Coral growth parameters are sensitive to environmental changes and are useful as palaeoclimatic proxies (Lough and Barnes, 1997; 2000; Draschba *et al.*, 2000; Cohen *et al.*, 2004). Statistical analyses allow researchers to determine the strength of the correlation between climatic data and coral density bands. Bessat and Buiges (2001) linked variations in two centuries (1800 – 1990) of coral growth data of a *Porites lutea* sample from Moorea, French Polynesia with climatic variations. Several datasets of regional climatic variability were used for comparison, including air temperature data and the Southern Oscillation Index, which is the Tahiti-Darwin sea-level pressure index of El Niño-Southern Oscillation (ENSO) events (Ropelewski and Jones, 1987), as described in Section 2.3.4.1 on Page 19.

Bessat and Buiges (2001) calculated a significant correlation between changes in annual calcification along the core and variations in air temperatures. The annual calcification rate also corresponded strongly with records of air temperature in a study of coral from the Great Barrier Reef, Australia by Lough and Barnes (1997; 2000). The data suggested that a rise in temperature from 20 to 21 °C would increase the calcification rate by about 3.5% (Lough and Barnes, 1997). In the study by Bessat and Buiges (2001), a rise in temperature of 1 °C increased the calcification rate by approximately 4.5%. A linear regression of air temperature versus skeletal density indicated that a rise in temperature of 1 °C would increase the density rate by 10.5% (Bessat and Buiges, 2001).

Bessat and Buiges (2001) indicated that the growth characteristics of their *Porites lutea* samples were highly variable and suggested several modes of annual linear extension, density and calcification rate, which included short-term (seasonal and annual) environmental pulse events and decadal variability. The annual density of the core generally was characterised by long-term variations, while annual extension and annual calcification were characterised by higher frequency variations. These results are consistent with the results of Lough and Barnes (1997). Spectral analysis of the Bessat and Buiges (2001) record indicated a strong concentration of variance at the Quasi-Biennial (approximately 2.5 year), ENSO (approximately 4.7 year to 6.6 year) and decadal-scale (approximately 21.9 year) frequency bands. Climate variability in the Indian Ocean occurs over a range of timescales. Spectral analysis of instrumental records and El Niño–Southern

Oscillation indices revealed that the dominant variance occurs over a broad range of periods from 3 to 10 years (Barnett, 1991; Barnett and Latif, 1998). ENSO events that cause temperature variations tend to affect linear extension and consequently the calcification rate (Lough and Barnes, 1997; Bessat and Buiges, 2001).

### *2.3.1.3 Analysis*

During storage at the Marine Geoscience Unit since 1993, the core had broken into a number of pieces, which were carefully fitted together. The two oldest pieces did not show banding as clearly as the others and were left out of the study. Once the coral core had been pieced together, it was taken to the radiology department at Entabeni Hospital, Durban, South Africa, for a Computerised Tomography (CT) Scan, using a GE Lightspeed 16 Slice Scanner, working at 380 mA and 140 kV. The approximate time of each scan was 10 s. During a CT scan, a low-dose X-ray tube and detector rotate around a patient (in this case the coral) to produce data from multiple angles. To limit the Heel effect, which is the result of a non-uniformity of an X-ray beam across the diameter of the cone of radiation (Chalker *et al.*, 1985), each piece of coral was scanned individually to utilise the central beam area where intensity was uniform.

The scans clearly showed the banding of the core (Figure 2.2). The selected pieces covered 116 years, and climatological analysis was possible through a collection of length, density and calcification data along the growth axis of the core (Figure 2.2). When the pieces did not fit together exactly, due to a bad breakage, linear interpolation was used to provide missing values.

The scanning computer offered the option of calculating density at points along the core. The density of these points were highly correlated with the pixal values (calculated with the 'PIXVAL' MATLAB function) of the scanned image. The mathematical relationship between density and pixal values was calculated through linear least squares regression analysis, and pixal values along the core were then converted to density values. Average annual density was calculated as well as the density of each alternate dark and light band. The length of bands was measured accurately using the 'IMDIST' function, written in MATLAB specifically for this purpose (Appendix 1).

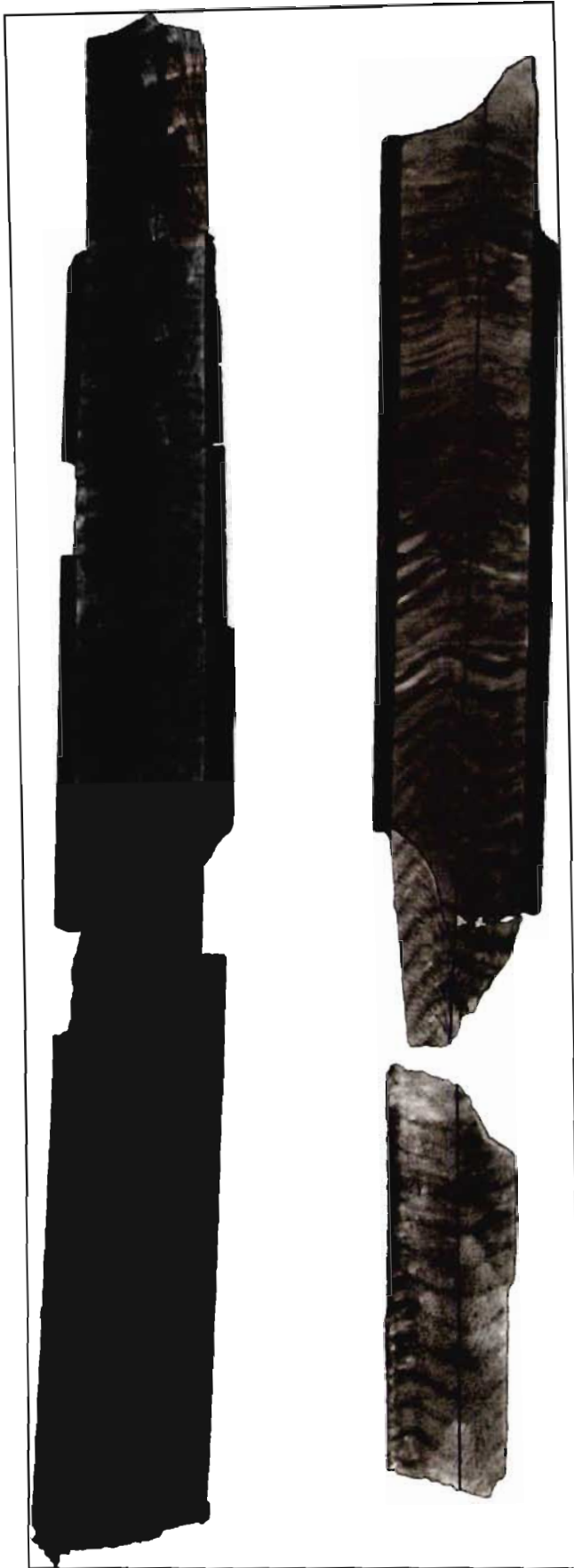


Figure 2.2 – Computerised Tomographical coral images showing axis of measurement.

The calcification rate was defined by Bessat and Buiges (2001) as the product of the linear extension rate and the average density at which the skeleton was deposited in making the extension. The calcification rate along the length of the core was calculated for further analysis. This record was then compared with recorded and modelled climatic datasets.

### 2.3.2 Stalagmite Data

Professor Karin Holmgren of Stockholm University provided the Makapansgat stalagmite data. Holmgren (such as Holmgren, 1996; Holmgren *et al.*, 1995; 1999; 2001; 2003) has played an important role in the collection and analysis of speleothems from southern African sites, such as Lobatse and Makapansgat, and in the climatic interpretation of speleothem isotopic data.

Holmgren *et al.* (2003) derived values of  $\delta^{18}\text{O}$  and  $\delta^{13}\text{C}$  with a time resolution of approximately 10 years over a period of 6600 years from stalagmite T7 from Cold Air Cave (24° 1' S 29° 11' E) in the Makapansgat valley (Holmgren *et al.*, 1999; 2001). Dating of the first 3500 years of the record was carried out with high-precision uranium-series thermal ionisation mass spectrometry (TIMS) and this forms part of the 6600 year series which is less securely dated by alpha spectrometry (Holmgren *et al.*, 2001). A 24 000 year record for this cave is also available from stalagmite T8, dated by  $^{230}\text{U}/^{234}\text{Th}$  methods (Holmgren *et al.*, 2003). After 10 000 BP, however, data resolution drops to a measurement about every 50 years. This study made use of the dataset with the 10 year resolution, extending to 10 000 BP, for the wavelet analyses described in Chapter 6, and the dataset extending to 6600 BP for the back-projections described in Chapter 4. For the purpose of accuracy, the dataset to 6600 BP was selected for the back-projections as this was the period of overlap for the T7 and T8 stalagmites, and thus a data comparison had been possible (Holmgren *et al.*, 2003). The wavelet analysis was used as a qualitative assessment of cyclicity and therefore it was deemed appropriate to make use of the less-secure dataset extending to 10 000 BP.

### 2.3.3 Pollen Data

The palynological data from the study of thermal spring sediments at Wonderkrater (24° 26' S 28° 45' E) was provided by Professor Louis Scott of the University of the Free State.

56 sediment layers, extending to 8 m depth, were dated and shown to cover a 20 000 year history (Scott *et al.*, 2003). Overall, 107 species were identified, although there were a small number of unknown species, and the relative abundance of each species type was recorded. To summarise the data, these 107 species were allocated to 1 of 13 groups named 'Forest and Forest edge', 'Mesic woodland', 'Woodland', 'Dry Woodland', 'Herbs', 'Asteraceae', 'Stoebe type', 'Fynbos', 'Chenopodiaceae and Amaranthaceae', 'Aquatics', 'Monolete fern spores', 'Cyperaceae' and 'Poaceae'.

#### 2.3.4 Recorded Data

Meteorological data for the regions of study were requested from the South African Weather Service (SAWS). Many of the datasets do not extend back further than 50 years. The Natal Sharks Board provided a record of sea surface temperatures at Richards Bay and this was strongly correlated with the modelled sea-surface temperatures for Sodwana Bay from the NOAA-CIRES (2000) dataset. NASA *et al.* (1995) also offer a dataset of modelled sea-surface temperatures from across the globe, and the values for Sodwana Bay were useful for comparison with the recorded dataset for Richards Bay and with the back-projections derived from the coral data.

##### 2.3.4.1 Southern Oscillation Index

There is no broadly accepted classification system indicating how much warming over exactly what region is required to meet the criteria of an 'El Niño' event. NIÑO3, which refers to the sea-surface temperature (SST) anomaly in the NIÑO3 region (90° W – 150° W, 5° S – 5° N) of the eastern equatorial Pacific, is commonly used as an index of El Niño (Cane, 2005). Alternatively, the Southern Oscillation Index (SOI), which is defined as the normalised pressure difference between Tahiti and Darwin, Australia, is also commonly applied. These two indices are well correlated.

The SOI was selected for this study due to the availability of the data and was calculated using the method presented by Ropelewski and Jones (1987). It uses a second normalisation step, and is the standard for the Climate Analysis Centre, National Centre for Atmospheric Research (NCAR) in the United States.



Table 2.1 shows the various recorded and modelled datasets used in the study.

**Table 2.1 – Recorded and modelled datasets used in this study**

PLACE	DATA TYPE	DATES	POSITION	USED FOR	SOURCE
Cape St Lucia	Daily rainfall	1950 - 2005	28° 30' S 32° 24' E	Sodwana Bay (27° 31' S 32° 41' E)	SAWS (2005)
Cape St Lucia	Daily maximum temperature	1960 - 2005	28° 30' S 32° 24' E	Sodwana Bay (27° 31' S 32° 41' E)	SAWS (2005)
Sodwana Bay	Monthly averaged sea-surface temperature	i) 1885 - 1995 ii) 1970 – 2000	27° 31' S 32° 41' E	Sodwana Bay (27° 31' S 32° 41' E)	i) NASA <i>et al.</i> (1995) ii) NOAA-Cires (2000)
Richard's Bay	Monthly averaged sea-surface temperature	1980 - 2003	28° 47' S 32° 06' E	Sodwana Bay (27° 31' S 32° 41' E)	Natal Sharks Board (2005)
Lake St Lucia	Monthly averaged salinity	1958 - 2000	28° 01' S 32° 29' E	Lake St Lucia (28° 01' S 32° 29' E)	KZN Wildlife (2005)
Darwin and Tahiti	Southern Oscillation Index (normalised pressure difference between Tahiti and Darwin, Australia)	1866 - 2004	Darwin: 12° 28' S 130° 51' E  Tahiti: 17° 32' S 149° 34' W	Sodwana Bay (27° 31' S 32° 41' E)	NCAR (2005)
Makopane	Daily rainfall	1930 - 2005	24° 16' S 29° 00' E	Makapansgat (24° 01' S 29° 11' E)	SAWS (2005)
Makopane	Daily maximum temperature	1930 - 2005	24° 16' S 29° 00' E	Makapansgat (24° 01' S 29° 11' E)	SAWS (2005)
Vryheid	Daily rainfall	1925 - 2005	27° 47' S 30° 48' E	Vryheid (27° 47' S 30° 48' E)	SAWS (2005)

## 2.4 SUMMARY

It is obvious that a number of potential data sources exist for the development of palaeoclimatic records, including glaciological, geological, biological and historical sources. No data source is ideal, and specific sources prove to be more viable and accurate in certain regions. The selection of a data source usually depends on whether the source type is present in the region of study, and on the availability of funds, time, equipment and expertise. This study will involve the use of two extensive, high-resolution datasets, namely the stalagmite isotope dataset from Makapansgat, provided by Professor Holmgren of Stockholm University, and pollen abundance data for Wonderkrater, provided by Professor Louis Scott of the University of the Free State. An original proxy record, derived from a *Porites lutea* coral head from Sodwana Bay, extending back 116 years from the present, will be used to indicate short-term climatic fluctuations over the last century. For comparison with these datasets, a number of recorded and modelled climatic datasets will be utilised, but these generally do not extend beyond 1950.

### **3. SOUTHERN AFRICAN PALAEOCLIMATES: A REVIEW**

#### **3.1 INTRODUCTION**

In palaeoclimatic records from the polar and temperate latitudes there is clear evidence that ice sheets and glaciers expanded and contracted repeatedly during the Quaternary period. Most of these events have been researched and documented extensively, which has provided detailed palaeoclimatic sequences for many parts of the northern hemisphere – particularly for North America and Europe (Dawson, 1992). Uncertainty exists over much of the rest of the globe, particularly in the largely unglaciated parts of the subtropics and tropics where the geomorphological impacts of climate change are less distinct (Meadows, 2001). Unlike South America (Clapperton, 1993), glaciation did not occur over semi-arid southern Africa during the Quaternary, and rainfall variations have had a greater influence on the landscape than temperature (Meadows, 1988). Although palaeoclimatic evidence in the southern Africa region is more limited than in many other regions, a number of reliable, continuous, high-resolution datasets have been collected from various sources, including isotopic data from stalagmites, pollen data from sediments, and growth data from tree-ring studies.

Selected investigations of Quaternary climate changes in southern Africa will be presented in this chapter. Southern Africa is defined as the area of the African continent south of approximately 17° S and comprising the territories of Angola, Botswana, Lesotho, Mozambique, Namibia, South Africa, Swaziland and Zimbabwe (Meadows, 2001). Although this study focuses on case studies from South Africa, and one located on the Botswanan border with South Africa, reference will be made to conditions across the southern African region. This region comprises a varied but coherent set of geographical and climatic characteristics (Meadows, 2001) and the climatic changes inferred from palaeoclimatic records from specific sites in South Africa give an indication of conditions at other sites in the region. The nature of the relationship between sites will be presented and discussed.

### 3.2 CASE STUDIES

Very little is known of southern African palaeoclimates prior to the start of the Quaternary, approximately 2 million years ago. Glacial periods occurred during the pre-Phanerozoic at around 2000 million BP and 600 million BP (Frakes, 1979) but their causes remain unclear (Lindesay, 1990). Permo-Carboniferous glacial evidence from southern Africa suggests that Gondwanaland lay over the pole at approximately 320 million BP (Tyson, 1986). During the Jurassic, beginning around 180 million BP, intense volcanic activity occurred in the region and temperatures would have been lowered by increased atmospheric turbidity over extended periods (Tyson, 1986). During the Cretaceous, beginning approximately 120 million BP, the break-up of Gondwanaland commenced, and southern African climates varied with the changing position of the subcontinent, the formation of the proto-Atlantic and proto-Indian oceans, and the initiation of Antarctic ice formation (Lindesay, 1990).

Towards the end of the Miocene, commencing at around 25 million BP, precursors of the Agulhas and Benguela current systems were in existence around southern Africa, which was then roughly in its present latitudinal position (Shannon, 1985). During the Tertiary period, tectonic uplift of approximately 500 m at 50 million BP, and of approximately 700 m at 2.5 million BP occurred as a result of global tectonic and orogenic activity (Lindesay, 1990). Temperature decreases associated with increases in subcontinental elevation were probably greater than those experienced during glacial cooling (Partridge, 1985).

There is substantially more information on the climates of southern Africa for the Late Quaternary period (Deacon and Lancaster, 1988) compared to the periods preceding it. From a temperature maximum at 125 000 BP to a temperature minimum at the Last Glacial Maximum, a series of rapid warmings followed by slow variable declines to progressively lower minima occurred at high latitudes in the southern hemisphere (Tyson, 1999b). A deuterium isotope record (Figure 3.1) from the Vostok ice core, Antarctica (Jouzel *et al.*, 1987) provides a temperature index, indicating the successive lowering of temperature maxima and minima until the Last Glacial Maximum was reached in this region at approximately 20 000 BP.

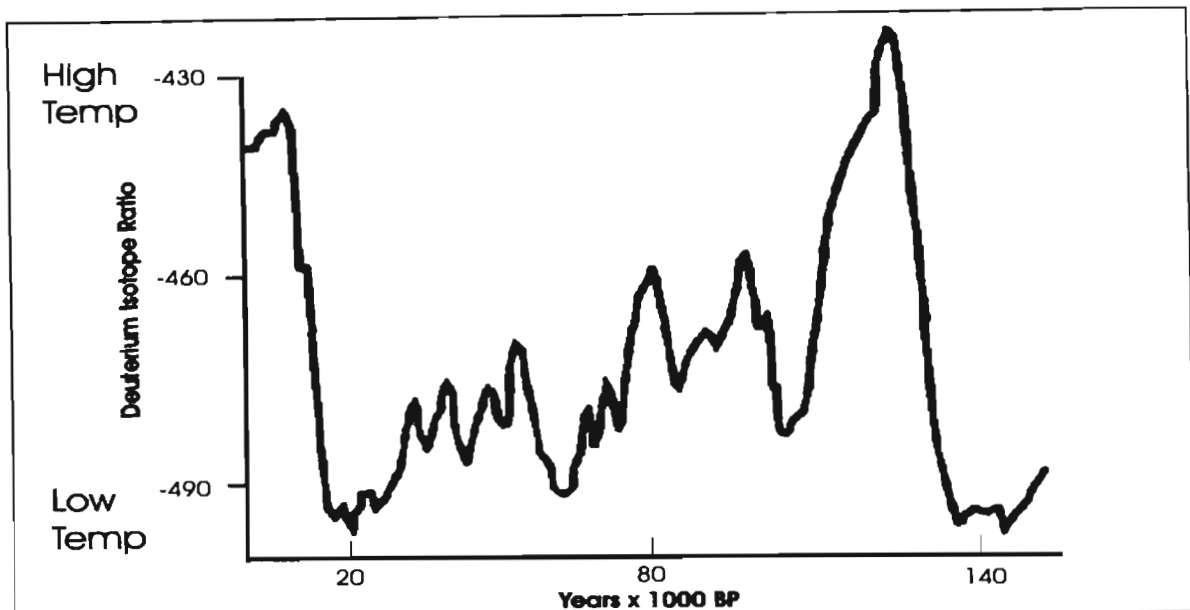


Figure 3.1 – Deuterium Isotope Index of the Vostok Ice core (Jouzel *et al.*, 1987 in Tyson, 1999b, 339).

Since there is little reliably dated palaeoclimatic data available for the period prior to 40 000 BP, this study focuses on the last 40 000 years of palaeoclimatic history, with particular focus on the last 20 000 years during which the two important palaeoclimatic episodes referred to as the Last Glacial Maximum (LGM) and the Holocene Maximum or Altithermal occurred (Partridge *et al.*, 1990). The following case studies were selected because they are semi-continuous, securely dated, well-documented analyses carried out for a range of timescales. They are arranged in ascending order according to the length of the record, which was determined by how far back features were confidently dated. All dates are given in years AD, calendar years BP (before 1950 or 2000 AD as indicated) or in radiocarbon years BP (uncalibrated radiocarbon years before 1950 AD). This will be specified for each study.

The case studies include tree-ring studies dating back to 700 BP, the Verlorenvlei sediment and palynological studies dating back to the Last Glacial Maximum at approximately 18 000 BP, Wonderkrater palynological studies dating back to 20 000 BP, Makapansgat stalagmite studies dating back to 24 400 BP, the Congo II Cave stalagmite study dating back to 47 000 BP, Border Cave sediment and micromammalian studies dating back to 49 000 BP, Lobatse Cave speleothem studies dating back to 50 000 BP, the Boomplaas micromammalian study dating back to 80 000 BP and the sediment and palynological studies at Tswaing Crater with evidence dating to beyond 200 000 BP. The main study sites are shown in the Figure 3.2.

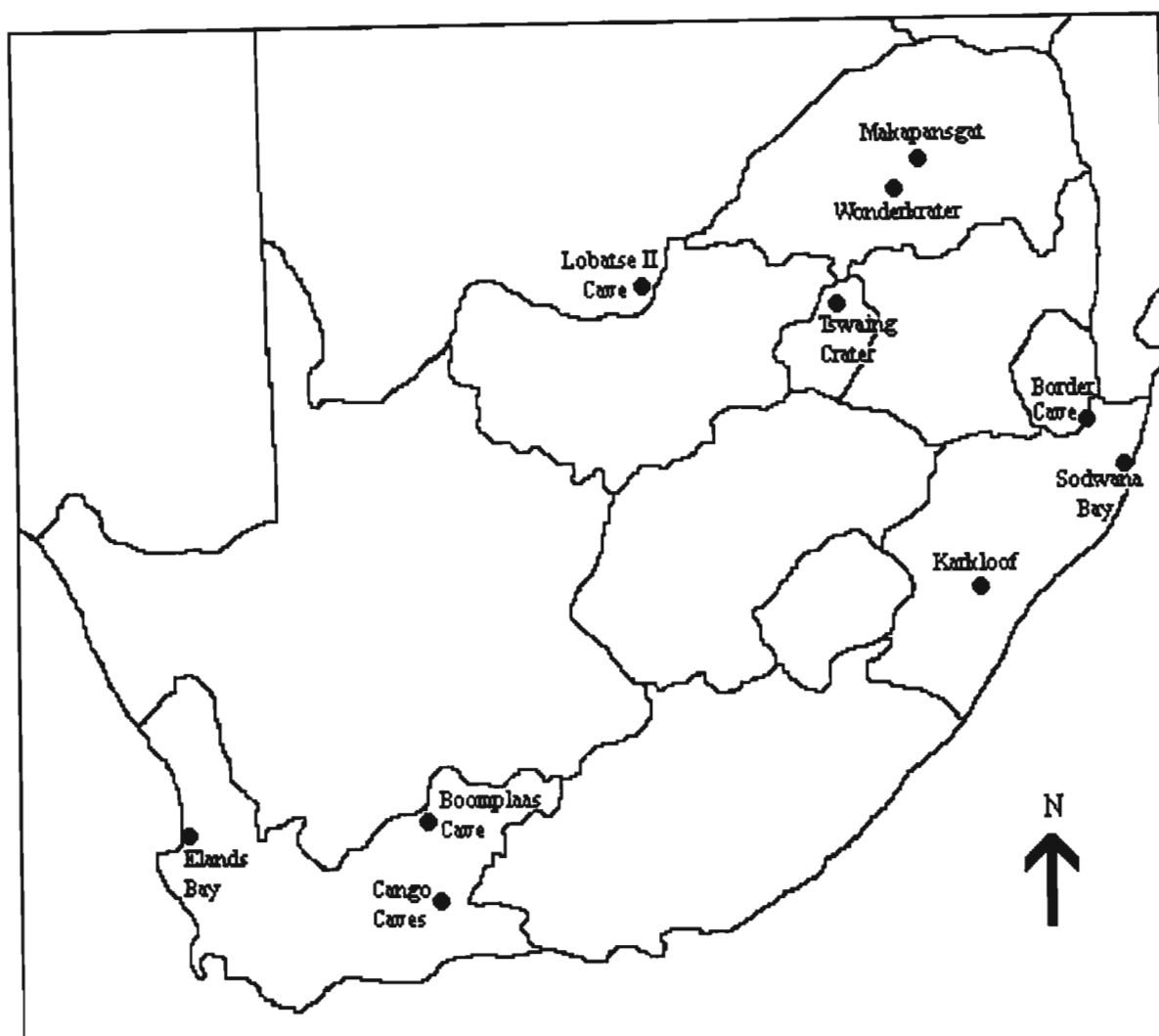


Figure 3.2 – Map indicating main study sites.

### 3.2.1 Tree-ring Studies

Few dendrochronological investigations have been conducted in southern Africa because of the apparent scarcity of trees adequately long-lived to provide information on the prehistoric environment, and the lack of information on the suitability of the indigenous arboreal flora for dendroclimatological work. Although tree-ring data from South Africa are limited, those available have been used successfully to support observations in palynological or isotope records.

Before Hall (1976) published the results of his dendrochronological study, archaeologists working in southern Africa had mostly circumstantial evidence for climate changes in the post-Pleistocene period, and had been forced either to rely on extrapolation or to assume

general climatic stability for the Holocene. Hall (1976) worked on a large specimen of indigenous yellowwood (*Podocarpus falcatus*) which had been felled in 1976 in the Karkloof forest, 25 km north-east of Howick, KwaZulu-Natal (29° 24' S 30° 12' E). The tree grew in the upper catchment area of a tributary of the Mpolweni River. Annual growth rings of trees located in this type of environment are more likely to reflect climate change than specimens from the bottom of valleys, where continuously high water tables desensitise growth patterns (Hall, 1976).

Initial analysis showed that the specimen had 597 growth rings, and since there was variability in annual growth, the specimen exhibited the basic dendroclimatological principle of sensitivity (Hall, 1976). Each ring was considered to represent summer wet seasonal growth (low density tissue) followed by winter dry seasonal growth (high density tissue). As such, growth commenced in this specimen at around 1300 AD (Hall, 1976).

Biological processes cannot occur faster than supported by the most limiting factor (Liebig, 1840), and Hall (1976) suggested that this is likely to be precipitation as the climate of the Karkloof is characterised by pronounced rainfall seasonality without much frost or low temperature (Phillips, 1973). Thus the variations in growth increments in the *Podocarpus falcatus* specimen were taken as an index of precipitation fluctuations over the last six hundred years. The data extending back to 1320 was plotted by Hall (1976) and is shown below in Figure 3.3.

The growth record indicates peaks (and therefore rainfall peaks) at approximately 1497, 1590, 1790, 1817, 1825 and 1857 AD. The growth values have increased over the course of the record with a growth peak in approximately 1497 of less than 2.5 mm per annum while the growth peaks of the 1800s and 1900s reached over 3 mm per annum. Rainfall variability appears to have increased substantially between the 1300s and 1800s.

Gillooly (1975) studied the growth patterns of a number of trees in the Rustenberg area (25° 38' S 27° 11' E) of the former Transvaal (now Gauteng), and found a strong correlation with annual rainfall over the previous 60 years. Furthermore, the years of exceptionally low tree growth in the nineteenth century, which occur at around 1800, in the early 1820s, in the late 1840s and in the early 1860s, were co-incident with severe famines

recalled by interviewees (Bryant, 1929; Webb and Wright, 1976). It would be reasonable to assume that a major cause of the famines was low rainfall (Bryant, 1929).

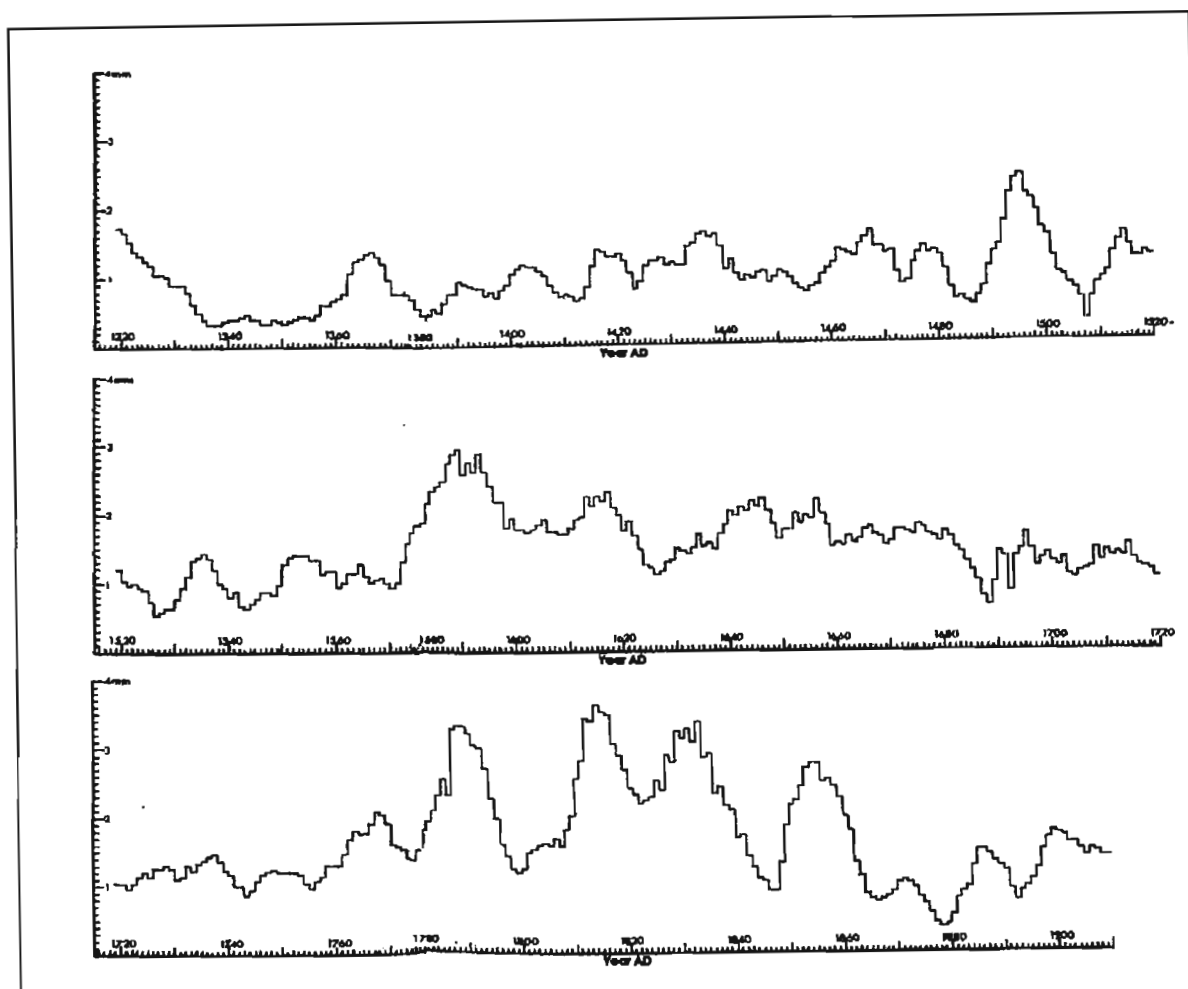


Figure 3.3 – Tree-ring record from Hall (1976, 699) with annual growth increments in millimetres.

Tree-ring data series from around the country show corresponding fluctuations but the nature of the correlation between sites depends on the location. For example, increased growth rates from 1550 to 1600 AD and from 1800 to 1850 AD in the *Podocarpus falcatus* tree from KwaZulu-Natal (Hall, 1976) correspond well with a *Podocarpus falcatus* record for Knysna (34° 05' S 23° 03' E) (Thackeray, 1996; Thackeray and Potze, 2000), but these data are out of phase with a *Widdringtonia cedarbergensis* tree-ring record (Dunwiddie and LaMarche, 1980) for Cedarberg (32° 25' S 19° 12' E), in the winter rainfall region of the Western Cape. The reasons for this correlation are linked to the north-south atmospheric shifts proposed by Tyson (1986) and are outlined in Section 3.4.1 on Page 61, and discussed extensively in Chapter 5.



### 3.2.2 Verlorenvlei

The coastal fishing settlement of Elands Bay (32° 19' S 18° 09' E) is situated in a small marine embayment, 180 km north of Cape Town. The area around Elands Bay is unique due to the presence of an aquatic ecosystem, comprising a river, swamp and semi-estuarine coastal lake, which provide valuable freshwater resources to the otherwise marginal, coastal landscape. This wetland system is collectively referred to as the 'Verlorenvlei' (Meadows, 2001).

The Verlorenvlei lies within the Sandveld biome of the West Coast and the geology of the region consists of Palaeozoic rocks, Malmesbury shales and sandstones, overlain by Tertiary and recent unconsolidated sands (Meadows, 2001). The area has a semi-arid climate, receiving a distinctly winter rainfall with precipitation of less than 300 mm per annum (Sinclair *et al.*, 1986). The plant communities have acquired a variety of survival features, such as succulence and spinescence (Sinclair *et al.*, 1986).

A series of cores was extracted from the Verlorenvlei using a variety of coring techniques (Baxter and Meadows, 1999). The cores were subjected to a range of physical, chemical and biological studies, including analyses of particle size, geochemistry, stable isotope content, and shell, charcoal and pollen analyses. A detailed Quaternary palaeoenvironmental history was developed from the evidence. The sediment cores were compared with cores from cave and open archaeological sites within a radius of approximately 20 km (Baxter, 1997). Many of the cores were dated by conventional radiocarbon methods while others were chronologically correlated using appropriate stratigraphic and biological indicators (Baxter and Meadows, 1999). Dates are given in uncalibrated radiocarbon years BP (before 1950 AD).

The Verlorenvlei area has experienced a complex sequence of events over the last 40 000 years in response to variable environmental inputs, including temperature and rainfall fluctuations, sea-level change and human activity. A palynological study indicated vegetation changed in response to fluctuating precipitation, and at the Last Glacial Maximum (at around 18 000 BP), Baxter (1997) suggests that significantly higher rainfall was experienced, and scrub forest, which is at present a restricted community in the area, was a dominant element. The changes in vegetation over time, as proposed by Baxter

(1997) and discussed in Meadows (2001), are presented in Figure 3.4 and this record gives an indication of rainfall changes in the region.

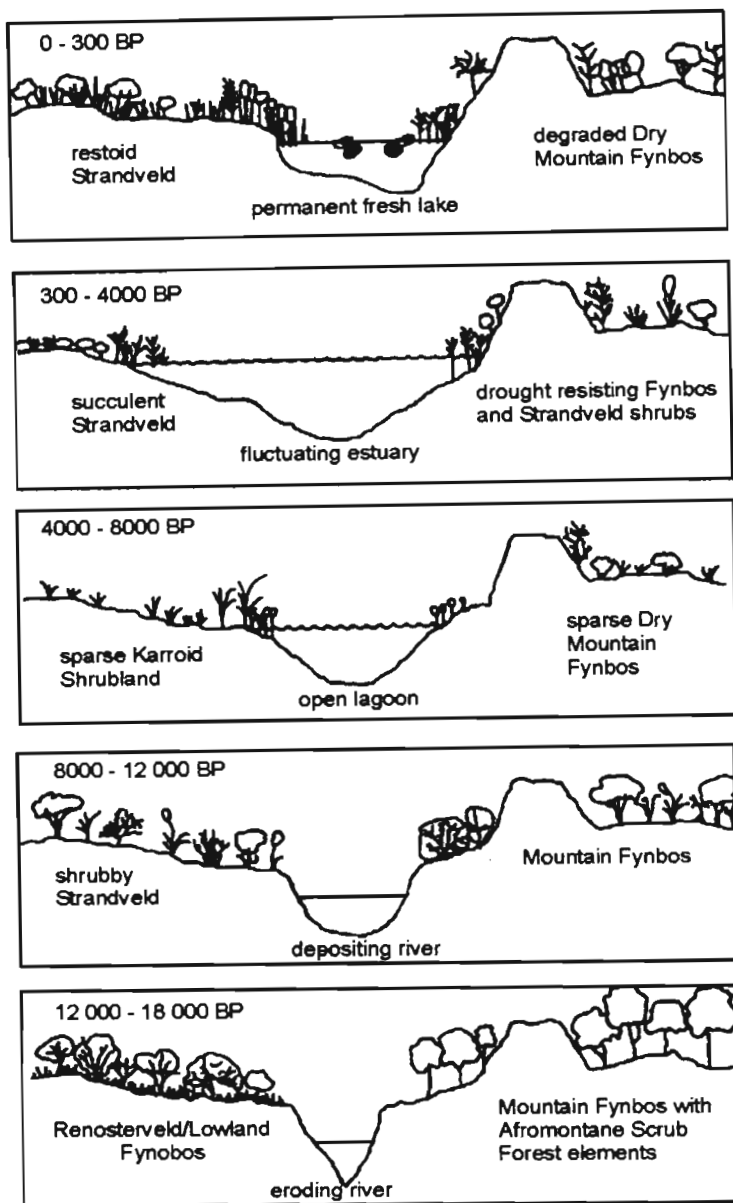


Figure 3.4 - Summary of Quaternary vegetation changes at Verlorenvlei (Baxter, 1997 In Meadows, 2001, 49).

It is apparent that rainfall decreased progressively from the Last Glacial Maximum and by approximately 8000 BP, sparse Karroid Shrubland was the dominant vegetation type along the lagoon, while sparse, dry mountain Fynbos dominated the higher areas. By 4000 BP, succulents had developed around the fluctuating estuary, and drought resistant Fynbos and Strandveld shrubs had developed in the higher regions, suggesting a further decrease in rainfall. Rainfall then increased from about 300 BP when restoid Strandveld replaced the succulents around a then permanent fresh lake.

However, rainfall was not the exclusive control on vegetation, and the study revealed that sea-level change had the greatest influence on pollen spectra of the Verlorenvlei sites, particularly during the Holocene. Baxter and Meadows (1999) provided a detailed summary of Holocene sea-level change from the evidence gathered in the sediment and pollen studies. They suggest that by 8500 BP, sea-levels had reached the lower Verlorenvlei valley and until about 7200 BP, the system formed a sheltered lagoon. After approximately 7200 BP, evidence indicates that the system returned to a more dynamic estuarine-riverine environment and there is the possibility of strong tidal or even wave action in the lower reaches. By 6500 BP, the sea had receded, causing significant changes in the sedimentary characteristics and density of fossil organisms. After a phase of aeolian deposition, sea-levels commenced rapid advancement, and by 6000 BP estuarine conditions had returned to Verlorenvlei (Baxter and Meadows, 1999).

Sediments indicate that the rising sea-level from 5500 BP onwards extended the influence of marine conditions beyond the Grootdrift coring sites. By 4340 BP, the Verlorenvlei sediments were texturally similar to those of the earlier lagoonal phases and this is followed by the termination (or later removal) of sediment accumulation in the upper reaches of the study site. Proxy archaeological evidence suggests that the hiatus is due to substantial sea-level regression, probably to below present levels, and the sediments would have been eroded by the regressing sea and fluvial rejuvenation. There was a minor sea-level increase at 1500 BP (Baxter and Meadows, 1999).

Baxter and Meadows (1999) summarised their findings in a revised sea-level curve for the west coast of southern Africa as presented in Figure 3.5. The curve is compared with those of Jerardino (1995) and Miller *et al.* (1993). There is a correlation between the Baxter and Meadows (1999) and the Miller *et al.* (1993) curves but major changes in sea-level appear to commence a couple of hundreds of years earlier in the Miller *et al.* (1993) curve. The Baxter and Meadows (1999) and Jerardino (1995) curves show a general increase in sea-level from the Early Holocene until after 4000 BP, followed by a general decrease in sea-level until the present.

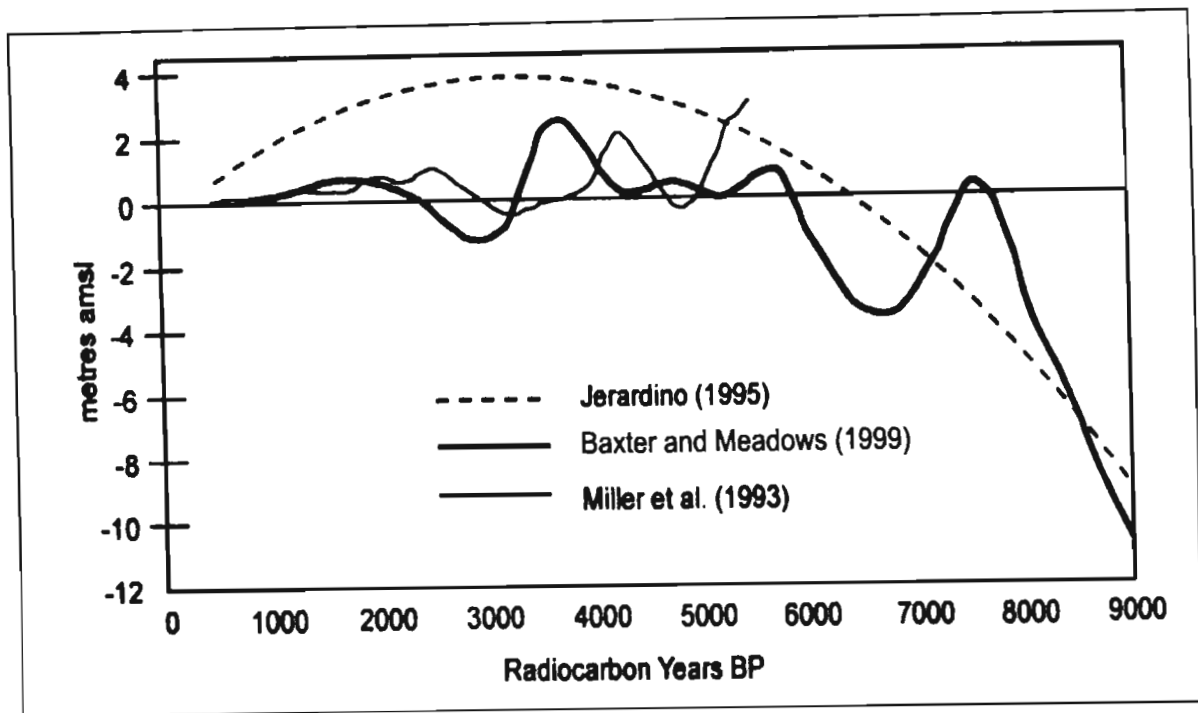


Figure 3.5 - Holocene sea-level curves from Jerardino (1995), Miller *et al.* (1993) and Baxter and Meadows (1999) (Baxter and Meadows, 2001, 77).

Other than an interpretation of sea-level and rainfall from Verlorenvlei data, temperature deductions were made and these were compared with other records for the region. For example, Cohen *et al.* (1992) proposed that sea surface temperatures along the west coast of South Africa rose from 10.5 to 13.5 °C between 10 000 and 8000 BP. The authors were unsure whether this was caused by enhanced retroflexion of warm Agulhas waters into the South Atlantic and Benguela system, or a decrease in cold upwelling off the west coast. The latter explanation is supported by the terminal Pleistocene pollen data from Elands Bay Cave (Baxter, 1997), which suggest warmer temperatures at that time (Baxter and Meadows, 1999).

It is difficult to isolate regional climate changes from a specific locality's evidence, but inferences can be made if they are supported by other sources of evidence for the region. From the Verlorenvlei case study, and other supporting evidence from the Western Cape, it can be concluded that Quaternary environments in the region were highly dynamic. Of interest is the similarity between the sea-level curve presented in Baxter and Meadows (1999), shown in Figure 3.5, and the temperature curves for other regions of southern Africa. This exemplifies the close link between ocean and atmosphere and shows that sea-level curves can be indicative of conditions on a regional, and perhaps even global, scale.

Another point of interest is the apparent contrast between rainfall conditions during the Last Glacial Maximum at Verlorenvlei, and over southern African as a whole. Evidence for the summer rainfall areas of southern Africa indicates a substantially drier Last Glacial Maximum while palynological evidence for Verlorenvlei suggests it was significantly wetter at this time. It is obvious that a distinction exists between the rainfall fluctuations of the summer and winter rainfall regions of southern Africa and this must be kept in mind during the development of a general palaeorainfall model. The reasons for this regional contrast will be examined in Chapter 5.

### 3.2.3 Wonderkrater

An analysis of the pollen in thermal spring sediments from Wonderkrater (24° 26' S 28° 45' E) gave new insight into environmental fluctuations during the Late Quaternary in the Mixed Bushveld (Low and Rebelo, 1996) region of the Savanna biome (Rutherford, 1997). This is an area believed to offer few sources of palaeoclimatic information (Scott *et al.*, 2003) and the Wonderkrater pollen data provided the first substantial record of local vegetation change (Scott, 1982a; 1982b).

Several boreholes were drilled at the site, and boreholes 3 and 4 (B3 and B4), at depths of 1.85 m and 8.05 m respectively, provided partially overlapping sequences (Scott *et al.*, 2003). B4 indicated a 30 cm sand layer at around 4.35 m depth (Figure 3.6). Below this layer, the section proved difficult to date but montane forest pollen was present and it is clear that *Podocarpus* trees existed around the spring during its early history. *Podocarpus* was later replaced by indicators of dry woodland (Scott *et al.*, 2003).

B3 provides an ostensibly continuous record of the last 14 000 years from above the base of sand at about 4.85 m. The one metre layer of peat below the sand contains pollen from the end of the Last Glacial Maximum with the upland fynbos elements Ericaceae, *Cliffortia* and *Passerina* signifying a vegetation depression of at least 1000 m and a temperature depression of 5 - 6 °C (Scott, 1982a). This vegetation was steadily replaced by varieties of the contemporary tropical savanna, with Combretaceae and associated woody species. Evidence of Chendopodiaceae and Amaranthaceae towards the end of Pleistocene times and arid woodland in the Early Holocene suggests a period of strong evaporative conditions (Scott *et al.*, 2003).

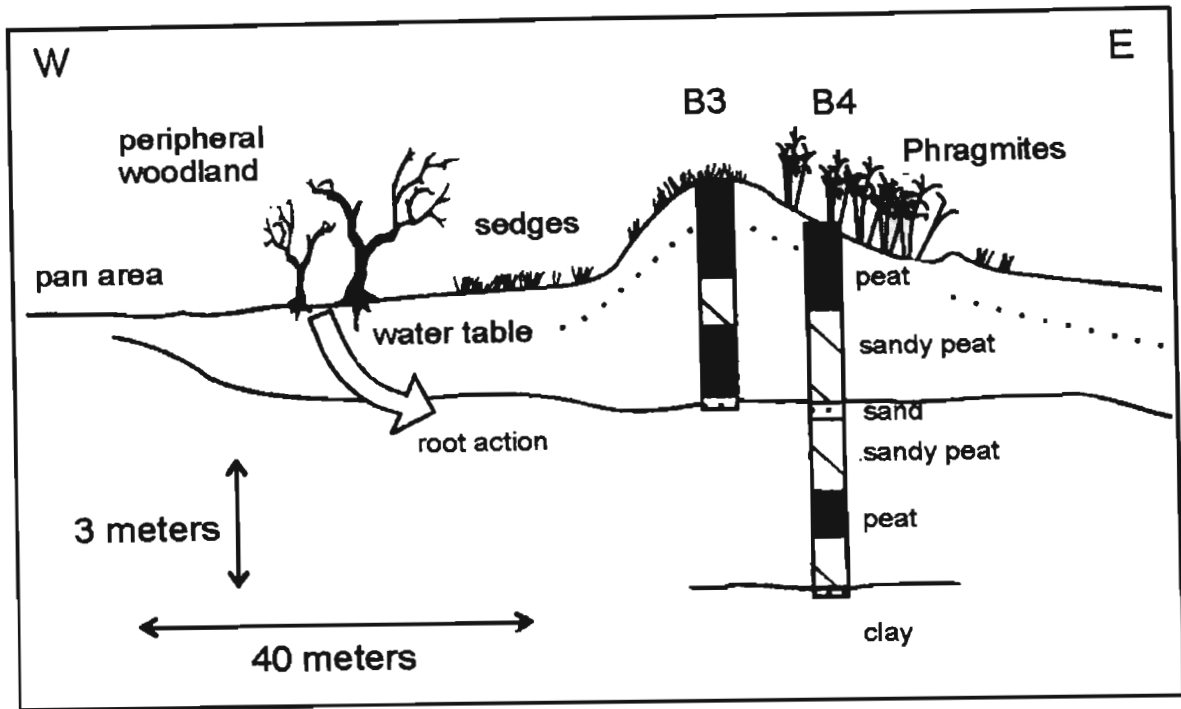


Figure 3.6 – Wonderkrater boreholes 3 and 4 (Scott *et al.*, 2003, 484).

Exploratory boreholes 1 and 2 (B1 and B2) were cored in 1971 by Van Zinderen Bakker (Scott *et al.*, 2003) but their exact location cannot be identified and therefore their stratigraphic relation with B3 and B4 is unknown. Their pollen contents and radiocarbon dates were, however, relevant to the assessment of the age of the peat deposits because they show that a distinct peat pollen zone, evident in B4, has an uncalibrated age of 24 300 years (Scott *et al.*, 2003).

Principal components analysis (PCA) was used to ordinate the Wonderkrater pollen data and the results provided Late Quaternary temperature and moisture indices (Figure 3.7) for the region (Scott and Thackeray, 1987; Scott, 1999; Scott *et al.*, 2003). Linking the patterns found within this pollen record with local and global events has proved problematic due to a low dating resolution. To solve this problem, a comparison was made with the stalagmite sequences of the nearby Makapansgat Valley (24° 1' S 29° 11' E), which has a higher resolution and had been securely dated by uranium series dating techniques (Holmgren *et al.*, 2003). The climatic variability and vegetation changes revealed by the stalagmite record can be assumed to be evident in the Wonderkrater pollen sequence. On the basis of anomalies and similarities between the two data sets, local and regional environmental changes could be explored (Scott *et al.*, 2003). All dates are provided in calendar years BP (before 2000 AD).

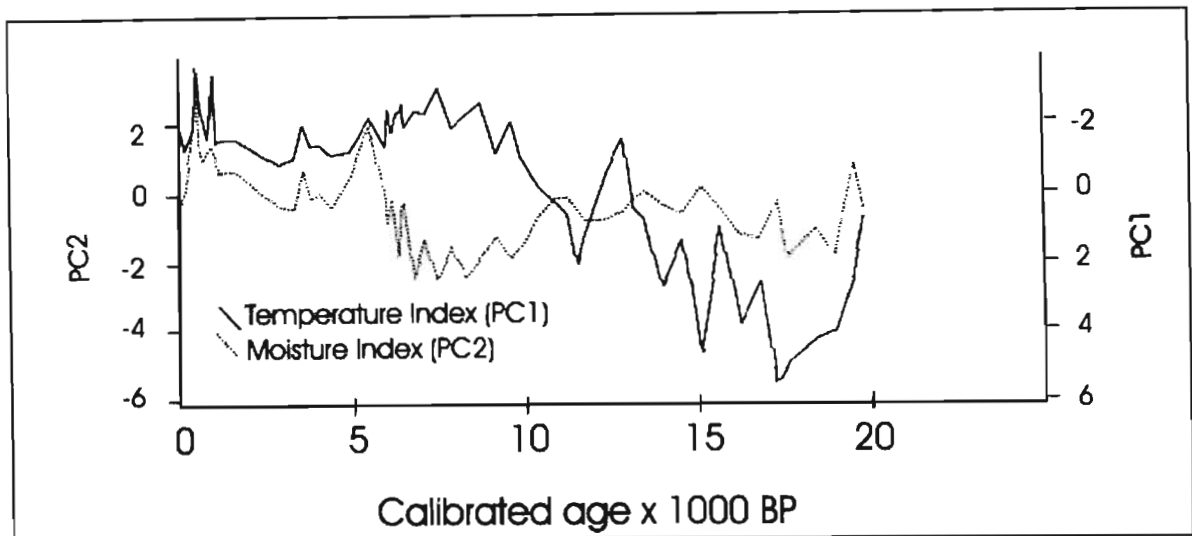


Figure 3.7 – Temperature and moisture indices for Wonderkrater (Scott *et al.*, 2003, 487).

The Wonderkrater sequence indicates a temperature minimum at approximately 17 200 BP and increasing temperatures are indicated until 13 000 BP. Subsequently slightly cooler but evaporative conditions with Chenopodiaceae and Amaranthaceae occurred until about 11 000 BP. At 8500 BP, there is an increase in grass pollen at Wonderkrater but the dryness index, which is independent of Poaceae, indicates that desiccation continued and grew stronger. The replacement of swampy Cyperaceae with grass pollen at around 8500 BP implies that the spring was shrinking, resulting in a spread of dry grass into the area (Scott *et al.*, 2003). The pollen data shows a relatively open savanna with Kalahari trees, shrubs and dry grassland similar to the present vegetation of the Kalahari thornveld (Scott *et al.*, 2003).

Warmer temperatures are indicated for Wonderkrater from 11 000 to 6000 BP. Cooling is apparent after 6000 BP such that temperatures reached their lowest values for the Holocene by about 3000 BP, with moderate dryness indicated for this time. The presence of fern spores in the record for this period suggests that the swamp appeared bracken-like. A significant increase in Asteraceae occurred from about 3000 to 2000 BP, and a high grass pollen count supports the inference from the Makapansgat isotope record of a cool, grassy environment for this period. Asteraceae pollen, which does not form part of the temperature index, was related independently to slightly cooler conditions between 3000 and 2000 BP in an analysis of the distribution of modern taxa in the region (Scott, 1982a). The  $\delta^{13}\text{C}$  enrichment between 3000 and 2000 BP in both the Makapansgat T8 and T7

stalagmites indicates strong grass growth (C4 species), and weak tree and small shrub growth (C3 species) (Holmgren *et al.*, 1999; Holmgren *et al.*, 2003). This appears to clash with the strong Asteraceae presence at Wonderkrater. If it is assumed that the Asteraceae spread was regional, affecting also the Makapansgat region, then other C3 plants such as trees must have decreased in favour of grass to maintain the high  $\delta^{13}\text{C}$  values of the stalagmite. The Wonderkrater pollen sequence supports such a scenario as there are low arboreal pollen percentages for this period (Scott *et al.*, 2003). The data resolution between 3000 and 2000 BP is low due to rapid sedimentation, and samples need to be reanalysed at smaller depth intervals (Scott *et al.*, 2003) to improve the quality of the record. Strong oscillations in temperature and moisture conditions have occurred over the last 1000 years as indicated by variations in pollen type (Scott *et al.*, 2003).

A comparison of the Wonderkrater record with the Vostok deuterium isotope index (Jouzel *et al.*, 1987) showed close parallels, which confirmed that the interpretation of the first principal component as a temperature index was valid. However, the major warming events occurred approximately 1000 years earlier in the Vostok record, as shown in Figure 3.8. The reasons for these lags will be examined in Chapter 5.

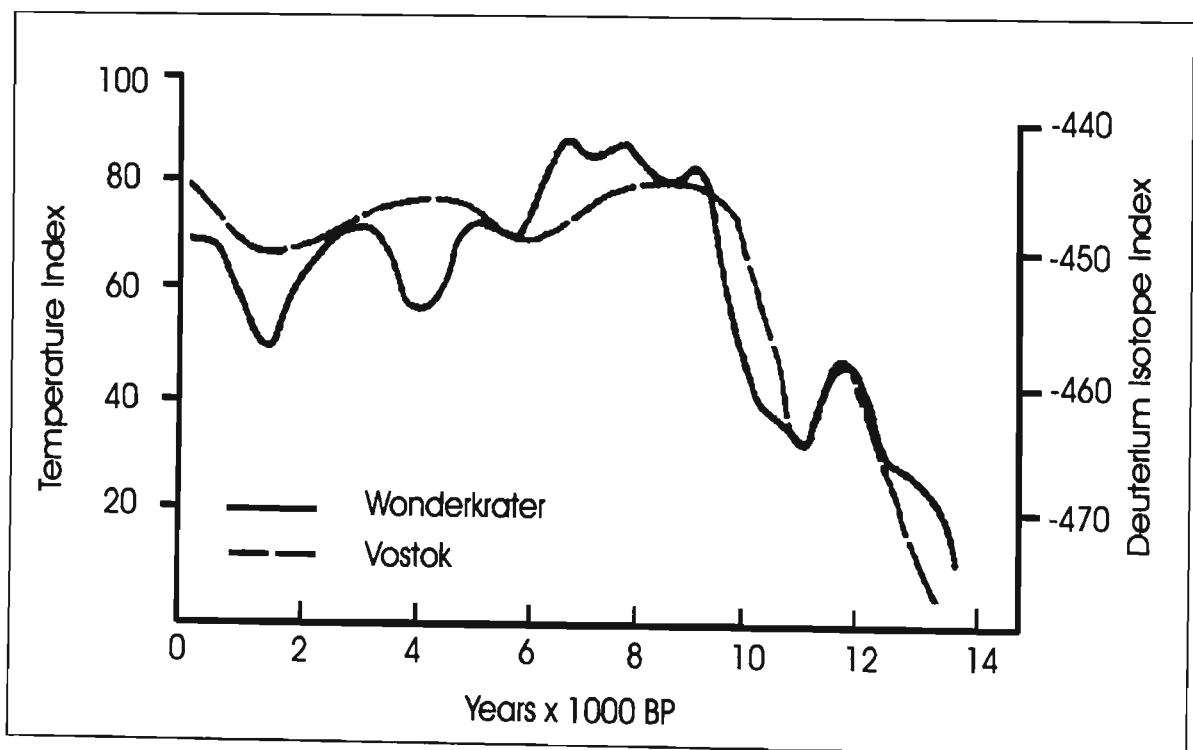


Figure 3.8 – Comparison of Wonderkrater temperature index and Vostok deuterium isotope ratio records (Tyson, 1999b, 339).



### 3.2.4 Cold Air Cave

Holmgren *et al.* (2003) established a high-resolution palaeoclimatic record through stable isotope analysis of stalagmites from Cold Air Cave in the Makapansgat Valley (24° 01' S 29° 11' E) in the north-eastern interior of South Africa, approximately 30 km south of Polokwane at an altitude of about 1500 m above sea-level (Finch *et al.*, 2003). Cold Air Cave is one of a series of caves located in the lower Precambrian dolomitic karst system of the Malmani Subgroup, Transvaal Supergroup (Holmgren *et al.*, 2003). The Makapansgat Valley is in the summer rainfall region of southern Africa and vegetation in the area consists of North-Eastern Mountain Sourveld to Sourish Mixed Bushveld (Acocks, 1953) or Mixed Savanna (Scholes, 1997).

The cave has a distal distance greater than 100 m and the entrance to the cave is approximately 0.7 m in diameter, resulting in poor ventilation and a high relative humidity (Finch *et al.*, 2003). The sampled stalagmites were located roughly 100 m from the entrance and at a distance of 10 m from each other, each beneath a separate fissure in the roof of the cave. The fissures act as conduits from a surface catchment above the cave to the speleothems below (Holmgren *et al.*, 2003).

High precision, uranium-series thermal ionisation mass-spectrometry (TIMS) was used to date the last 3500 calendar years (before 2000 AD) of  $\delta^{18}\text{O}$  and  $\delta^{13}\text{C}$  deposition at a resolution of approximately 10 years, which forms part of a 6600 year record dated by alpha-spectrometry (Holmgren *et al.*, 1999). In order to confirm the results from one continuous (T7) and one semi-continuous specimen (T5), a third stalagmite (T8), was later collected and studied. T8 has provided a high resolution record back to 24 400 BP (Holmgren *et al.*, 2003) through  $^{230}\text{U}/^{234}\text{Th}$  dating and close sampling for isotope analysis.

A comparison of the colour density of the stalagmite's grey and brown banding with tree-ring widths revealed that the growth layers were annual (Holmgren *et al.*, 2003). Growth-layer widths and rainfall were positively correlated, as were colour and temperature (Svanared, 1998). Colour levels on the stalagmite were controlled by changes in the vegetation above the cave. During warm, wet spells, plant growth rates increased, particularly of grasses, and increased infiltration and mobilisation of organic matter from the soil caused deeper colouring of the stalagmite (Holmgren *et al.*, 1999). Increasing

values of  $\delta^{18}\text{O}$  and  $\delta^{13}\text{C}$  represent warmer, wetter conditions and decreasing values represent cooler, drier conditions (Holmgren *et al.*, 2003). The  $\delta^{13}\text{C}$  record corresponds to changes in vegetation cover such that fluctuations can be interpreted as changes in the relative amounts of C4 grasses over time (Holmgren *et al.*, 1999). Higher values suggest periods of a greater abundance of C4 grasses and warmer and wetter summer conditions, while more arid conditions are associated with diminished grass cover and lower C4 values (Holmgren *et al.*, 1999).

Due to the close proximity of the Wonderkrater site to Makapansgat, the Wonderkrater temperature and moisture indices, derived from principal component analysis of the pollen abundance data, were compared with the Makapansgat  $\delta^{18}\text{O}$  and  $\delta^{13}\text{C}$  records, which provide temperature and moisture indices respectively for the region (Figure 3.9).

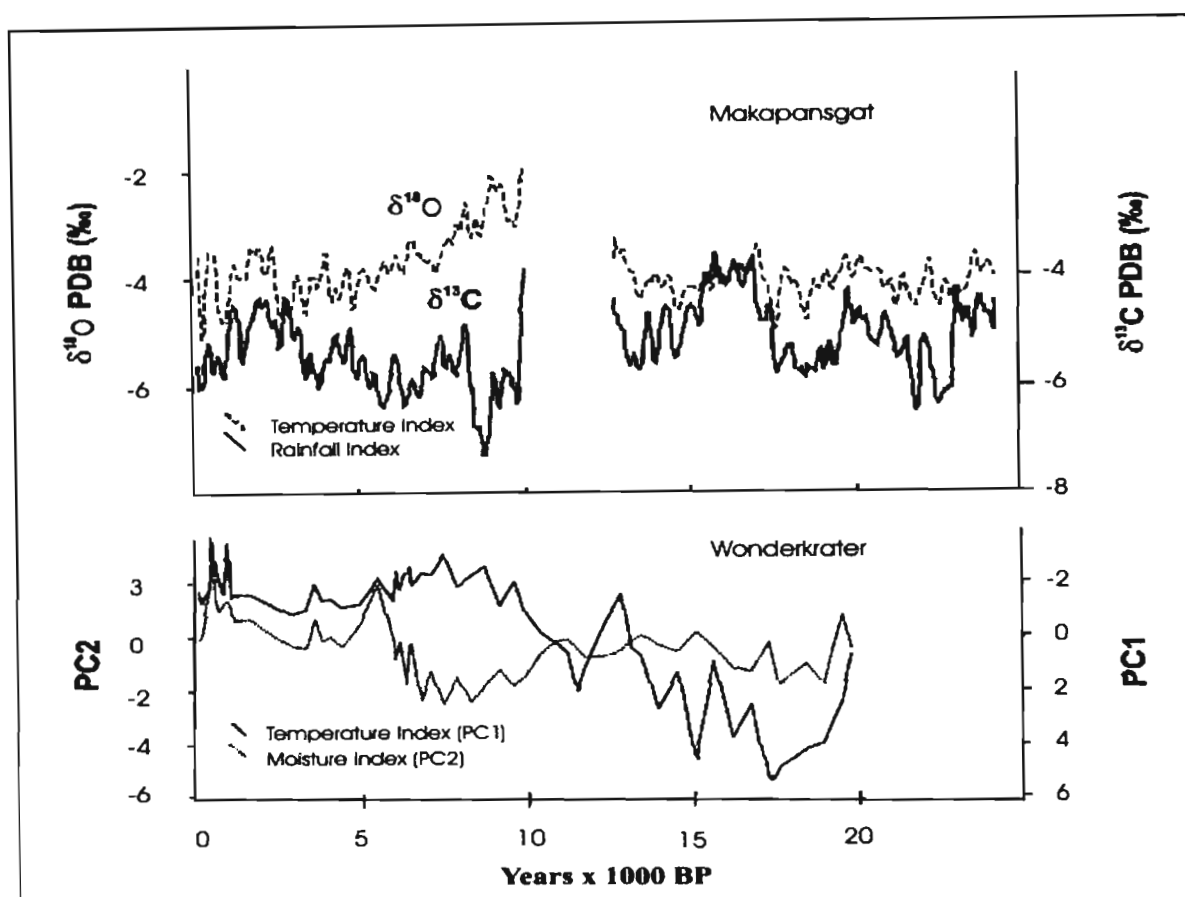


Figure 3.9 – Comparison between Wonderkrater (Scott *et al.*, 2003, 487) and Makapansgat (Holmgren *et al.*, 2003) temperature and moisture indices, with  $\delta^{18}\text{O}$  and  $\delta^{13}\text{C}$  expressed relative to the Pee Dee belemnite (PDB) standard.

The records are similar except for a major difference in the Makapansgat  $\delta^{18}\text{O}$  record where there is little contrast between the Last Glacial Maximum and the Late Holocene,

although the Early Holocene shows high isotope values (Holmgren *et al.*, 2003; Scott *et al.*, 2003). It is difficult to give reasons for this deviation except that it may be caused by environmental factors on a local scale yet to be identified, or oxygen isotope fractionation in the stalagmite (Holmgren *et al.*, 2003). On a millennial scale, however, it can be concluded that the curves are similar.

In the 24 000 year Makapansgat T8 record, there is a break between 12 700 and 10 000 BP. It is likely that the hiatus in stalagmite growth is related to the termination of drip caused by the commencement of drier conditions (Holmgren *et al.*, 2003). Evidence of a drying and cooling of the environment has been discovered in many regions in Africa during this interval, which has been identified at sites across the globe and is referred to as the 'Younger Dryas'.

At 8500 BP, the  $\delta^{13}\text{C}$  values at Makapansgat increased rapidly, which was interpreted at first as a moistening of the environment. At this time there was an increase in grass pollen at Wonderkrater but the dryness index, which is independent of Poaceae, indicates that desiccation continued and intensified (Scott *et al.*, 2003). It becomes apparent that moist conditions are not always indicated by increased  $\delta^{13}\text{C}$  in the Makapansgat record as the change to more grassy conditions can be the result of the predominance of dry grass and a decline of woody elements. This clearly shows the importance of relying on more than one record for interpretation. One requires records based upon different data sources— pollen and stalagmite isotopes in this case — for improved understanding.

The colour banding and increasing  $\delta^{18}\text{O}$  values just prior to 5200 BP suggest warm, humid conditions with denser vegetation cover during the Holocene Altithermal than previously (Lee-Thorp *et al.*, 2001). The warm and moist period continued until 3200 BP when its termination corresponds with a sharp vegetation change and rapid cooling. One can infer a cool but grassy environment between 3000 and 2500 BP. Highest C4 grass values over the last 10 000 years are indicated between 2500 and 2100 BP, which coincides with the peak C4 abundance in the Congo stalagmite (Talma and Vogel, 1992).

After warming between 2500 and 2100 BP, temperatures decreased to a local temperature minimum at approximately 1100 BP (900 AD). The four centuries from 1100 to 700 BP (900 to 1300 AD) were generally warmer but variable, with warm periods interrupted by

short cool periods, and this is the regional expression of the Medieval Warm Epoch (Holmgren *et al.*, 1999). During the Little Ice Age, which extended from around 700 to 190 BP (1300 to 1810 AD),  $\delta^{18}\text{O}$  decreased by approximately 2.5% between 370 and 300 BP (1630 and 1700 AD) to reach its lowest value in the entire 3000 year record between 300 and 250 BP (1700 and 1750 AD) when temperatures may have been as much as 1 °C cooler than today (Holmgren *et al.*, 2001). In the following 110 years,  $\delta^{18}\text{O}$  was enriched by more than 3%, and by 190 BP (1810 AD) the Little Ice Age had effectively ended.

### 3.2.5 Cango II Cave

Stable isotope studies have been carried out on the Pleistocene-Holocene V3 stalagmite from Cango II Cave (33° 23' S 22° 13' E) in the limestone formation of the Swartberg Mountains in the Little Karoo, near Oudtshoorn in the Western Cape (Talma and Vogel, 1992). This Cango stalagmite was collected about 1100 m from the cave opening. Here the air temperature is a constant 17.5 °C and relative humidity is greater than 95%. All dates in this section older than 5000 years are in  $^{14}\text{C}$  years BP (before 1950 AD). The last 5000 years in Figure 3.10 have been calibrated to calendar years BP (before 1950 AD).

$^{230}\text{Th}$  and  $^{14}\text{C}$  dating was conducted and palaeotemperatures and vegetation indicators were derived for the last 47 000 years (Talma and Vogel, 1992). The  $^{230}\text{Th}/^{234}\text{U}$  and  $^{14}\text{C}$  dating series showed vast discrepancies (Vogel, 1983a). A tentative adjustment to the  $^{230}\text{Th}/^{234}\text{U}$  ages suggested that a cooling trend from 30 000 to 19 000 BP, as inferred from a mean  $\delta^{18}\text{O}$  change of approximately 0.5% in the Cango II Cave stalagmite, is consistent with the cooling trend from 51 000 to 21 000 BP that was inferred from a  $\delta^{18}\text{O}$  shift of 0.35 to 0.4 % at Lobatse II Cave (Holmgren *et al.*, 1995).

Since the isotopic composition of the cave drip water could be estimated back 30 000 years using the results of studies of the Uitenhage artesian aquifer (Vogel, 1983b; Talma *et al.*, 1984; Heaton *et al.*, 1986), carbonate deposition temperatures were calculated to produce the temperature record shown in Figure 3.10. It can be inferred that a slow temperature decrease occurred from about 30 000 BP towards minimum temperatures between 19 000 and 17 000 BP, co-incident with the Last Glacial Maximum which was recorded in various other sources for the region.

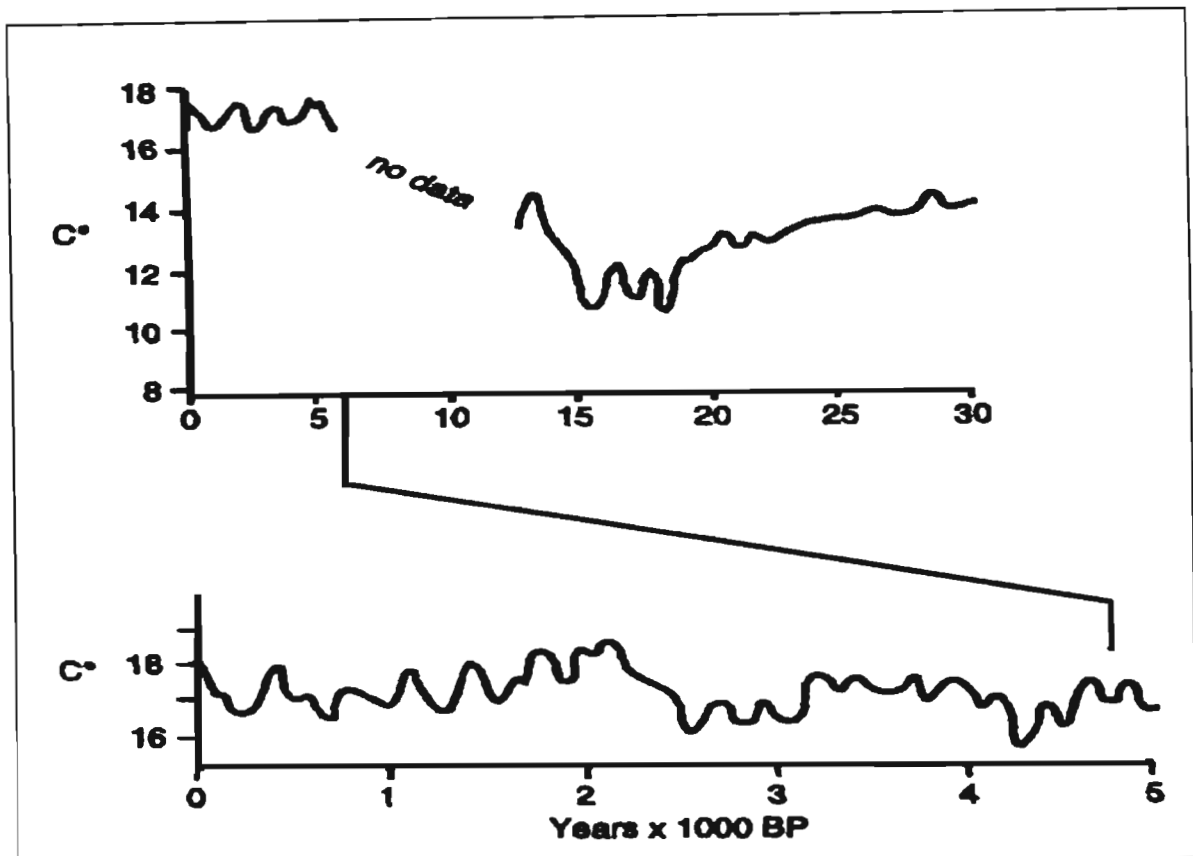


Figure 3.10 – Temperature record from Cango II Cave (Talma and Vogel, 1992) in Tyson (1999b, 337). Ages in  $^{14}\text{C}$  BP except for those less than 5000 BP which are in calendar years BP.

Temperatures increased from the Last Glacial Maximum until 13 800 BP when stalagmite growth was halted. On the recommencement of growth at 5000 BP, the temperatures varied within 1 and -2 °C relative to present-day temperatures. Two major cooling events occurred over the last 5000 years: the first from 4700 BP to 4200 BP, and the second from 3200 to 2500 BP. During the period between these two events, warmer conditions prevailed. The second period of cooling, between 3200 and 2500 BP, coincides with a neoglacial period documented extensively at sites across the globe. This cooling period was also detected in studies of sediments off the Benguela Coast (Johnson, 1988). Thereafter, warmer conditions prevailed for about a thousand years. The effects of the Little Ice Age are apparent in the speleothem record from about 1000 to 200 BP (950 to 1750 AD) but with some warming between 500 and 400 BP (1450 and 1550 AD).

$\delta^{13}\text{C}$  variations in the stalagmite were used to develop a vegetation history of the region through the use of  $\delta^{13}\text{C}$  values as an indicator of the C4/C3 status of the vegetation cover of the area (Talma and Vogel, 1992). Minimum values correspond to nearly complete C3 cover while maximum  $\delta^{13}\text{C}$  values are indicative of a slightly greater C4 grass cover than

at present. The  $\delta^{13}\text{C}$  data from Cango II Cave show less variation and are less enriched in  $\delta^{13}\text{C}$  than the stalagmite from Lobatse II because of the southerly position of the Cango Caves in an ecozone that was dominated by C3 vegetation during the Pleistocene (Talma and Vogel, 1992).

$\delta^{13}\text{C}$  values for the glacial period were low compared to those of the Holocene, suggesting increased C3 cover at the Last Glacial Maximum. The  $\delta^{13}\text{C}$  maximum occurs at around 2000 BP when maximum C4 cover occurred. The higher C4 values are postulated to be caused by a higher mean temperature during the wet season (Vogel *et al.*, 1978). However, the slow increase of  $\delta^{13}\text{C}$  from 5000 BP towards 2000 BP does not correlate with the constant  $\delta^{18}\text{O}$  derived temperatures for the same period. Talma and Vogel (1992) suggest that at this time the seasonality of the rainfall tended more toward winter rainfall than the present rainfall pattern of the area which is non-seasonal.

### 3.2.6 Border Cave

Border Cave (26° 57' S 31° 54' E) is located in KwaZulu-Natal at 600 m altitude in the Lebombo Mountains. The climate is humid-subtropical with predominantly summer rainfall. Butzer *et al.* (1978a) provided an initial palaeoclimatic interpretation of the sedimentary column using various climatic indicators within the layers. A subsequent analysis of the micromammalian fauna (Avery, 1982b) allowed further palaeoclimatological interpretation of the sediments. The cave sedimentary sequence was dated by  $^{14}\text{C}$  methods and this indicated that the top 30% of the sequence formed during the last 50 000 years (Butzer, 1984a). All dates in this section are in radiocarbon years BP.

Butzer (1984a) presented an overall interpretation of the climate history of the dated column as shown in Figure 3.11. The record suggests warm conditions from approximately 49 000 to 39 000 BP, followed by cold conditions from about 39 000 to 33 000 BP. Warming recommenced after approximately 28 500 BP. It is suggested that dense grass cover and bush existed in the region from the Mid-Upper Pleistocene until approximately 49 000 BP, after which this vegetation was replaced by open grassland from around 49 000 until after 13 000 BP. Neither of these vegetation types resembles the modern vegetation (Avery, 1982b). These temperature and vegetation inferences were later confirmed by a re-evaluation of the data by Thackeray and Avery (1990).

		BORDER CAVE		Lebombo Mine	
HOLOCENE	EARLY	-2.0 ka			Subhumid
	MID				
PLEISTOCENE	LATE	-13.3 ka			Subhumid
	MID	Grit		Cool	
		-28.5 ka			
		-33 ka		Cold	
		Spell Hor I -39 ka		Warm	Subhumid
		>49 ka		Cold	
	EARLY	Spell Hor II		Warm	Humid
		Spell Hor III Minor Soil Spell Hor IV Homo		Cold	
		Major Soil		Very Humid	

Figure 3.11 – Palaeoclimatic record from Border Cave (Butzer, 1984a, 240).

### 3.2.7 Lobatse II Cave

Lobatse II Cave (25° 12' S 25° 42' E) is a Proterozoic dolomite cave located in Botswana, close to the border with South Africa. Lobatse borders the sand plains of the Kalahari and the erosion surface of the eastern hardveld, which is an area with virtually no palaeoclimatic data available (Deacon and Lancaster, 1988). The record thus offers an invaluable source of information for the region. The cave is located in the same Proterozoic bedrock formation as Wolkberg Cave but Lobatse II Cave proved more suitable for stalagmite analysis due a narrow entrance shaft and a cave interior with a high relative humidity (Holmgren, 1996). The climatic inferences from Lobatse II Cave were

similar to those of previous studies of caves in South Africa such as Talma *et al.* (1974) and Talma and Vogel (1992).

The cave is located in a region of dominantly C4 vegetation as a result of the low latitude position in a summer rainfall region (Holmgren *et al.*, 1995). Stable isotope analysis and radiocarbon and uranium-series dating of speleothems from the site commenced in 1991. The  $\delta^{13}\text{C}$  values of the stalagmite collected at Lobatse II range from 1 to -6.5, indicating that C4 plants had been the dominant biomass throughout the period of stalagmite growth (Holmgren *et al.*, 1995).

The record was dated using radiocarbon and uranium methods and all dates in this section are in calendar years BP (before 1950 AD). Large shifts in  $\delta^{18}\text{O}$  and  $\delta^{13}\text{C}$  were observed between two main periods of deposition. Between 50 000 and 49 000 BP, the warmest conditions across the record are indicated. It is evident that there was a change from warmer humid conditions with some C3 vegetation between 51 000 and 43 000 BP to colder conditions with drought-resistant C4 plants between 27 000 and 21 000 BP. There is a gradual temperature decrease of about 2 °C from 50 000 BP until the Last Glacial Maximum after 20 000 BP (Holmgren *et al.*, 1995).

It is probable that between 51 000 and 47 000 BP, the region was influenced by both summer and winter rainfall (Holmgren *et al.*, 1995). From 47 000 BP, the climate became drier with a decreasing proportion of winter rainfall, and vegetation comprised predominantly C4 species, particularly grasses. After 43 000 BP, it was too dry for any major calcite precipitation in the cave, but some deposition occurred again at about 35 000 BP. The period (43 000 - 27 000 BP) between the two main periods of deposition shows irregular speleothem formation, bounded by two hiatuses, indicating very dry conditions at these times (Holmgren *et al.*, 1995). The heavily enriched  $\delta^{13}\text{C}$  values just before the growth hiatuses at 43 000 and 21 000 BP may be a result of kinetic fractionation due to highly evaporative conditions, and thus the interpretation of a transition to drier climatic at this time seems likely (Holmgren *et al.*, 1995).

Between 28 000 and 27 000 BP major calcite precipitation recommenced after the period of discontinuous precipitation. Some warming occurred between 27 000 and 26 000 BP when an increase in C3 biomass is indicated. Progressively drier conditions, interrupted by



wetter episodes, possibly with both summer and winter rainfall at 25 000 and 23 500 BP, halted speleothem growth after 21 000 BP but before 15 000 BP (Holmgren *et al.*, 1995). A second speleothem from Lobatse II cave extended the record beyond the Last Glacial Maximum and results indicated that stalagmite growth recovered slightly, suggesting moister conditions after the Last Glacial Maximum. This supports the findings of a study in the Kalahari (Shaw and Thomas, 1996) that documents a wetter episode from about 16 000 to 13 000  $^{14}\text{C}$  BP.

Average growth rates between dated sections showed that decreasing growth was associated with decreasing humidity, which suggests that rainfall is the major limiting factor for speleothem growth in semi-arid areas (Holmgren, 1996). After growth of the speleothems was precluded, their surfaces were corroded, particularly after the cave was opened up in the Holocene and colonised by bats (Holmgren, 1996). It is likely that biogenic corrosion hinders present speleothem formation more than the limited amount of water available (Holmgren, 1996).

Both Lobatse II Cave and Wolkberg Cave (Talma *et al.*, 1974) contain Pleistocene-Holocene speleothems with several growth hiatuses. Although the isotope data of Wolkberg Cave is inadequate for a comprehensive comparison with Lobatse II cave, trends toward colder and drier conditions at the Last Glacial Maximum and before 50 000 BP are clear in both data sets. The dry periods recorded at Lobatse (which are indicated by the hiatuses between 43 000 and 27 000 BP and the enriched  $\delta^{13}\text{C}$  values before 51 000 BP, at about 46 000 to 43 000, 26 000, 24 000 and 22 000 BP) correspond with cooling cycles documented in marine cores (Bond *et al.*, 1992) and ice cores (Mayewski *et al.*, 1994) in the North Atlantic. Although this correlation is speculative, the isotope record in stalagmites from Lobatse II may reflect climate changes at a global scale (Holmgren *et al.*, 1995; Holmgren and Shaw, 1999).

Some of the wetter episodes in the Lobatse record correspond with the Cockcroft *et al.* (1987) model of increasing winter rainfall in the summer rainfall regions of southern Africa. This is associated with an equatorward migration of the westerlies. Such strengthening of the westerlies generally led to drier conditions over the most of the summer rainfall region. It is apparent from the Lobatse II record, and other records from the Kalahari and Namib (such as Grey and Cooke, 1977; Heine, 1981; 1982; Lancaster,

1983; Vogel, 1983a; Ward *et al.*, 1983; Deacon *et al.*, 1984; Helgren, 1984), however, that conditions in these regions often deviated from this general trend, and at times, increases in winter rainfall tended to increase the average rainfall and cause moister conditions.

### 3.2.8 Boomplaas Cave

Boomplaas Cave (32° 14' S, 22° 07' E) is located 800 m above sea-level in the Cango Valley, in the limestone foothills of the Swartberg Mountains to the south of the Karoo in the Western Cape. The dominant vegetation type is Fynbos (Deacon *et al.*, 1984).

Excavations at Boomplaas Cave provided a number of different indicators of climatic changes over the last 80 000 years (Deacon *et al.*, 1984). Radiocarbon dating methods were applied and all dates in this section are in radiocarbon years BP. These indicators included materials that reflect temperature and rainfall changes directly through weathering and sedimentary processes, and indirectly in charcoal, pollen and micromammalian remains (Deacon *et al.*, 1984).

Although prehistoric humans may have been partly responsible for the accumulation of small mammals in the cave deposits, it is thought that the main agents were owls, which discard the bones of their prey in pellets (Avery, 1982a). Principal components analysis of the relative abundance of micromammalian faunal assemblages was used to develop a proxy palaeotemperature series for Boomplaas (Thackeray, 1987) as shown in Figure 3.12. Indicators of increased aridity include an increase in the bush Karoo rat (*Otomys unisulcatus*) in the micromammalian record, and the lack of woodland taxa in the charcoal samples (Thackeray, 1987). The lowest diversity of pollens, charcoals and micromammals (Figure 3.12) correlates with the Last Glacial Maximum at approximately 19 000 BP when conditions were both cold and dry, as is recorded in other records across southern Africa. There is evidence of warming before 14 000 BP with a rapid increase in micromammalian diversity, and the re-establishment of woodland in the valley. The charcoals also show a marked increase in taller woody taxa such as *Olea*, which is indicative of increased precipitation. From about 11 000 BP, charcoals indicate that thicket taxa became more common in the valley. These were replaced by *Acacia karoo* in the Late Holocene (Deacon *et al.*, 1984).

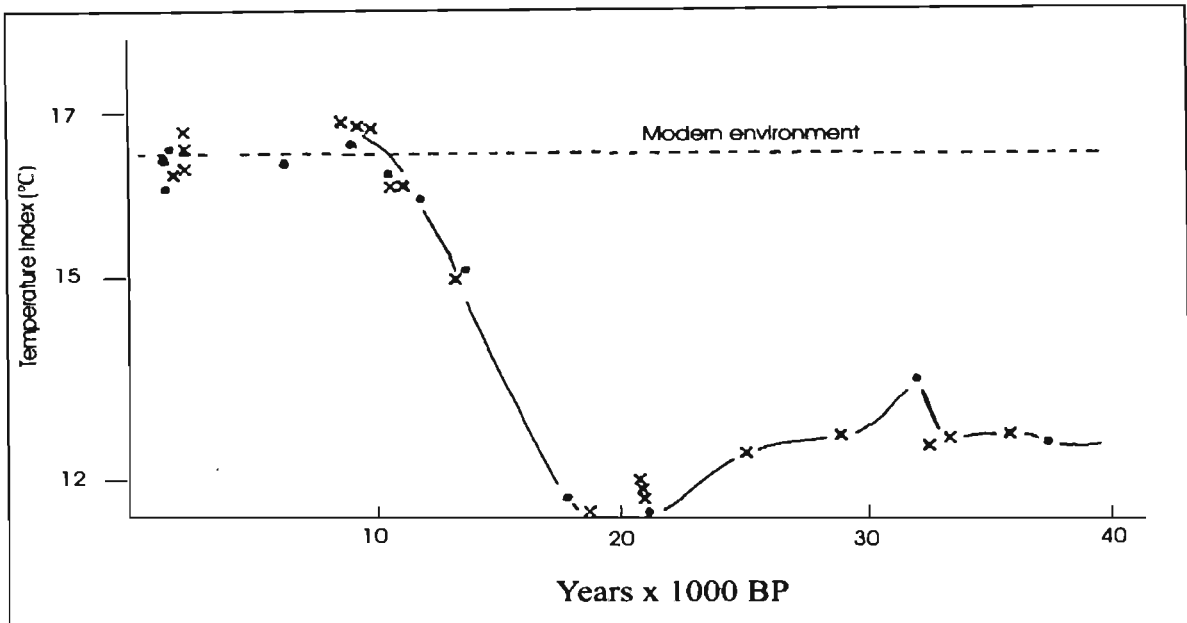


Figure 3.12 – Temperature index for Boomplaas, with dots indicating assemblages dated by carbon isotope assays on charcoal samples and crosses indicating assemblage of uncertain age (Thackeray, 1987, 298).

Some records of environmental change collected at Boomplaas, such as the micromammalian and charcoal records, proved to be more sensitive to local habitat changes. Others, such as the analysis of large mammals, were influenced more by agents of accumulation (Thackeray, 1987). However, the merit of this study lies in the combined weight of various sources of evidence of environmental change over the last 80 000 years. These could support the results from the main thrust of study which was the principal component analysis of the micromammalian faunal content of the sediments.

### 3.2.9 Tswaing Crater (Pretoria Saltpan)

The Tswaing Crater (25° 35' S 28° 05' E) is a circular crater with a diameter of 1130 m situated 40 km north-north-west of Pretoria. The crater was formed almost exclusively in Nebo granite of the Bushveld Complex. The current vegetation at the crater consists of 'Sourish Mixed Bushveld' (Acocks, 1953) and the climate is subtropical and dry sub-humid (Partridge *et al.*, 1993).

The crater provided valuable data for the reconstruction of environmental conditions based on a comprehensive sedimentary sequence. No other terrestrial record of similar length and continuity exists in the region. The continuous raised rim around the crater and its location within a homogenous lithology (with the exception of small areas of intrusive rocks and

Karoo grit) are of importance for a palaeoclimatic study of the crater sediment layers as the rim has allowed the crater to function as a closed hydrological system, while its inner surface can be considered to be a uniform source of clastic sediment (Partridge *et al.*, 1993). Because of the isolation of the crater it is possible to associate changes in the principal constituents of the sequence with changes in precipitation and evaporation, and the sedimentary record can thus be translated as a local index of aridity (Partridge *et al.*, 1993).

Between 1988 and 1989, a group headed by Partridge conducted a study of the area. A core drilling procedure penetrated 90 m of largely fine-grained lacustrine sediments, followed by 61 m of sand and boulders. Fractured granite bedrock was reached at about 151 m (Partridge *et al.*, 1993). The sediments were dated using radiocarbon analysis on the upper 20 m of the core. The sediments indicated a regular increase in age to 39 900 BP at 19.7 m depth. Assuming that the rate of accumulation of sediment remained the same for the whole period since the formation of the crater, the lower part of the crater sediments would have formed after 180 000 BP (Partridge, 1999). Fission track dating indicated an age of 200 000 years. All dates quoted in this section are in calendar years BP (before 1950 AD).

The palynological studies of the cores (Scott, 1988b) provided a vegetation history of the site, which gave an indication of palaeoclimatic conditions. During the period between 100 000 and 82 000 BP, the vegetation surrounding the lake changed from dry bushveld to broad-leaved savanna (Partridge, 1999). Between 80 000 and 33 000 BP, generally cool but variable climatic conditions occurred which were conducive to the establishment of upland yellowwood (*Podocarpus falcatus*) forest elements. Warmer periods are recorded between 79 000 and 75 000 BP, between 62 000 and 60 000 BP, and between 44 000 and 38 000 BP, when more woody savanna elements are indicated for the region (Partridge, 1999).

The lacustrine sediments in the crater were deposited in alternating fresh and saline lake environments. Diatoms lived in this environment and fluctuating vegetation communities developed along the edges (Partridge *et al.*, 1997). A principal components analysis of the palynological data from the 1988/1989 study produced a basic palaeotemperature curve from the PC1. However, due to the absence of pollen in some layers, the Last Glacial Maximum and the Holocene Altithermal are not reflected in the curve (Partridge *et al.*,

1993). An analysis of the diatoms preserved in the 1988/1989 core produced the only diatom sequence of this timescale in southern Africa. Diatoms are present in most parts of the core and record both the long-term evaporative concentration of the lake and more rapid climatic variations (Partridge, 1999).

Analysis of the sediments from the 90 m core produced a proxy regional rainfall series (Partridge *et al.*, 1997) as shown in Figure 3.13. Despite poor temporal resolution of the Tswaing Crater data, a valuable deduction emerged from this multidisciplinary study - principally that southern African Quaternary climate change, or at least in an area representing summer rainfall subhumid climates, correlates with the Milankovitch precessional cycle (Partridge *et al.*, 1997). The correspondence between January insolation and the proxy rainfall record for the last 200 000 years is evident in Figure 3.13. It also emerged that climate changes have been of considerable magnitude, and conditions over the last 200 000 years have been both warmer and cooler, and moister and drier compared to present conditions.

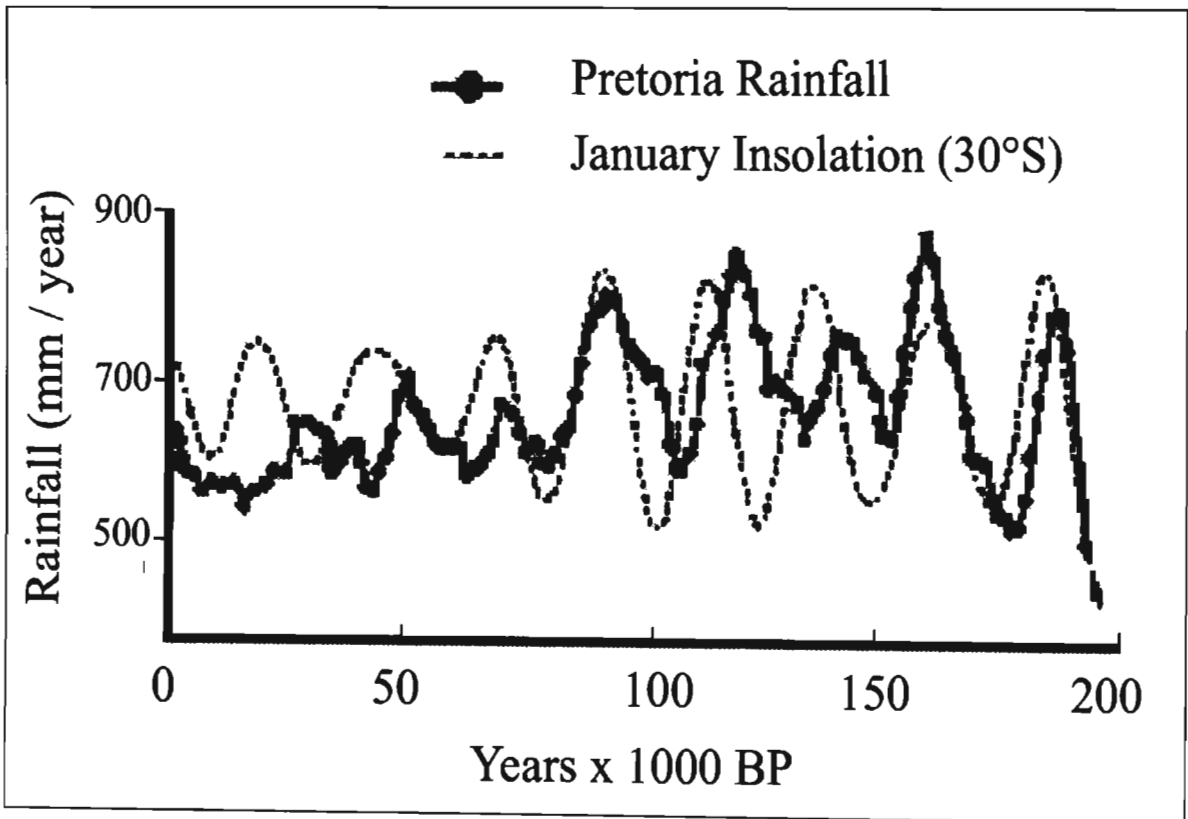


Figure 3.13 – Correlation between Pretoria rainfall and January insolation over 200 000 years (Partridge *et al.*, 1997, 1128).

### 3.3 SYNTHESIS: THE CLIMATIC TIMELINE

It is possible to compile a synthesis of knowledge of the palaeoclimatological history of southern Africa using the selected case studies and others, which were not considered sufficiently extensive in their time range or resolution to warrant an individual report in Section 3.2. Previous syntheses include those by Deacon and Lancaster (1988), Lindsay (1990) and Tyson (1991; 1999b) but new evidence, such as the Makapansgat data (Holmgren *et al.*, 2003) and the extension of the dated Wonderkrater sequence (Scott *et al.*, 2003), have become available since their publication.

Although the longer southern African palaeoenvironmental records extend to the Upper Pleistocene (130 000 BP) and beyond (the Tswaing Crater record, for example, extends beyond 200 000 BP), a useful dating framework is available for around 40 000 years from radiocarbon methods. Few datasets extend beyond this point due to dating problems and the difficulty involved in locating and extracting extended sequences. For this reason, the synthesis will focus on the period subsequent to 40 000 BP although a description of conditions just prior to this period will be presented to contextualise the climatic situation.

According to Partridge *et al.* (1990), the following time slots have been agreed upon for the study of southern African palaeoclimates of the last 40 000 years based upon a relative homogeneity within each period and a discontinuity between periods: 40 000 – 30 000 BP, 30 000 – 25 000 BP, 25 000 – 21 000 BP, 21 000 – 17 000 BP, 17 000 – 12 000 BP, 12 000 – 10 000 BP, and 10 000 BP – the present. This study will outline the salient features of these time periods but will also highlight conflicting evidence as local conditions at certain sites may not reflect the regional trend.

It is now understood that there is a discrepancy between calendar years and radiocarbon years due to fluctuations in atmospheric  $^{14}\text{C}$  concentration over geological time. However, Partridge *et al.* (1990) directly compare various radiocarbon-dated southern African records with the Vostok ice core record, which is on a calendar year timescale. Here the Boomplaas record, for example, shows a correlation with the Vostok record (Tyson, 1999) before calibration. Tyson (1999) performs a similar comparison of the uncalibrated radiocarbon-dated Cango Cave record with the isotopically-dated Makapansgat dataset beyond the LGM. Although the lack of calibration may bring the detected correlations into

question by some, it is possible that calibration would have introduced further errors. Using the Boomplaas record as an example, an LGM at 20 000  $^{14}\text{C}$  BP would provide a calibrated date of around 24 000 calendar years BP (Fairbanks *et al.*, 2005) in contrast with the results of Makapansgat study, the Vostok ice core and many other data sources which date the LGM between 18 000 and 21 000 calendar years BP. It appears that calibration offsets these chronologies which may have been adjusted according to a known date of the LGM, although the authors do not document this or any other assumptions made.

A resolution was reached to follow the example set by authors such as Partridge *et al.* (1990) and Tyson (1999) and not attempt any complicated calibration procedures, since the aims of the study involved the search for general trends over extended timescales. The broad time divisions beyond the LGM (e.g. 25 000 – 30 000 BP, 30 000 – 40 000 BP) are sufficient to incorporate the differences between calendar and radiocarbon years considering the inherent problems with radiocarbon dating, particularly in records analysed before accelerated mass spectrometry (AMS) techniques were widely adopted. A discussion of the palaeoclimates during the time periods designated by Partridge *et al.* (1990) follows and the dates provided are thus rough approximations based mainly on uncalibrated radiocarbon records. The dates presented are likely to be adjusted in the future as authors update their work with more advanced dating and calibration procedures.

Prior to 49 000 BP, roof spall horizons at various sites, including Border Cave and Bushman Rock Shelter in Mpumalanga, are indicative of frost action (Deacon *et al.*, 1983). A cooler period prior to 49 000 BP is also indicated by pollen samples for Florisbad (Scott and Nyakale, 2002), micromammals from Border Cave (Avery, 1982b), and larger mammals from the Border Cave site (Klein, 1980). By 49 000 BP, at Border Cave, conditions had become warmer and moister, followed by another cool, dry period indicated by a spall horizon for the period 39 000 to 33 000 BP (Butzer, 1984a). At approximately 39 000 BP, at the Makgadigadi Depression, in the central Kalahari, lake levels were low (Deacon *et al.*, 1983), also indicating increased aridity.

### 3.3.1 40 000 – 30 000 BP

Between 30 000 and 40 000 BP temperatures appear to have been intermediate between the LGM and the present (Deacon *et al.*, 1983). Biological and geological evidence indicates

that all regions of southern Africa, except parts of the eastern areas of Mpumalanga and KwaZulu-Natal, were wetter than today during at least part of this period (Partridge *et al.*, 1990). Evidence from Lobatse II Cave (Holmgren *et al.*, 1995) indicates that a short period of moistening occurred in this region at approximately 35 000 BP. Moistening is also indicated at Tswaing Crater from 40 000 to 30 000 BP and the site was moister than presently by approximately 30 000 BP (Partridge *et al.*, 1997).

### **3.3.2 30 000 – 25 000 BP**

#### *3.3.2.1 Temperature*

Temperatures remained low in most regions with some warming towards the end of the period according to evidence from Border Cave (Butzer, 1984a) and Lobatse II Cave (Holmgren *et al.*, 1995). Isotopic measurements at Congo and Uitenhage indicated mean temperatures around 4 – 5 °C lower than at present (Talma and Vogel, 1992) but with some warming from approximately 26 000 BP.

#### *3.3.2.2 Rainfall*

Sediments from the Tswaing Crater (Partridge, 1999), the decline of fossil diversity at Boomplaas Cave in the Congo Valley (Thackeray, 1987), and the enriched  $\delta^{13}\text{C}$  values at Lobatse II Cave in Botswana suggest a progressive drying during this period. Drier conditions appear to have occurred throughout the subcontinent with the exception of the Namib and Kalahari, which seem to have been almost uniformly wetter than at present (Partridge *et al.*, 1990). For example, evidence from Wonderwerk Cave, in the south-eastern Kalahari, suggests a moist and cold climate with frost (Butzer, 1984a).

### **3.3.3 25 000 – 21 000 BP**

#### *3.3.3.1 Temperature*

Cooler conditions continued into this period (Partridge *et al.*, 1990) as indicated by the Congo II Cave (Talma and Vogel, 1992) and Lobatse II Cave (Holmgren *et al.*, 1995) datasets. According to the Congo II Cave (Talma and Vogel, 1992) and the Makapansgat



Cold Air Cave records (Holmgren *et al.*, 2003), there was cooling, followed by warming with a local temperature peak before 22 000 BP, followed by further cooling. Overall, temperatures at the end of this period were cooler than those at the start of the period.

### 3.3.3.2 Rainfall

In the southern and eastern parts of the subcontinent, the climate apparently remained dry (Butzer *et al.*, 1978a; Price-Williams *et al.*, 1982; Butzer, 1984a). There is evidence for a small increase in wetness in the Karoo (Beaumont, 1986), in the northern Kalahari (Grey and Cooke, 1977; Deacon *et al.*, 1984; Helgren, 1984), the south-western Kalahari (Heine, 1981; 1982) and the south-western region of the Western Cape (Butzer, 1984a). However, evidence also has been reported for drier conditions in the Kalahari (such as Cooke and Heine, 1983; Helgren and Brooks, 1983) and at Boomplaas Cave in the southern Cape (Deacon *et al.*, 1983; Deacon and Lancaster, 1984). Further conflicting evidence exists for the Namib as Lancaster (1983), Vogel (1983a) and Ward *et al.* (1983) state that conditions were wetter than presently, while Heine and Geyh (1984) and Partridge *et al.* (1990) propose that conditions were significantly drier. Moistening in the northern and central former Transvaal (Marker, 1974) and the central interior (Butzer, 1984a; 1984b) is indicated by some sources while others indicate drying (Scott, 1982a; Partridge, 1999; Holmgren *et al.*, 2003). These discrepancies may be the result of dating problems or alternatively, as some sources suggest, there may have been some moistening until 23 500 BP followed by rapid increases in aridity towards the LGM at 18 000 BP.

### 3.3.4 21 000 – 17 000 BP

#### 3.3.4.1 Temperature

The LGM occurred during this period and temperatures reached their lowest values of approximately 5 – 6 °C less than at present over most of the region (Heaton *et al.*, 1986). At this time, periglacial conditions occurred at high elevations, such as in the Drakensberg and Lesotho (Hastenrath and Wilkinson, 1973; Lewis and Dardis, 1985) and perhaps even on the Highveld (Linton, 1969). At Wolkberg Cave, in the former Transvaal, at the time of the Last Glacial Maximum, temperatures were 8 °C lower than at present (Talma *et al.*, 1974). A 5.5 °C temperature drop is evident in samples from artesian groundwaters of the

Uitenhage aquifer (Vogel, 1983b; Talma *et al.*, 1984; Heaton *et al.*, 1986), while the Congo II Cave V3 speleothem indicates a mean temperature 5 °C lower than presently (Vogel, 1983b). The Wonderkrater pollen sequence for this time suggests a 100 m drop in vegetation zones which corresponds with a drop of 5 – 6 °C (Scott, 1982a).

The isotope record from the Congo II Cave V3 speleothem reveals that in the southern coastal region of South Africa, coldest conditions were observed before 18 000 BP (Talma and Vogel, 1992). The Wonderkrater pollen sequences and the isotope records of Makapansgat suggest that coldest conditions were experienced at around 17 500 BP (Scott *et al.*, 2003; Holmgren *et al.*, 2003). In the Western Cape, lowest temperatures were recorded at Nelson Bay Cave between 18 660 and 16 700 BP, and at Boomplaas Cave between 21 220 and 18 600 BP (Deacon *et al.*, 1983). Stute and Talma (1998) concluded that a similar temperature drop occurred at Stampriet, Namibia, which clearly indicates that cooling occurred over a large area of the subcontinent. These findings correspond with a number of less thorough regional proxy records indicating generally drier and colder conditions at this time (Partridge, 1997; Thomas *et al.*, 2000).

#### 3.3.4.2 Rainfall

Between 20 000 and 18 000 BP, regional and local desiccation occurred. Cooke and Heine (1983) and Helgren and Brooks (1983) state that it was particularly dry in the Kalahari, and Tyson (1999b) suggests that a minimum of less than 40% of present mean annual rainfall was experienced across the region. The rainfall at the time of the Last Glacial Maximum is estimated to be about 25% lower at the Tswaing Crater than the present precipitation of around 750 mm (Partridge, 1999). Southern Cape sites also indicate drier conditions (Deacon *et al.*, 1983; Deacon and Lancaster, 1984) and a  $\delta^{13}\text{C}$  minimum occurred at Congo Caves at approximately 18 000 BP (Talma and Vogel, 1992). The Makapansgat stalagmite record indicates drier conditions and sparser grass cover from 19 500 to 17 500 BP (Holmgren *et al.*, 2003). Speleothem growth at Lobatse Cave was halted at some point after 21 000 BP but before 15 000 BP (Holmgren *et al.*, 2003). The eastern region of the subcontinent remained dry (Price-Williams *et al.*, 1982; Butzer, 1983) with Tyson (1999b) suggesting that the smallest diminution in rainfall occurred here.

There are indications that the concurrence of aridity with coolest temperature did not prevail across the entire subcontinent. Butzer (1983; 1984a) and Meadows and Baxter (1999) suggest a wet LGM for the south-western region of the Western Cape, and Shaw and Thomas (1996) record a wetter Kalahari out of phase with other subtropical deserts.

### 3.3.5 17 000 - 12 000 BP

#### 3.3.5.1 Temperature

During the period from 17 000 to 12 000 BP, temperatures were generally lower than those at present, although it is clear from the isotope analysis of samples from the Uitenhage aquifer (Vogel, 1983b; Talma *et al.*, 1984; Heaton *et al.*, 1986), the Vostok ice core (Jouzel *et al.*, 1987) and Cango II Cave (Talma and Vogel, 1992), and using various biological indices (Thackeray, 1987; Scott *et al.*, 2003), that the post-glacial warming trend was firmly established during this period. Warming is observed in terrestrial lake sediment records for a similar period from African mid- to low-latitudes (such as Gasse and Van Campo, 1998; Johnson *et al.*, 2002). These correlate well with trends in southern hemispheric tropical and polar ice records (Thompson *et al.*, 1995; Blünier *et al.*, 1998; Steig *et al.*, 2000).

After the warming, there was a return to colder conditions around 15 000 BP, as indicated in the Cango II Cave (Talma and Vogel, 1992), the Wonderkrater (Scott *et al.*, 2003) and the Makapansgat data (Holmgren *et al.*, 2003), and this appears to be a local manifestation of the Antarctic Cold Reversal recorded in ice cores from Antarctica (Blünier *et al.*, 1998). Formerly thought to be unique to southern polar records, this reversal is now traceable from pole to equator in the southern hemisphere (Holmgren *et al.*, 2003). This was followed by renewed warming after about 13 500 BP (Holmgren *et al.*, 2003).

#### 3.3.5.2 Rainfall

A significant increase in wetness accompanied warming from around 17 000 BP onwards to around or slightly above present levels in most regions (Partridge *et al.*, 1990). Regional contrasts diminished in many areas. Although some data suggest periods of dry conditions (such as that of Butzer *et al.*, 1978a; Heine, 1981; 1982; Avery, 1982a; Price-Williams *et*

*al.*, 1982; Butzer, 1984b; Deacon *et al.*, 1983), most evidence suggests that the wetter conditions established after 18 000 BP continued to prevail until about 12 000 BP over most of southern Africa (Coetzee, 1967; Butzer *et al.*, 1973; Grey and Cooke, 1977; Scott, 1982a; Lancaster, 1983; Helgren and Brooks, 1983; Butzer, 1983; 1984a; 1984b; Deacon *et al.*, 1983; Deacon *et al.*, 1984; Helgren, 1984; Thackeray, 1987; Partridge *et al.*, 1990; Partridge, 1993; 1997; Holmgren *et al.*, 1995; Shaw and Thomas, 1996).

Butzer *et al.* (1973) indicate that at around 16 000 BP, rainfall at Alexandersfontein was about double that of present. Kent and Gribnitz (1985) presented similar findings for Swartkolkvloer in the north-eastern Cape for the period from 16 000 to 14 000 BP. For two to three millennia after 16 000 BP, there is also evidence of greater moisture in the north-western interior (Lancaster, 1979; Cooke and Verstappen, 1984). Data from the south-western Cape suggest a persistence of moister conditions in this region (Butzer, 1984a) although there is data that suggest the opposite (Avery, 1982a; Deacon *et al.*, 1983; Deacon and Lancaster, 1984). According to the Makapansgat record (Holmgren *et al.*, 2003), rainfall decreased after about 16 000 BP, with a slight increase between 14 000 and 13 500 BP, followed by further decreases that caused the cessation of drip by 12 700 BP. Partridge *et al.* (1990) suggest that in the Kalahari, a wetter trend was maintained from the previous period. Talma and Vogel (1992) suggest that over most of the region, the proportion of summer rainfall increased while that of winter rainfall decreased.

### **3.3.6 12 000 – 10 000 BP**

#### *3.3.6.1 Temperature*

The warming trend following the LGM was interrupted by a sudden cooling associated with the Younger Dryas before 12 000 BP. This is evident in the Wonderkrater pollen record (Scott and Thackeray, 1987; Scott *et al.*, 2003) and from mollusc stable isotope data for the Atlantic coastal region (Cohen *et al.*, 1992). The Wonderkrater sequence indicates a disruption in the warming trend and the commencement of slightly cooler and intensely evaporative conditions with an increase in abundance of the pollen taxa Chenopodiaceae and Amaranthaceae between 11 500 and 10 000 BP (Scott, 1982a; Scott *et al.*, 2003). Thereafter the warming trend was re-established over much of the subcontinent.

### 3.3.6.2 Rainfall

During this period, the eastern and southern parts of the subcontinent appear to have been similar to the present (Partridge *et al.*, 1990). There are a few reports of conditions wetter than the previous period south of about 27° S (Coetzee, 1967; Butzer *et al.*, 1973; Butzer, 1983; Deacon and Lancaster, 1984), but evidence consistently suggests that to the north of about 27° S, conditions grew progressively drier. The Makapansgat study shows a drastic and abrupt change in climate at 12 700 BP. The hiatus which occurs from 12 700 to 10 200 BP was most probably related to the cessation of drip caused by the onset of drier conditions (Holmgren *et al.*, 2003). The neighbouring Wonderkrater pollen record suggests that strongly evaporative conditions prevailed at this time (Scott *et al.*, 2003).

Further evidence of a drying of environments in Africa during this interval, which in northern Europe and elsewhere is defined as the 'Younger Dryas' (or Heinrich 0 event), includes the work of Coetzee (1967), Tankard (1976), Grey and Cooke (1977), Butzer *et al.* (1978b), Price-Williams *et al.* (1982), Butzer (1983; 1984a; 1984b), Deacon *et al.* (1983), Vogel (1983b), Deacon and Lancaster (1984), Deacon *et al.* (1984), and Holmgren *et al.* (1995). Lake Victoria sediments indicate lower lake levels at around 12 500 BP (Stager *et al.*, 2002), and both cool and dry conditions between 12 000 and 10 300 BP are indicated by a low mass accumulation rate of biogenic silica in Lake Malawi (Johnson *et al.*, 2002), although this interval was followed by an abrupt reversion to warmer and wetter Holocene conditions and increasing mass accumulation rates. Other lake records from equatorial and northern Africa indicate that humid conditions were established earlier than this, possibly as early as 11 500 BP (Gasse, 2000).

## 3.3.7 10 000 – 4000 BP

### 3.3.7.1 Temperature

Across southern Africa, available evidence indicates that conditions were warmer between 8000 and 4000 BP than at present, and the Holocene Maximum is thought to have occurred at approximately 6000 BP (Partridge *et al.*, 1990) when temperatures were at their highest values since the last interglacial at 125 000 BP (Tyson, 1999b). The Makapansgat Cold Air Cave stalagmite record (Holmgren *et al.*, 2003) indicates warm conditions between 10 000

and 6000 BP. The Wonderkrater trend (Scott *et al.*, 2003) does not follow the Makapansgat  $\delta^{18}\text{O}$  curve exactly, but higher temperatures for the period are indicated (Figure 3.9, Page 37). Due to the limitations of the Makapansgat oxygen record and the Wonderkrater temperature curve, an exact correlation should not be expected.

Sea-level curves (Figure 3.5, Page 31) for the Western Cape indicate rising sea-levels from 9000 BP, with a peak at around 5800 BP (Baxter and Meadows, 1999). The Miller *et al.* (1993) curve suggests that highest sea-levels over the last 6000 years were experienced at this point but the Baxter and Meadows (1999) curve suggests that there was a higher peak at 3500 BP. High sea-levels in the region at the Holocene Altithermal are indicative of warmer conditions experienced across the globe, which caused a melting of polar ice.

Warming between 8000 and 4000 BP accords well with the Early Holocene warming documented in Antarctic ice cores (Masson *et al.*, 2000), in marine cores from the South Atlantic (Hodell *et al.*, 2001) and in Kilimanjaro ice cores (Thompson *et al.*, 2002). Speleothems from northern Norway reveal a Holocene temperature maximum between 9500 and 7500 BP, and the snowline data from the Swiss Alps indicate a temperature maximum between 8000 and 6000 BP (Negendank, 2003).

The Wonderkrater temperature index shows a gradual mid-Holocene cooling after 6000 BP (Holmgren *et al.*, 2003) with temperatures reaching minimum values for the period by around 3000 BP (Scott *et al.*, 2003). This corresponds well with the isotope records of Cold Air Cave, Makapansgat (Holmgren *et al.*, 2003). The Verlorenvlei sea-level curves also demonstrate a minimum for the last 6000 years at around 3000 BP (Miller *et al.*, 1993; Baxter and Meadows, 1999). Global evidence exists of mid-Holocene cooling recorded in Antarctic ice cores (Masson *et al.*, 2000), in South Atlantic marine sediments (Hodell *et al.*, 2001) and in glacial evidence from New Zealand (Porter, 2000).

### 3.3.7.2 Rainfall

At 10 000 BP, the weight of evidence suggests moist conditions (Cockcroft *et al.*, 1987) for the central and western regions of the subcontinent and tropical Africa (Butzer *et al.*, 1973; 1978b; Van Zinderen Bakker, 1982; Lancaster, 1983; Butzer, 1983; 1984a; Deacon and Lancaster, 1984; Holmgren *et al.*, 2003; Scott *et al.*, 2003) while conditions in the

eastern and southern parts of southern Africa remained similar to those of the earlier period (Scott, 1982a; Price-Williams *et al.*, 1982; Deacon and Lancaster, 1984).

From around 10 000 BP, both the Makapansgat stalagmite (Holmgren *et al.*, 2003) and Wonderkrater pollen records (Scott *et al.*, 2003) suggest that conditions were becoming drier. The stalagmite record shows a rapid decrease in rainfall after 10 200 BP to reach a minimum between 9000 and 8400 BP (Holmgren *et al.*, 2003). However, evidence for continued regional desiccation comes from the Wonderkrater pollen record. After 8500 BP, increased grass cover is indicated at Makapansgat and at Wonderkrater (Scott *et al.*, 2003) but the pollen spectra at the latter site indicate a dry, grassy, sparsely wooded ecosystem similar to that of the present semi-arid Kalahari thornveld (Scott *et al.*, 2003). The increase in grass pollen is coincident with a decrease in Cyperaceae pollen, representing a dry-land grass spread into the wet areas (Scott, 1982a; Scott *et al.*, 2003). Moistening appears to recommence at around 7000 BP in the Wonderkrater record (Scott *et al.*, 2003) to reach a maximum at approximately 5500 BP. Linear dune construction in Zambia at 10 000 to 8000 BP (O'Connor and Thomas, 1999) suggests widespread arid conditions (Holmgren *et al.*, 2003). Equatorial and northern Africa lake records (Gasse, 2000) and the Kilimanjaro ice-core record (Thompson *et al.*, 2002) document a short but strong dry event at 8300 to 8200 BP.

After 8000 BP, however, and until about 4000 BP, the weight of the evidence suggests that most of southern Africa was becoming moister (Heine, 1981; 1982; Van Zinderen Bakker, 1982; Butzer, 1983; 1984a; 1984b; Scott and Vogel, 1983; Deacon, *et al.*, 1983; Cockcroft *et al.*, 1987) and even the eastern region of the subcontinent was decidedly wetter than at present during at least the latter part of this period (Partridge *et al.*, 1990). Exceptions include the south-western Cape (Tankard, 1976; Klein, 1980; Avery, 1982a), Karoo (Partridge *et al.*, 1990) and Namib (Partridge *et al.*, 1990). Regional variations in climate do not appear to have been marked between 7000 and 4000 BP. The degree of uniformity of wetter conditions appears to be similar to that which prevailed between 25 000 and 21 000 BP. A notable contrast between these periods does exist, however, as between 25 000 and 21 000 BP the south-western Cape was much wetter than between 8000 and 4000 BP (Cockcroft *et al.*, 1987).

### 3.3.8 4000 BP – Present

Temperatures and moisture levels of the latter part of the Holocene were characterised by continuous fluctuations of small amplitude. Isotopic evidence from the V2 stalagmite from Cango II Cave (Talma and Vogel, 1992) indicates that temperatures did not depart by more than 2 °C from the present mean over the last 5000 years. The Makapansgat stalagmite record for the last 4000 years (Holmgren *et al.*, 2003) accords with the lower-resolution Wonderkrater pollen record (Scott *et al.*, 2003) and high grass and Asteraceae pollen counts support the inference from the isotope record of a cool, grassy environment from 3000 to 2000 BP. The dune record from Zambia (O'Connor and Thomas, 1999) indicates arid conditions until 2000 BP. Evidence for drier, colder conditions in equatorial Africa come from the Kilimanjaro ice cores (Thompson *et al.*, 2002) and from glacier expansion on Mount Kenya (Karlén *et al.*, 1999).

A reconstruction of the climate over the last 2000 years was developed by Tyson and Lindsay (1992) and is shown in Figure 3.14. This was derived from the last 2000 years of the Cango Cave record (Talma and Vogel, 1992), a high-resolution record of foraminifera collected off the coast of Walvis Bay (Johnson, 1988), and Bushveld pollen analyses (Scott, 1993). The integrated record was enhanced by lower resolution data from the isotopic analysis of mollusc shells at Elands Bay (Cohen *et al.*, 1992), pollen analysis of Hyrax middens at Blydefontein (Scott, 1991) and annual records of tree-ring data from the Karkloof (Hall, 1976) and the Cedarberg (Dunwiddie and LaMarche, 1980). The record was developed further by dated point observations of a variety of environmental proxies including micromammalian evidence at Blinkkop (Thackeray *et al.*, 1983; Thackeray, 1987; Avery, 1988) and Abbott's Cave (Avery, 1991), the described cooling at Border Cave at 1425 AD (Thackeray, 1987), changing environmental conditions at Craigrossie at 1350 AD (Scott, 1989), changes in Free State pans from 800 to 1150 AD (Butzer, 1984a; Scott, 1988a), and the incidence of buried soils after 1700 AD at Blydefontein (Bousman *et al.*, 1988). The record was supplemented by data from peat layers at sites in the southern region of the Western Cape (Scholtz, 1986), in the Nuweveld (Sugden and Meadows, 1989) and in Lesotho (Hanvey and Marker, 1994). Lake-level fluctuations in Malawi (Crossley *et al.*, 1983), riverine sediments in northern Namibia (Vogel and Rust, 1990), archaeological evidence in central west-coast Namibia (Burgess and Jacobson, 1984) and historical records (Vogel, 1989) were also utilised.



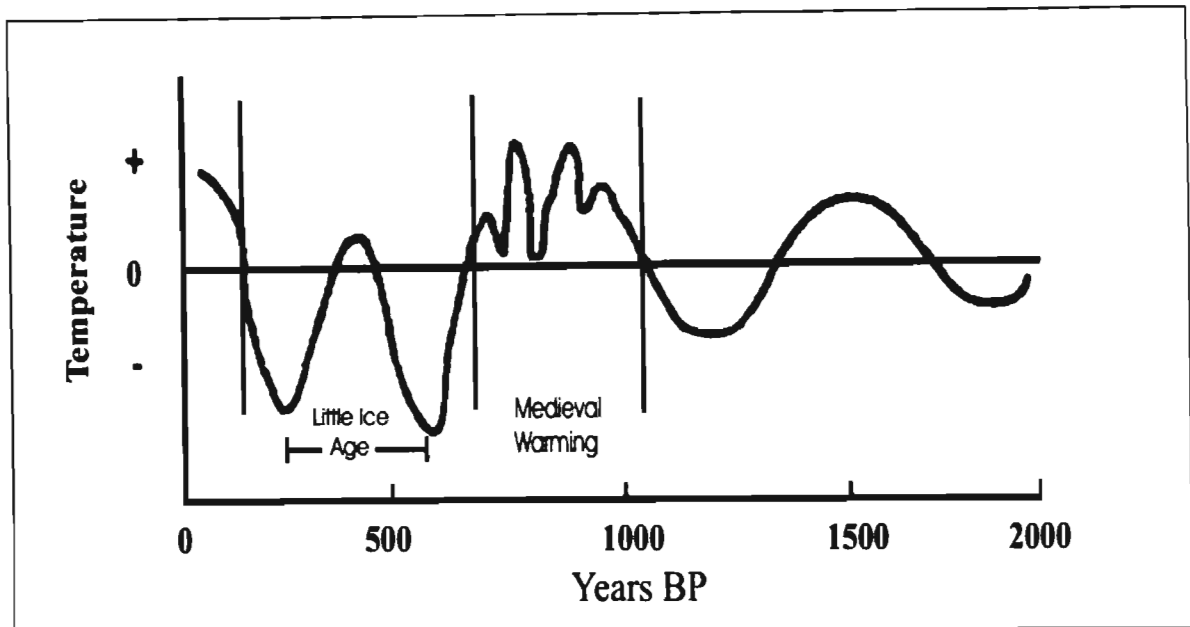


Figure 3.14 – Generalised temperature conditions of the last 2000 years for southern Africa relative to current mean temperature at 0 (Tyson, 1999b, 342).

From this integration of data, it was possible to surmise that over much of southern Africa, cooling occurred from about 1900 to 1750 BP (500 to 200 AD), warming from 1750 to 1400 BP (200 AD to 550 AD) and cooling and drying thereafter until 1100 BP (850 AD). The period from 1100 to 700 BP (850 to 1250 AD) was highly variable, but generally warmer and wetter, corresponding to the Medieval Warm Epoch that has been described in many parts of the world. The intermittent drier episodes during this period, however, were intense enough to result in signs of aridity in central southern Africa (Scott and Brink, 1991), pan formation in the western Free State Province (Butzer, 1984a) and dune formation in the south-western Kalahari (Thomas *et al.*, 1997). The 500 year cooling from 700 to 150 BP (1250 to 1800 AD), considered to be the local manifestation of the Little Ice Age, was interrupted by a warm period from about 500 to 330 BP (1450 to 1620 AD). Cooling, drying and an increase in major flood events during the Little Ice Age are evident in tree-ring analyses from distant sites (Hall, 1976; Dunwiddie and LaMarche, 1980; Thackeray, 1996), in foraminifera levels in sediment cores taken off the west coast of Namibia (Johnson, 1988), in the Cango II Cave record (Talma and Vogel, 1992), in river sediment analyses from Namibia (Vogel and Rust, 1990), in changing levels of Lakes Malawi and Chilwa (Crossley *et al.*, 1983), and in high-resolution palynological analyses from the Kuiseb Valley, Namibia (Scott, 1996).

The accuracy of the Tyson and Lindsay (1992) model has been confirmed by a number of other records, including a coastal mollusc isotope record (Cohen *et al.*, 1992; Cohen and Tyson, 1995), which indicates a sea-surface temperature drop during the Little Ice Age, and a dated record of shifting distributions of Iron Age villages in central and southern Africa (Huffman, 1996). Further confirmation was derived from a palaeoflood record of the lower Orange River (Zawada *et al.*, 1996), which indicated increased flooding during the Little Ice Age, and from high-resolution climatic series from the central plateau of the Northern Province (Holmgren *et al.*, 2003; Scott *et al.*, 2003). A cool, dry period, commencing at approximately 1450 BP (550 AD), is evident in the Wonderkrater palynological record (Scott *et al.*, 2003). The Makapansgat Cold Air Cave stalagmite grey-level variations and the  $\delta^{18}\text{O}$  record indicate warmer, moister conditions from 1125 to 685 BP (875 to 1315 AD). The  $\delta^{13}\text{C}$  record indicates recurrent periods of declining C4 grass cover and moisture availability during the medieval period in otherwise warmer, wetter conditions. The Little Ice Age maximum, at approximately 300 BP (1700 AD), shows the most marked  $\delta^{18}\text{O}$  deviation in the entire Makapansgat stalagmite record (Holmgren *et al.*, 2003). Inverse modelling of borehole temperature profiles indicated that after 150 BP (1800 AD), the effect of the recent global warming after the Little Ice Age became apparent throughout the subcontinent (Jones *et al.*, 1999). The boreholes were located at various sites in the Northern Cape, North West and Gauteng provinces.

### **3.4 TELECONNECTIONS**

Teleconnections are defined as atmospheric and oceanic linkages between distant climatic events. They indicate a statistical relationship between climatic conditions on one part of the globe and those at a widely separated region. Significant teleconnections became apparent during the development of the southern African palaeoclimatic synthesis, and in the comparison of this synthesis with documented records from across the globe. These teleconnections will be discussed below.

#### **3.4.1 Southern Africa**

At present, changes in rainfall of the winter and summer rainfall regions are 180° out of phase (Lindsay *et al.*, 1986; Muller and Tyson, 1988; Tyson, 1986). It is likely that this

inverse correlation extended back into the past and this inference is supported by a study of various tree-ring datasets (Tyson *et al.*, 2002a). Over a 376 year period of record overlap, the approximately 80 year oscillation in the *Podocarpus falcatus* tree-ring dataset from the Karkloof in KwaZulu-Natal (Hall, 1976), which falls in the summer rainfall region of southern Africa, is 180° out of phase with that of the *Widdringtonia cedarbergensis* tree-ring record of Dunwiddie and LaMarche (1980) from the winter rainfall region. Tyson (1999a) surmised that when changes driven primarily by tropical circulations extend sufficiently far south, the conditions experienced in the two regions have a positive correlation, as is the case when temperate or sub-polar westerly circulations expand sufficiently far north. However, if expansion in both cases is insufficient to cover the entire region, which is normally the case, conditions in these two regions are likely to correlate poorly or inversely, as at present. The changes in the non-seasonal rainfall region long the southern coastal areas of South Africa may be difficult to interpret due to influences from both the summer and winter rainfall regions (Tyson, 1999a).

Cool periods that occurred at both the Makapansgat Cold Air Cave and Cango Cave sites (such as the Little Ice Age at 300 BP and those at around 1150 BP at 1550 BP) lasted longer at the more southerly site, while warmer periods, such as the Medieval Warm Epoch, and the warming trends centred on 1350 BP and 1800 BP, extended for longer at the lower-latitude site, as shown in Figure 3.15. The Makapansgat and Cango II Cave datasets used by Tyson (1999a) were in calendar years before 1950 AD. The Little Ice Age began at the Cango II Cave site approximately a century before it began at Makapansgat, and ended approximately a century after. In contrast, the most prolonged period of warming at Makapansgat, which occurred between 1600 and 2000 BP, began around 200 years earlier at Makapansgat than at Cango, and ended around 100 years after. Climate model results (such as Rind and Overpeck, 1993) suggested a north-south gradient in climate change responses and this is consistent with the atmospheric model proposed by Tyson (1986), and later extended (Tyson, 1999a). The model indicates that an expansion of the circumpolar vortex of westerly winds, coupled with contraction of tropical easterlies, is associated with cooler and drier conditions, while the reverse coupled contraction and expansion of westerly and easterly winds is associated with warmer and wetter conditions. This model is described extensively in Chapter 5.

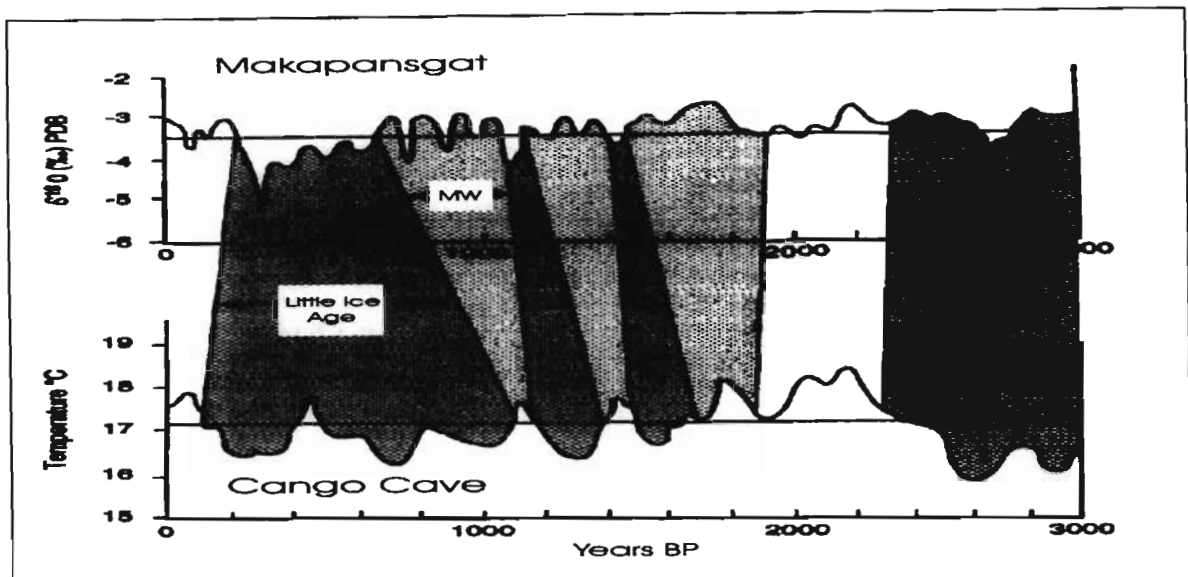


Figure 3.15 – Comparison of Makapansgat  $\delta^{18}\text{O}$  (expressed relative to the Pedee belemnite, PDB, standard) curve and Cango II Cave palaeotemperature curve, with MW = Medieval Warming (Tyson, 1999b, 345).

The times when the peaks and troughs in the Makapansgat and Cango records are  $180^\circ$  out of phase, such as at 700 BP and 1300 BP (Figure 3.15), are representative of instances when the tropical warming had reached the more northerly site with contraction of the circumpolar vortex, but had not extended sufficiently far south to reach southern South Africa. Alternatively, expansion of the westerlies northward had reached the more southerly site but not the more northerly site (Tyson, 1999a).

This model is further supported by the proposal of Scott (1993) that the Holocene Altithermal advanced southwards over the subcontinent as shown in Figure 3.16. This is indicative of a gradual southward progression of warmer, moister conditions associated with the expansion of the tropical easterlies.

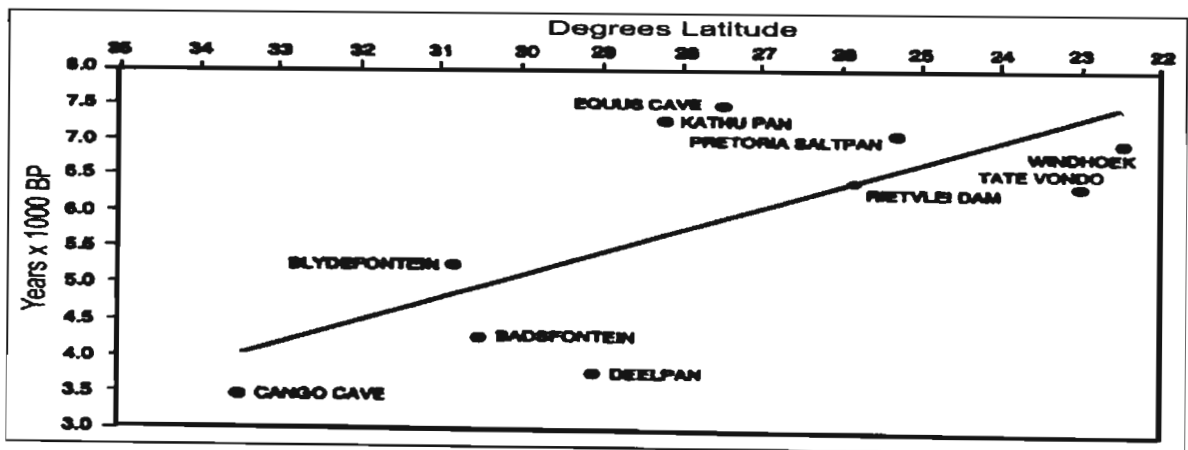


Figure 3.16 – Southward advance of Holocene Altithermal (Scott, 1993 in Tyson, 1999b, 341),

### 3.4.2 Africa

Tree-ring data series from southern African show a corresponding or inverse relationship with the Lake Naivasha, Kenya, record depending on the position of the site. For example, droughts between 450 BP and 400 BP (1500 and 1550 AD) and 200 and 150 BP (1750 and 1800 AD) in the record from Lake Naivasha (Verschuren *et al.*, 2000) are coincident with periods of favourable environmental conditions and strong growth in *Podocarpus falcatus* trees from KwaZulu-Natal (Hall, 1976) and Knysna (Thackeray, 1996; Thackeray and Potze, 2000). Similarly, lower tree growth at the two localities between 730 BP and 700 BP (1220 – 1250 AD), between 460 and 440 BP (1490 - 1510 AD) and between 130 and 100 BP (1820 – 1850 AD) correspond to higher lake levels in Lake Naivasha (Verschuren *et al.*, 2000). The Naivasha lake-level record (Verschuren *et al.*, 2000) and a *Widdringtonia cedarbergensis* tree-ring record (Dunwiddie and LaMarche, 1980) from the winter rainfall region of South Africa are more in phase, as is the present South African winter rainfall region's climate variability from the meteorological record (Lindesay and Vogel, 1990; Mason and Lindesay, 1993).

A clear correspondence between moist conditions and periods of reduced solar activity (the Wold, Sporer and Maunder Minima) has been observed in the Lake Naivasha region, with highest lake levels in the last 1100 years recorded during the Maunder Minimum (Verschuren *et al.*, 2000). In the Makapansgat record the opposite occurs, and most arid conditions occur during the Maunder Minimum (Tyson *et al.*, 2000; Tyson *et al.*, 2002b). Over Africa as a whole, the precessional low, which occurred at the beginning of the Holocene, is clearly evident in the inverse response of lakes on either side of a line 10 – 15° south of the equator. In the south, low lake levels indicate dry conditions associated with the weakening of incoming solar radiation while areas to the north show high lake levels, reflecting the northward shift in the position of the Inter-Tropical Convergence Zone (Tyson and Partridge, 2000). Once again these relationships are caused by the north-south shifts of the pressure belts and will be extended on in Chapter 5.

### 3.4.3 Global

The Makapansgat record (in calendar years before 2000 AD) has a high-resolution of approximately 10 years until 10 000 BP, followed by a hiatus and then an approximately

50 year resolution from 12 600 BP to 24 400 BP. This record is extremely valuable for comparison with other high-resolution records to ascertain the nature of teleconnections across the globe (Holmgren *et al.*, 2003). Many records for the southern hemisphere indicate strong teleconnections with southern Africa. For example, the cooling which occurred at approximately 320 BP (1630 AD) at Makapansgat is apparent in cave speleothem records (Wilson *et al.*, 1979) and dendrochronologies for New Zealand (Xiong, 1995) and north Patagonia in Argentina (Boninsegna, 1992), and in a Tasmanian tree-ring record (Cook *et al.*, 1991). It also correlates with  $\delta^{18}\text{O}$  values in the Quelccaya summit core from the Peruvian Andes (Thompson *et al.*, 1985) and a record of snow accumulation (Thompson, 1992) from the region for a similar time period.

Intervals of depleted  $\delta^{18}\text{O}$  in the Makapansgat record (Holmgren *et al.*, 2003), which occurred after approximately 23 500, at 19 000 BP and again after 15 500 BP, are consistent with shifts observed in the Mozambique Channel marine core record (Bard *et al.*, 1997). Similar trends are observed in the Taylor Dome ice-core record from Antarctica (Steig *et al.*, 2000), but not with exact temporal correspondence. Shifts in the Makapansgat record appear to lead those in the Antarctic cores but there are large error limits for the Pleistocene part of the Makapansgat record (Holmgren *et al.*, 2003), and thus further evidence of this teleconnection needs to be gathered before the lag rate can be securely established.

Teleconnections with sites in the northern hemisphere are also apparent. Cooling events dated at 525 BP (1475 AD) and 300 BP (1700 AD) were identified from an integrated temperature dataset derived from multivariate analysis of reliable high-resolution multiproxy data for the northern hemisphere as a whole (Mann *et al.*, 1998) and these events are evident in the Makapansgat record. Furthermore, the southern African precessional low, which occurred at the beginning of the Holocene, was associated with intensely evaporative conditions in the Makapansgat record (Holmgren *et al.*, 2003) amongst others (such as Partridge *et al.*, 1997; Scott *et al.*, 2003). This corresponds with the findings of Wang *et al.* (1999) from a speleothem record from China, but an inverse correlation is evident because of the location of the site in the northern hemisphere (Holmgren *et al.*, 2003).

The Rind and Overpeck (1993) model indicates that there are theoretical teleconnections between southern Africa and parts of Greenland and Scandinavia and this is evident, for example, in the correlation between the Greenland GISP2 ice core  $\delta^{18}\text{O}$  record (Alley *et al.*, 1997) and the Makapansgat isotope record over the last three millennia (Holmgren *et al.*, 2003). Holmgren *et al.* (1999) showed that centennial-scale warming and cooling episodes were similar at the two sites. Furthermore, the lowering of temperature at Makapansgat, that reached a minimum at 1700 AD, corresponds with a minimum in deuterium levels in a Greenland Ice Core Project (GRIP) record (Jouzel, 1998). Other extreme events in these records correspond closely and the same events in the last 1000 years are recorded in a dendrochronological study from northern Sweden (Briffa *et al.*, 1992).

### 3.5 SUMMARY

Very little is known of southern African palaeoclimates prior to the start of the Quaternary, approximately 2 million years ago. Although more is known of the Quaternary, reliably dated, continuous records for the southern African region rarely extend beyond the last 40 000 years – with the record from the Tswaing Crater, which extends beyond 200 000 BP (Partridge *et al.*, 1997), offering an obvious exception. From an analysis of a few carefully selected records, extending across sources and timescales, a number of common rainfall and temperature trends were detected for the last 40 000 years, clearly indicating that these trends were controlled by the interaction of the ocean and atmosphere on a regional scale.

When coincident fluctuations occurred across southern Africa, the nature of the relationship between sites was either corresponding or inverse. An investigation of these relationships made the nature of regional teleconnections apparent. A study of documented palaeoclimatic records from elsewhere in Africa and across the globe allowed for the detection of larger-scale teleconnections. While regional, short-term fluctuations appeared to be controlled by the seasonal north-south shifting of the pressure belts, global long-term teleconnections appeared to be controlled by the solar precession cycle or changes in solar activity. These teleconnections can now be explored in the context of established atmospheric models in Chapter 5.

## **4. PALAEOCLIMATIC ANALYSIS: THE GENERAL MODELS AND COMPARISONS**

### **4.1 INTRODUCTION**

The regional synthesis presented in Chapter 3 allowed for the detection of general palaeotemperature and palaeorainfall trends across the summer rainfall region of southern Africa. In this chapter, generalised temperature and rainfall models for the summer rainfall region are presented, as well as the results of their comparison with a 6600 year stalagmite record from Makapansgat and a 10 000 year palynological record from Wonderkrater. A 100 year coral record is presented to show climate changes over the short-term and this record is compared with recorded climatic variables.

### **4.2 METHODOLOGY**

#### **4.2.1 Regional Rainfall and Temperature Models**

The aim of this section is to extract and plot the dominant southern Africa climatic trends of the last 40 000 years on an original timeline based on the synthesis of existing data. The climatic records derived from the Karkloof, Cedarberg and Knysna tree-ring studies, from the Verlorenvlei, Border Cave, Boomplaas Cave and Tswaing Crater physical and biological analyses of sediment, from the Wonderkrater palynological study, from the Makapansgat Cold Air Cave, Lobatse II Cave and Cango II Cave stalagmite isotope analyses, and from various other documented studies, were utilised in the search for general climatic trends. These general trends appear to be representative of the summer rainfall region of southern Africa, and thus exclude the winter rainfall areas of the Western Cape and the non-seasonal rainfall region along the southern coast. Despite being summer rainfall regions, the trends do not necessarily comply with records from the Kalahari and Namib due to their general lack of correspondence with the remainder of the summer rainfall region.



An attempt was made to provide a scale of change when the palaeoclimatic records in the literature provided estimated rainfall and temperature values. However these values were indicative of local conditions of the site and are not necessary applicable to the entire region. Thus a qualitative interpretation of these curves is necessary, and they should be viewed as generalised models of maxima and minima over time.

#### **4.2.2 Back-projection of Climatic Variables for Sodwana Bay and Makapansgat**

Pearson product-moment correlation coefficients indicated the strength of the linear relationship (MATLAB, 2004) between the Sodwana Bay and Makapansgat (Holmgren *et al.*, 2003) proxy-records and various climatic variables. If a high correlation was established, a linear least squares regression analysis was performed to determine the mathematical relationship between the palaeoclimate record and the recorded variable. A back-projection of the data over the length of the proxy-record was then possible. In the case of the Sodwana Bay coral data, the back-projections were compared with various other recorded and modelled datasets. In the case of the Makapansgat data, these back-projections were compared with the general models of southern African annual mean temperature and rainfall developed from the regional synthesis, as described in Section 4.2.1.

#### **4.2.3 Principal Component Analysis of Wonderkrater Pollen Data**

One of the difficulties in multivariate statistics is the visualisation of a multivariate dataset. In a dataset with many variables, groups of variables often change together such that multiple variables can be related by one or a few factors that explain the overall behaviour of the system. In many systems there are only a few such driving forces and the dataset can be made more compact through the substitution of a group of variables with a single variable (MATLAB, 2004). Principal components analysis (PCA) is a quantitatively rigorous method for achieving this simplification through the generation of a set of variables called 'principal components' (MATLAB, 2004). Each principal component is a linear combination of the original variables. The principal components are all orthogonal to each other in order to limit redundancy (MATLAB, 2004).

The first principal component is a single axis in multidimensional space such that when the observations are projected onto this axis, a new variable is formed with maximum variance among all possibilities for the first axis. The second principal component is another axis in multidimensional space, perpendicular to the first, such that a projection of the observations onto this axis generates another new variable with greatest variance among all possible choices of this second axis. The full set of principal components is as large as the original set of variables, but usually one considers the first principal components that together exceed 80% of the total variance of the original data (MATLAB, 2004).

The Wonderkrater dataset comprised species abundance figures at various time intervals. As in Scott *et al.* (2003), a principal component analysis (PCA) of the pollen data was conducted, using MATLAB in this case. Through an examination of the new variables, it was possible to develop a deeper understanding of the driving forces that generated the original data. The first two principal components were compared with the general models of southern African annual mean temperature and rainfall developed from the regional synthesis as described in Section 4.2.1.

### **4.3 RESULTS AND DISCUSSION**

#### **4.3.1 General Models of Southern African Climate Change**

The synthesis of palaeoclimatic records allowed for the development of general rainfall and temperature models representative of the summer rainfall region of southern Africa. These models do not apply to the Kalahari and Namib, which tend to deviate from general trends of the rest of the summer rainfall region.

##### *4.3.1.1 Temperature*

The general model of southern Africa annual mean temperature derived from the regional synthesis is shown in Figure 4.1. Between 40 000 and 30 000 BP, temperatures were low but higher than during the Last Glacial Maximum. This is a phase of increasing temperature, increasing to a point slightly higher than that of today. The period from 30 000 to 25 000 BP was a phase of decreasing temperatures across the region. Over various

parts of the region, there is evidence that temperatures dropped to levels 4 – 5 °C lower than at present. Between 25 000 and 21 000 BP, cool conditions continued with a small rise in temperature before 22 000 BP followed by continued cooling. The general temperature curve clearly indicates the Last Glacial Maximum at approximately 18 000 BP when the lowest mean temperatures over the 40 000 period occurred. Temperatures of 5 – 6 °C less than the present mean occurred in most regions.

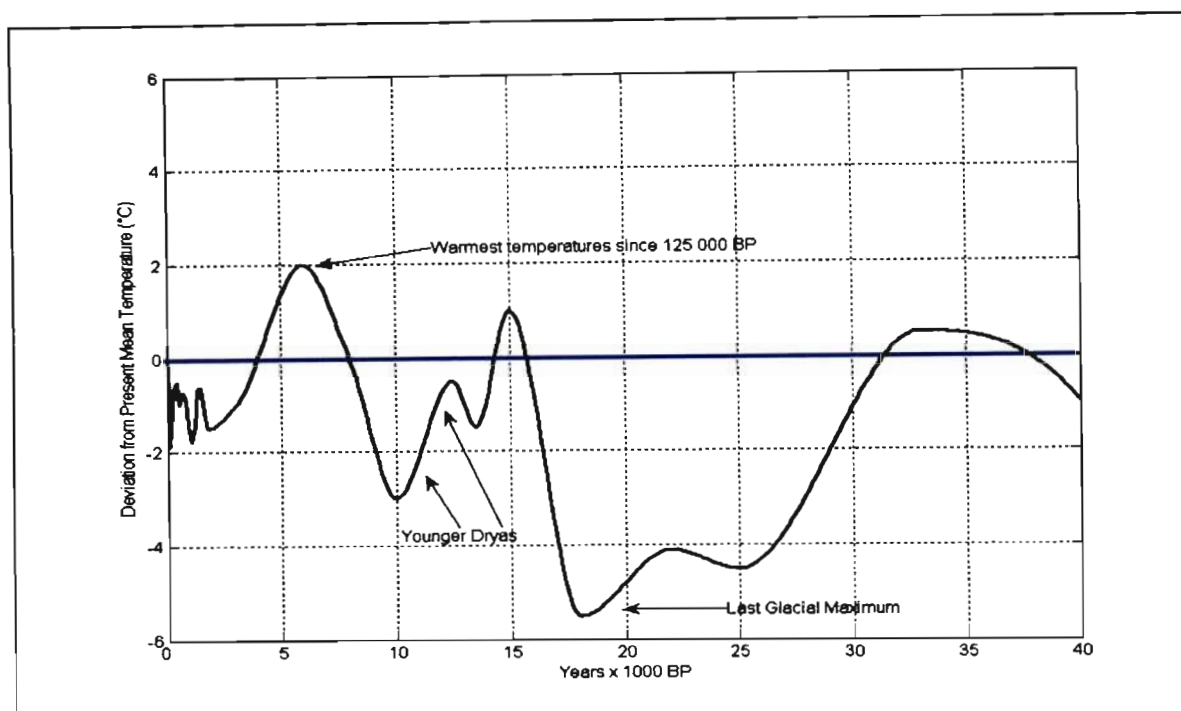


Figure 4.1 – General model of southern African annual mean temperature for the last 40 000 years.

Rapid warming occurred after 17 000 BP until cooling recommenced at approximately 15 000 BP associated with the Antarctic Cold Reversal. Renewed warming occurred after about 13 500 BP. Temperatures were lower than at present, but continued to increase until a sudden cooling took place before 12 000 BP associated with the Younger Dryas. Between 12 000 and 10 000 BP, continued cooling occurred followed by warming and moistening from about 10 000 BP. Conditions were warmer than at present by about 8000 BP with highest temperatures since 125 000 BP experienced at around 6000 BP. Thereafter cooling occurred, reaching a local minimum by around 3000 BP.

Temperatures stayed within 2 °C less than mean over the last 5000 years. Conditions were warm and moist between 4300 to 3200 BP, with cooling between 3000 and 1750 BP, followed by warming until 1400 BP, and cooling until 1100 BP. Conditions then grew

warmer until 700 BP (1250 AD) followed by cooling until 150 BP (1800 AD), with a slightly warmer period from 500 to 300 BP (1450 to 1650 AD). Warming has continued until the present and at around 250 BP (1700 AD) mean annual temperatures were about 1 °C cooler than at present.

Selected sources that support various trends in the model are indicated in Figure 4.2.

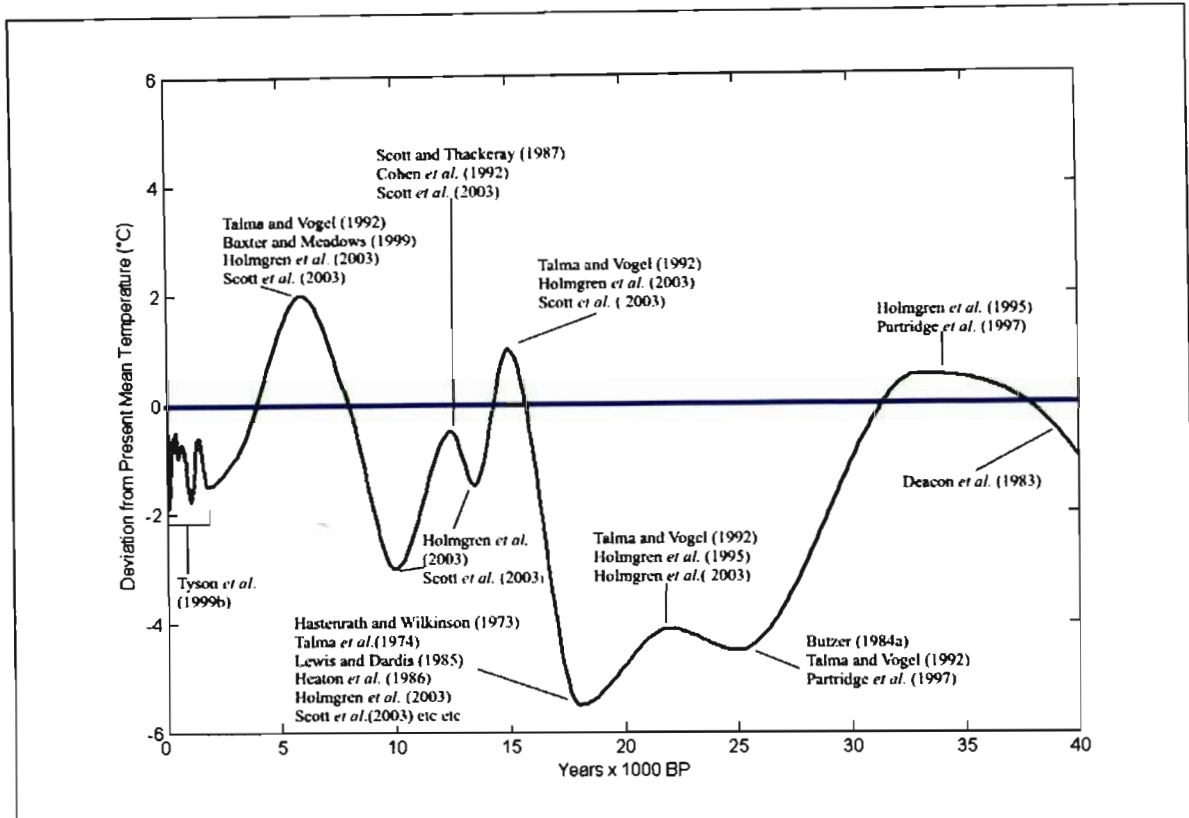


**Figure 4.2 – Southern Africa regional corroboration of major events in general model of southern African annual mean temperature for the last 40 000 years.**

Tyson (1999b) synthesised the findings of the Makapansgat Valley into a regional palaeoclimatology for the summer rainfall region for the last 3000 years, and this is shown in Figure 4.3, also with corroborating data sources indicated. The Medieval Warming from approximately 1100 to 700 BP (900 to 1300 AD) is evident in Figure 4.2 and Figure 4.3. The regional manifestation of the Little Ice Age from 700 to 150 BP (1300 to 1850 AD), with some warming between 500 and 300 BP (1500 to 1700 AD), is also apparent.

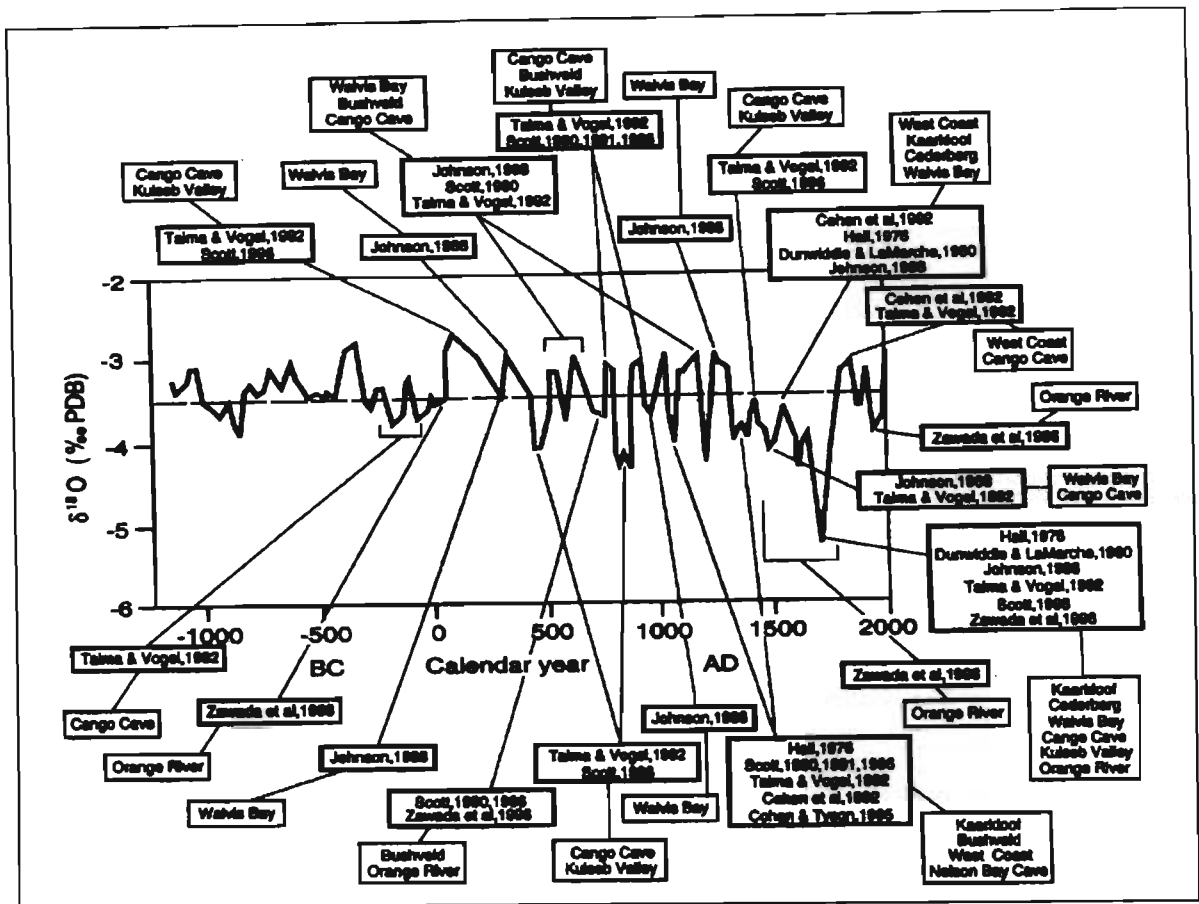


Figure 4.3 – Southern African regional corroboration of major events in the Makapansgat  $\delta^{18}\text{O}$  record over the last 3000 years (Tyson, 1999b, 344).

#### 4.3.1.2 Rainfall

The general model of southern African annual mean rainfall for the summer rainfall region is shown in Figure 4.4. Between 40 000 and 30 000 BP, conditions were moister than at present, during at least the latter part of this period. During the period from 30 000 to 25 000 BP, conditions grew drier. Between 25 000 and 21 000 BP, the region remained dry but there is evidence of increasing moisture towards the end of this period followed by renewed drying at 21 000 BP. At Tswaing Crater, rainfall was less than 75% of present annual mean rainfall by 17 500 BP. There is evidence an increase in moisture from 18 000 BP, peaking at approximately 15 000 BP with drying until about 13 500 BP when a short-lived increase in rainfall occurred in some areas. Thereafter drying continued until 10 000 BP.

At 10 000 BP the region was generally moistening, but there is some evidence of continued dry conditions during the early part of the Holocene in the eastern and southern parts.

Rainfall was still lower than presently at Makapansgat between 9000 and 8400 BP. By 7000 BP, however, even the arid interior was moister than presently, which persisted until about 4000 BP. From 4000 BP to the present, there were only minor fluctuations in rainfall. Moistening conditions were experienced from about 1500 until 1200 BP, and drying until 1100 BP. Conditions then grew moister until 700 BP (1250 AD) followed by drying until 150 BP (1800 AD). Moisture availability has increased from this point until the present.

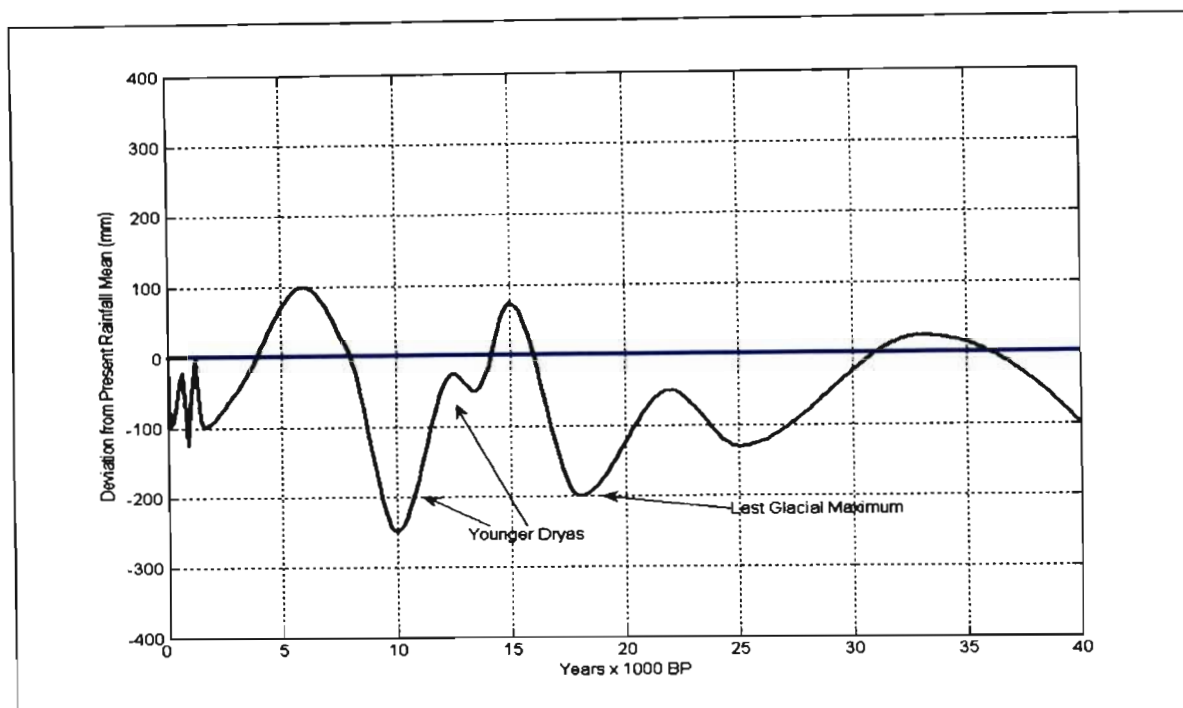


Figure 4.4 – General model of southern African annual mean rainfall for the last 40 000 years.

The general model of southern African annual mean rainfall generally correlates with the general model of southern African annual mean temperature with warmer temperatures associated with higher rainfall. An exception to this general trend can be seen when comparing the Younger Dryas with the Last Glacial Maximum in the Makapansgat and Wonderkrater curves in Figure 4.5. There was a cessation of drip at Makapansgat at the Younger Dryas but drip continued through the Last Glacial Maximum, suggesting that it may have been drier and more evaporative during the Younger Dryas than at the Last Glacial Maximum. Moisture levels at Wonderkrater at the Last Glacial Maximum and during the Younger Dryas were similar. However, temperature records for both sites clearly indicate cooler temperatures for the Last Glacial Maximum compared to the Younger Dryas.

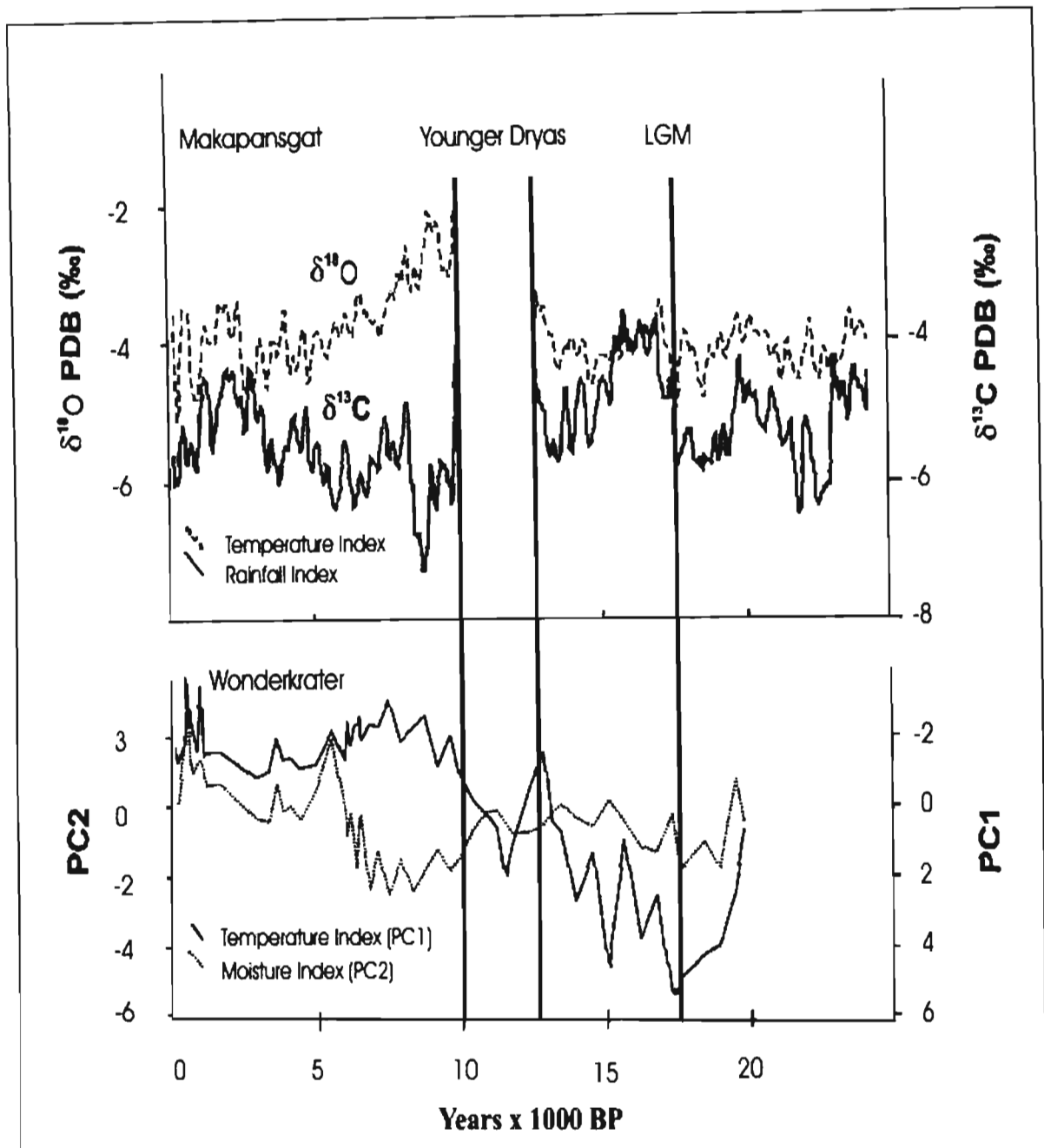


Figure 4.5 – Temperature curves,  $\delta^{18}\text{O}$  and PC1, and moisture curves,  $\delta^{13}\text{C}$  and PC2, for Makapansgat and Wonderkrater respectively. Younger Dryas and Last Glacial Maximum (LGM) are labelled. Note that temperatures increase between the LGM and the Younger Dryas, while moisture levels decrease in the Makapansgat record and remain similar in the Wonderkrater record (adapted from Scott *et al.*, 2003, 487).

#### 4.3.2 A Climatic Record for the Last 116 Years from Sodwana Bay

Short-term climatic fluctuations at a seasonal resolution are evident in the coral record from Sodwana Bay.

#### 4.3.2.1 Calcification and Temperature

Ramsay (1994) proposed that the low density coral bands are formed during the late austral summer (February – March) in the Sodwana Bay region. For ease of analysis, regular time intervals were required and the high density bands were assumed to form in the austral winter (May to October) and the low density bands during the austral summer (November to April). A similar assumption was made in the study by Bessat and Buiges (2001).

A negative correlation exists between the mean seasonal coral calcification rate along the growth axis of the core and mean seasonal recorded sea-surface temperatures for Richards Bay. A correlation between temperature and calcification also was detected in the studies of Lough and Barnes (1997; 2000) and Bessat and Buiges (2001). The statistics of the correlation and regression analysis are shown in Table 4.1.

**Table 4.1 – Statistics of the correlation between calcification and sea-surface temperature**

x	Mean calcification
y	Mean sea-surface temperature for Richards Bay
r	-0.95
r <sup>2</sup>	0.90
Degrees of freedom (dof)	25
Calculated t-value	19.99
Critical t-value (25 dof, 95% confidence level)	1.71
Mathematical relationship	$y = -0.00018 (x) + 27.52$
Calculated F-value	418.12
Critical F-value (1 dof in numerator, 25 dof in denominator, 95% confidence level)	4.24

A one-tailed Student's t-test was conducted to determine whether the correlation coefficient indicates a statistically significant relationship between the two variables. The calculated t-value of 19.99 is greater than the critical value ( $p = 0.95$ ) of 1.71 for 25 degrees of freedom. Therefore one can accept that there is a statistically significant relationship between the two variables.



A linear regression analysis was conducted to determine the mathematical relationship between the two variables. This regression analysis accounted for 90% of the variance. A Fischer's Test (F-test) was conducted to determine whether the observed relationship between the dependent and independent variables occurred by chance. The F-value for this regression analysis was 418.82, which indicated a probability of  $4.01 \times 10^{-17}$  that this relationship occurred by chance. Furthermore, the critical F-value ( $p = 0.95$ ) for 1 degree of freedom in the numerator, and 25 degrees of freedom in the denominator is 4.24. The calculated F-value of 418.12 is greater than 4.24 and therefore it is extremely unlikely that the relationship occurred by chance.

A comparison of the back-projected sea-surface temperature and modelled values (NOAA-CIRES, 2000) is shown in Figure 4.6. The projected sea-surface temperature curve indicates a gradual increase in temperature since the early 19<sup>th</sup> century until the present, which is reflection of the global warming trend across the globe. Similar results are shown in Figure 4.9 in the correlation between air temperature and calcification.

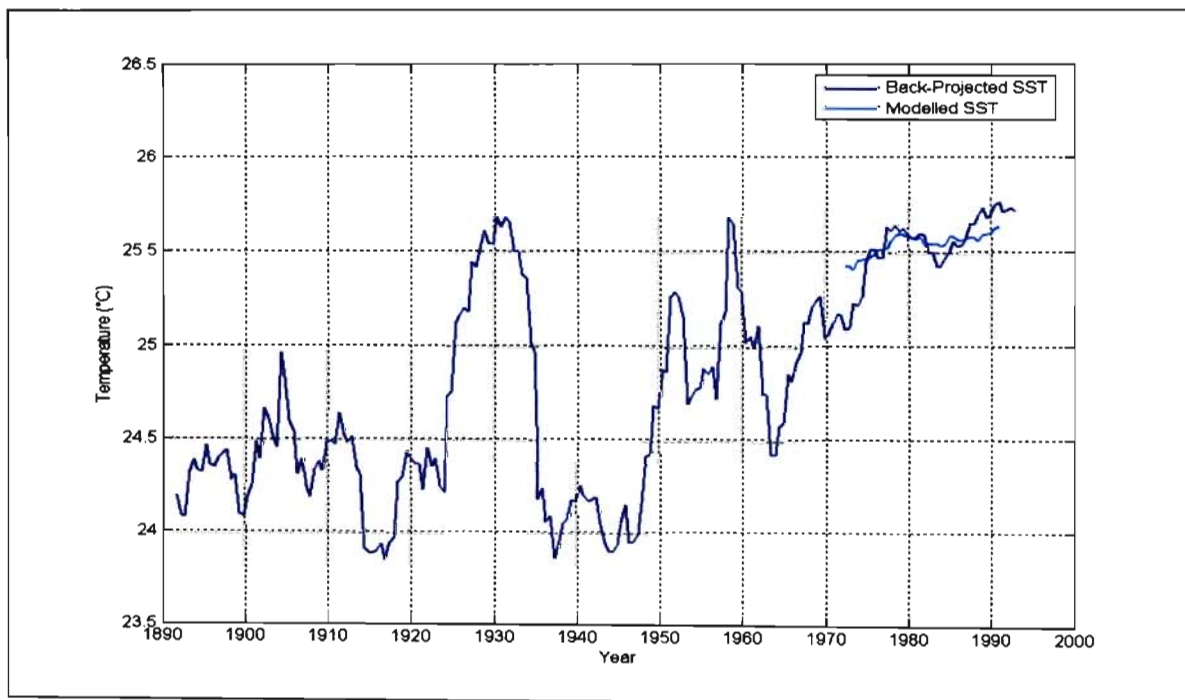


**Figure 4.6 – Comparison of sea-surface temperatures (SST) back-projected from coral calcification and modelled sea-surface temperatures (SST) (NOAA-CIRES, 2000).**

The influence of El Nino on sea-surface temperatures over southern African is clear in the correlation between back-projected sea-surface temperatures and the Southern Oscillation

Index anomalies over the extent of the coral record (Figure 4.7). Since there is a clear correspondence between the Southern Oscillation Index and sea-surface temperatures off the KwaZulu-Natal coast, it is expected that El Nino cycles will be detected in the analysis of cyclicity of the coral dataset in Chapter 6.

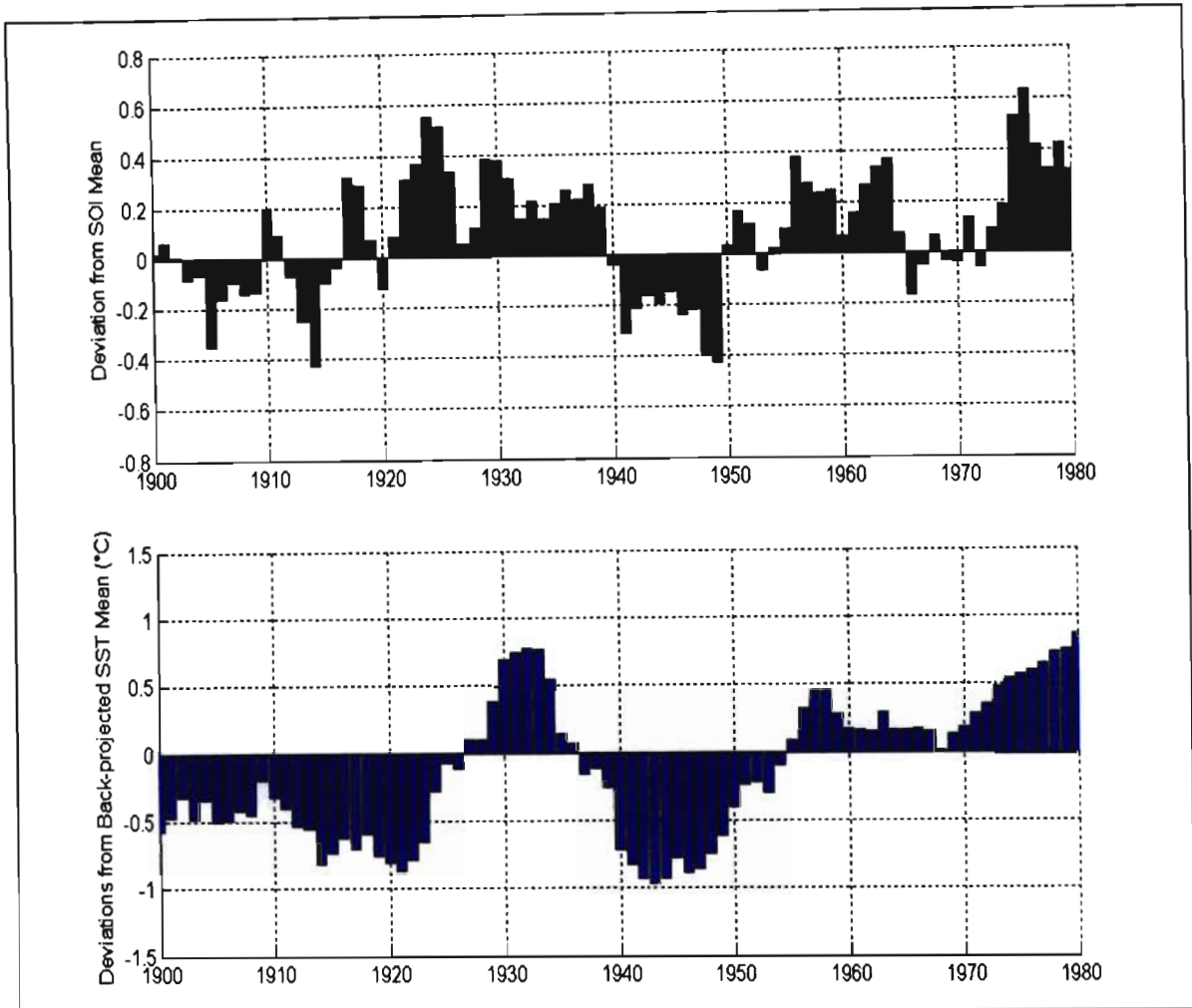


**Figure 4.7 – Comparison of sea-surface temperature (SST) anomalies back-projected from coral calcification and Southern Oscillation Index (SOI) anomalies (NCAR, 2005).**

Seasonal mean air temperatures for Cape St. Lucia were negatively correlated with the coral’s seasonal mean calcification rate. It was calculated that a five year running mean of air temperature produced the closest correlation with calcification (Figure 4.8). This is indicative of the ocean taking longer than air to warm up and cool down due to water having a high thermal capacity.

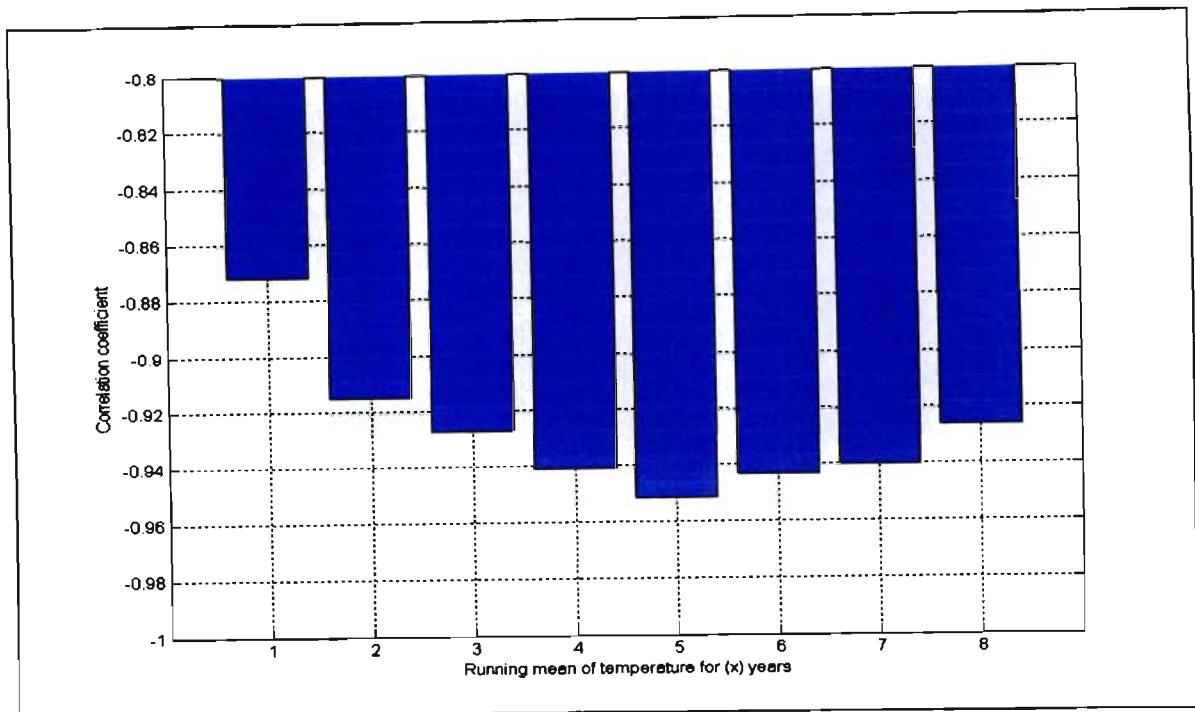


**Figure 4.8 – Correlation between calcification values and air temperature running means with a peak at a 5 year running mean**

The statistics of the correlation and regression analysis of a 5 year running mean of air temperature for Cape St. Lucia (calculated seasonally) and seasonal mean coral calcification values are shown in Table 4.2.

**Table 4.2 - Statistics of the correlation between calcification and air temperature**

x	Mean calcification
y	Five year running mean of air temperature for Cape St. Lucia
r	-0.95
r <sup>2</sup>	0.89
Degrees of freedom (dof)	55
Calculated t-value	21.18
Critical t-value (55 dof, 95% confidence level)	1.67
Mathematical relationship	$y = -0.00021 (x) + 28.37$
Calculated F-value	454.31
Critical F-value (1 dof in numerator, 55 dof in denominator, 95% confidence level)	4.02

A one-tailed t-test was conducted to determine whether the correlation coefficient indicates a statistically significant relationship between the two variables. The calculated t-value of 21.18 is greater than the critical value ( $p = 0.95$ ) of 1.67 for 55 degrees of freedom. One can thus accept that there is a statistically significant relationship between the two variables.

A linear regression analysis was conducted to determine the mathematical relationship between the two variables. This regression analysis accounted for 89% of the variance. An F-test was conducted to determine whether the observed relationship between the dependent and independent variables occurred by chance. The F-value for this regression analysis was 454.31 which indicated a probability of  $2.96 \times 10^{-28}$  that this relationship occurred by chance. Furthermore, the critical F-value ( $p = 0.95$ ) for 1 degree of freedom in the numerator, and 55 degrees of freedom in the denominator is 4.02. The calculated F-value of 454.31 is greater than 4.15 and therefore it is extremely unlikely that the relationship occurred by chance.

The back-projected and recorded air temperature records are shown in Figure 4.9.

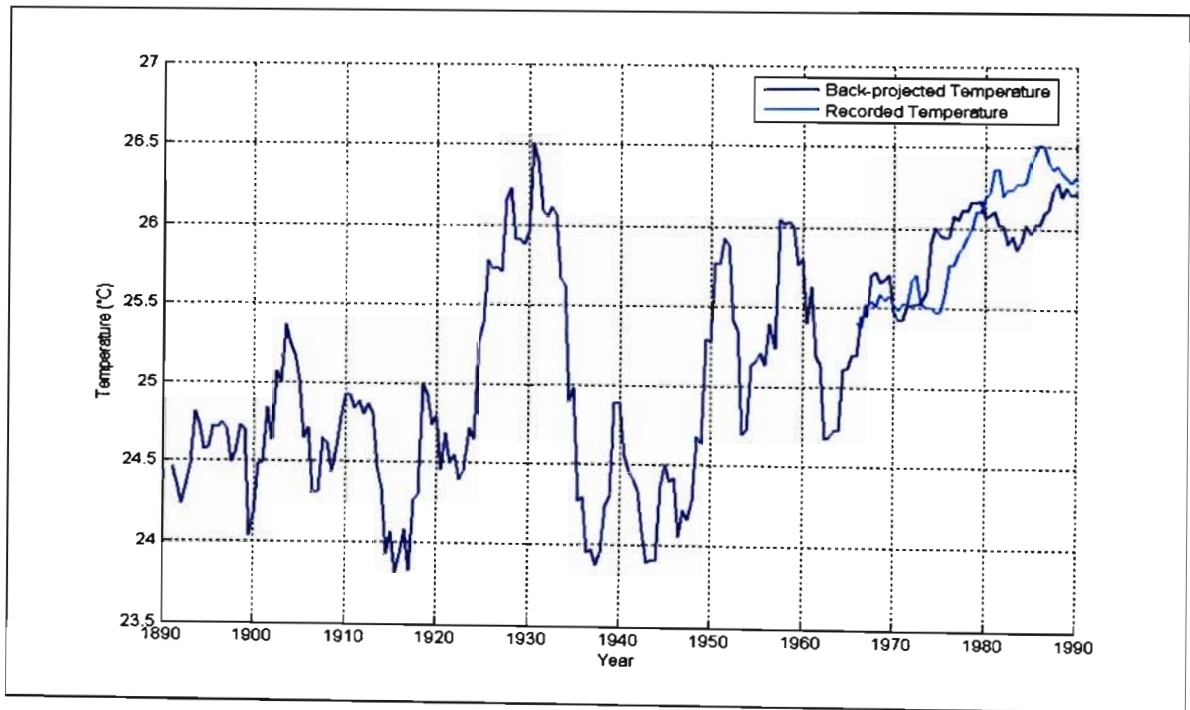


Figure 4.9 – Comparison of back-projected air temperatures from coral calcification and recorded air temperatures (SAWS, 2005).

According to Tyson and Preston-Whyte (2000), warmest conditions in the meteorological record for South Africa as a whole occurred in the 1920s and this is clearly indicated in the temperature peak in the late 1920s and early 1930s in Figure 4.9. Tyson and Preston-Whyte (2000) describe a drop in temperature in the 1960s which is also represented in the back-projected temperature record from the coral calcification rate. The authors propose that over the period from 1861 to 1980, the southern hemisphere's averaged combined land-marine temperature rose by 0.48 °C and the regionally averaged South African surface rock temperatures rose by 0.67 °C. This rise in temperature is clearly indicated in Figure 4.9 with mean air temperatures for the Sodwana Bay site increasing by more than 1.5 °C between 1893 and 1990. This temperature increase has been related to global warming (Tyson and Preston-Whyte, 2000).

Decadal surface rock temperature profiles indicate that surface temperatures over southern Africa since 1850 have followed hemispheric trends (Tyson and Preston-Whyte, 2000) as shown in Figure 4.10. The South African temperature curve correlates well with the coral-derived temperature record. The South African temperature curve indicates a peak between 1920 and 1930, which corresponds with the peak in the coral-derived record at approximately 1930 in Figure 4.9, and a second peak centred at 1960, which corresponds with the peaks between 1950 and 1960 in Figure 4.9.

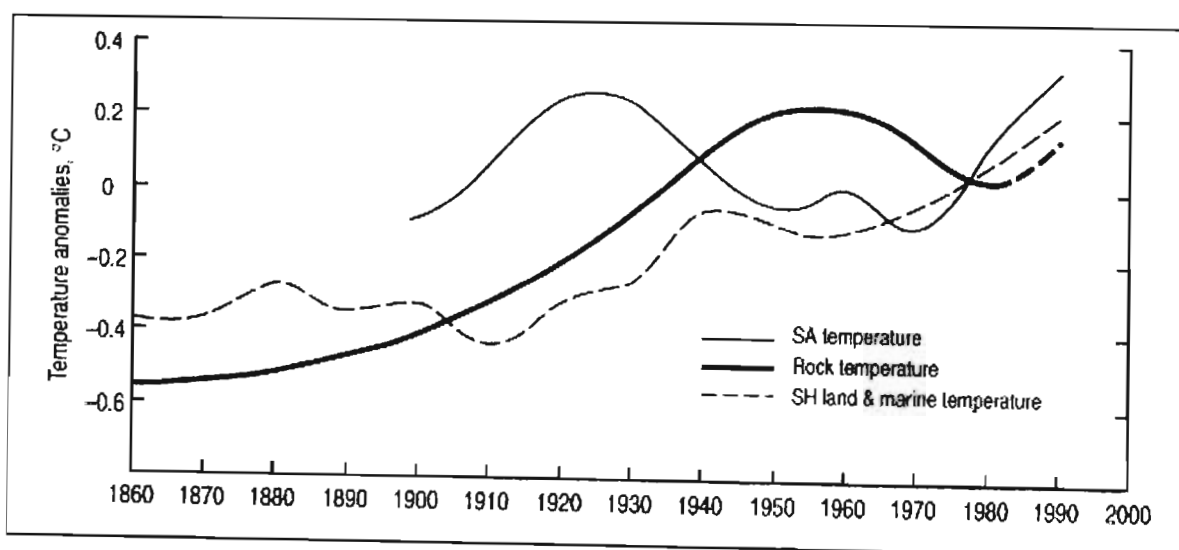


Figure 4.10 – Decadal southern hemisphere combined land-sea temperatures compared with South African regional maximum annual air temperature and borehole-derived surface rock temperature anomalies (Tyson and Preston-Whyte, 2000, 324).

#### 4.3.2.2 Length and Rainfall

A positive correlation exists between seasonal mean changes in length along the coral core growth axis and seasonal mean recorded rainfall for Cape St. Lucia. The statistics of the correlation and regression analysis are shown in Table 4.3

**Table 4.3 – Statistics of the correlation between length and rainfall**

x	Mean change in length
y	Mean rainfall for Cape St. Lucia
r	0.81
r <sup>2</sup>	0.65
Degrees of freedom (dof) in the denominator	85
Calculated t-value	11.03
Critical t-value (85 dof, 95% confidence level)	1.66
Mathematical relationship	$y = 37.62(x) + 89.55$
Calculated F-value	126.32
Critical F-value (1 dof in numerator, 85 dof in denominator, 95% confidence level)	3.95

A one-tailed t-test was conducted to determine whether the correlation coefficient indicates a statistically significant relationship between the two variables. The calculated t-value of 11.03 is greater than the critical value ( $p = 0.95$ ) of 1.66 for 85 degrees of freedom. Therefore one can accept that there is a statistically significant relationship between the two variables.

A linear regression analysis was conducted to determine the mathematical relationship between the two variables. This regression analysis accounted for 65% of the variance. An F-test was conducted to determine whether the observed relationship between the dependent and independent variables occurred by chance. The F-value for this regression analysis was 126.32 which indicated a probability of  $1.72 \times 10^{-18}$  that this relationship occurred by chance. Furthermore, the critical F-value ( $p = 0.95$ ) for 1 degree of freedom in the numerator and 85 degrees of freedom in the denominator is 3.95. The calculated F-

value of 126.32 is greater than 3.95 and therefore it is extremely unlikely that the relationship occurred by chance.

Back-projected rainfall is compared with recorded rainfall (SAWS, 2005) in Figure 4.11. The back-projection corresponds well with the rainfall record presented by Tyson and Preston-Whyte (2000) for the last 100 years gathered through an analysis of historical and meteorological records. The rainfall peak between 1910 and 1920 is indicative of the wet period of 1916 – 1924 (Tyson and Preston-Whyte, 2000). Rainfall then drops during the 1920s, indicative of the dry period in the overall southern African record extending from 1925 – 1932. The slight rainfall drop at around 1940 may be a local manifestation of the dry spell extending from the 1940s to early 1950s (Tyson and Preston-Whyte, 2000). Increasing moisture in the 1950s is representative of the moist spell indicated from 1953 (Tyson and Preston-Whyte, 2000). Tyson and Preston-Whyte (2000) suggest that the lowest rainfall year over the region during the period 1905 to 1981, was during the year 1932 – 1933, which is co-incident with the lowest back-projected rainfall values across the period of the coral record.

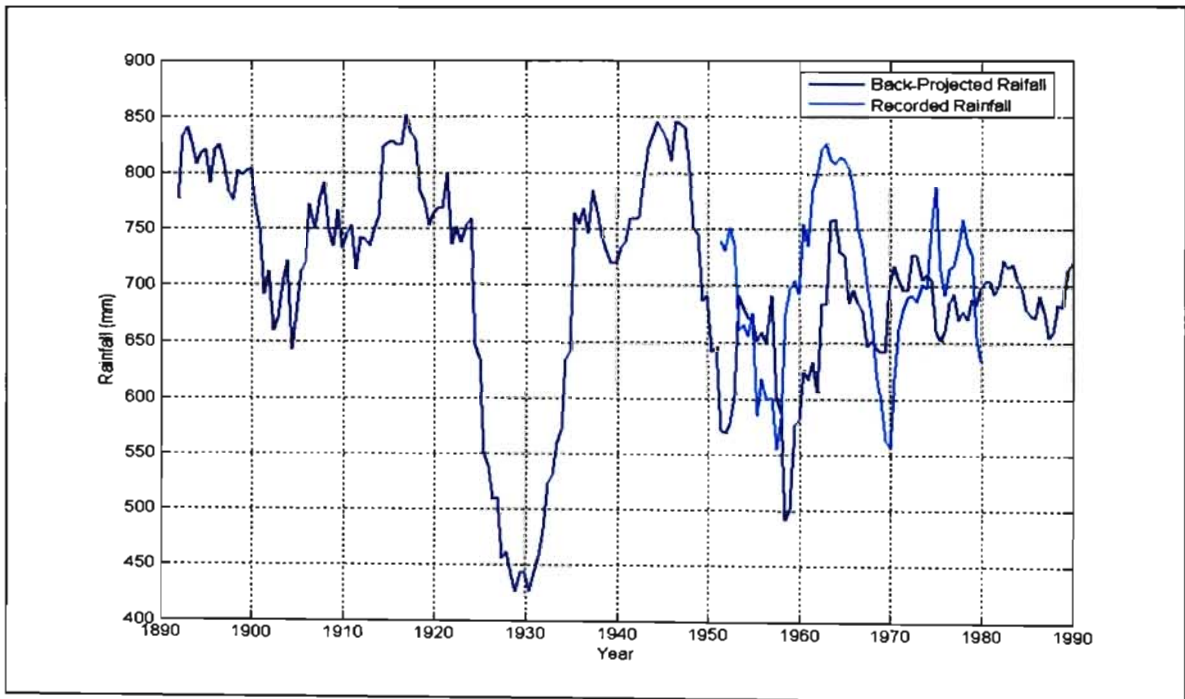


Figure 4.11 - Comparison of back-projected rainfall from coral length and recorded rainfall (SAWS, 2005).

The back-projections appear to offer a qualitative guide to rainfall changes over the record, indicating maxima and minima but not necessarily providing accurate rainfall values.

### 4.3.3 A Climatic Record for the Last 6600 Years from Makapansgat

#### 4.3.3.1 $^{18}\text{O}$ and Temperature

A high correlation exists between the ten year mean of daily maximum temperature for Makopane and  $^{18}\text{O}$  isotope concentration, with decadal resolution, in the stalagmite. The statistics of the correlation and regression analysis are shown in Table 4.4.

**Table 4.4 - Statistics of the correlation between  $^{18}\text{O}$  and mean daily maximum air temperature**

x	$^{18}\text{O}$
y	Mean daily maximum air temperature for Makopane
r	0.96
$r^2$	0.93
Degrees of freedom (dof) in the denominator	5
Calculated t-value	5.03
Critical t-value (5 dof, 95% confidence level)	2.02
Mathematical relationship	$y = -1.97(x) + 14$
Calculated F-value	25.31
Critical F-value (1 dof in numerator, 5 dof in denominator, 95% confidence level)	6.61

A one-tailed t-test was conducted to determine whether the correlation coefficient indicates a statistically significant relationship between the two variables. The t-value of 5.03 is greater than the critical value ( $p = 0.95$ ) of 2.02 for 5 degrees of freedom. Therefore one can accept that there is a statistically significant relationship between the two variables.

A linear regression analysis was conducted to determine the mathematical relationship between the two variables. This regression analysis accounted for 93% of the variance. An F-test was conducted to determine whether the observed relationship between the dependent and independent variables occurred by chance. The critical F-value ( $p = 0.95$ ) for 1 degree of freedom in the numerator, and 5 degrees of freedom in the denominator is



6.61. The calculated F-value of 25.31 is greater than 6.61, and therefore it is unlikely that the relationship occurred by chance.

The relationship established between the variables allowed a back-projection of the annual mean maximum daily temperature over 6600 years as shown in Figure 4.12. The back-projection indicates a deviation of less than 3 °C about the mean over the last 6600 years. There is evidence of cooling between 3800 and 2900 BP, warming until around 2700 BP followed by cooling until around 2200 BP, warming until 1600 BP, cooling until 1200 BP, then warming until 700 BP. This was followed by cooling until 500 BP and warming until 300 BP, cooling until 150 BP, and warming until present. The back-projection indicates the Climatic Optimum between 6000 and 5800 BP, and a temperature minimum at approximately 2900 BP, which is also the temperature minimum in the Wonderkrater record. The back-projection shows evidence of the Medieval Warming (1100 to 700 BP) and the Little Ice Age (700 – 150 BP), albeit with a warming period between 500 and 300 BP.

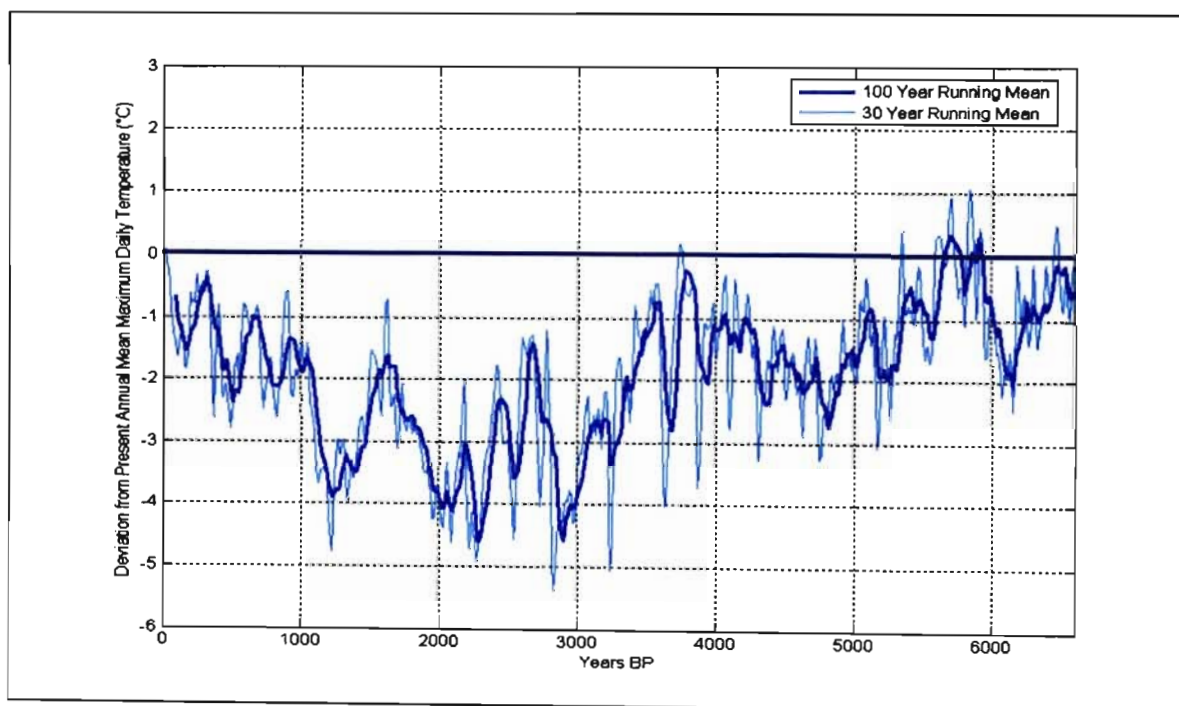


Figure 4.12- Back-projection of the deviation from present annual mean maximum daily temperatures (0) over 6600 years for Makapansgat.

A comparison of the back-projected mean maximum daily temperatures over 6600 years and the general model of southern African annual mean temperature is shown in Figure

4.13. The model and the back-projected temperatures are not expected to match exactly as the model reflects general trends across southern Africa.

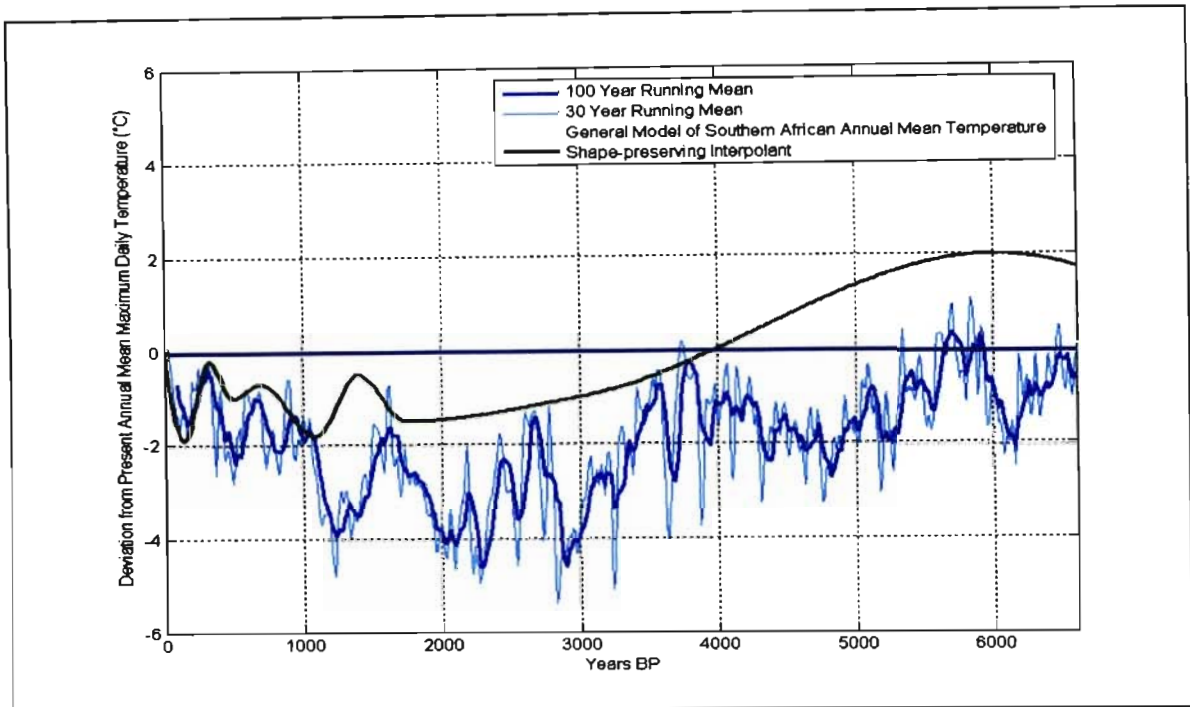


Figure 4.13 – Comparison of the back-projected record of deviation from present annual mean of maximum daily temperature (0) for Makapansgat and the general model of southern African annual mean temperature.

The proxy-record shows a trend of decreasing temperatures from about 6000 BP to a minimum at roughly 3000 BP, which agrees with the general model of southern African annual mean temperature. Both records show the Climatic Optimum at around 6000 BP and a local temperature peak at around 1500 BP followed by decreasing temperatures until around 1100 BP. The rise in temperature between 1100 and 700 BP in the model and back-projected record is comparable. The general drop in temperature from 700 BP until 150 BP (with an increase between approximately 500 and 330 BP) associated with the Little Ice Age is also evident.

#### 4.3.3.2 $^{13}\text{C}$ and Rainfall

A high correlation was calculated between the ten year mean of January rainfall (highest rainfall month for the region) for Makopane and  $^{13}\text{C}$  isotope concentration, with decadal resolution, of the stalagmite. The statistics of the correlation and regression analysis are shown in Table 4.5

**Table 4.5 - Statistics of the correlation between  $^{13}\text{C}$  and mean January rainfall**

x	$^{13}\text{C}$
y	Mean January rainfall for Makopane
r	0.97
$r^2$	0.93
Degrees of freedom (dof) in the numerator	1
Degrees of freedom (dof) in the denominator	5
Calculated t-value	6.44
Critical t-value (5 dof, 95% confidence level)	2.02
Mathematical relationship	$y = -60.75(x) - 149.86$
Calculated F-value	41.53
Critical F-value (1 dof in numerator, 5 dof in denominator, 95% confidence level)	6.61

A one-tailed t-test was conducted to determine whether the correlation coefficient indicates a statistically significant relationship between the two variables. The t-value of 6.44 is greater than the critical value ( $p = 0.95$ ) of 2.02 for 5 degrees of freedom. Therefore one can accept that there is a statistically significant relationship between the two variables.

A linear regression analysis was conducted to determine the mathematical relationship between the two variables. This regression analysis accounted for 93% of the variance. An F-test was conducted to determine whether the observed relationship between the dependent and independent variables occurred by chance. The calculated F-value of 41.53 is greater than the critical F-value ( $p = 0.95$ ) of 6.61, therefore it is extremely unlikely that the relationship occurred by chance.

The calculated relationship between the variables was used to back-project rainfall over 6600 years as shown in Figure 4.14. Major rainfall minima occurred at approximately 4100 BP, 3200 BP, 2500 BP, 2100 BP, and at 800 BP. Rainfall maxima are indicated at approximately 4500 BP, 4300 BP, 3000 BP, 2800 BP, 1000 BP and 300 BP.

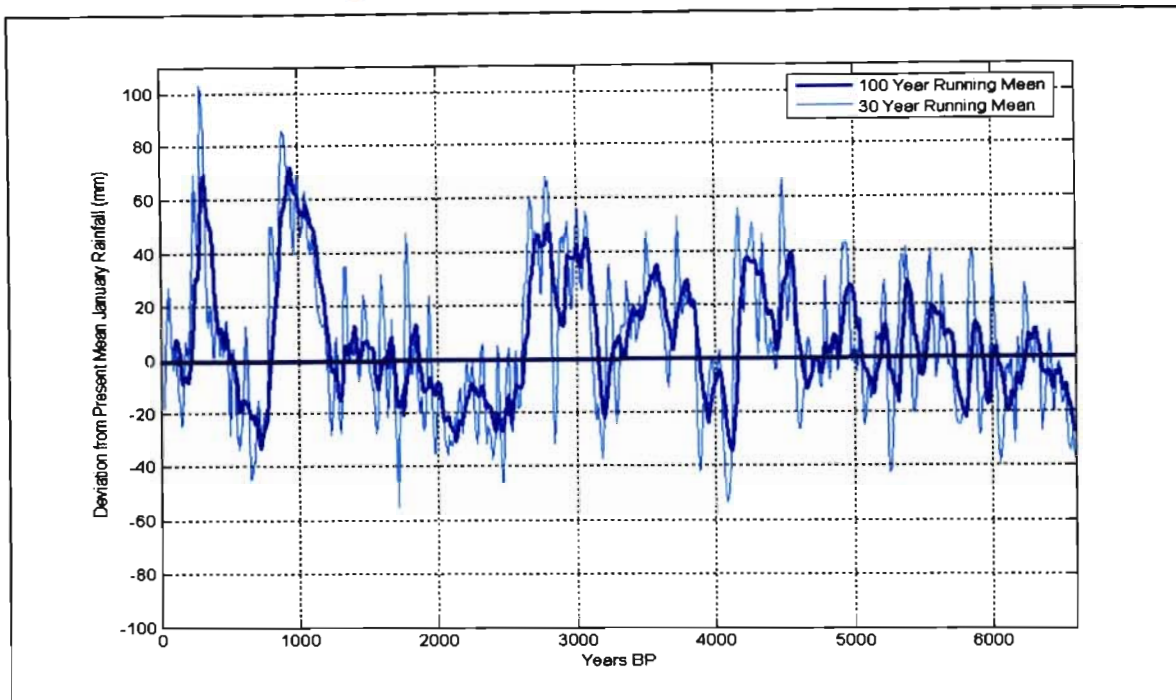


**Figure 4.14 – Back-projection of deviation from present mean January rainfall (0) over 6600 years for Makapansgat.**

The general model of southern African annual mean rainfall is compared with the back-projected rainfall curve in Figure 4.15.

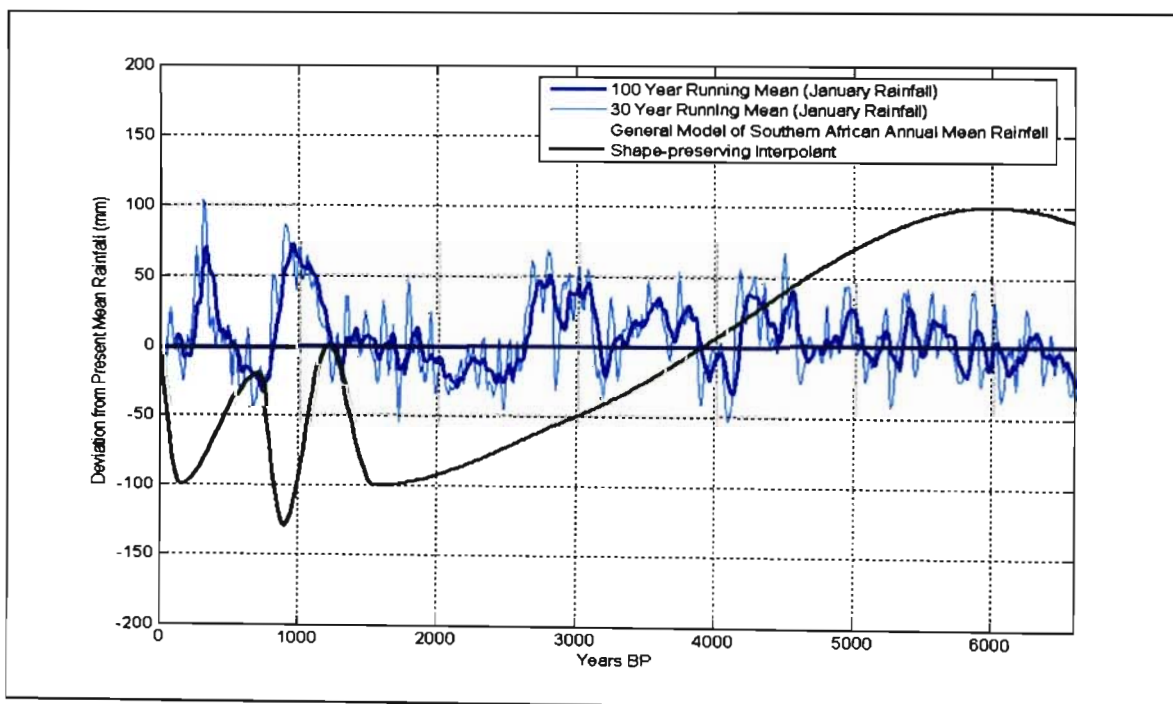


**Figure 4.15 – Comparison of the back-projected record of deviation from present mean January rainfall (0) for Makapansgat and the general model of southern African annual mean rainfall.**

Some deviation between the two signals is expected as the model depicts the general trends across the summer rainfall region of southern Africa. The rainfall peaks which occurred at approximately 1000 BP and 300 BP in the back-projected rainfall are evident in general model although the timing of the peaks is not identical. It is clear that the Makapansgat signal has less variability about the mean than the general model, suggesting a local moderating mechanism. Further investigation of the site is necessary to determine what this mechanism may be.

#### 4.3.4 A Climatic Record for the Last 10 000 Years from Wonderkrater

Scott *et al.* (2003) provided pollen abundance data for cores collected at Wonderkrater. A principal components analysis of 15 selected pollen taxa provided two principal components, which together accounted for 59.1% of the variability in the data (Figure 4.16).

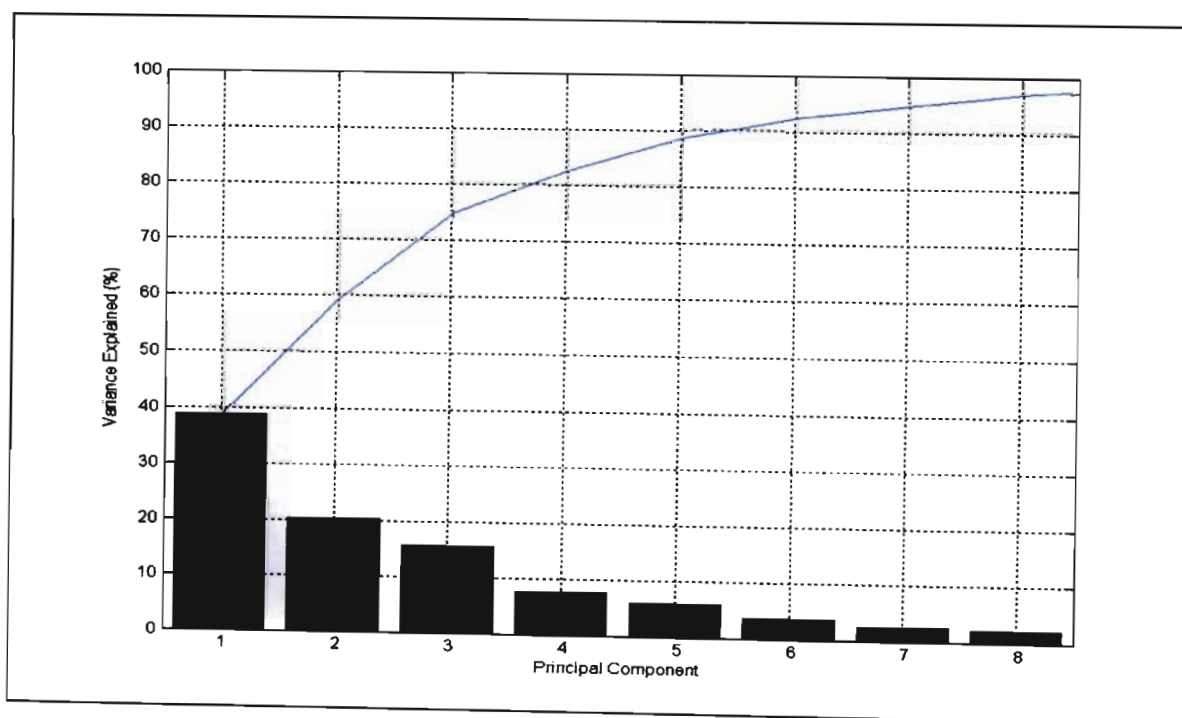


Figure 4.16 - Variance explained by principal components with line of cumulative variance.

A plot of the principal component weightings of the 15 taxa is shown in Figure 4.17. The contrast in distribution along the axes was used to construct temperature and moisture indices. Taxa such as *Ericaceae*, *Cliffortia*, *Artemisia* and *Passerina* appear to have low PC1 values while *Burkea*, *Combretaceae*, *Tarchonanthus* and *Capparaceae* have high PC1

values. Thus, the first principal component appears to show a gradual transition from cool fynbos (low PC1 values) to warm woodland (high PC1 values). Combretaceae occur in warm, moist environments of the tropics and subtropics, while *Tarchonanthus* and Capparaceae are associated with drier conditions. Thus a high PC2 value appears to represent moist conditions while a low PC2 value represents dry conditions.

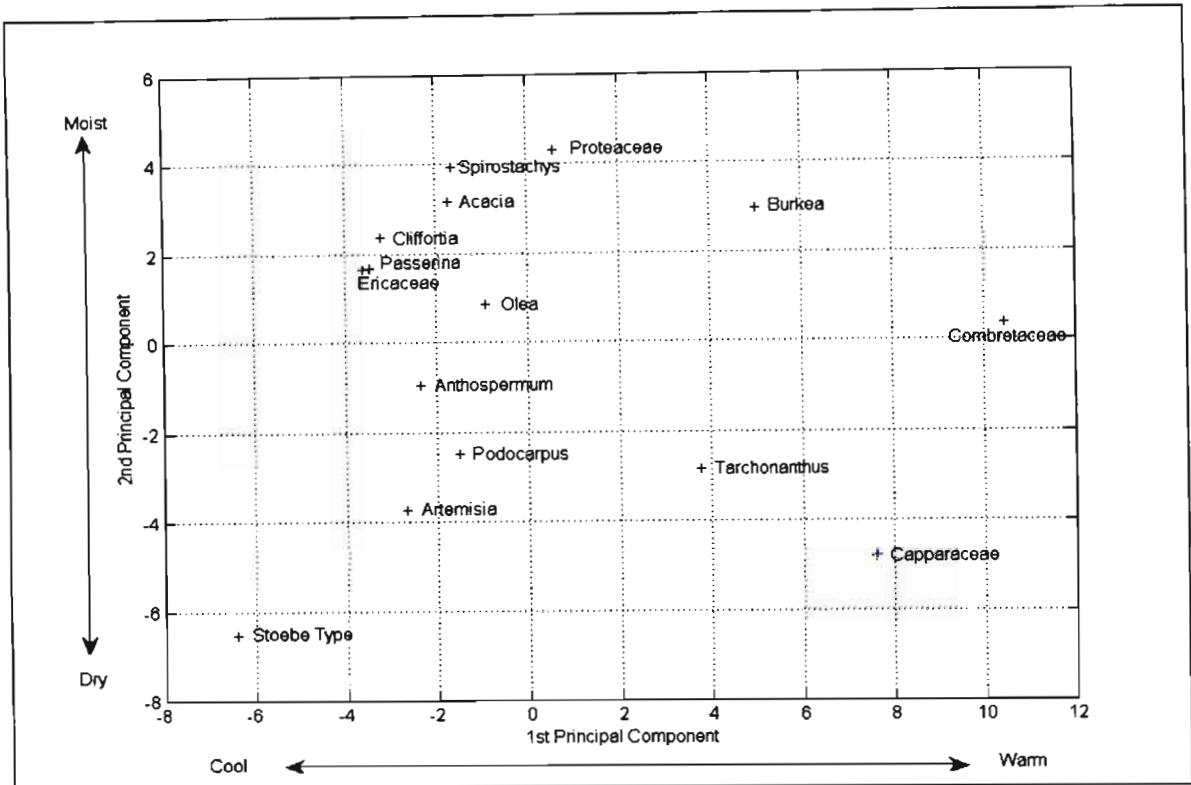


Figure 4.17 - Principal component weightings of 15 selected pollen taxa.

The temperature and moisture indices derived from PC1 and PC2 respectively are represented in Figure 4.18. The PC1 temperature index shows warming from the Last Glacial Maximum (at approximately 18 000 BP) until a temperature peak at about 12 800 BP followed by cooling until 11 700 BP. Thereafter temperatures generally increase until the Holocene Maximum or Altithermal at around 6000 BP when temperatures commenced a general decrease until the Medieval Warming period from 1100 BP. The PC2 rainfall index shows a gradual increase of moisture from the Last Glacial Maximum to the present. Minor peaks in moisture generally correspond with peaks in the temperature record. Moisture values for the region do not show much variation about the mean

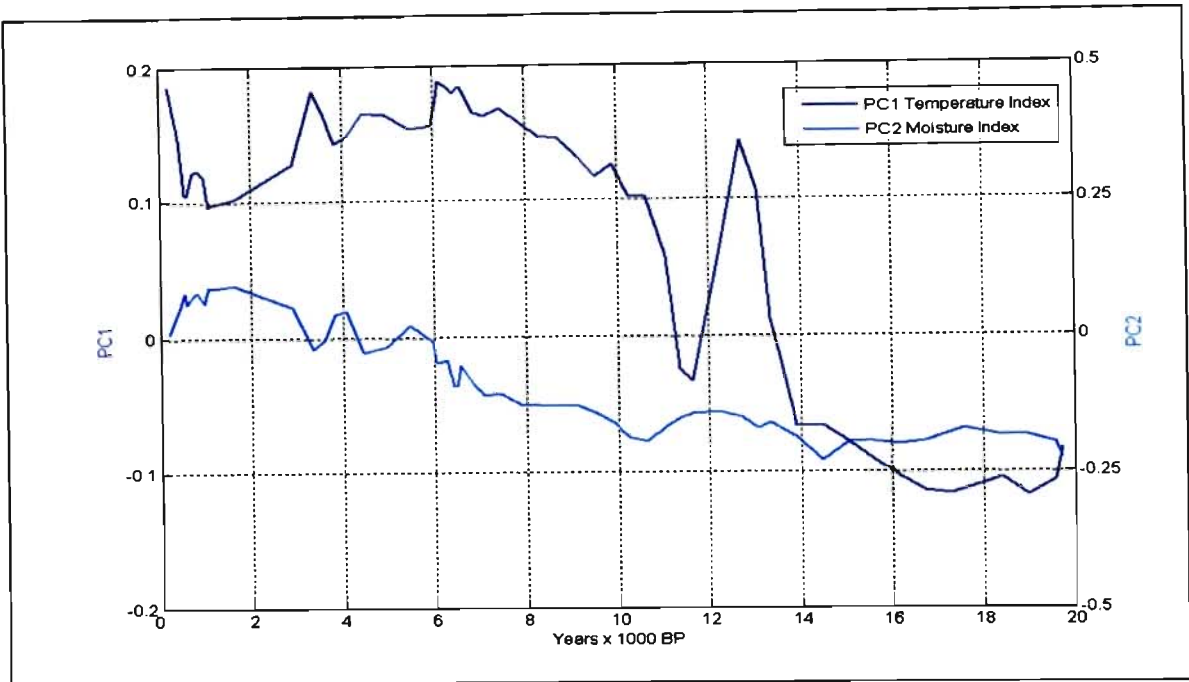


Figure 4.18 - First two principal components with PC1 representing a temperature index and PC2 representing a moisture index for Wonderkrater.

#### 4.3.4.1 PC1 and Temperature

The Wonderkrater temperature index is compared with the general model of southern African annual mean temperature in Figure 4.19.

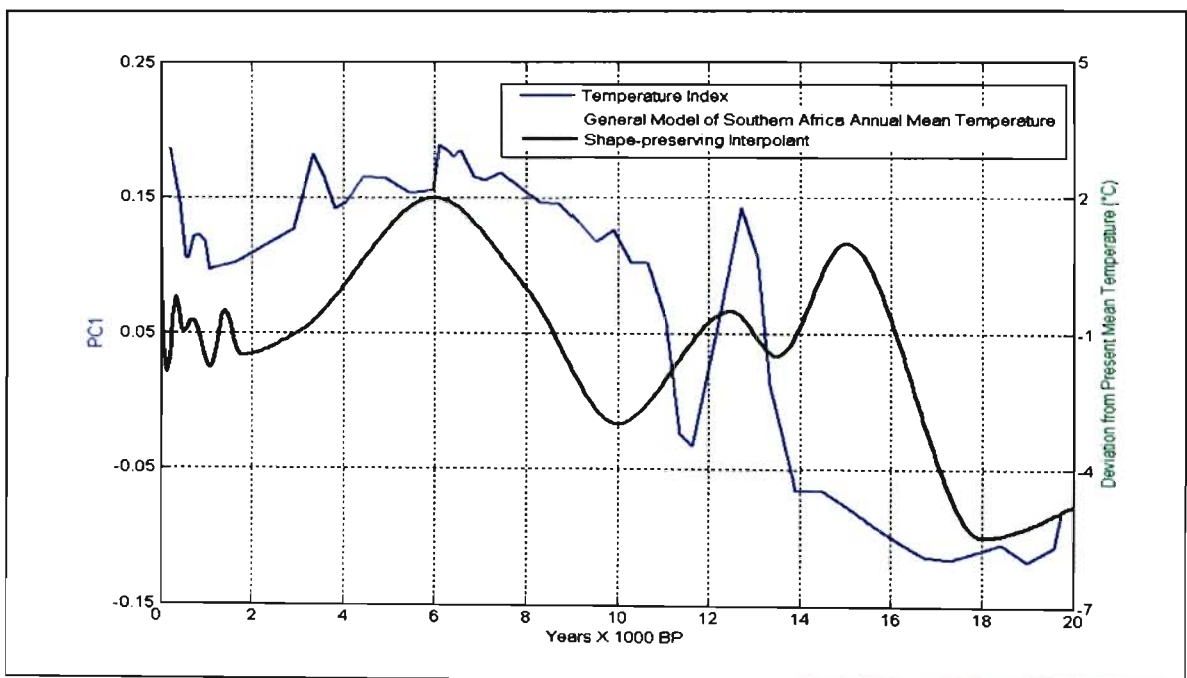


Figure 4.19 – Comparison of the Wonderkrater PC1 temperature index and the general model of southern African annual mean temperature.

The model and the index show a general warming from the Last Glacial Maximum. After a peak at about 12 500 BP, cooling commences, and a Younger Dryas minimum at about 11 700 BP according to the index, but at about 10 000 BP according to the model. Discrepancies occur as the general model is based on records with radiocarbon year age scales while the Wonderkrater record has been calibrated according to the Makapansgat uranium-series calendar year age model. At around 6000 BP, the warmest temperatures across the record are shown in both the model and index. There is evidence of the Medieval Warming (1100 BP – 700 BP) in both the index and the model, but subsequent cooling associated with the Little Ice Age (700 BP – 150 BP) is absent from the index.

#### 4.3.4.2 PC2 and Rainfall

The rainfall index is compared with the general model of southern African annual mean rainfall in Figure 4.20. Both the model and the Wonderkrater moisture index indicate increased dryness at the Last Glacial Maximum and during the Younger Dryas. The rainfall minimum associated with the Younger Dryas occurs at around 10 500 BP according to the index, but at around 10 000 BP according to the model. There is an increase in moisture from the Younger Dryas until about 6000 BP. Thereafter moisture decreases towards the present according to the general model, or recovers somewhat from 3300 BP until 1600 BP in the moisture index before decreasing towards to the present.

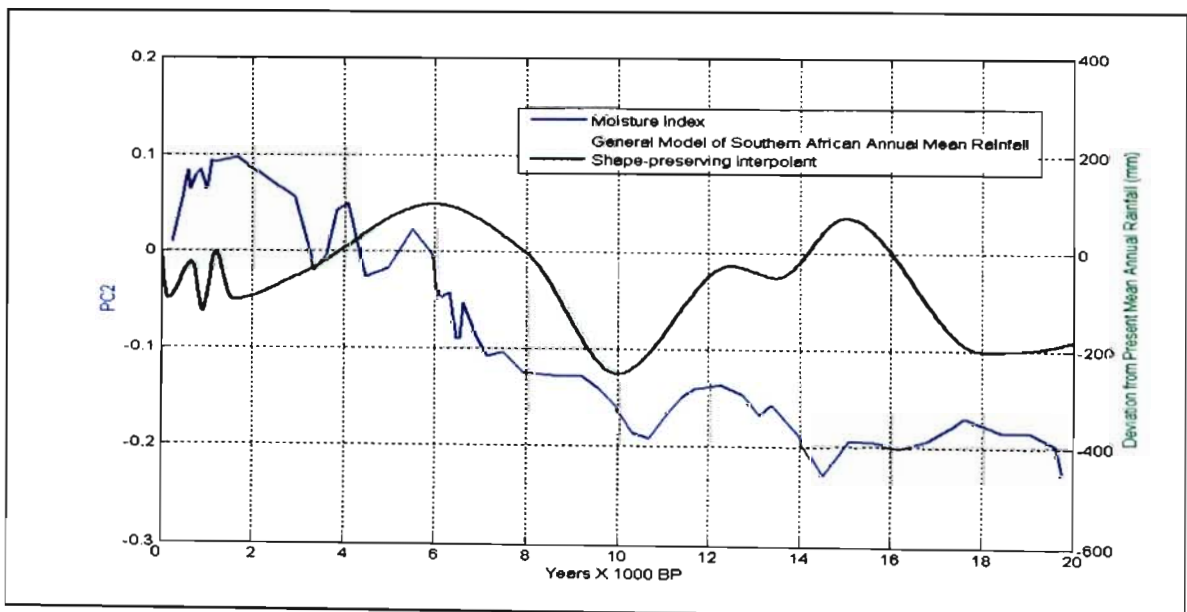


Figure 4.20 - Comparison of the Wonderkrater PC2 moisture index and the general model of southern African annual mean rainfall.



#### **4.4 SUMMARY**

A synthesis of current knowledge of southern African climate change clearly indicated that palaeotemperature and palaeorainfall records show similar trends across most of the summer rainfall region of southern Africa. Areas of discrepancy include the Kalahari and the Namib deserts. Based on these general trends, the general model of southern African annual mean temperature and the general model of southern African annual mean rainfall for the summer rainfall region were developed.

High correlation coefficients between proxy-records and measured climatic variables allowed for the back-projection of the climatic variables over the length of the proxy-records. The 116 year coral record from Sodwana Bay provided back-projections of air temperature, sea-surface temperature and rainfall. These back-projections were then compared with recorded and modelled values and showed a high level of correspondence. The stalagmite record from Makapansgat provided back-projections of temperature and rainfall over 6600 years. These were compared with the general models and also showed a high level of correspondence. Temperature and rainfall indices for Wonderkrater were derived from a principal component analysis of pollen abundance data. Once again, these indices showed a correspondence with the general models.

The existence of common climatic trends indicates that there are teleconnective processes in action across the southern African summer rainfall region, and an investigation of atmospheric and oceanic interaction in the region of the subcontinent would assist in the determination of the processes driving these fluctuations in temperature and rainfall. Atmospheric circulation models are investigated in Chapter 5 in an effort to identify climate forcing mechanisms and the nature of their teleconnections across the region.

## **5. ATMOSPHERIC CIRCULATION: PAST AND PRESENT**

### **5.1 INTRODUCTION**

It is important first to establish the mechanisms controlling present climate before attempting to understand palaeoclimates. This chapter will provide an examination of the atmospheric conditions that give rise to present climate, and provide an example of a quasi-regular disturbance to this general circulation in the form of the El Niño-Southern Oscillation. Although the degree of anthropogenic impact on present climate is uncertain, it is reasonable to believe that past climates were controlled by forces similar to those that are in action today. One can thus infer the causes of variability in the past by examining what causes similar variations at present. The palaeoclimatic fluctuations outlined in Chapter 4 will be examined in the context of established models of atmospheric circulation to ascertain the driving forces behind these changes.

### **5.2 THEORIES OF ATMOSPHERIC CIRCULATION**

#### **5.2.1 Mean Atmospheric Circulation Models**

Tyson (1986) developed a model that highlighted the changes in atmospheric circulation between the extended wet spells and dry spells that had been identified as forming an approximately 18 year rainfall cycle in southern African meteorological records (Tyson, 1971). Tyson suggested that the components of the circulation over southern Africa undergo a reversal between these wet and dry spells, and regional contrasts between the eastern and western parts of the subcontinent exist at all times.

Tyson (1986) postulated that the ascending limb of the African Walker cell is situated over tropical Africa during the extended wet spells (Figure 5.1). The subtropical westerly jet intensifies to the south of the subcontinent, particularly to the south-east in the region of Marion Island. Upper tropospheric (200 hPa) zonal winds become anomalously easterly at about 20° S while lower in the atmosphere (500 hPa), flow is anomalously westerly. At 30° S, the zonal anomaly in the upper levels is westerly and easterly below.

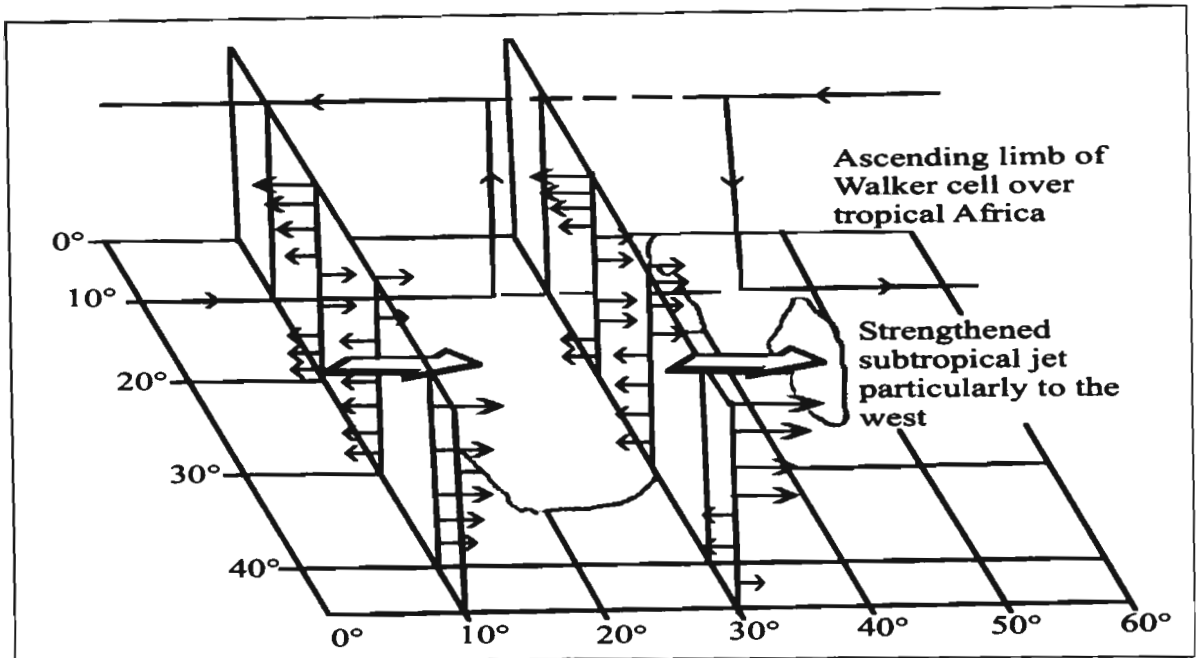


Figure 5.1 - Model of zonal wind component anomalies over southern Africa during wet spells (Tyson and Preston-Whyte, 2000, 332).

During the dry periods (Figure 5.2), the descending limb of the African Walker cell is situated over tropical Africa, and upper tropospheric (200 hPa) zonal wind components become anomalously westerly at about 20° S. Lower in the atmosphere (500 hPa) flow is anomalously easterly. At 30° S, the zonal anomaly in the upper levels is easterly and westerly below (Tyson and Preston-Whyte, 2000).

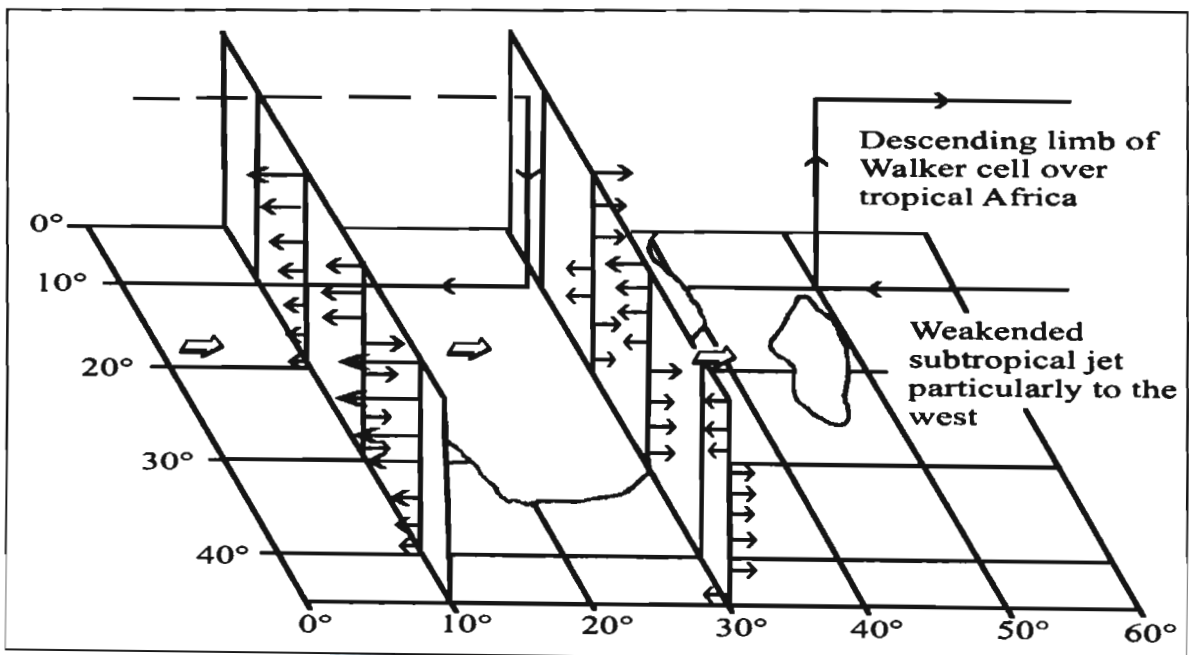
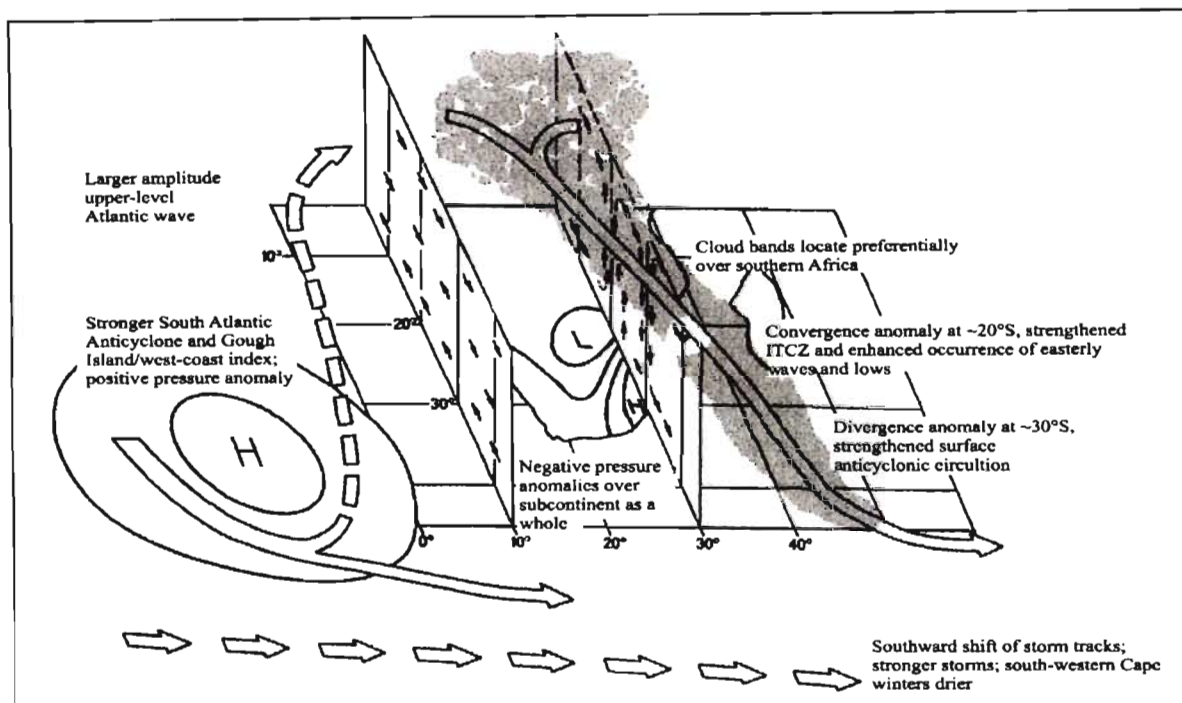


Figure 5.2 - Model of zonal wind component anomalies over southern Africa during dry spells (Tyson and Preston-Whyte, 2000, 332).

In the Hadley-cell mode along the west coast during wet spells, upper level meridional flow is poleward and near-surface flow is equatorward (Figure 5.3). Over the eastern and central parts of the subcontinent, the meridional structure is more complex with divergence anomalies developing at 30° S and convergence anomalies developing at 20° S, strengthening the Inter-Tropical Convergence Zone (ITCZ). The formation of easterly wave disturbances and tropical lows is promoted, and the inflow of moist air from the east and north-east increases. Negative pressure anomalies prevail over most of the subcontinent (Tyson and Preston-Whyte, 2000).



**Figure 5.3 - Model of anomalous meridional circulations during wet spells with positions of upper-tropospheric Atlantic wave, cloud formation zones, surface expressions of South Atlantic High, and location of storm tracks. ITCZ = Inter-Tropical Convergence Zone (Tyson and Preston-Whyte, 2000, 333).**

During dry spells, the meridional flow anomalies reverse on both sides of the subcontinent. Along the west coast in the Ferrel-cell mode, upper-level meridional flow is anomalously equatorward and lower tropospheric flow is poleward (Figure 5.4). At 30° E, the divergence anomaly at 20° S weakens the Inter-Tropical Convergence Zone and decreases the incidence of easterly waves in the region. The convergence anomaly at 30° S weakens surface anticyclones, weakens the north-south pressure gradients and decreases moisture advection, which is more from the Atlantic Ocean than Indian Ocean. The overall pressure anomaly is positive over the subcontinent.

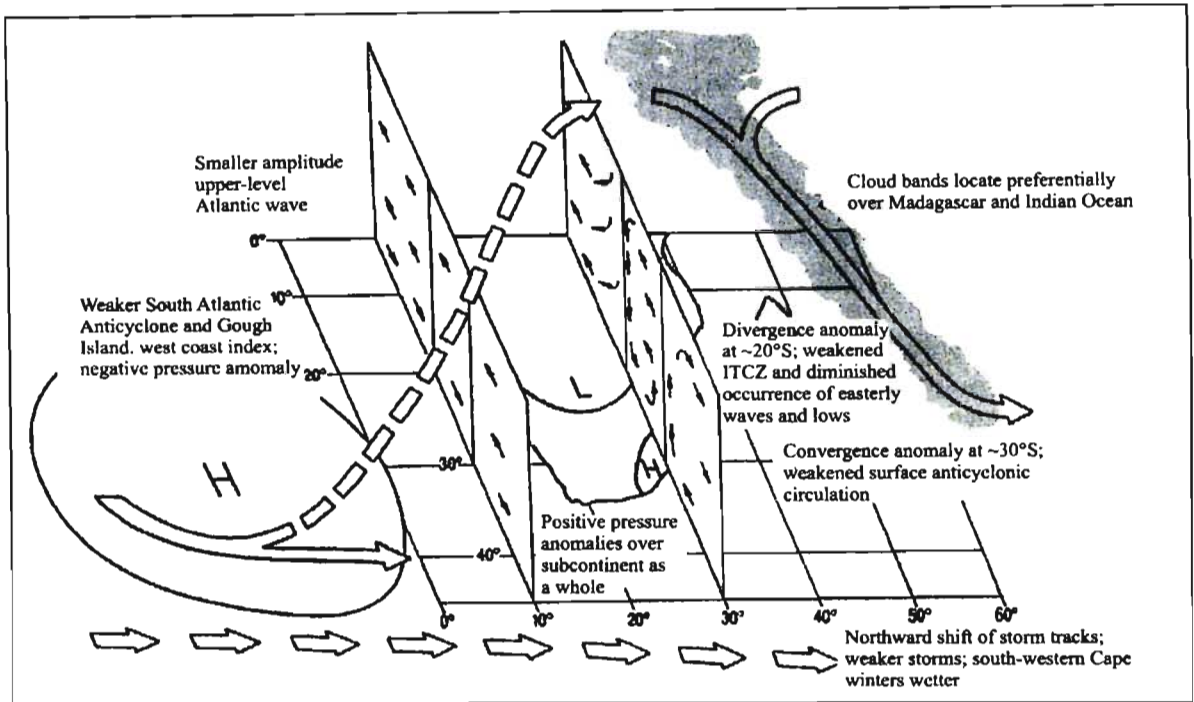


**Figure 5.4 - Model of anomalous meridional circulations during dry spells with positions of upper-tropospheric Atlantic wave, cloud formation zones, surface expressions of South Atlantic High, and location of storm tracks. ITCZ = Inter-Tropical Convergence Zone (Tyson and Preston-Whyte, 2000, 333).**

During wet spells, the trough of the planetary wave associated with the African cloud band is located to the west and rainfall occurs preferentially over the summer rainfall region of southern Africa (Tyson, 1999a), as shown in Figure 5.5. Westerly storm tracks shift southwards resulting in less winter rainfall in the winter rainfall region of the Western Cape. Increased advection of thermal vorticity causes storms to be stronger along their southerly tracks (Tyson and Preston-Whyte, 2000).

During dry spells, the planetary wave over the Atlantic weakens, and the zone of major cloud bands moves eastward towards the Indian Ocean (Tyson, 1999a), as shown in Figure 5.6. The subtropical jet is weakened, meridional fluxes of energy are lessened, north-south temperature gradients increase, and westerly storm tracks move north, carrying more winter rain to the Western Cape from weakened storms. The summer rainfall region becomes drier, and the winter rainfall region becomes wetter and expands inland. The frequency of winter rainfall increases in the summer rainfall region but not sufficiently to compensate for the loss of summer rainfall (Tyson, 1999a).

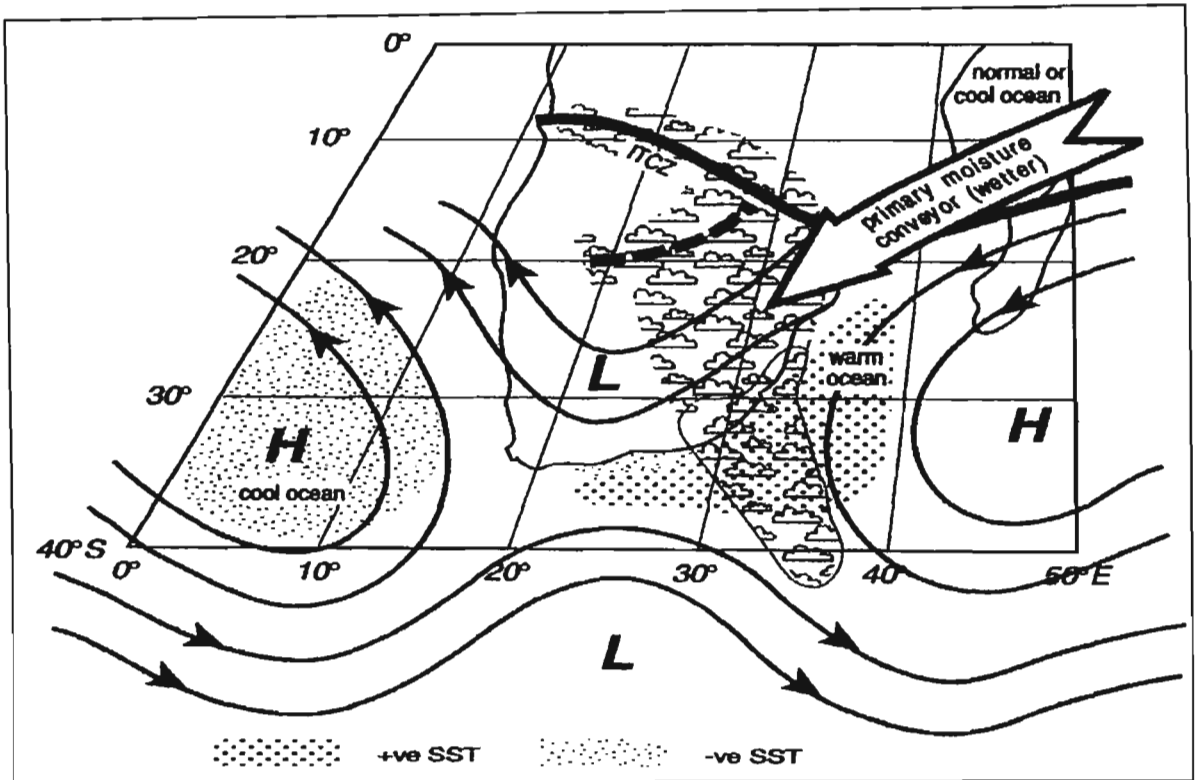


Figure 5.5 - Conceptual model illustrating changing circulation controls, sea-surface temperatures, moisture-transport conveyors and loci of tropical convection during wet spells (Tyson and Preston-Whyte, 2000, 335).

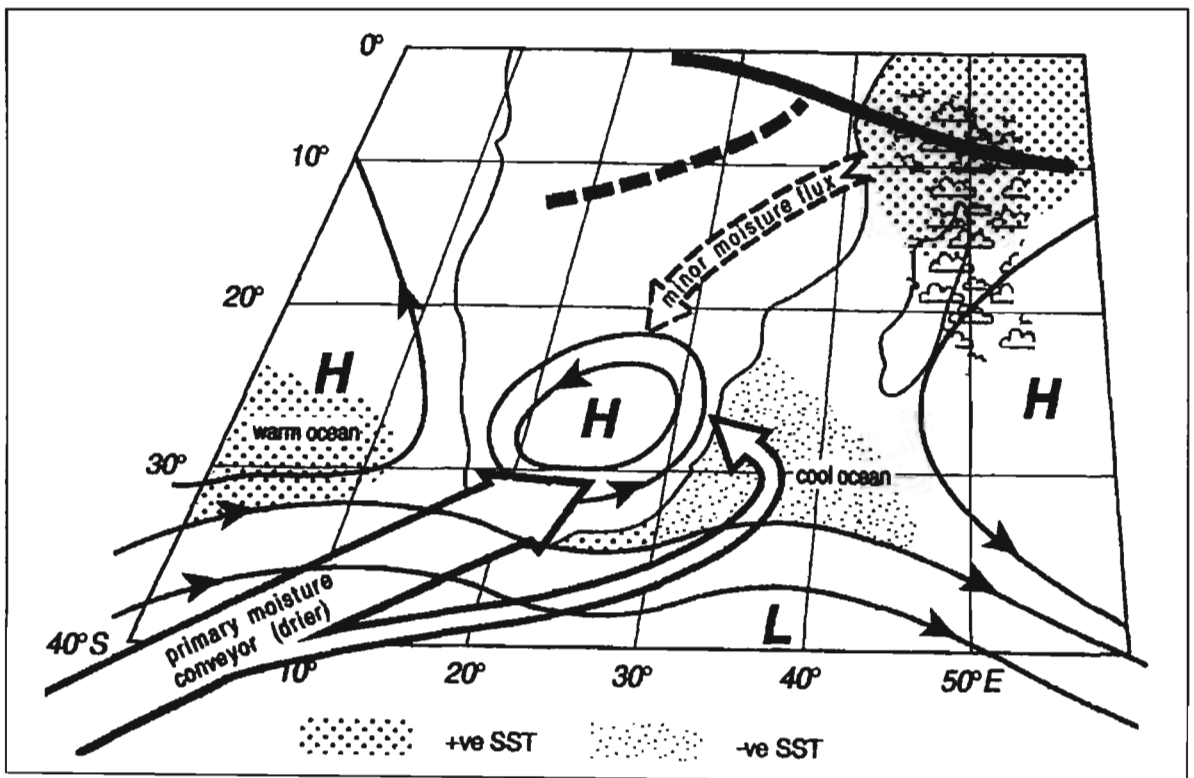


Figure 5.6 - Conceptual model illustrating changing circulation controls, sea-surface temperatures, moisture-transport conveyors and loci of tropical convection during dry spells (Tyson and Preston-Whyte, 2000, 335).

Tyson (1999a) updated this model to include the effects of sea-surface temperature. During wet spells, the Atlantic Ocean in the vicinity of Gough Island cools, the Agulhas region warms, and the Indian Ocean north of Madagascar cools. The primary moisture transport pattern is from the north-west. During the dry periods, the sea surface temperature pattern reverses and primary moisture transport is from the south-west.

In summary, Tyson (1986; 1999a) highlighted that warmer wetter conditions are initiated by a southward expansion of the tropical easterlies, whereas drier cooler conditions occur when there is an equatorward expansion of the westerlies. When the tropical easterlies penetrate further south, they spread warmer and wetter conditions and more summer rainfall to the higher latitudes of southern Africa. Conversely, the expansion of the westerlies northwards causes cooler and drier conditions and a greater proportion of winter rain to wider areas.

### **5.2.2 The El Niño Model**

El Niño events are quasi-periodic (every 3 to 7 years) intense, extended periods of oceanic warming. An El Niño event, which is experienced across the entire tropical Pacific Ocean, is characterised by warm sea-surface temperatures in the eastern and central regions of the Pacific, and by changes in the depth of the thermocline and strength of surface ocean currents (Philander, 1990). During an El Niño event, sea-surface temperatures can increase by 4 °C over a quarter of the circumference of the globe (Mason, 2001). La Niña is the opposite of El Niño and occurs in years when warming is anomalously weak and the eastern Pacific Ocean surface is cooler than in other years (Philander, 1990).

The Southern Oscillation is the atmosphere's complement to El Niño. During a typical summer, low pressure systems lie over the Pacific and Indian Oceans, and high pressure systems lie over the eastern equatorial Pacific and the South American Pacific coast. During El Niño, the high pressure systems move westward, and the low pressure systems typically over the African to Australian region shift eastward (Walker, 1924; Walker and Bliss, 1932). Consequently, the Indonesian-Asian low-pressure is weakened, preventing monsoon conditions, and drought results. The eastward migration of low pressure causes heavy rains over Peru and Ecuador, which temporarily greens the semi-desert landscape (Philander, 1990).

It was four decades after the work of Walker (1924) was published that the linkages between the ocean and atmosphere were established and the concept of the El Niño-Southern Oscillation (ENSO) was developed. Through analysis of meteorological and oceanographic data, Bjerknes (1966; 1969) concluded that the normal zonal atmospheric cell circulation, termed 'Walker Circulation', is disturbed during ENSO events. Bjerknes (1969) initially noted that the Pacific is 4 - 10 °C colder in the east than in the west although the equatorial oceans all receive about the same solar insolation. Through further investigation, he concluded that this phenomenon is caused by equatorial upwelling and the transport of cold water from the South Pacific, which are processes driven by the easterly trade winds. These winds are partially due to the temperature contrast of the ocean, which causes higher pressures in the east, and surface air to blow down the gradient from east to west. Thus it was clear that the normal state (Figure 5.7b) of the tropical Pacific is maintained by a coupled positive feedback system involving the ocean and atmosphere (Bjerknes, 1966; 1969).

Increased interest in the climatic impacts of the El Niño phenomenon led to investigations into the role of the thermocline in this dynamic system. It was realised that colder temperatures in the east drive stronger easterlies, which in turn drive greater upwelling, lift the thermocline up more strongly, and increase the transport of cold waters, making the temperatures colder still. Thus the thermocline plays an important role in this oceanic-atmospheric interaction by enforcing a continuously synergizing cycle (Cane, 2005), and any disturbance to the thermocline may result in an atmospheric disruption which extends beyond the tropics.

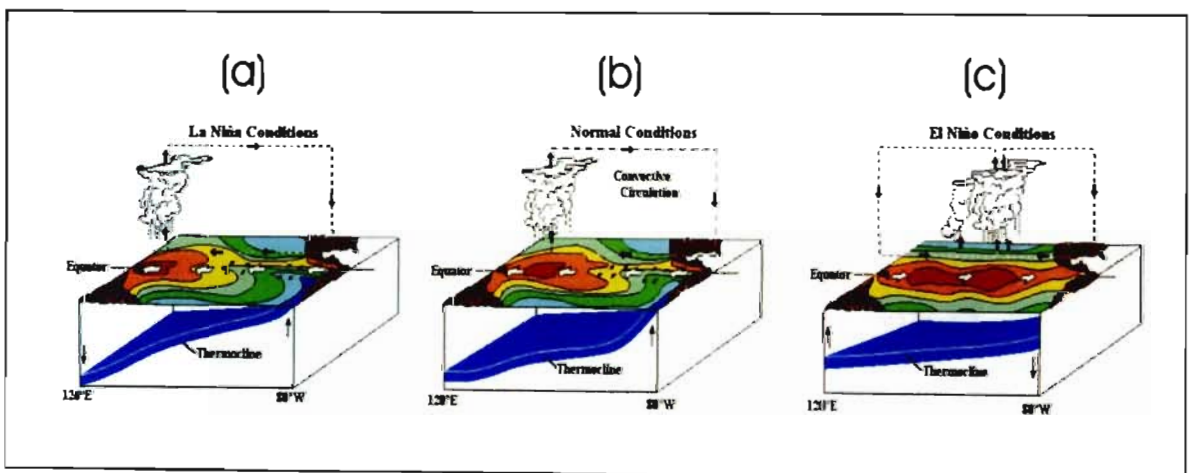


Figure 5.7 - (a) La Niña, (b) Normal and (c) El Niño conditions (NOAA, 2005).



The El Niño state is the result of a disturbance to this mechanism. For example, if the thermocline is depressed, the east starts to warm (Figure 5.7c). Then the east-west sea-surface temperature contrast is reduced, so the pressure gradient and the winds weaken. The weaker winds bring weaker upwelling, a sinking thermocline, and slower transport of cold water. The weakened pressure gradient allows warmer water from the western Pacific to surge eastwards, and sea-level flattens. The characteristics of La Niña, normal and El Niño events are described in Table 5.1.

**Table 5.1 - Summary of atmospheric and oceanic features of La Niña, Normal and El Niño states (adapted from Philander, 1990; Mason, 2001; Cane, 2005)**

LA NIÑA	NORMAL	EL NIÑO
Every 1.5 to 3.5 years	When El Niño and La Niña conditions are not occurring	Every 3 to 7 years
Strengthened easterlies drive surface waters westward	Easterlies drive surface waters westward	Easterlies weaken and warm waters travel eastward
Thermocline deepens in the west, shallows in the east (steep thermocline)	Thermocline deeper in the west than the east	Thermocline deepens in the east, shallows in the west (less steep thermocline)
Higher atmospheric pressure in west, lower pressure in the east	Higher atmospheric pressure in west, lower pressure in the east	Higher atmospheric pressure in east, lower pressure in the west
Trade winds cause surface waters to accumulate around Indonesia – raising the sea-level in this region	Trade winds cause surface waters to accumulate around Indonesia – raising the sea-level in this region	Pressure gradient weakens and allows warmer water from the western Pacific to surge eastwards, and sea-level flattens
Surface waters reaching the west (e.g. Indonesia) are warm	Surface waters reaching the west (e.g. Indonesia) are warm	Surface waters reaching the east (e.g. Peru) are warm
Intense rainfall in Indonesia; intense drought in Peru	Rainfall in Indonesia; drought in Peru	Rainfall in Peru and Ecuador; drought over Indonesia, Sri Lanka, southern India, Philippines, Australia, southern Africa and central America

ENSO is now widely recognised as a climatic phenomenon that originates as a tropical ocean-atmosphere disturbance but has global climate repercussions extending into the temperate zones (Philander, 1990). Climatologists ascertain that during ENSO years, not only does the Indonesian-Asian monsoon system fail, but Africa and the western Pacific can experience severe drought, western North American summers are hot and dry, and the

southeastern United States can experience anomalously high winter rainfall (Cane, 2005). Intense El Niño events tend to occur once every decade and during extreme events, such as the 1982 - 1983 ENSO, drought and flooding cause property damage, agricultural losses, and the loss of lives (Glynn, 1990).

Bjerknes' (1966; 1969) mechanism explained why the system has two distinct states (with La Niña being an intensification of the normal state) but not why it oscillates between them. Various explanations for the fundamental dynamics of the ENSO cycle have been suggested. Some authors focus on wave propagation, others focus on the recharge-discharge of the equatorial ocean heat or the role of ocean-atmosphere interactions in the western Pacific. Cane (2005) suggests that these are different descriptions of the same basic physics. The wave propagation theory describes how westerly wind anomalies in the central and eastern equatorial Pacific generate a downwelling, eastward-moving equatorial Kelvin wave, which produces positive sea-surface anomalies. The same westerly wind anomalies cause slower, westward-moving upwelling Rossby waves that usually reflect at the western boundary a few months later in the form of upwelling Kelvin waves. It is the reflection of these waves that ultimately provides the mechanism for the erosion of El Niño conditions. This succession of downwelling followed by upwelling Kelvin waves is referred to as the 'delayed oscillator' mechanism (Mason, 2001).

The ocean-atmosphere interaction theory, on the other hand, suggests that the oscillations are caused by internally generated dynamics between the ocean and the atmosphere (Philander, 1990). In this theory the delayed oscillator mechanism is the depth of the tropical thermocline. The warm layer depth changes associated with ENSO are too large to be caused by merely exchanges of heat with the atmosphere and are, instead, the result of wind-driven ocean dynamics (Philander, 1990). While the rate of change of winds and sea-surface temperatures in the ENSO cycle are similar, the slow thermocline changes are not in phase with the winds driving them. This provides the delayed mechanism for the oscillation (Cane, 2005). If the coupling was stronger, the direct link from westerly wind anomaly to deeper eastern thermocline to warmer sea-surface temperature and back to increased western anomaly would increase too rapidly for the out-of-phase signals to catch up and there would be no oscillation (Cane, 2005). This 'coupling strength' is determined by various physical factors including how strong the mean wind is, the mean atmospheric temperature and humidity, and the depth and slope of the thermocline, which influences

changes in the temperature of upwelled water from a given wind-driven change in the thermocline depth (Cane, 2005).

In simple linear analyses, the ENSO period is highly variable and determined mostly by the coupling strength rather than the time for waves to travel back and forth across the Pacific. In nonlinear models, which are better representations of reality, this holds and the cycle repeats itself every 2 - 7 years (Cane, 2005). In addition to its quasi-regular recurrence, ENSO frequencies vary over decadal, centennial and possibly millennial timescales. There is no accepted theory explaining what sets the average period of the ENSO cycle (Cane, 2005) and there is much debate over the causes of the irregular cycle. Some attribute it to low-order chaotic dynamics and some simply to noise in the climate system (Cane, 2005).

Despite its intricacy, integrated ocean-atmosphere programs that model future ENSO have been developed and continue to be improved. Several ENSO models predicted the intense 1997 - 1998 El Niño event (Philander, 1990), which was implicated in catastrophic flooding in coastal Peru and Ecuador, and drought in the Altiplano of Peru and Bolivia, the Nordeste region of Brazil, and Indonesia, New Guinea and Australia (Cane, 2005).

### **5.3 PRESENT CONDITIONS**

#### **5.3.1 Mean Atmospheric Circulation and Travelling Disturbances**

The atmospheric circulation of southern Africa is dominated by semi-permanent subtropical high-pressure cells, and the mean circulation over the region is anti-cyclonic through most of the year, except near the surface. Due to the position of southern Africa in the subtropics, this mean atmospheric circulation is occasionally disturbed by travelling systems that develop in the tropics to the north or the temperate latitudes to the south (Tyson and Preston-Whyte, 2000).

In summer, near-surface circulation (at 850 hPa) consists of a weak low pressure cell centred over the central interior and linked by a trough across the northern Cape and Botswana to a tropical low (Figure 5.8a). Middle and upper tropospheric (500 and 200

hPa) flow is easterly north of about 23° S (Figure 5.8c). A weakening of convection results in the establishment of the dominant high-pressure cell by March. The air over Zimbabwe, Zambia and northern Botswana is still moist at this time, and the flow of air from the north may bring autumnal rains to the western part of South Africa. In winter, the anticyclonic systems intensify further and move northward, and the low-level winter mean pressure field at 850 hPa is strongly anticyclonic (Figure 5.8b). As the upper-level circumpolar westerlies expand (Figure 5.8d), the upper tropical easterlies are displaced equatorward (Tyson and Preston-Whyte, 2000).

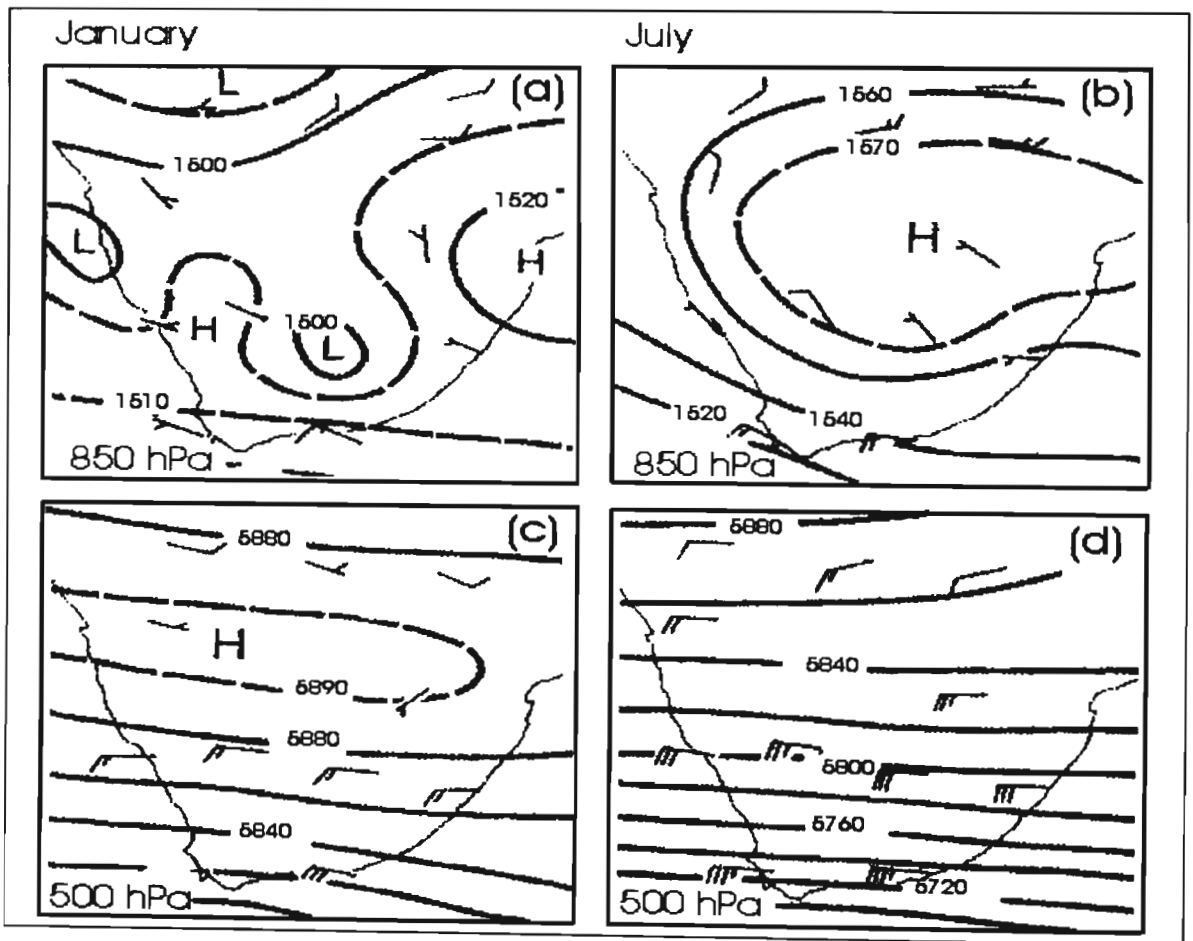


Figure 5.8 – Monthly mean winds, contours of the 850 and 500 hPa surfaces (gpm) (Tyson and Preston-Whyte, 2000, 177).

The subtropical control of the semi-permanent South Indian, South Atlantic and Continental high pressure systems, indicated in Figure 5.9, varies significantly over the course of the year. The South Indian and South Atlantic Anticyclones move about 6° northward in winter, and the South Atlantic high may ridge eastward and to the south of the continent. Extensive ridging may result in the budding of a separate high that travels

eastward into the Indian Ocean before becoming absorbed by the South Indian high-pressure system (Tyson and Preston-Whyte, 2000).

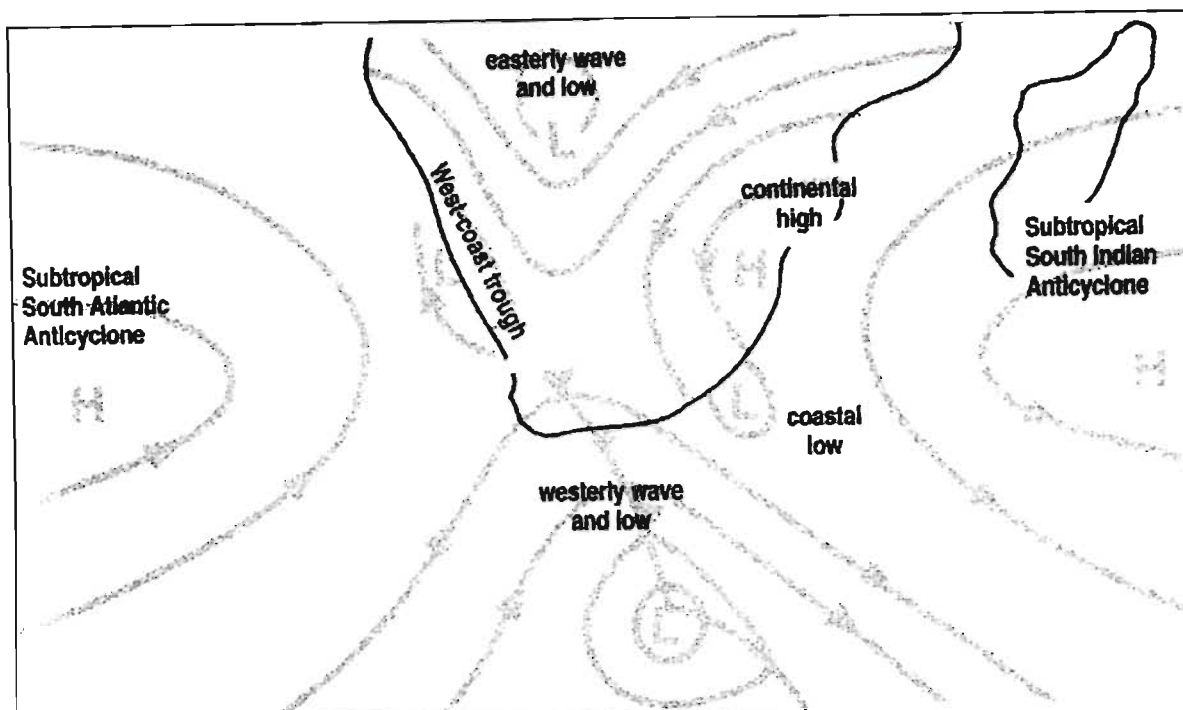


Figure 5.9 – Important features of the surface atmospheric circulation over southern Africa (Tyson and Preston-Whyte, 2000, 179).

While the mean circulation of the atmosphere controls the climate of the subcontinent, daily weather situations are mainly controlled by synoptic smaller-scale disturbances originating in temperate and tropical circulations. Temperate influences are experienced through travelling disturbances in the westerlies in the form of westerly waves and lows (Figure 5.9) and are typically winter features (Tyson and Preston-Whyte, 2000). Westerly perturbations on a local scale include west-coast troughs and shallow coastal lows.

Westerly waves have a peak frequency of occurrence in the range of 2 – 8 days. Surface convergence is produced to the rear of a westerly trough while south-westerly airflow and divergence occurs to the east and ahead of the trough line at the 500 hPa level and above. This results in the gentle uplift of air and precipitation to the rear of the surface trough while ahead of the trough, subsidence causes fine, clear conditions. Rainfall associated with these systems rarely occurs inland of the escarpment, although inland rainfall may be caused indirectly by the squall-line convection related to the fronts that accompany these waves. The troughs may form deep low pressure systems associated with heavy rains. A

cut-off low is a more intense form of the westerly trough. This is a cold-cored depression formed from a trough in the upper westerlies that is displaced towards the equator and deepens into a closed circulation reaching down to the surface. These are unstable systems with strong convergence at the surface, strong upper air divergence, and can cause flood-producing rains. Cut-off lows causing heavy rains occur with a semi-annual variation that peaks from March to May and September to November (Tyson and Preston-Whyte, 2000).

Disturbances in the tropical easterly flow occur in the form of easterly waves and lows (Figure 5.9). These are associated with the Inter-Tropical Convergence Zone (ITCZ) and the warm, humid easterly winds between the ITCZ and the subtropical high-pressure belt. Easterly waves over southern Africa are semi-stationary in character and form in deep easterly currents in the region of an easterly jet. Low-level convergence occurs to the east of the surface trough while at 500 hPa and above, flow is divergent, which causes strong uplift and sustained rainfall in the absence of strong instability. With the presence of unstable air, heavy rains may occur over a wide area to the east of the trough associated with winds of a northerly direction. Ahead of and to the west of the trough, subsidence occurs, causing clear skies and warm conditions (Tyson and Preston-Whyte, 2000).

An easterly low is also associated with surface convergence to the east of the low but with divergence occurring at higher levels than in case of easterly waves. Strong uplift occurs to the east while subsidence occurs to the west of the system. Heavy rainfall is usually associated with the system, accompanied by a northerly flow of air. Heavy rains on the plateau thus usually originate from a northerly direction. Tyson and Preston-Whyte (2000) suggest that it is these rains that differentiate abnormally wet years from dry years.

Tropical disturbances over South Africa usually take the form of easterly waves and only a few of these disturbances are in the form of warm-cored tropical cyclones. Tropical cyclones occur more regularly over the Indian Ocean, but typically recurve to the south before reaching land, moving south along the Mozambique channel. Occasionally, the storms cross the coast but rarely move inland of the escarpment. These storms are associated with heavy rainfall and flooding and occur almost exclusively in summer (Tyson and Preston-Whyte, 2000) when ocean temperatures in the region are at their warmest. The increased evaporation from the warm ocean surface provides moisture which

is entrained into these systems and ultimately provides energy, in the form of latent heat, to support their development.

### 5.3.2 Rainfall

Rainfall in present-day southern Africa occurs predominantly in summer, except in the Western Cape where more than 70% of rainfall occurs in winter over parts of this region, and along the southern coast where rainfall is received throughout the year (Figure 5.10). The Atlantic coast of southern Africa and the adjacent region, containing the Namib, western Karoo and Kalahari deserts, are much drier than the eastern regions of the subcontinent (Reason *et al.*, 2004). Annual rainfall varies from more than 800 mm over the eastern subcontinent to less than 100 mm over the arid western regions (Tyson, 1986).

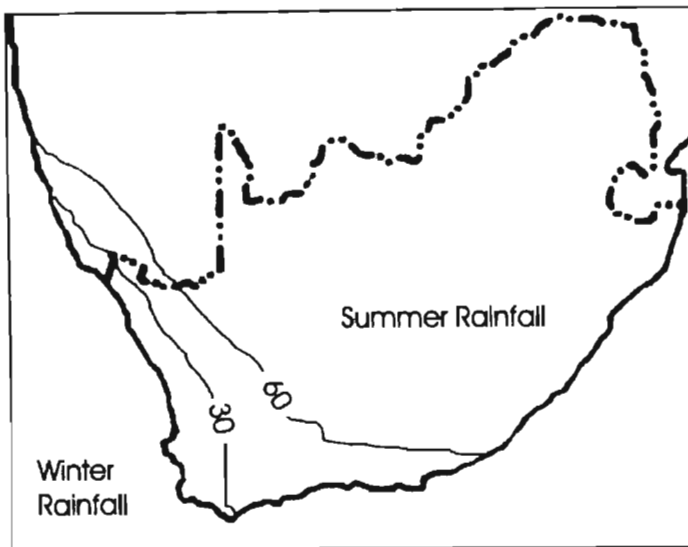


Figure 5.10 – Present day distribution of summer and winter rainfall regions in southern Africa with isolines indicating percentage annual rainfall received in summer (Cockcroft *et al.*, 1987).

Winter rainfall over the Western Cape is frontal in origin and develops due to the northward shift of the anticyclones over the South Atlantic in winter and the consequent development of a relative low pressure over the region. There is significant interannual variability and evidence suggests that this is related to sea surface temperature gradients of the South Atlantic (Reason *et al.*, 2003; 2004). The rest of subtropical southern Africa experiences summer rainfall, which is generated largely from convective thunderstorms (Harrison, 1984). In the interior this is typically associated with tropical-extratropical interaction causing cloud bands along the position of the African trough of the mid-

tropospheric planetary standing wave number four. Particularly in late summer, a strong confluence zone extends in a north-easterly direction towards the north-south oriented ITCZ across central southern Africa (Rouault *et al.*, 2003). When the cloud band is longitudinally displaced to the east, either due to displacement of the southern African convergence zone or due to changing planetary wave configuration, the regions receiving rainfall are likewise displaced, and the summer rainfall region of southern Africa becomes drier (Tyson, 1999a). Changes in the Walker Circulation linked to the El Niño-Southern Oscillation affect the climate of southern Africa in a similar way (Tyson and Preston-Whyte, 2000).

### 5.3.3 Disruptions to the Mean Circulation: El Niño

During El Niño events, the teleconnection from the equatorial Pacific Ocean to southern Africa is caused by an abrupt warming of the Indian Ocean along the east coast (Mason, 2001). This change in Indian Ocean sea-surface temperatures causes an atmospheric response over the region. Increased heat fluxes over the warmer oceanic areas of the tropical Indian Ocean increase *in situ* atmospheric instability (Mason, 2001), which weakens the pressure gradient onto the subcontinent. The easterly convergence is displaced to the east and north (Mason and Jury, 1997) and there is a weakening of the inflow of moist air over the land, which causes below-normal rainfall over most of the region (Tyson, 1986; Mason and Jury, 1997). This may lead to persistent droughts south of about 10° S (Lindesay, 1988; Mason and Jury, 1997; Mason, 2001). A further influence of El Niño events on southern Africa occurs via the southern hemisphere standing waves, as these experience a northward shift and a decrease in amplitude during El Niño warm events. Over southern Africa, this results in dry conditions since the northward shift of the westerlies brings substantially less moisture than air from the Indian Ocean (Mason, 2001).

Southern African climate variability is sensitive to a range of factors and this poses great challenges for predictability. Walker (1990) attempted to isolate factors clearly associated with ENSO by assessing the influence of South Atlantic and South Indian sea surface temperature anomalies on South African summer rainfall. More recently, Mulenga *et al.* (2003) separated interannual summer droughts over northeastern South Africa into ENSO and non-ENSO droughts. Non-ENSO droughts occurred due to an abnormally strong influence of relatively cool, dry South Atlantic air, which was advected over South Africa



as a result of a cyclonic anomaly located over the southeast Atlantic. These droughts were classified by Mulenga *et al.* (2003) as ones where the atmospheric circulation over the subtropical to mid-latitude South Atlantic had an anomalously strong role to play, whereas most other droughts were tropical in origin, via ENSO.

The variance in southern African rainfall linked by direct association to ENSO is approximately 20% (Lindesay, 1988). In the summer rainfall region of South Africa, the influence of ENSO on rainfall is strongest during the summer months of December to March as this is when the ENSO events have reached maturity and when tropical atmospheric circulation is usually dominant over most of the subcontinent (Lindesay, 1988). Over Zimbabwe, the early- and late-season rains (October and March) are affected more severely. The difference in timing of ENSO influence is indicative of the effect of El Niño on the normal meridional migration of the Inter-Tropical Convergence Zone. During the austral summer, tropical air normally extends southwards and the convergence zone reaches about 20° S by January (Lindesay, 1988). However, during El Niño events, convergence is weakened and shifted northerly and easterly (Mason and Jury, 1997).

Since the late 1970s, El Niño episodes have been unusually recurrent and persistent while the frequency of strong La Niña events has been low. This has been attributed to global warming due to an enhanced greenhouse effect (Mason, 2001). Since El Niño is associated with significant rainfall anomalies over most of the region, the possibility of changes in the frequency and intensity of ENSO events are a serious concern.

#### **5.4 APPLICABILITY OF MODELS TO PALAEOCLIMATES**

Theories of atmospheric circulation during the Quaternary over southern Africa have ranged considerably from those that suggest a symmetrical contraction and expansion of climatic belts around the equator (Van Zinderen Bakker, 1967; Hastenrath, 1972) to those proposing an asymmetric shifting of these belts (Butzer *et al.*, 1978b). Nicholson and Flohn (1980) and Newell *et al.* (1981) subsequently showed that both equatorward movement of the climatic belts and marked asymmetries of circulation occurred during glacial cooling. The most detailed and enduring model of palaeoclimatic conditions over southern Africa was developed by Van Zinderen Bakker (1967; 1976; 1978). The model

was based upon the shifting of the westerlies, easterlies and the Inter-Tropical Convergence Zone (ITCZ) to explain glacial and interglacial transitions and the model was later modified (Van Zinderen Bakker, 1982) to highlight the importance of intensification rather than shifting of the circulation features. Present analogues of palaeoclimatic conditions indicate that both displacement and intensification of circulations occurred and not one or the other as suggested previously.

The Tyson (1999a) model of north-south shifts in the pressure belts can be applied to wet or dry spells on a scale from decades to millennia and longer, and thus has applicability to changes in atmospheric circulation during the transition between glacial and interglacial periods (Tyson, 1999a). Over much of the late Quaternary, the mechanisms controlling the cycle of warm-wet and cold-dry periods appear to have operated under the precessionally controlled changes in receipts of solar radiation. The shorter events of the last 1000 years, in contrast, are more likely related to variations in solar activity (Tyson, 1999b).

The Tyson (1986) model for southern Africa accords well with findings for Australasia on decadal to millennial timescales as well. A southward shift and westward expansion of the subtropical high brings decreased westerlies and increased subsidence and drought to much of eastern Australia. The subtropical jet weakens over the continent and westerlies increase to the south, bringing stormy conditions and increased precipitation to the southern and western parts and to New Zealand (Pittock, 1973; Trenberth, 1975).

The model proposes that warmer and wetter conditions are initiated in the northern regions and advance southwards while cooler, drier conditions are detected first in southern regions and then advance northward (Tyson and Preston-Whyte, 2000). A comparison of the Cango Cave (Talma and Vogel, 1992) and Makapansgat (Holmgren *et al.*, 2003) records indicate that this is likely to be the case. Cool episodes at Cango cave prevail a century or two longer than at Makapansgat during the last six millennia, while warm episodes were longer at Makapansgat (Tyson, 1999b).

There is evidence that the El Niño-Southern Oscillation (ENSO) has acted as a disturbance to mean circulation for at least the past 130 000 years (Cane, 2005). There is much debate over the behaviour of El Niño over geological timescales but it is possible to surmise the strength and frequency of El Niño through a study of the solar precession cycle. In both

model and real versions of the modern climate, ENSO events develop through a growing season during the boreal summer and into the autumn, after which growth ceases and anomalies break down. Growth is caused by the Bjerknes feedback and there is a positive feedback for only part of the year. In model simulations of the early Holocene, for example, growth of anomalies ends in August before the summer is over and the shorter growing season does not allow anomalies to reach the peak values of today (Cane, 2005).

At the start of the Holocene, the equatorial oceans received about the same annual solar radiation but its seasonal distribution was different to the present. Due to a boreal summer perihelion, northern hemisphere insolation was stronger in the late summer and therefore the Inter-Tropical Convergence Zone (ITCZ), shifted towards the higher tropical latitudes. A critical link in the Bjerknes (1966; 1969) feedback is from sea-surface temperature to enhanced heating to changes in the winds (Cane, 2005). The heating is associated with low level convergence, and if the convergence cannot be shifted to the equator, the link fails and ENSO anomalies do not develop. Thus asymmetrical heating at the equator associated with a boreal or austral summer perihelion tends to weaken the development of El Niño, while a boreal or austral spring perihelion tends to strengthen El Niño development. This analysis omits mechanisms that might alter the outcome, such as the advection of subsurface temperature anomalies, but the results do correlate well with the comprehensive coupled general circulation model (Otto-Bleisner *et al.*, 2003).

Clement *et al.* (2001) used the Zebiak-Cane (1987) model to simulate El Niño events over the last 500 000 years. They identified two El Niño periods, a regular one of approximately 3 years which occurred when there was a boreal spring perihelion, and another more irregular period of approximately 4 years, which occurred when there was a boreal autumn perihelion. During the transition between these two modes, there were regular El Niño shutdowns when the system had no clearly defined mode of behaviour and periodically locked to the period of forcing (1 year). This transition period occurred during an austral summer and winter perihelion, thus giving a return period of 11 000 years for the ENSO shutdown, or half a precessional cycle (Clement *et al.*, 2001). The last shutdown occurred around the start of the Holocene (Clement *et al.*, 2001).

According to Timmerman *et al.* (2006), previous models such as the Zebiak-Cane model failed to simulate the annual cycle in the Pacific realistically. The key element for the

generation of the equatorial annual cycle is the northern position of the Intertropical Convergence Zone (ITCZ) associated with hemispheric land cover differences. The attendant meridional temperature asymmetry around the equator and the physical processes responsible for the annual cycle in the eastern equatorial Pacific are distinct from those for the interannual ENSO mode, and the amplitude of ENSO depends on the strength of the annual cycle in a complex manner (Chang *et al.*, 1994; Liu, 2002). One extreme case is that the annual cycle is absent, and thus the ENSO amplitude is determined simply by ENSO relevant processes. The other extreme case is a very strong annual cycle forcing, which prevents the generation of interannual ENSO anomalies. Clement *et al.* (1999, 2001) used an intermediate ENSO model with prescribed annual cycle to study the influence of orbital forcing over the last 500 000 years on ENSO strength. Because of the prescribed annual cycle in the model, the anomalous annual cycle simulated in response to orbital forcing arises primarily via ENSO physics. The Timmerman *et al.* (2006) model, which simulated the annual cycle more realistically, indicated that El Niño would be strongest during an austral summer perihelion (as at present) when the annual cycle is weakest, and weakest at a boreal summer perihelion when the annual cycle is strongest.

The three (winter, all-year, and summer) rainfall regions of southern Africa respond differently to El Niño (Tyson, 1986; Tyson and Preston-Whyte, 2000). El Niño produces drier conditions over the summer rainfall region and wetter conditions over the winter rainfall regions and La Niña results in the opposite (Lindesay, 1988; Mason and Lindesay, 1993; Allan *et al.*, 1996). Similarly, an inverse correlation is experienced over longer periods of wet and dry years (Muller and Tyson, 1988) and over centuries and millennia (Cockcroft *et al.*, 1987; Tyson, 1999a). In the all-year rainfall region, the nature of the correlation depends on whether the summer or winter atmospheric circulation is contributing more to the annual rainfall record (Tyson *et al.*, 2002a).

## **5.5 APPLICATION OF MODELS TO PALAEOCLIMATES**

The Tyson (1986; 1999a) atmospheric circulation model and the El Niño model can be applied to the palaeoclimates of southern Africa of the last 20 000 years. The following periods of analysis have been selected based on homogeneity in mean atmospheric

circulation within periods and a discontinuity between periods: 20 000 BP – 12 000 BP, 12 000 – 10 000 BP, 10 000 – 4000 BP, and 4000 BP to present.

### 5.5.1 20 000 to 12 000 BP

#### 5.5.1.1 *Mean Atmospheric Conditions*

CLIMAP (1981) made use of General Circulation Models (GCMs) to simulate global palaeoclimates using boundary conditions for defined time slices in the past. The results correlated well with various palaeoclimatic records. The findings of these studies support the assertion that at the Last Glacial Maximum, the equatorial zone of maximum sea-surface temperature and the Inter-Tropical Convergence Zone were displaced northward. Howard (1985) proposed that the Antarctic Ocean Convergence moved 5 - 8° and the Subtropical Convergence 3 - 5° equatorward over the oceans at this time. Palaeodune evidence indicated that the subtropical high-pressure system responsible for the Late Quaternary Kalahari dunefield, which formed at the time of the Last Glacial Maximum, was displaced about 2° northwards (Lancaster, 2000).

As the Last Glacial Maximum approached, the Tyson (1986) dry spell analogue would have prevailed with a progressive equatorward displacement of the circulation (Cockcroft *et al.*, 1987). The palaeorainfall record for this period suggests an equatorward displacement of the winter rainfall margin in the order of 8° over the western parts of the subcontinent (Cockcroft *et al.*, 1987) as shown in Figure 5.11. This is consistent with records of Karoo vegetation in an expanded winter rainfall region (Bayer, 1984).

The humidity record for the south-western parts of southern African indicates a wet Last Glacial Maximum, which can be attributed to the equatorward shift of the westerlies (Stuut and Lamy, 2004) and the movement of storm tracks northward (Tyson and Preston-Whyte, 2000). A summer rainfall regime remained only over the far eastern and north-eastern areas of South Africa and these regions would have been drier due to a weaker Walker Circulation and the absence of tropical easterly wind anomalies (Tyson and Preston-Whyte, 2000). Some of the reported findings of drier conditions in the southern Cape conflict with the model and are likely to be explained by local rainfall effects (Cockcroft *et al.*, 1987).

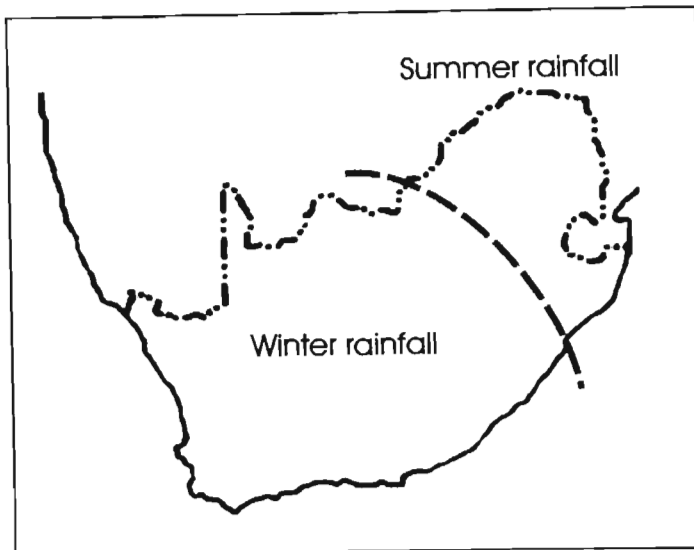


Figure 5.11 – Distribution of winter and summer rainfall regions at the Last Glacial Maximum (approximately 18 000 BP).

After the Last Glacial Maximum, contraction of the circumpolar westerlies occurred and storm tracks returned southwards. There was a progressive decrease in the extent of the winter rainfall region. There was a progressive moistening over the summer rainfall region due to the increased incursion and persistence of tropical easterly disturbances.

#### 5.5.1.2 Disturbances to the Mean: El Niño

According to the CLIMAP (1981) model results little or no cooling occurred in the tropics at the time of the Last Glacial Maximum. Coral and terrestrial records, however, show a significant cooling at this time. Mix *et al.* (1999) established a record of sea-surface temperatures from the time of the Last Glacial Maximum until the present from foraminifera assemblages and the authors proposed that at the Last Glacial Maximum, there was significant cooling in the eastern equatorial Pacific, creating a perpetual La Niña state. However, a study of foram geochemistry by Koutavas *et al.* (2002) indicated that the western Pacific cooled to a greater degree than the eastern Pacific, which weakened the temperature gradient and created more El Niño-like conditions at this time. This correlates with the results of the Zebiak-Cane model (Figure 5.12) and the hypothesised relationship with solar precession.

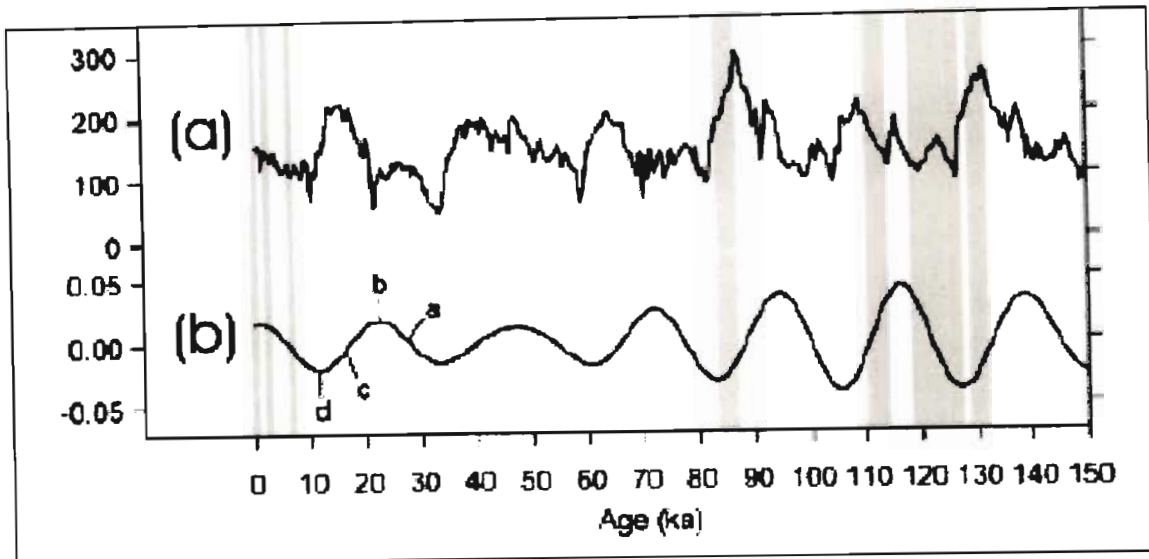


Figure 5.12 – (a) Zeblak-Cane model of El Niño-Southern Oscillation power over time and (b) solar precession with a = boreal autumn; b = boreal winter; c = boreal spring; d = boreal summer perihelion (Tudhope *et al.*, 2001, 1515).

Otto-Bleisner *et al.* (2003) proposes that at the Last Glacial Maximum, colder waters, which moved into the tropics from high latitudes, cooled and intensified the thermocline, which made the eastern Pacific more sensitive to small changes in wind. This weakened orbital control on El Niño and resulted in a stronger, more variable ENSO with a greater amplitude and higher frequency. After the Last Glacial Maximum, El Niño began to weaken towards a power minimum at around 10 000 BP (Figure 5.12).

## 5.5.2 12 000 to 10 000

### 5.5.2.1 Mean Circulation

An increase in aridity between 12 000 and 10 000 BP is likely to have occurred under a circulation regime similar to that postulated for present-day extended dry spells, but without the extensive equatorward displacement of the circulation that occurred during the previous period (Cockcroft *et al.*, 1987). The transition zone between the summer and winter rainfall regions shifted southwards from the Last Glacial Maximum and therefore moved closer to its present position. The position of the summer rainfall and winter rainfall regions during this period are shown in Figure 5.13.

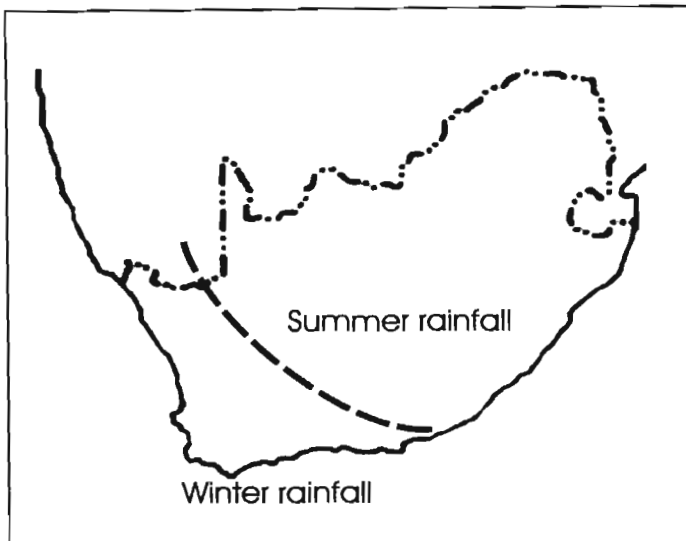


Figure 5.13 – Distribution of summer and winter rainfall regions 12 000 – 1000 BP.

Dry conditions would have resulted from a deficiency in summer rainfall over the summer rainfall region but the winter rainfall region of the south-western Cape was likely to have been wetter than presently. Butzer’s (1983) findings based on the presence of ferruginous horizons at Nelson Bay Cave on the southern Cape coast support this view.

#### 5.5.2.2 *Disturbances to the Mean: El Niño*

The frequency of El Niño episodes decreased substantially over this period due to the shift towards a boreal summer perihelion which increased asymmetrical heating at the equator (Cane, 2005). The Zebiak-Cane model clearly indicates the sudden drop in ENSO power (Figure 5.12) towards the end of this period.

### 5.5.3 10 000 to 4000 BP

#### 5.5.3.1 *Mean Circulation*

The moistening conditions of the interior between 9000 and 6000 BP were the result of increased summer rainfall associated with a circulation pattern similar to the present-day wet spell analogue (Cockcroft *et al.*, 1987) with a boosted Walker Circulation and greater tropical influence on rainfall. Weaker westerly circulation would have occurred over the southern part of the subcontinent, though further south, in the region of 45° S, it would have been stronger. The south-western Cape region would have been drier and there is



evidence of this in the findings of Tankard (1976), Klein (1980) and Avery (1982b). The model is similar to that proposed for Australasia at 9000 BP (Salinger, 1984) and is consistent with the theories of Nicholson and Flohn (1980) and Newell *et al.* (1981).

At the time of the Holocene Altithermal (8000 – 6000 BP), circulation was likely to have been controlled mainly by tropically induced disturbances in the easterlies as shown in Figure 5.14. Winter rainfall in the summer rainfall region was less than experienced at present and annual rainfall would have been higher than at present. The warming and increase in rainfall would have advanced southwards from the more tropical regions of southern Africa to reach the southern coast of South Africa (Scott, 1993). The poleward advance of increasing annual rainfall toward high latitudes was quasi-linear, commencing around 7500 BP at the Tropic of Capricorn and only at about 3500 BP on the southern coast of South Africa (Figure 5.14). The Altithermal conditions appear to have advanced poleward at a rate of 3 to 4 degrees of latitude per millennium (Tyson, 1999a).

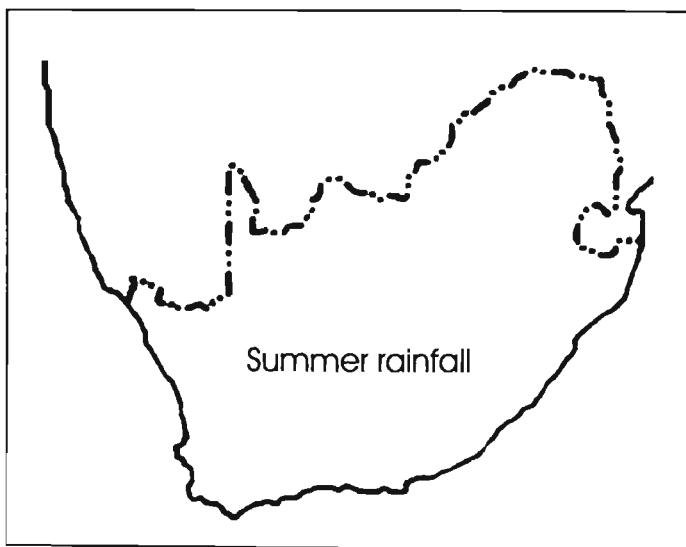


Figure 5.14 – The dominance of summer rainfall at the Holocene Altithermal (approximately 6000 BP).

#### 5.5.3.2 Disturbances to the Mean: *El Niño*

*El Niño* was systematically weaker during the early and middle Holocene as indicated in the results of a study of banded coral from Papua New Guinea (Tudhope *et al.*, 2001) and of foraminifera from seafloor sediments near the Galápagos Islands (Koutavas *et al.*, 2002). Koutavas *et al.* (2002) proposed that during the early Holocene, the zonal temperature gradient increased by 0.5 °C, and caused stronger trade winds and a more La

Niña-like state. Model results from Clement *et al.* (2001) and Timmerman *et al.* (2006) showed a weakened El Niño during the early and middle Holocene. The comprehensive coupled general circulation model showed a particularly weak amplitude El Niño–Southern Oscillation at 9000 BP (Otto-Bleisner *et al.*, 2003).

#### **5.5.4 4000 BP – Present**

##### *5.5.4.1 Mean Circulation*

The medieval warming from 1100 to 700 BP (850 to 1250 AD) and the Little Ice Age from 700 to 150 BP (1250 to 1800 AD) can also be linked to variations in the extent of the circumpolar vortex. A southward shift of the pressure belts increased the tropical influence on the summer rainfall region during the Medieval Warm Epoch with associated increases in rainfall in the summer rainfall region. During the Little Ice Age, a weakened influence of the tropical easterlies limited rainfall in the region. While the long-term shifts between wet and dry spells in the past had been strongly influenced by the solar precession cycle, the shorter events of the last 1000 years appear to be related to variations in solar activity (Tyson, 1999b).

##### *5.5.4.2 Disturbances to the Mean: El Niño*

El Niño strength continued to increase from a minimum at approximately 10 000 BP until the present (Tudhope *et al.*, 2001). According to the Timmerman *et al.* (2006) model, El Niño frequency should be at its highest over the last precessional cycle at present. This peak may also incorporate an anthropogenic influence as the increase in global warming is likely to increase El Niño frequency and weaken the orbital influence (Mason, 2001).

## **5.6 SUMMARY**

Wet and dry spells have occurred on decadal scales during the period of meteorological record and similar spells can be detected in palaeoclimatic records going back several centuries. Tyson (1986) introduced a model of the atmospheric circulation changes that result in these alternating wet and dry spells. These mechanisms relate to latitudinal shifts

of the westerly and easterly wind belts, *in situ* intensification of semi-permanent circulation cells, meridional shifts in the African cloud band and convergence zone, fluctuations in amplitude and position of the mid-tropospheric standing waves, and changes in sea-surface temperature (Tyson, 1999a). General circulation models have highlighted the importance of these mechanisms on the scale of decades to centuries and beyond (Tyson, 1999a). On the scale of millennia, additional forcing by precessional changes in solar radiation modulates rainfall receipt over wide areas. A boreal summer perihelion causes a northward shift of the pressure belts and an increase in the strength and persistence of dry spells, while an austral summer perihelion causes a southward shift and an increase in strength and persistence of wet spells over the summer rainfall region of southern Africa.

It is apparent from palaeoclimatic records that warmer periods in the summer rainfall region over geological history have also been moister. At first this seemed counter-intuitive as present-day droughts, occurring on approximately monthly scales, are associated with warm temperatures. On decadal, centennial and longer timescales, however, the major circulation changes that occur override these local effects, and generally warmer conditions are associated with increased rainfall, while cooler conditions are associated with decreased rainfall. The reasons for this relationship become clear in the Tyson (1986) model. At these longer timescales, a poleward expansion of the tropical easterlies causes warmer and wetter conditions over southern Africa south of 20° S, while an expansion equatorward of the westerlies and associated frontal disturbances results in cooler, drier conditions in the summer rainfall region (Tyson, 1999a). The winter rainfall region shows an inverse relationship with the summer rainfall region, and cool periods are generally moist while warm periods are dry. Major adjustments of atmospheric circulation causing the association of warmer and wetter, and cooler and drier conditions in the summer rainfall region have been sustained for at least 200 000 years on multi-decadal and longer timescales (Tyson, 1999a).

These mean circulation fluctuations exert a strong influence on climate, but disturbances moderate their control. The El Niño–Southern Oscillation is a quasi-regular disturbance to this mean circulation and is associated with increasing aridity over the summer rainfall region of southern Africa. Despite its strength being ultimately controlled by solar precession, El Niño is an example of an internal climate change mechanism which distorts

the atmospheric patterns which would exist in world of purely external solar control on atmospheric circulation. Chapter 6 offers an analysis of various internally and externally controlled climatic cycles, and a discussion of their interaction and influences on southern African climate.

## 6. SOUTHERN AFRICAN CLIMATIC VARIABILITY

### 6.1 INTRODUCTION

Glacial and interglacial periods, and the fluctuations of temperature and rainfall that occur within these periods, are a consequence of mechanisms that alter either the total amount of energy available to the geosphere-hydrosphere-cryosphere-atmosphere system (Figure 6.1), or the storage and transmission of energy within this system (Lindesay, 1990). Climatologists can therefore distinguish two principal types of climate change mechanism: factors that affect the amount of energy received from the sun, known as external factors, and internal factors, which influence the transfer of energy within the global system. External mechanisms of climate change include variations in solar output and adjustments in the orbital parameters of the Earth, while internal mechanisms include plate tectonics, changes in the cryosphere and oceans, and adjustments in atmospheric composition (Lindesay, 1990).

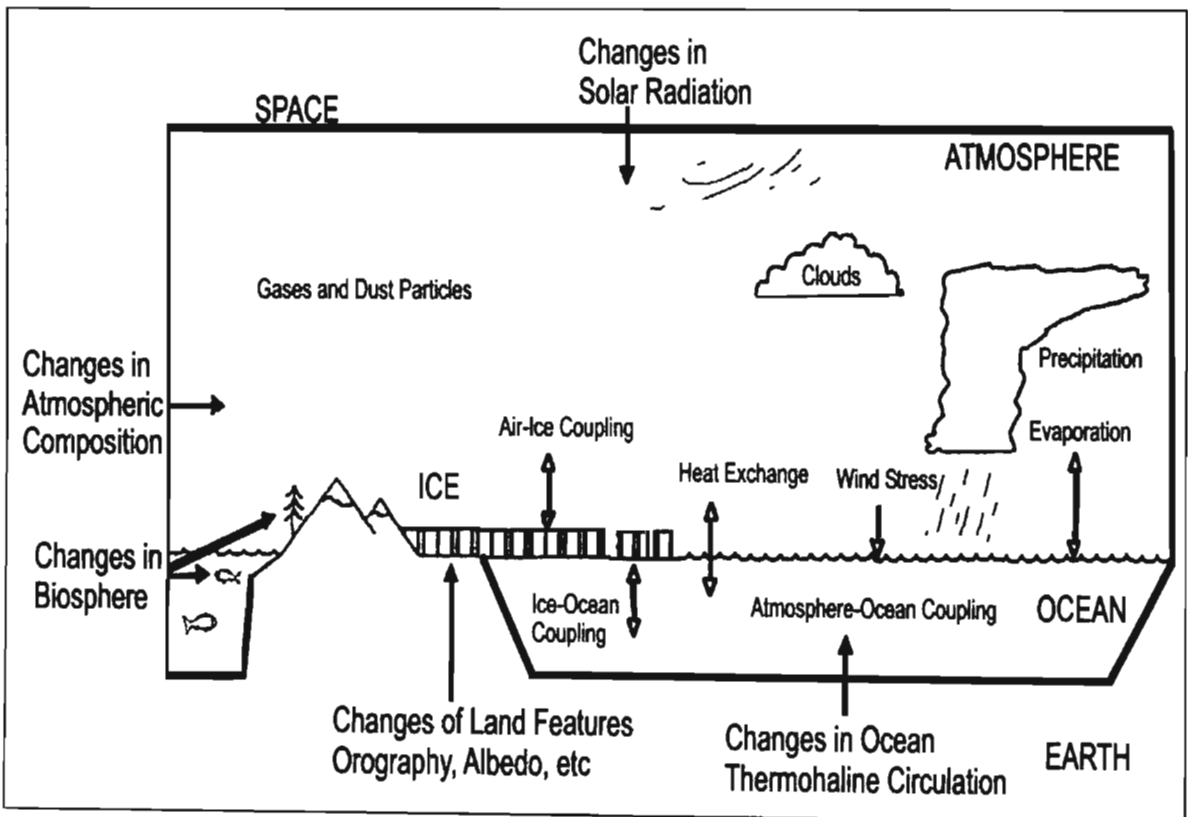


Figure 6.1 – The geosphere-hydrosphere-cryosphere-atmosphere system (Bradley, 1999, 16).

### 6.1.1 External Mechanisms of Climate Change

Isolating the causes of climate change is difficult as the geosphere-hydrosphere-cryosphere-atmosphere system is complex and a change in any component causes feedbacks in other parts. Furthermore the signals of many of the mechanisms of climatic change are weak, and thus are difficult to distinguish from background noise (Lindesay, 1990). Two external mechanisms of climate change that have been identified and extensively studied are orbital variations, which change the astronomical relationship between the Earth and the sun, and variations in solar output. The former mechanism affects the distribution of energy provided to the Earth-atmosphere system, while the latter alters the amount of energy initially available to the system (Lindesay, 1990).

The orbital variations determining the relationship between the Earth and the sun have three major components, which are termed the 'Milankovitch cycles'. The eccentricity of the Earth's orbit, in which the orbit varies from more elliptical to more circular, changes on a timescale of about 100 000 years (Figure 6.2a). The obliquity of the elliptic, which is the tilt of the Earth's axis in relation to the orbital plane, fluctuates approximately  $1.5^\circ$  about a mean of  $23.1^\circ$  with a period of approximately 40 000 years (Figure 6.2b). The precession of the equinoxes determines the time of year when the earth is closest to (perihelion) and furthest from (aphelion) the sun. This affects the distribution of solar energy in time and space in a cycle with a period of 19 000 to 23 000 years (Figure 6.2c), and a generalised periodicity of approximately 22 000 years (Oliver and Hidore, 1984; Henderson-Sellers and Robinson, 1986; Lindesay, 1990).

The oscillatory features of the Milankovitch cycles can be calculated, and combinations of the three cycles can be correlated with long-term climatic variations. The role of these cycles in controlling climate is evident in the recurrence of the Milankovitch periods (approximately 22 000, 40 000 and 100 000 years) in various palaeoclimatic datasets. Evidence from marine sediment and ice cores indicates the presence of the Milankovitch cycles in the Earth's extended temperature record (Hays *et al.*, 1976; Hecht and Imbrie, 1979; Imbrie and Imbrie, 1980; Pisias and Shackleton, 1984; Imbrie, 1985; Pisias and Imbrie, 1986; Jouzel *et al.*, 1987; Pestiaux *et al.*, 1987; Berger, 1988).

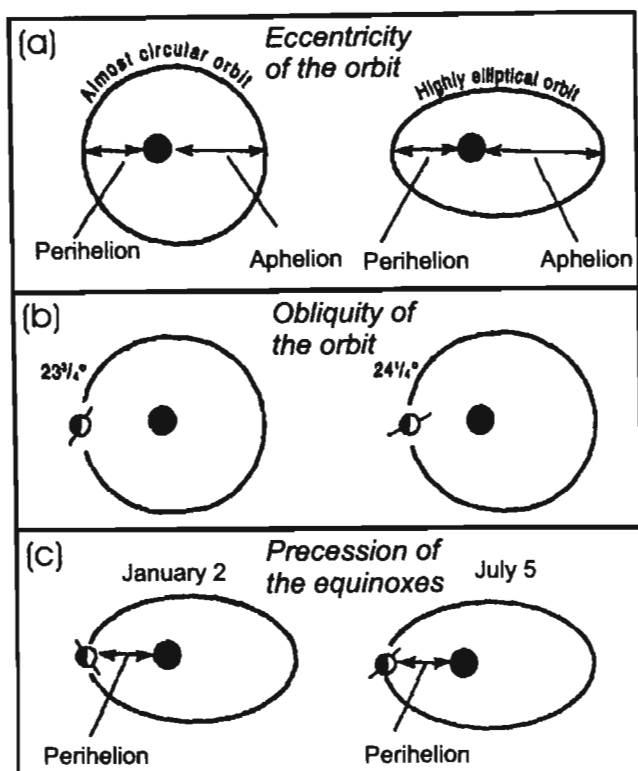


Figure 6.2 – The Milankovitch cycles showing (a) eccentricity of the orbit, (b) obliquity of the orbit and (c) precession of the equinoxes (Tyson and Preston-Whyte, 2000, 55).

Rainfall in the summer rainfall region of southern Africa fluctuates in an approximately 23 000 year cycle (Partridge *et al.*, 1997). The correlation between the rainfall changes at Tswaing Crater (Partridge *et al.*, 1997) and the Milankovitch precession solar radiational curve for the approximate latitude of the site over the last 200 000 years is shown in Figure 6.3. Rainfall changes at this site were clearly influenced by solar precession.

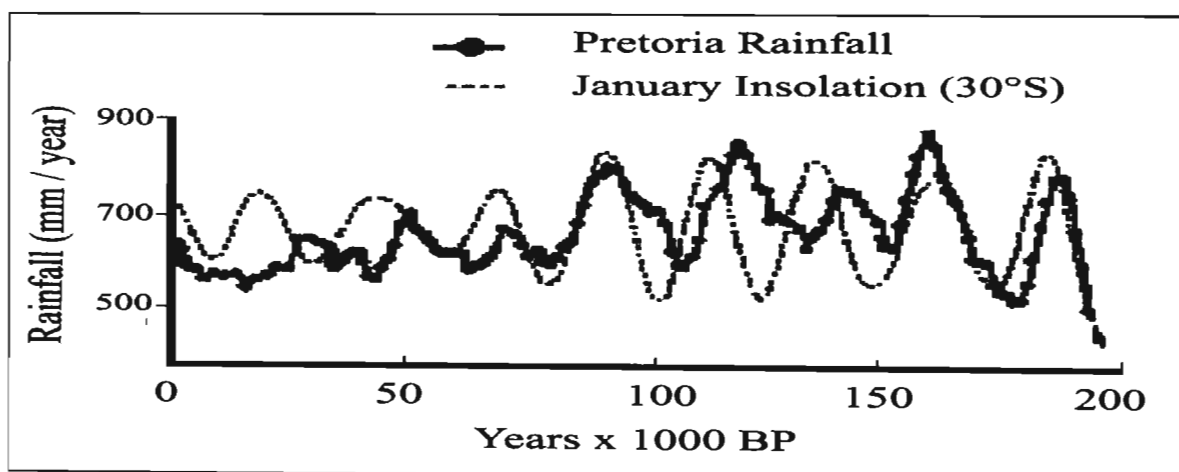


Figure 6.3 - Pretoria rainfall and January insolation at 30° S (Partridge *et al.*, 1997).

Although variations in the Earth's orbit appear to have had a major influence on the succession of glacials during the Quaternary, and on climatic changes during the Holocene (Lindesay, 1990), Milankovitch forcing is not adequate alone for modelling past global ice volumes or future climatic changes accurately. The incorporation of long-period variations in atmospheric CO<sub>2</sub>, for example, greatly improves models, as changes in atmospheric CO<sub>2</sub> level intensify and complicate the effects of Milankovitch signals (Lindesay, 1990). The exact mechanisms by which the relatively small variations in the Earth's orbit and axis direction cause significant climate variations are not well established, but some theories will be presented in Section 6.1.2.

The second widely-studied external mechanism of climate change is solar variability associated with visible activity such as flares or sunspots. Long-term changes in solar activity, on timescales of 100 years or more, have been linked with climatic variations such as the Little Ice Age (Schuurmans, 1981; Lamb, 1982). The five centuries of the Little Ice Age represent the longest perturbation in the 3000 year record of the Makapansgat Valley and correspond with the decline in solar irradiance that occurred during the Maunder Minimum from 355 to 285 BP (1645 to 1715 AD), the Sporer Minimum at approximately 500 BP (1500 AD) and an unnamed minimum at approximately 650 BP (1350 AD) (Hoyt and Schatten, 1997). A clear correspondence between moisture conditions over the last 1000 years in the summer rainfall region of southern Africa and periods of solar inactivity has been observed in a number of records, with coolest and driest conditions occurring during these minima (Tyson *et al.*, 2000).

The approximately 11 year sunspot and 22 year solar magnetic cycles have been statistically linked with various climatic parameters (Willet, 1987; Reddy *et al.*, 1989). Although the amplitudes of the climatic variations concerned are often too small to be easily detected in most records, scientists have linked the 22 year solar magnetic cycle with significant variations in global marine air temperatures (Newell *et al.*, 1989). The 11 year sunspot cycle has also been correlated with stratospheric temperature variations and the phase of the tropical stratospheric wind reversal, known as the Quasi-Biennial Oscillation (QBO) (Labitzke and van Loon, 1987; 1989; Tinsley, 1988; Van Loon and Labitzke, 1988), which modulates the effect of El Niño on southern Africa (Tyson and Preston-Whyte, 2000).



### 6.1.2 Internal Mechanisms of Climate Change

While external mechanisms of climate change control the amount of solar energy received by the Earth, internal mechanisms influence the flow of the energy once it is part of the Earth's systems. To comprehend past, present and future climates, scientists must understand the processes which currently control variations of climate on timescales from years to decades. Within this time frame, external parameters such as solar variability have a small influence on climate, and it is the internal factors, including changes in the composition of the atmosphere, oceanic temperature variations and large-scale atmospheric circulation anomalies, that have the greatest affect (Lindesay, 1990).

Changes in the geosphere have influenced climate over geological timescales. Continental drift, for example, led to significant climatic adjustments as Gondwanaland broke apart and the continents edged towards their present positions. Changes in ocean basin configurations, the development of the present oceans and current systems, and sea-level changes, have all affected the climates of the continents over time (Lindesay, 1990). Also on geological timescales, variations in ice cover, particularly over the poles, have been substantial. During cooler periods, terrestrial and sea ice cover has increased, enhancing the albedo of the affected areas and thus decreasing absorption of solar radiation. Furthermore, the low thermal conductivity of snow and ice limits heat exchange between the surface and the atmosphere. In this way, a positive feedback occurs which reinforces the growth of snow and ice masses, and the reverse of these processes reinforces a contraction of the cryosphere during warmer periods (Lindesay, 1990).

Fluctuating atmospheric composition, which controls the radiation and heat balance of the Earth-atmosphere system, is another important internal climate change mechanism (Thompson, 1989). The relative concentrations of the constituent gases and particulate matter within the atmosphere have shown significant variations over time (Lindesay, 1990). A rise in atmospheric turbidity causes increased reflection of solar radiation and a lowering of surface temperature (Henderson-Sellers and McGuffie, 1987). Despite attempts to establish a volcanic signal in surface air temperature by measuring the frequency of large volcanic eruptions that eject particulates into the upper troposphere and stratosphere (Lamb, 1982), only the largest eruptions appear to have a detectable effect on climate (Hare, 1979; Mass and Portman, 1989). Two recent large eruptions, namely Mount

Agung in 1963 and El Chichon in 1982, coincided with major warm events in the Pacific Ocean, leading to suggestions that Pacific warmings may be caused by volcanic dust (Handler, 1984; 1986). It is more likely, however, that the coincidence of this volcanic event with an El Niño event disguised the cooling effects that are to be expected in the one to two years following a major eruption (Lamb, 1982; Mass and Portman, 1989).

While atmospheric dust concentrations are relevant, it is the trace gases present in the troposphere and stratosphere that play the decisive role in determining the radiation balance of the Earth-atmosphere system. The most important gases in the atmosphere are carbon dioxide (CO<sub>2</sub>), water vapour (H<sub>2</sub>O), methane (CH<sub>4</sub>), nitrous oxides (NO<sub>x</sub>) and chlorofluorocarbons, collectively known as the 'greenhouse gases' (Lindesay, 1990). These gases restrict the loss of long-wave (with a wavelength between 7 and 100 µm) terrestrial radiation to space. The greenhouse effect plays a critical role in regulating the temperature of the Earth-atmosphere system (Lindesay, 1990) and without the presence of these gases in the atmosphere, Earth would be on average 33 K colder than its present mean temperature of 288 K (Ramanathan *et al.*, 1989).

The most important greenhouse gas is CO<sub>2</sub>, the natural levels of which have varied considerably over geological time in synchrony with glacial and interglacial periods (Gribben, 1989). Fluctuations in CO<sub>2</sub> and CH<sub>4</sub> naturally occur as part of the carbon cycle, which is one of several biogeochemical cycles that are a manifestation of life on Earth. The carbon cycle maintains an approximate balance between green biomass, photosynthesis, forest soils (Handler, 1984) and the oceans (Bolin, 1986) when undisturbed. As a result, natural CO<sub>2</sub> levels can be considered to be constant over timescales less than a millennium (Moore and Bolin, 1986).

Berner *et al.* (1979) published groundbreaking work that indicated that the CO<sub>2</sub> content of the air trapped in ice from the glacial sections of the Greenland and Antarctic cores was about two thirds of the CO<sub>2</sub> content of air trapped in ice from the interglacial sections. Since colder, more saline oceans would limit CO<sub>2</sub> solubility by an amount that would explain only approximately 10% of this difference (Bradley, 1999), other factors had to be considered. This stimulated investigations into changes in ocean chemistry over geological timescales (Broecker, 1981; 1982a; 1982b).

Since the ocean carbon content is 50 to 60 times greater than that of the atmosphere, any change in the amount of oceanic uptake or loss of CO<sub>2</sub> would have a significant impact on atmospheric CO<sub>2</sub> levels (Broecker, 1982b). It was known that when major climate changes took place, changes in the Earth's orbit preceded the changes in CO<sub>2</sub>, and that the changes in CO<sub>2</sub> preceded changes in ice cover. But despite a number of theories, exactly how CO<sub>2</sub> variations and long-term climatic change on the scale of thousands of years are related remained a mystery for many years of scientific investigation (Lindesay, 1990).

Detailed studies of ocean chemistry revealed that fluctuations in CO<sub>2</sub> are caused by alterations in the rate of oceanic overturning and hence mixing of CO<sub>2</sub> through the ocean mass (Moore and Bolin, 1986), and also by the rate of extraction of CO<sub>2</sub> from the atmosphere by plankton in the oceanic mixed layer (termed the 'biological pump') (McCarthy *et al.*, 1986; Takahashi, 1986). At higher latitudes, this process is particularly effective at bolstering the Milankovitch mechanism of climatic change (Berner *et al.*, 1979; Delmas *et al.*, 1980; Neftel *et al.*, 1982). Broecker (1981) hypothesised that the plankton living at high latitude polar regions formed the link between the slight temperature changes of the Milankovitch cycles and the start and end of a glacial period. The author suggested that the transfer of nutrients from eroding continental shelves, exposed by marine regression, raised the productivity level of the ocean, and the increased biomass in the surface waters acted as a 'biological pump' to draw down atmospheric CO<sub>2</sub>. This theory dominated for a number of years but further research indicated that CO<sub>2</sub> changes could not be purely the result of the erosion of shelf sediments as these could not occur fast enough to produce the changes that had occurred - such as a 60 ppm CO<sub>2</sub> change in approximately 100 years (Lindesay, 1990).

To be viable, hypotheses began to call upon the redistribution of carbon, phosphorus, and fixed nitrogen in the sea (Broecker and Takahashi, 1984; Knox and McElroy, 1984; Sarmiento and Toggweiler, 1984; Siegenthaler and Wenk, 1984). However, such redistributions are only feasible if ocean mixing and biological cycling change substantially over a short period of time. This is highly unlikely in these complex and carefully balanced systems. Furthermore, evidence of nutrient variations, in particular dissolved phosphate, did not reveal significant changes between glacial and interglacial periods (Boyle and Keigwin, 1982), and sea-level changes tended to lag orbital forcings and CO<sub>2</sub> changes by several thousands of years. The proposal of nutrient redistribution,

however, was not entirely incorrect as it is now known that the redistribution of nitrogen, which is a key nutrient limiting biological productivity in many parts of the ocean, plays an important role in changes of atmospheric CO<sub>2</sub> levels, albeit not a dominant role (Bradley, 1999).

Scientists realised that there were more complicated links between climate and oceanic systems and new theories suggested that major climate changes occurred as a result of the joint operation of the atmosphere and ocean (Sarmiento and Toggweiler, 1984; Siegenthaler and Wenk, 1984; Knox and McElroy, 1984; Broecker and Takahashi, 1984). It was known that the degree of upwelling of carbon-rich deep waters affected the amount of CO<sub>2</sub> returned to the atmosphere. A scientific breakthrough occurred when Broecker and Takahashi (1984) suggested that a change in the water transfer rate between the cold- and warm-water spheres of the ocean would bring about a redistribution of CO<sub>2</sub> between these reservoirs and influence global climate.

Circulation of water at the ocean surface is essentially a response to the overlying atmospheric circulation that causes drag at the surface (Bradley, 1999). Circulation of deeper waters, on the other hand, is caused by density variations which result from differences in temperature and salinity caused by sensible and latent heat fluxes, precipitation, and runoff from continental areas, particularly the ice caps. In areas where surface waters become relatively dense, due to cooling or evaporation, the waters will sink to the level of equilibrium with surrounding water masses (Bradley, 1999). In areas of sea ice formation, salt is expelled from the water during the freezing process. These waters have a high density and thus experience sinking. Dense waters flow away from the source region as either bottom waters or intermediate waters depending on their relative density (Bradley, 1999).

At present, Antarctic bottom water originates from areas of sea-ice formation adjacent to Antarctica, and North Atlantic deep water (NADW) forms in the Norwegian Sea and in the region of Greenland (Bradley, 1999) as shown in Figure 6.4. Deepwater presently does not form in the North Pacific where waters are less saline than in the North Atlantic (Bradley, 1999).

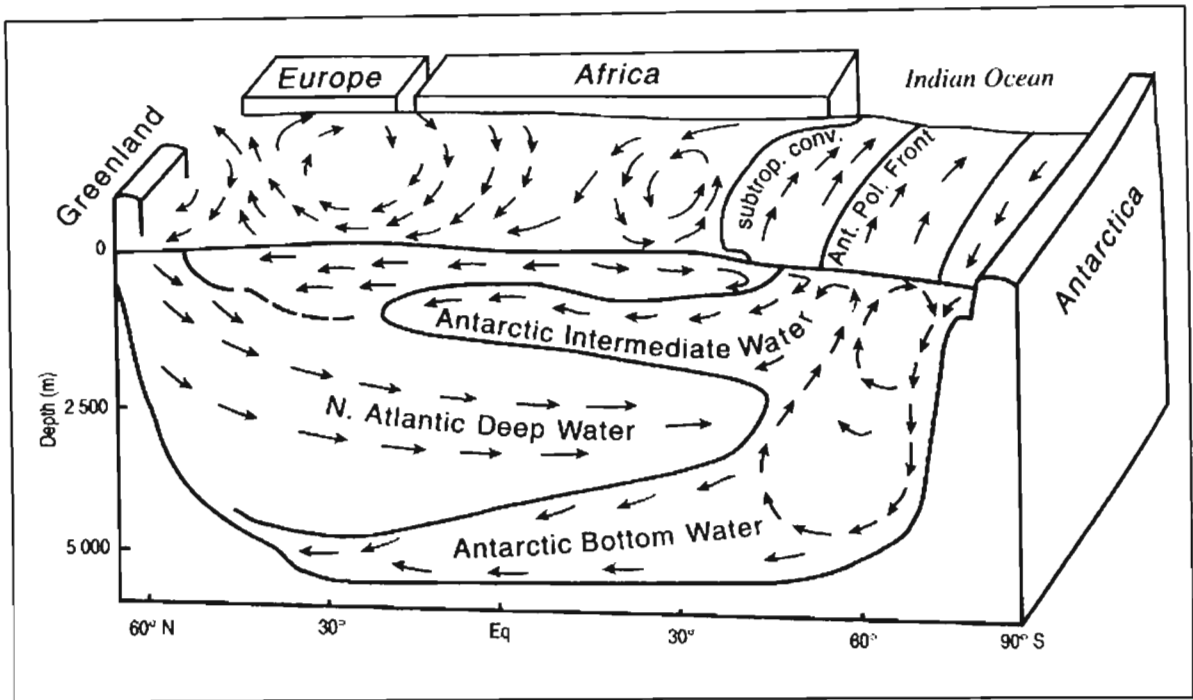


Figure 6.4 – Idealised thermohaline circulations in the Atlantic Ocean (Tyson and Preston-Whyte, 2000, 226).

Deep thermohaline flow from the Atlantic Ocean travels through the Indian Ocean to the Pacific Ocean. The belt then rises and returns to its region of origin through the warm, saline, surface waters in the Gulf Stream and associated North Atlantic Drift (Figure 6.5).

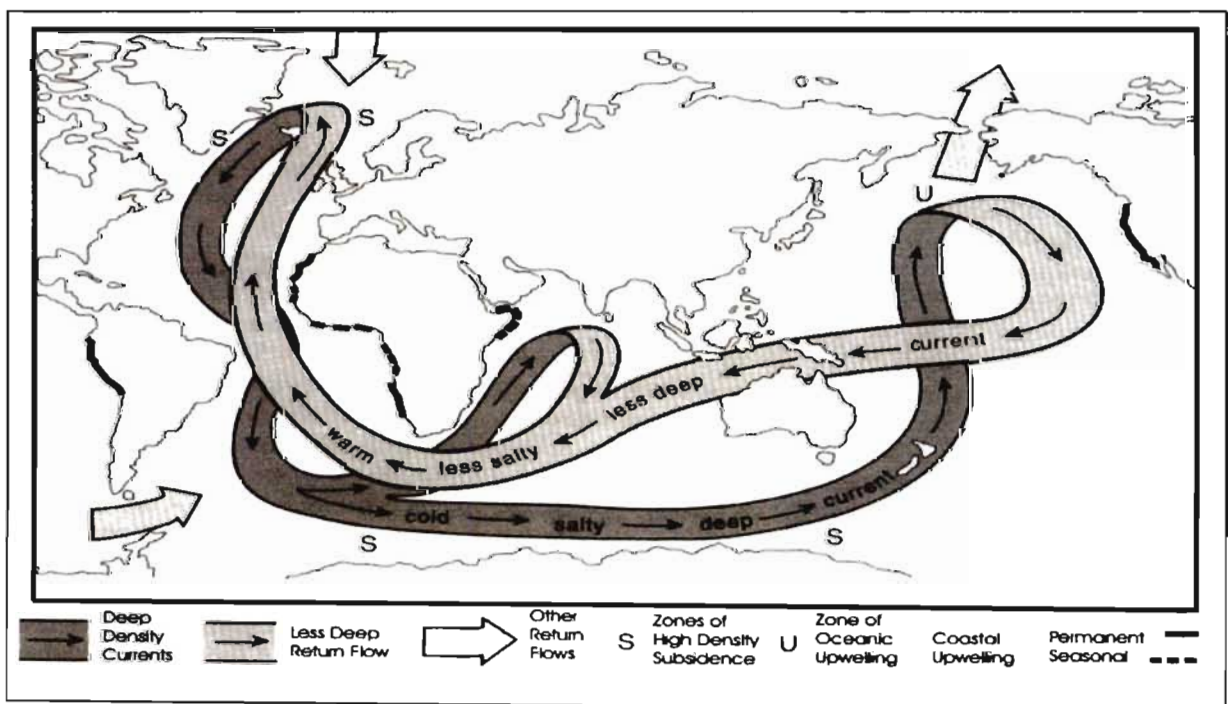


Figure 6.5 – Broecker's concept of the deep-ocean thermohaline conveyor belt (Tyson and Preston-Whyte, 2000, 227).

The major forcing mechanism of the conveyor is in the high-latitude region of the North Atlantic Ocean. Here the thermocline is weak and only small changes in regional climate can prevent the sinking of water, which is necessary to produce the subsurface flow of intermediate water to the south. In such a situation, the conveyor may stop or reverse. Consequently a small climate change in the region can cause a global climatic event (Bradley, 1999).

The North Atlantic thermohaline circulation can be thought of as having two distinct modes. If the freshwater flux to the North Atlantic were to increase, such as when the major ice sheets melted, it would create an upper layer of low salinity water which may shut down the process of North Atlantic deep water formation (Bradley, 1999). This would, in turn, 'turn off' the conveyor belt, with an associated reduction of Gulf Stream water flowing in to replace that lost through sinking and with a reduction in deep water sequestration of carbon dioxide. With less heat transported to the North Atlantic and generally colder conditions, there is less freshwater runoff and expansion of the ice sheets. When the conveyor is 'off', the rate of salt export from the North Atlantic (in the North Atlantic deep waters) is less than the rate of salt build-up resulting from evaporation and water vapour export to adjacent regions. Salinity gradually increases until some critical density is reached and the conveyor 'switches back on' (Bradley, 1999).

It was Oeschger *et al.* (1984) who initially came to the conclusion that the ocean-atmosphere system has more than one stable mode of operation and a switch between modes, with an associated change in amount of deep water production in the North Atlantic, would produce a rapid regional climate change with global impacts. Abrupt warmings, followed more gradual coolings, are evident in the Greenland Ice Core Project (GRIP) record as indicated in Figure 6.6. During the warmings, ice-flow debris were deposited on the ocean floor producing a layer rich in polar foraminifera. Although the exact physics still needs to be explained, the switch between modes can be tracked using two variables. The first variable indicates whether water is being stored in or released from the large northern hemisphere glacial ice caps adjacent to the Atlantic. The other is a measure of the transport of salt through the deep sea. As water resides for many hundreds of years in the deep sea, changes in the deep ocean salinity distribution are an important element in the oscillator (Broecker *et al.*, 1985).

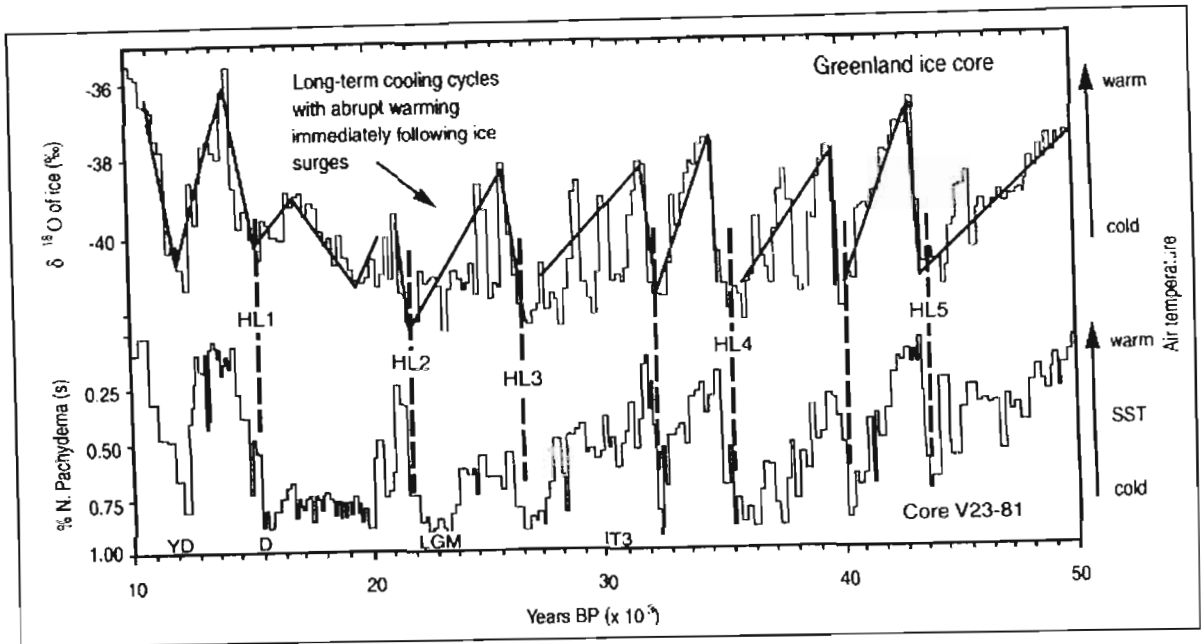


Figure 6.6 – A comparison of the GRIP ice core oxygen-isotope record and the relative abundance of polar foraminifera in the North Atlantic sediment core V23-81. YD denotes Younger Dryas, D deglaciation, LGM Last Glacial Maximum, IT3 Interstadial 3 and HL Heinrich layer (Tyson and Preston-Whyte, 2000, 337).

Mechanisms likely to affect the thermohaline circulation on various timescales are shown in Figure 6.7.

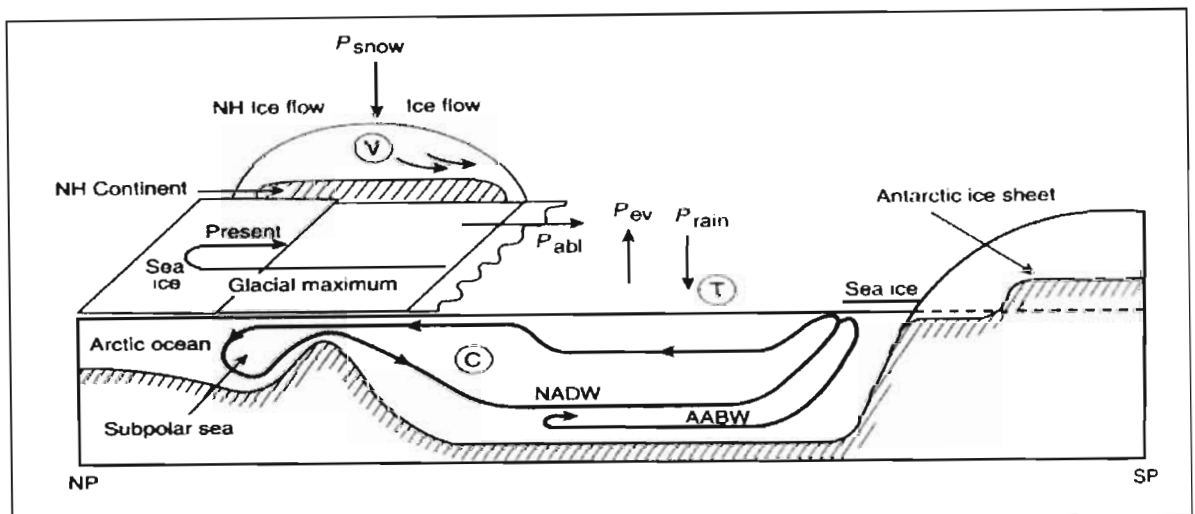


Figure 6.7 – A section through the Atlantic Ocean to show the mechanisms likely to affect thermohaline circulation on various timescales (Tyson and Preston-Whyte, 2000, 338).

Alterations to the hydrological cycle, expressed in terms of the water fluxes of precipitation minus evaporation ( $P_{rain} - P_{ev}$ ) for the ocean, and snowfall minus ablation ( $P_{snow} - P_{abl}$ ) for snow and ice, are due to changes in ocean temperature. The formation of North Atlantic deep water (NADW) is affected by changes in ice volume and extent (V),

and regulates the intensity of the thermohaline circulation (C). Changes in Antarctic bottom water (AABW) formation are likewise affected by the thermohaline process and in turn regulate the overall thermohaline circulation of the system. The thermohaline circulation affects the temperature of the overall system (T) and is also affected by it. Changes in the thermohaline system impact southern African climate as shown, for example, by the teleconnections between the Makapansgat Valley and Greenland (Tyson and Preston-Whyte, 2000).

In the present-day ocean, deep water production corresponds to salt enrichment in the Atlantic, and thus it is possible to hypothesise that during glacial time the opposite was true and that salt was being enriched in the Pacific and deep water flow was the reverse of current conditions. This claim is supported by studies of oxygen isotopes in north Pacific cores, which suggest that deep water may have been produced in the Pacific Ocean during glacial time (Broecker *et al.*, 1985). On the other hand, it is possible that the rate of salt enrichment in the Atlantic was considerably less during glacial times, causing a reduction in deep water production rather than a reverse in flow. A reduction in deep water formation during glacial times is supported by cadmium data from benthic foraminifera that act as powerful tracers of deep water formation (Boyle and Keigwin, 1982).

The current rate of production of deep water in the northern Atlantic region is roughly 20 000 000 m<sup>3</sup>.s<sup>-1</sup> (Broecker, 1979), and the water supplying the source region for the deep water has a temperature of approximately 10 °C, while the new deep water leaving the source region has a temperature of approximately 2 °C. Therefore around 2.092 x 10<sup>19</sup> kilojoules of heat are released to the atmosphere each year, an amount equivalent to almost 30% of the solar heat reaching the surface of the Atlantic Ocean in the region to the north of 35° N (Broecker *et al.*, 1985). This heat is released to the atmosphere by sensible and latent heat exchange and is dependent on sea-surface temperature (Tyson and Preston-Whyte, 2000).

To assess the spatial impact of a quantitative change in released heat, an experiment was performed by Broecker *et al.* (1985) using the general circulation model (GCM) for the atmosphere developed by the Goddard Institute for Space Studies. Air temperatures for a model run with present ocean temperatures were compared with those of a model run with the surface ocean temperature in the region north of the glacial polar front lowered to the



levels estimated by CLIMAP (1981) for glacial time. The air temperature anomaly caused by this change in sea-surface temperature extended across Europe and a decrease in temperature was seen in north-eastern North America, whereas no anomaly was seen in the United States or over Antarctica. These results corresponded neatly with pollen and ice-core evidence for the Younger Dryas event (Broecker *et al.*, 1985). Although this experiment does not confirm that the Younger Dryas event definitely was caused by changes in the rate of deep water production in the northern Atlantic, it does suggest that if such fluctuations were to have occurred, they would have produced climate change with a similar pattern (Broecker *et al.*, 1985).

Lowell *et al.* (1995) studied carbon-dated glacial till material and proposed that the glaciers of the southern hemisphere advanced and retreated in synchrony with northern hemispheric air temperature records, such as during the glacial collapse around 14 000 BP, which occurred 1300 years before the major north Atlantic thermohaline switch at 12 700 BP. Bond and Lotti (1995) studied a high-resolution record of continental material in two North Atlantic Ocean cores. They compared these with temperature estimates from an ice core from the Greenland Ice Core Project (GRIP) and sea-surface temperatures from ocean records, and found that the depositional events were related to discharges from the Icelandic ice cap and the Gulf of St Lawrence. These depositional events correlated well with air temperature events in the Greenland cores, but not as well with the North Atlantic sea-surface temperature records. This suggested that ice surges were initially driven by external atmospheric forcing rather than North Atlantic thermohaline circulation changes. Fresh water released rapidly during the Heinrich events, in turn, disrupted deep water formation, thereby forcing the sudden switch between glacial and interglacial modes of thermohaline circulation. This suggests that other mechanisms of atmospheric CO<sub>2</sub> change precede thermohaline circulation changes, and new theories focus on the interaction of the oceanic alkalinity and biological pumps through carbonate compensation (Sigman and Boyle, 2000).

From this brief summary it is clear that several factors are operating simultaneously to cause shifts between glacial and interglacial periods and to cause higher frequency changes as well. The initial driving force of the glacial-interglacial cycle appears to be orbital forcing, although there are additional feedbacks, such as those involving sea-surface temperature changes, thermohaline circulation changes, surface wind stress, and nutrient

and alkalinity fluctuations. It is evident that a great deal more research on this topic is necessary to increase understanding of the complex interactions between components of the system, and it is likely that our current understanding of the topic may be revised considerably in coming years.

In conclusion it is important to note that the discovery of the abrupt switch between climate modes went against thinking at the time as previously climate change theories had been dominated by the assumption that the response to gradual solar forcings would be smooth. Despite resistance towards the theory of abrupt climate change, subsequent records supported the theory - such as the Vostok ice core (Jouzel *et al.*, 1987), the Greenland ice cores (Chappellaz, 1993) and the Makapansgat stalagmite records (Holmgren *et al.*, 2003). Proof of these abrupt changes supported the 'white Earth catastrophe' theory. This theory presented a situation in which the Earth would be gradually covered with ice. The greatly increased reflectivity of the surface would cause the temperature to suddenly fall below freezing point, and thereby stabilise the change. On the other hand, a 'greenhouse catastrophe' is also possible. If the carbon in sediments were gradually released to the atmosphere, the enhanced infrared absorption would raise the planetary surface temperature and ultimately carbonate minerals and organic residues would no longer form. The major anthropogenic impact on climate lies in the contribution of industrial and other processes to the natural levels of CO<sub>2</sub> in the atmosphere (Lindesay, 1990). Global warming associated with this rise of CO<sub>2</sub> may cause the air temperature to be raised sufficiently to produce greater concentrations of atmospheric water vapour which is a far more efficient absorber of heat, thereby creating a positive feedback effect, and locking the Earth into a trend of temperature increase (Pearman, 1988; Ramanathan *et al.*, 1989).

## **6.2 CLIMATIC CYCLICITY**

The climate of southern Africa is intrinsically variable (Tyson, 1986) with evidence of seasonal, annual, decadal, millennial and longer cycles. Climatic variability is complex and there are a number of forcing factors that interact with one another through the record (Reason *et al.*, 2004). Researchers have linked some regular climatic variations with major external forcing mechanisms of solar and orbital fluctuations. The Maunder Minimum in

solar activity (Lamb, 1982), for example, coincided with the Little Ice Age (Grove, 1988). Other than these major climate-forcing factors, this variability is thought to be influenced remotely via ENSO (Nicholson and Entekhabi, 1986; Lindesay, 1988; Mason and Jury, 1997; Nicholson and Kim, 1997; Reason *et al.*, 2000; Reason *et al.*, 2004), by variability in the neighbouring Indian and Atlantic Oceans (Hirst and Hastenrath, 1983; Ogallo *et al.*, 1988; Walker, 1990; Mason, 1995; Reason and Mulenga, 1999; Reason, 1999; Behera and Yamagata, 2001; Rouault *et al.*, 2003; Reason *et al.*, 2004) and by local land surface processes (Zheng and Eltahir, 1998; Douville *et al.*, 2001; Reason *et al.*, 2004).

### 6.2.1 Cycles on a Milankovitch Scale

Studies of deep sea cores provided a history of climate change over the past million years (Emiliani, 1955; Broecker and Van Donk, 1970). Long-term fluctuations tend to be correlated with global climate-forcing factors such as the solar radiation fluctuations caused by orbital eccentricities (Partridge, 1997). Alternating glacial and interglacial conditions occurred consistently over the period of these records with a quasi-periodicity of approximately 100 000 years (Broecker and Van Donk, 1970) and this cycle is linked to the eccentricity of the Earth's orbit. The records of these climatic cycles are not symmetrical and show prolonged periods of glacial expansion ended by rapid warming.

Further study indicated that the long intervals of glacial expansion are modulated by cycles of approximately 20 000 and 40 000 year duration (Imbrie *et al.*, 1984), which can be linked in timing and amplitude to fluctuations in seasonal discrepancies caused by the Earth's orbital changes (Berger *et al.*, 1984; Imbrie *et al.*, 1984). For example, the 23 000 year cycle of the precession of the equinoxes has a strong influence on global climate. Presently the perihelion occurs in January in the southern hemisphere summer and the aphelion in July in the southern hemisphere winter (Tyson, 1999b). This causes the southern hemisphere summers and winters to be more severe than those experienced in the northern hemisphere.

When the perihelion occurs during the southern hemisphere summer (Figure 6.8a), the southern hemisphere summer Inter-Tropical Convergence Zone (ITCZ) strengthens, and tropical forcing of summer southern African climates increases and moister conditions occur. Drier conditions prevail over Africa north of the equator. When the aphelion occurs

in the southern hemisphere summer (Figure 6.8b), the temperature gradient between equator and South Pole weakens, as does the southern hemisphere summer ITCZ. Tropical forcing at this time weakens and drier conditions occur in the southern hemisphere, with moister conditions over Africa north of the equator (Tyson, 1999b).

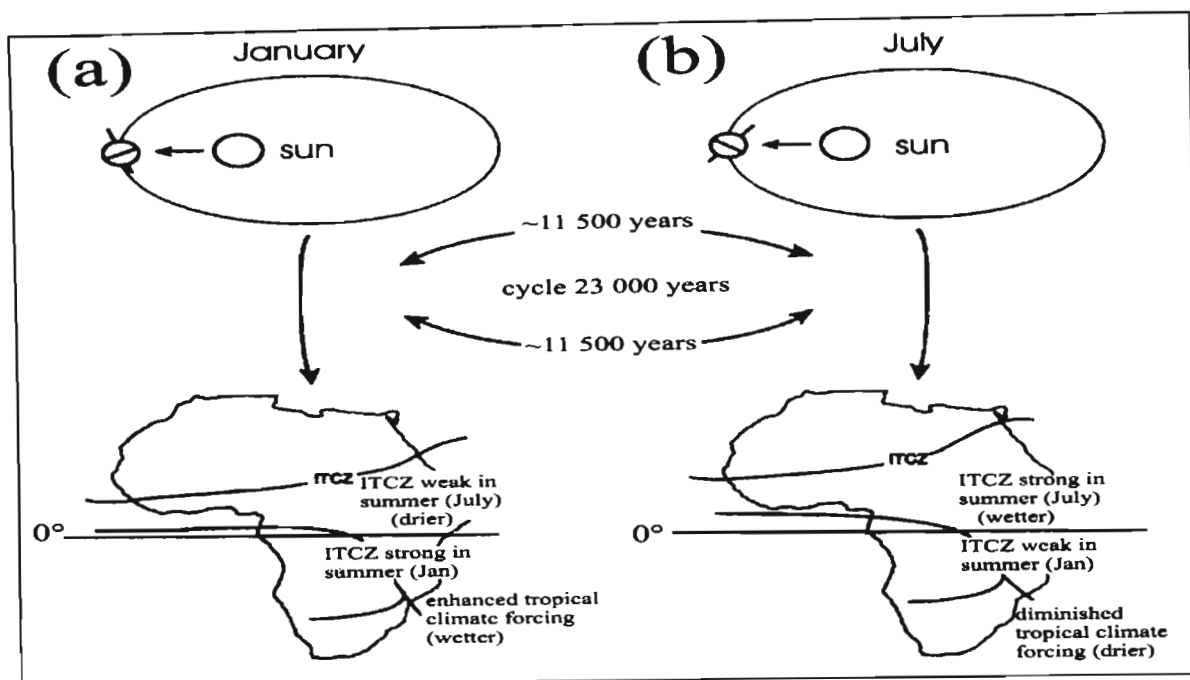


Figure 6.8 – Precession of the equinoxes (Tyson and Preston-Whyte, 2000, 311) with (a) austral summer perihellion and (b) boreal summer perihellion.

Thus climate fluctuations associated with the precessional changes are 180° out of phase in Africa south and north of the equator (Tyson, 1999b). A clear corroboration of the model lies in evidence that the rainfall at the Tswaing Crater has fluctuated in an approximately 23 000 year cycle over the last 200 000 years while rainfall over Africa north of the equator fluctuated in an inverse oscillation of approximately 23 000 years over the same time period (Partridge *et al.*, 1997).

### 6.2.2 Cycles on a Millennial Scale

Heinrich (1988) found evidence of increases in iceberg debris every 7000 to 10 000 years in deep-sea cores. He associated these increases with destabilisation of the Laurentide Ice Sheet. These 'Heinrich events' were profound and catastrophic, and occurred at the boundaries of major climatic transition when periods of long-term cooling were followed by abrupt warming and associated deposition of ice-flow debris on to the ocean floor,

producing a sediment layer rich in foraminifera (Tyson and Preston-Whyte, 2000). CH<sub>4</sub> records in ice cores indicate changes in atmospheric CH<sub>4</sub> during Heinrich events, and this suggests a global imprint of these oscillations since CH<sub>4</sub> is produced primarily in tropical wetlands by anaerobic bacteria (Chappellaz, 1993).

Similar to the Heinrich events (Heinrich, 1988) every 7000 to 10 000 years during the last ice age, Bond (1996) reported evidence from deep sea cores of iceberg advances involving smaller glaciers that occurred every 1000 to 3000 years. Approximately four of these advances, termed Dansgaard-Oeschger events and identified originally by Dansgaard *et al.* (1973), would occur between the larger Heinrich events, and together make up a Bond Cycle. Although the amount of ice-carried debris in deep-sea cores was far lower during the warmer Holocene, Bond (1996) found that indicative periodic layers in the cores continued after most glaciers had melted. This evidence indicated an underlying, persistent climate cycle that operates whether or not large ice sheets exist. There is evidence to suggest that these Dansgaard-Oeschger events are globally synchronous (Bond *et al.*, 1999) and Rahmstorf (2003) proposed that the events are paced by a regular cycle of approximately 1500 years. There has been only a 2% deviation from this in the five most recent events for which dating is more precise. The regularity of the cycle suggests the external controlling mechanism of solar forcing.

### **6.3 METHODOLOGY: WAVELET ANALYSIS**

An important aspect of palaeoclimatological analysis involves identifying dominant patterns within datasets. Mathematical transforms may be applied to signals to derive information that is not clear in the raw data. The Fourier transform, for example, has been applied extensively as a method of pattern analysis and signal processing (Priestly, 1981). When a Fourier transform is applied to a signal in the time domain, it results in a frequency and amplitude representation of that signal. Researchers must then attempt to link the patterns observed with the mechanisms responsible, which, in turn, provides a greater understanding of the system processes (Bradshaw and McIntosh, 1994).

Fourier analysis, which assumes a fundamental stationarity of the data, is not always suitable for an analysis of climatic data for two main reasons. Firstly, these datasets usually consist of multi-scale patterns in a nested or hierarchical structure, and secondly, the

records are not always periodic or stationary (where frequency does not vary over time) either because the record is not long enough to capture the entire period of low-frequency signals, or the events themselves are aperiodic, rare or clustered (Bradshaw and McIntosh, 1994). The power spectra calculated for data which are non-sinusoidal in form often exhibit edge effects which may be mistakenly taken as high frequency components (Bradshaw, 1991). The method is often applied without prior detrending, which, in the presence of a trend, may disguise low-order frequencies (Priestly, 1981; Chatfield, 1989).

Daubechies (1992, 10) defines the wavelet transform as ‘...a tool that cuts up data, functions or operators into different frequency components and then studies each component with a resolution matched to its scale’. Wavelet analysis had its origins in signal and image processing (Daubechies, 1990; 1992; Farge, 1992) but the technique has gained wide acceptance in geophysics and the atmospheric sciences. In the latter it has been used in studies of tropical convection (Weng and Lau, 1994), past climates (Bolton *et al.*, 1995), the El Niño-Southern Oscillation (Gu and Philander, 1995; Wang and Wang, 1996; Torrence and Compo, 1998; Torrence and Webster, 1999; Allan, 2000), the North Atlantic Oscillation (Higuchi *et al.*, 1999), and has been applied to proxy palaeoclimatic records and recorded climatic data for southern Africa (Tyson *et al.*, 2002a).

Wavelet analysis is a method which has been developed for the analysis of multi-frequency data which may be neither stationary nor sinusoidal in form (Argoul *et al.*, 1989; Bradshaw 1991; Bradshaw and Spies, 1992). The method transforms a one dimensional time series (or frequency spectrum) to a two dimensional time-frequency image. Wavelet analysis thus offers an improvement to Fourier analysis which offers no time-frequency information, which is relevant when the amplitudes and periods of dominant oscillations are time dependent. Wavelet analysis offers a localised time-frequency analysis, and short signal pieces have significance. While Fourier analysis involves the multiplication of a signal by a sinusoid to determine the frequency content of that signal, wavelet analysis is an iterative process of scaling and shifting the original waveform, comparing it to a wavelet and assigning a coefficient of similarity. Scale approximates with the frequency band so that a high frequency corresponding to a small scale.

The problems associated with a Fourier analysis on non-stationary climatic data are highlighted in Figure 6.9. The Fourier analysis of a hypothetical dataset indicates two

cycles - one with a period of around 22 years and another of around 26 years (Figure 6.5a). The wavelet analysis shows that this is in fact one cycle with frequency modulation over time (Figure 6.5b). Furthermore, the Fourier results give no indication that this cycle weakens after 1950, which is clearly shown in the results of the wavelet analysis.

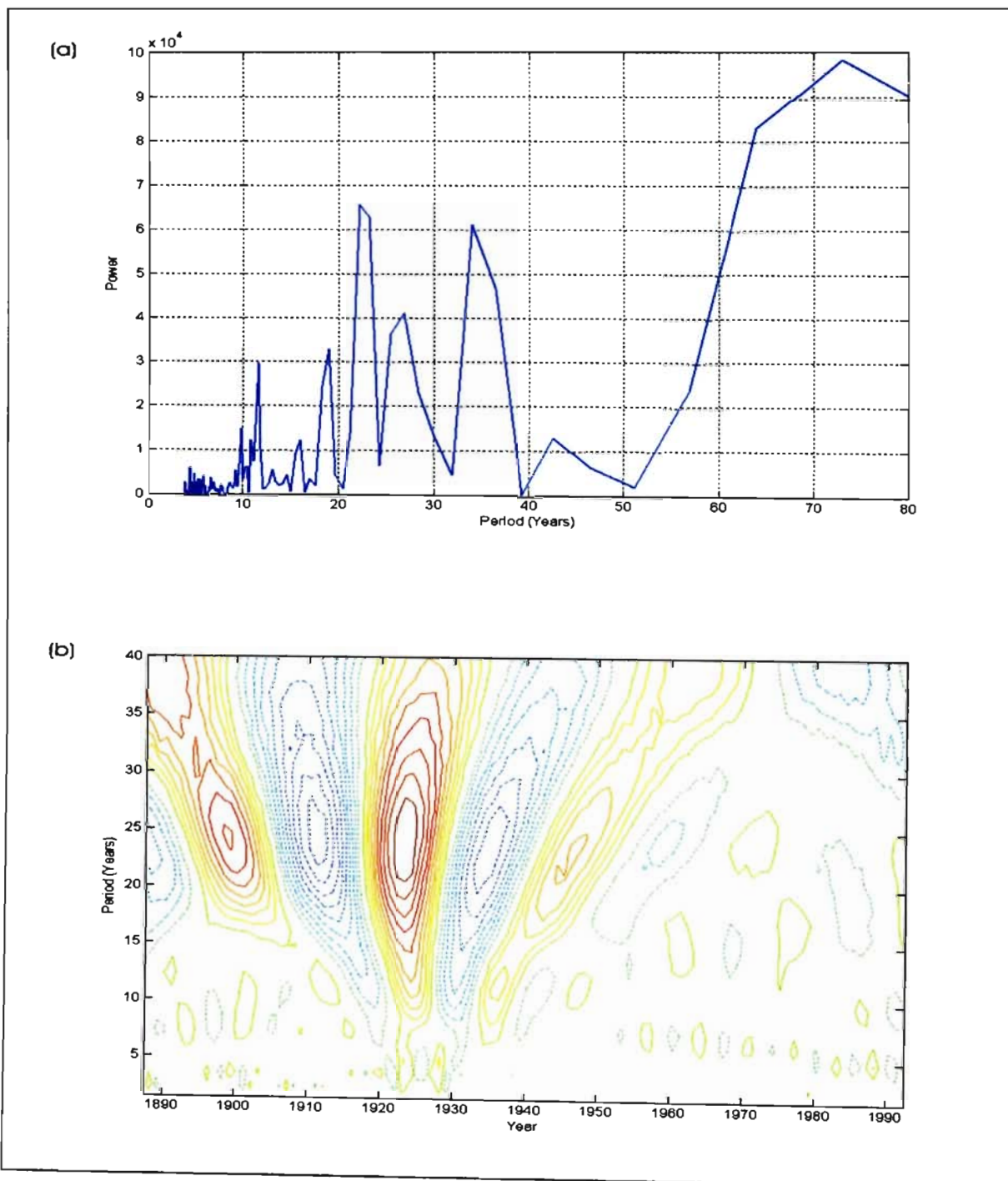


Figure 6.9 – Comparison of the (a) Fourier analysis and (b) wavelet analysis of the same hypothetical dataset, with positive values of the wavelet indicated by solid lines and negative values indicated by dotted lines.

Details of this method of analysis, including the specification of statistical significance and coherence are given in Lau and Weng (1995) and Torrence and Compo (1998). There are a number of wavelets commonly used in analysis and each has specific properties. These small localised waves have a particular shape and finite duration, and they tend to be irregular and asymmetric, although some are symmetric, such as the Mexican Hat and Morlet wavelets. The type of wavelet chosen for a study is relatively arbitrary – except when some wavelet property is required for a specific application. Sometimes the best way to determine how well a particular wavelet transform works on a dataset is visual, and various wavelets can be applied to the data and the results compared (G.R.J. Cooper, 2005, pers. comm.).

For this study, the Morlet wavelet (Figure 6.10) was selected. This is a non-orthogonal, symmetrical wavelet which provides good results with smooth data that can be considered to be composed of sinusoidal functions (G.R.J. Cooper, 2005, pers. comm.). It was selected because it was applied with success to climate data by Tyson *et al.* (2002a), and was recommended by G.R.J. Cooper (2005, pers. comm.) who is the leading local expert in this field.

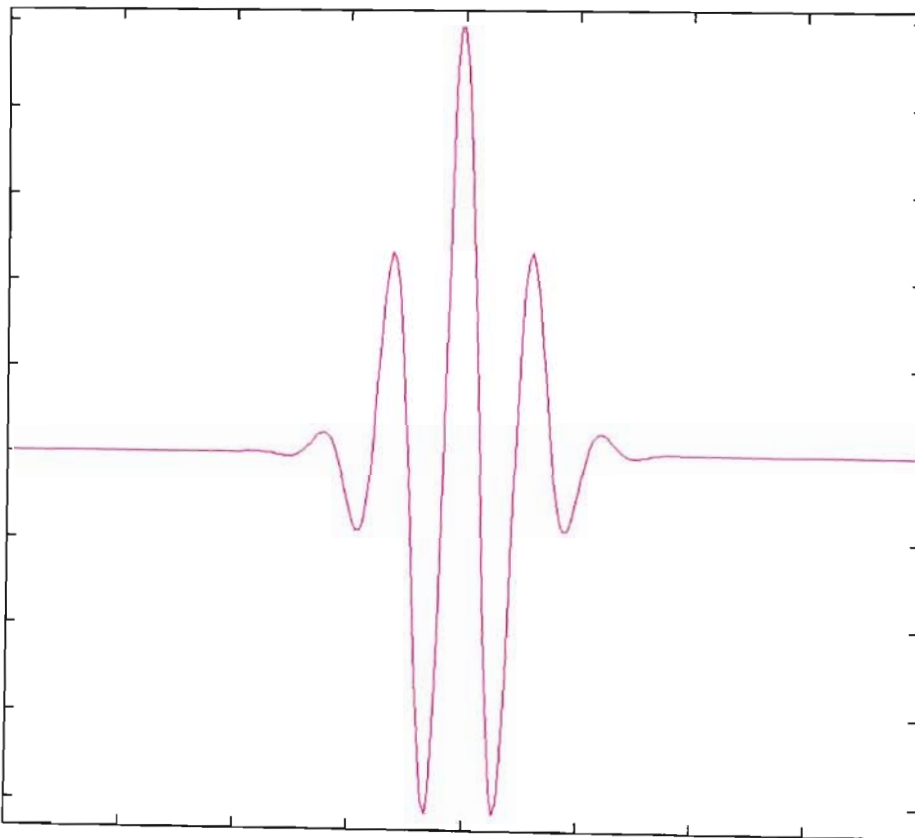


Figure 6.10 - Morlet(x) =  $\exp(-x^2 / 2) * \cos(5x)$  (MATLAB, 2005)



Tyson *et al.* (2002a) applied the continuous wavelet transform rather than the discrete wavelet transform to various palaeoclimatic datasets. Discrete wavelet analysis relies on a subset of scale and position based on the power of two – rather than every possible set of scale and position in the The continuous wavelet transform was preferred because of the greater number of scales at which it can be calculated for a given dataset, which aids in the visual presentation of results. The real version, as opposed to the complex version, of the Morlet wavelet was applied in the following analyses. This resulted in the calculation of real, continuous coefficients of similarity, which were contoured as a function of time and cycle period in the wavelet figures, following an adjustment to convert scale to frequency. The MATLAB script written for this purpose is shown in Appendix 2c.

Instead of portraying the temporal stability of the signal by plotting the absolute values of the continuous wavelet transform as is usually done, the signed coefficients were contoured to establish phase relations between the different frequency components. It is believed that this facilitates a clear interpretation of the data by providing a helpful distinction between positive and negative amplitude peaks (Tyson *et al.*, 2002a; G.R.J. Cooper, 2005, pers. comm.). Thus a persistent oscillation appears as an unbroken ridge of positive values in standard presentation, but as a series of positive and negative values in the presentation used here, with the instantaneous sign of the oscillation indicated by the sign of the wavelet transform. In the subsequent wavelet figures, positive values of the wavelet transform are indicated by solid lines, while negative values are indicated by dotted lines.

Inherent in wavelet analysis is the assumption that the data is cyclic (Torrence and Compo, 1998). If the data is not cyclic, there are problems near the edge of the time series as the wavelet runs off the end of the time axis. Wrap-around effects can be limited by padding the time series with zeroes, although this reduces the wavelet power at the edges. Zero padding to twice the dataset is usually recommended but Torrence and Compo (1998) suggest that padding to the next power of two allows for negligible wrap-around effects while still allowing for a fast analysis. The MATLAB script written to pad the climate records with zeroes is shown in Appendix 2a. Padding with zeroes introduces discontinuities at the endpoints and as the scale increases, the amplitude near the edges is decreased as more zeroes enter the analysis. The ‘cone of influence’ is the region of the

wavelet spectrum in which edge effects become important, and is mathematically defined as the  $e$ -folding time for the autocorrelation of the wavelet power at each scale (Torrence and Compo, 1998). Since this study is viewing the wavelets results as qualitative, G.R.J. Cooper (2005, pers. comm.) suggested that it was not necessary to indicate a cone of influence in these results. However, if future studies require a measurement of changes in amplitude of the correlation coefficients, a cone of influence should be added to prevent misinterpretation in the zone of edge effects.

In order to overcome the problem of slightly irregular time intervals between data points in the proxy records, linear interpolation was used to provide regularly spaced data. This had little to no effect on the frequency of any oscillation that may be present in the data, but may have diminished their amplitude and make the wavelet analyses slightly more conservative (G.R.J. Cooper, 2005, pers. comm.). Whether oscillations should be tested for statistical significance is a debatable issue (Nicholls, 2000), particularly in the case of exploratory studies (Flueck and Brown, 1993). Such is the case here, and hypothesis testing may be misleading (Von Storch and Zwiers, 1999; Tyson *et al.*, 2002a), especially when the total data population and not just samples are being considered. In view of the contested relevance of significance testing in an exploratory study such as this, it has not been included. As such, cyclicity in the results of the study will be viewed as a qualitative indication of the possibility of a cycle at a particular frequency.

Wavelet analysis is a technique that allows a comparison of various types of record and at various timescales. The determination of oscillatory variations relying on single records is problematic and ideally a collection of overlapping records should be utilised. This has been achieved in this study. The cycles identified in recorded and proxy climatic datasets are compared with cycles documented by other authors, and the inferred causes of these cycles are presented in the context of existing solar and atmospheric-oceanic models. From the results it is possible to offer some insights on internal and external mechanisms of climate change in the southern African region, and on teleconnections at a regional, hemispheric and global scale.

## 6.4 RESULTS AND DISCUSSION

### 6.4.1 The Sodwana Bay Coral Record

Wavelet analyses of the coral density, length and calcification records reveal cyclicity in coral growth. The density record indicates a dominant approximately 22 year cycle (Figure 6.11), which is clear until 1950 when the signal weakens.

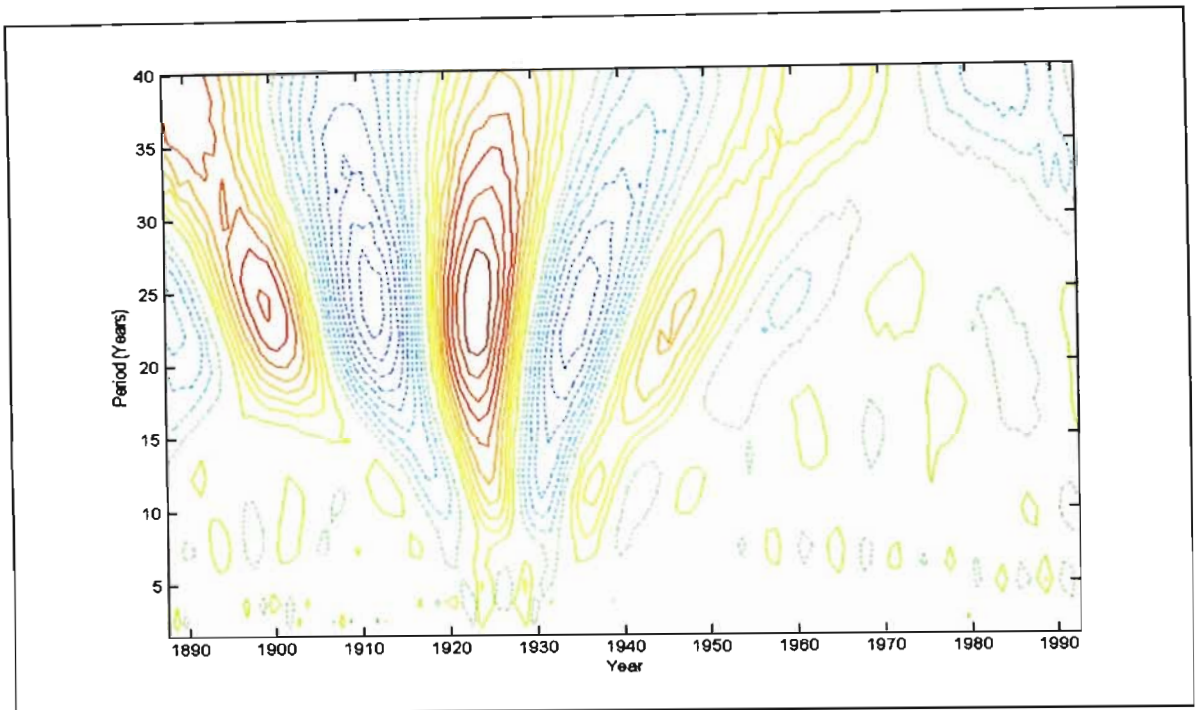


Figure 6.11 – Wavelet analysis of 116 year coral density record from Sodwana Bay using the Morlet wavelet, with positive values of the wavelet indicated by solid lines and negative values indicated by dotted lines.

#### 6.4.1.1 The 22 Year Cycle

The approximately 22 year cycle apparent in the coral record may be a reflection of the Hale cycle, which is a 22 year solar magnetic cycle (Labitzke and Van Loon, 1987). The magnetic field of the sun reverses during each Schwabe cycle of 11 years, and magnetic poles return to the same state after two reversals. A cycle of 21.9 years was noted in a study of *Porites lutea* at Moorea, French Polynesia (Bessat and Buiges, 2001). Similar results were observed in a 370 year old coral colony from the Galapagos Islands (Dunbar *et al.*, 1994). The evidence of this cycle at distant sites suggests a common global forcing mechanism, and this is likely to be the decadal cycle of solar activity.

There is some evidence of an approximately 11 year cycle (Figure 6.11) between 1910 and 1945 and this may be a reflection of the Schwabe cycle. However, the Schwabe cycle would maintain a regular period of 11 years while this appears to be a cycle that has experienced frequency modulation over the period of the coral record. It has a period of around 8 years in 1890 with a progressive period increase to a period of around 15 years in 1980.

According to Garric and Huber (2003), many palaeoclimatic proxies for interannual variability reveal power within the 7 – 15 year band extending back into geological history. Despite that the likely causes of this climatic variability are intrinsic, it is commonly attributed to the 11 year sunspot cycle. Allan (2000), for instance, has identified an 11 – 13 year band of variability aligning with prolonged El Niño and La Niña events. Therefore the quasi-11 year cycle apparent in the coral record may be a reflection of some internal climatic fluctuation rather than solar forcing despite the link between solar variability and coral growth suggested by Bessat and Buiges (2001) and Dunbar *et al.* (1994).

The Fourier analysis of the coral density data is shown in Figure 6.12. The results indicate the 11 year and 22 year cycles but also show evidence of the well-documented 80 year cycle.

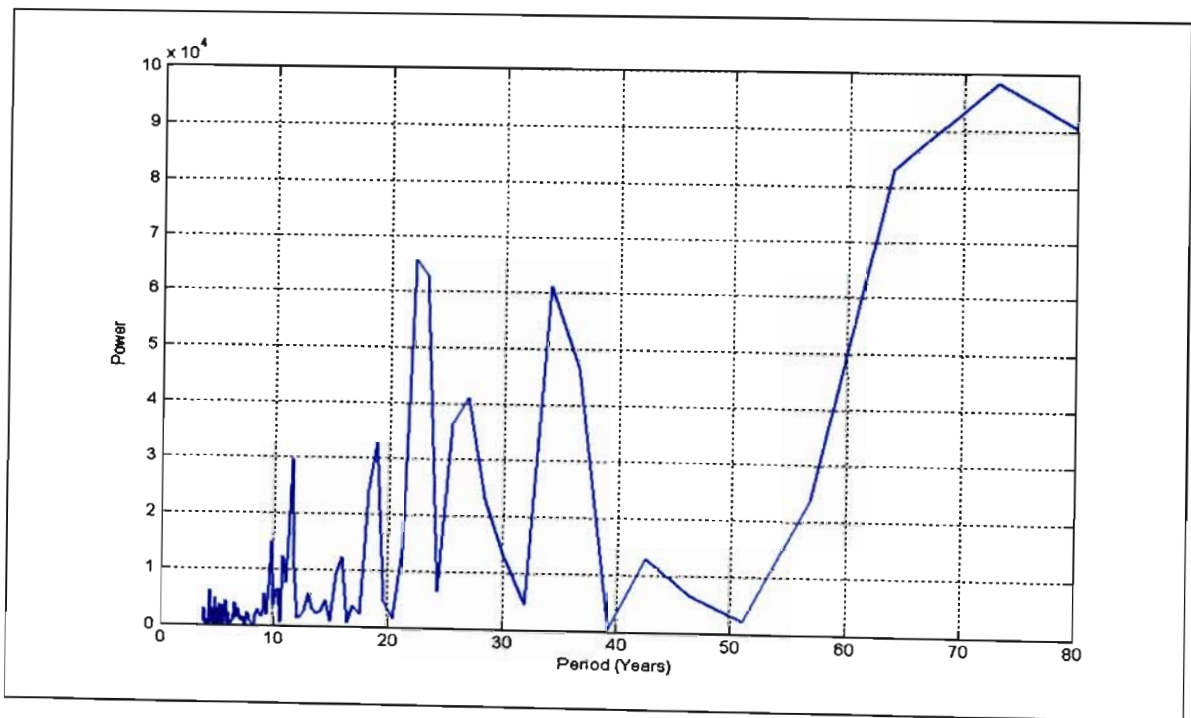


Figure 6.12 - Fourier analysis of 116 year coral density record from Sodwana Bay.

Although it may not seem appropriate to extract an 80 year cycle from a 120 year record, this cycle is considered valid in this instance because it has been identified in various other proxy records of southern African palaeoclimates. Cycles of approximately 19 and 26 year periods are evident but according to the wavelet analysis in Figure 6.11, these are the result of frequency modulation of the 22 year cycle. An approximately 35 year cycle is also evident in the Fourier analysis and weakly evident in the wavelet analysis at the edge of the wavelet range.

#### 6.4.1.2 The 80 Year Cycle

This cycle may also be reflection of a solar cycle: the Gleissberg cycle of around 80 years is linked to high and low phases of the 11 year Schwabe cycle (Hoyt and Schatten, 1997). It is apparent that coral density is sensitive to solar fluctuations. This 80 year oscillation is common in temperature, sea-level pressure and precipitation data (Tyson *et al.*, 2002a). It has been observed in long tree-ring records from South Africa (such as Hall, 1976; Dunwiddie and LaMarche, 1980; Thackeray, 1996; Thackeray and Potze, 2000) and in a run-off record for the Zambezi River at Victoria Falls (McCarthy *et al.*, 2000). It is evident in a number of records from other regions of the globe, such as the Greenland Camp Century oxygen isotope record (Dansgaard *et al.*, 1973), the Nile River flood series (Hameed, 1984; Hoyt and Schatten, 1997), in cosmogenic isotopes in tree-ring series (Hoyt and Schatten, 1997), in central England temperature data (Burroughs, 1992), and rainfall records from China (Zhu and Wang, 2001). Significant variability has been found in the 60 – 80 year band in global sea-surface temperature data (Folland *et al.*, 1999) and in the analysis of historical sea-surface temperature and mean sea-level pressures around the globe (Allan, 2000).

The Lough and Barnes (1997) and Bessat and Buiges (2001) coral studies indicated that the annual density of their cores was characterised by long-term variations while annual extension and annual calcification were characterised by high frequency variations. This is clear in the Sodwana Bay data as well. A wavelet analysis of the coral length data clearly indicates an 18 year cycle, a 6 - 9 year cycle, while a high frequency 1 - 3 year cycle appears periodically as shown in Figure 6.13.

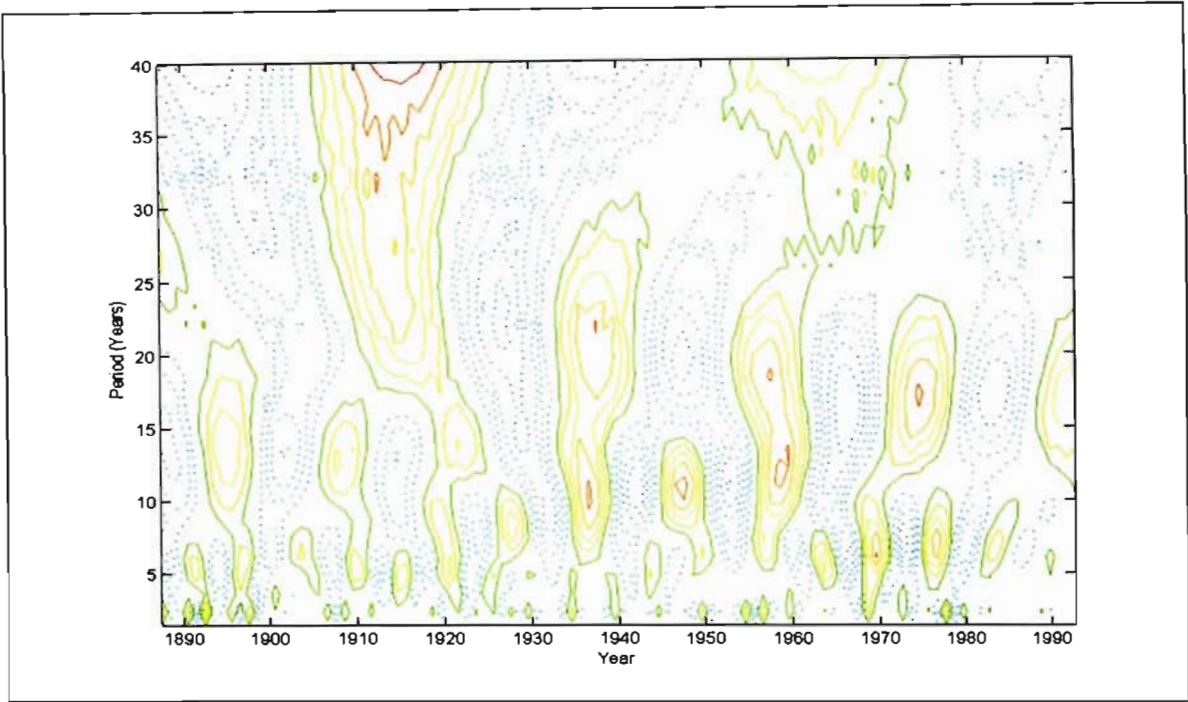


**Figure 6.13 – Wavelet analysis of 116 year coral length record from Sodwana Bay using the Morlet wavelet, with positive values of the wavelet indicated by solid lines and negative values indicated by dotted lines.**

There is some evidence of an approximately 45 year cycle at the edge of the wavelet range. It may seem inappropriate to derive a cycle from the edge of the range of the wavelet analysis, but this cycle is presented and discussed because of its prominence in the Fourier analysis of the length dataset (Figure 6.14).

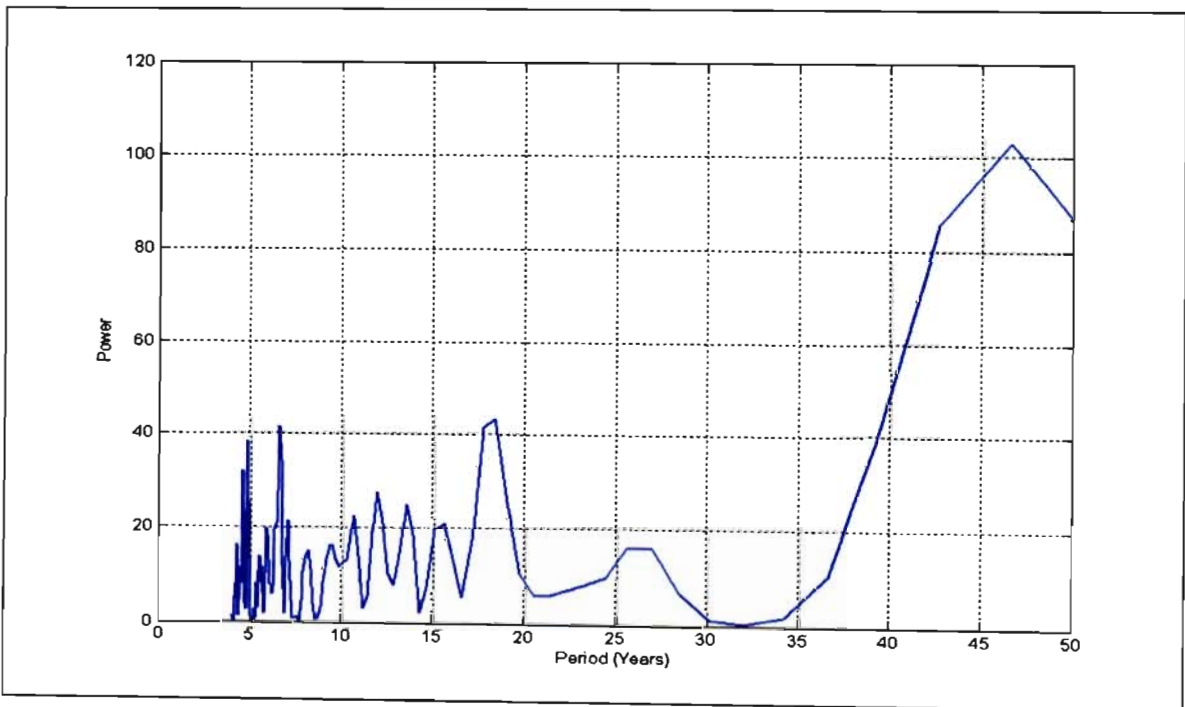


**Figure 6.14 – Fourier analysis of 116 year coral length record from Sodwana Bay.**

### 6.4.1.3 The Annual Cycle

There is a distinct seasonal variation in rainfall over southern Africa related to the annual cycle of the Inter-Tropical Convergence Zone (ITCZ), as shown in Figure 6.15, and the subtropical high pressure belt dominating southern African atmospheric circulation (Reason *et al.*, 2004). Rainfall over most of southern Africa increases when the ITCZ is in its summer position. This is caused by the poleward expansion of the tropical easterlies and associated increases in easterly wave disturbances and tropical lows in the region, which promote the inflow of moist air from the east and north-east. Over the southern parts of the Western Cape province, rainfall increases in winter due to the northward shift of the mid-latitude westerly wind belt and increased incidence of mid-latitude cyclones (Tyson and Preston-Whyte, 2000). These concepts were discussed extensively in Chapter 5.



Figure 6.15—Annual shifts in the Inter-Tropical Convergence Zone (ITCZ) (Engle, 2005).

### 6.4.1.4 The 2 – 3 Year Quasi-Biennial and the 4 – 8 Year El Niño Cycles

Variability at periods of 2 - 3 years and 5 - 8 years is evident in southern African climatic records (Nicholson and Entekhabi, 1986; Tyson, 1986). An approximately 6 - 8 year cycle is clearly evident in Figure 6.13, and can be attributed to the El Niño-Southern Oscillation (ENSO), which dominates interannual variability over the tropical southern hemisphere and beyond (Lindesay *et al.*, 1986; Lindesay, 1988; Venegas *et al.*, 1996; Reason *et al.*, 2000). In addition to moderating the sea-surface temperature of the Indian and South Atlantic Oceans, ENSO leads to changes in the regional atmospheric circulation, primarily

through the local Walker circulation (Lindesay, 1988; Reason *et al.*, 2000) and the South Indian Convergence Zone (Cook, 2001). In this way, El Niño acts on southern African climate to suppress rainfall in the summer rainfall region during the mature phase of El Niño, and enhances rainfall during La Niña events.

The link between southern African rainfall and ENSO is modulated by the Quasi-Biennial Oscillation (QBO), which is the quasi-periodic reversal of equatorial stratospheric winds in the region of the 50 hPa level (Tyson and Preston-Whyte, 2000). When the QBO is in its westerly phase, more than 36% of the interannual variability in the late summer period (January – March) in the summer rainfall region can be ascribed to the effect of ENSO. On the other hand, when the QBO is in its easterly phase, only up to 16% of the interannual variability is ENSO-related (Tyson and Preston-Whyte, 2000). The modulation of ENSO by the QBO occurs through the enhancement of convergence and divergence fields (Figure 6.16) such that when the QBO is in its westerly phase, divergence occurs over Madagascar which limits rainfall in the region, while convergence and increased rainfall occurs over southern Africa (Figure 6.16a). In its easterly phase, the converse situation occurs, with enhanced rainfall over Madagascar and low rainfall over southern Africa (Figure 6.16b).

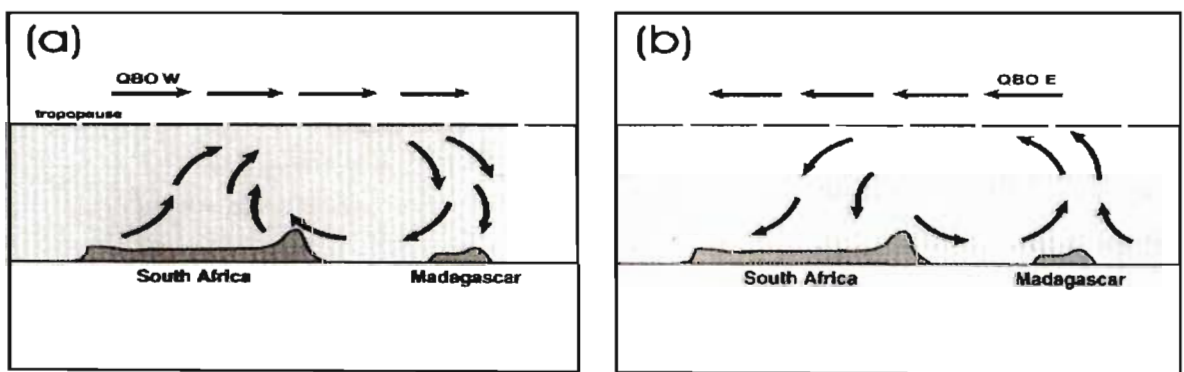


Figure 6.16 – Modulation of the El Niño-Southern Oscillation (ENSO) in the region of southern Africa by the Quasi-Biennial Oscillation (QBO) in its (a) westerly phase and (b) easterly phase (Tyson and Preston-Whyte, 2000, 235).

A marked 2 – 3 year oscillation associated with the QBO occurs over central southern Africa (Tyson and Preston-Whyte, 2000). This 2 – 3 year cycle is difficult to distinguish from the annual cycle in Figure 6.15 but a dataset with a higher resolution may allow a distinction to be made.



While interannual variability is dominated by ENSO over the tropical southern hemisphere, the Antarctic Oscillation or Southern Annular Mode (SAM) is the leading influence on mid- to high latitude atmospheric circulation. Fyfe (2003) and Simmonds *et al.* (2002) established that trends towards high index polarity in SAM limits mid-latitude cyclones over the hemisphere as a whole. Due to the influence of the South Indian and South Atlantic anticyclones on southern African climate, the hemispheric modulation of the subtropical high pressure belt would have significant impacts on southern African rainfall, particularly in over parts of the Western Cape (Reason, 2000; Reason *et al.*, 2003; 2004).

In addition to ENSO, various other South Indian Ocean sea-surface temperature patterns exist (Walker, 1990; Mason, 1995; Reason and Mulenga, 1999; Behera and Yamagata, 2001; Reason, 2002). In the South Atlantic Ocean, the Benguela warm and cold events (Hirst and Hastenrath, 1983; Reason *et al.*, 2004) and modulations of SST in the subtropics and midlatitudes (Reason *et al.*, 2004) are significant for different regions of the subcontinent. Furthermore, the tropical Atlantic develops its own zonal SST variability on interannual timescales, known as the Atlantic ENSO (Zebiak, 1993). Although variability in the South Indian Ocean is considered to have greater influence over southern Africa than that in the South Atlantic (Nicholson and Entekhabi, 1986; Walker, 1990; Mason, 1995; Mason and Jury, 1997), the climate impacts of the Atlantic on southern Africa are currently less understood and may be more significant than presently believed.

Thus there are a number of influences on variability on inter-annual timescales. While the El Niño cycle dominates southern African records, cycles of other periods may be detected associated with the Southern Annular Mode, the Atlantic ENSO, and Benguela warm and cold events. These cycles may at times weaken one another or bolster one another. The interactions are complex and further investigation is necessary to allow researchers to distinguish these cycles from one another and assess their interaction.

#### 6.4.1.5 The 18 Year Cycle

One of the strongest interdecadal signals (Reason *et al.*, 2004) in the southern hemisphere is an approximately 18 year cycle in summer rainfall over southern Africa (Tyson *et al.*, 1975). Climate variability in the range of 16 – 20 years has long been recognised in other

South African data series (Tyson, 1971; 1986; Tyson *et al.*, 1975), and in Zimbabwe (Ngara *et al.*, 1983) and Botswana (Jury *et al.*, 1992). It has been observed in river discharge, air temperature, sea-surface temperature, sea-level pressure and tree-ring data (Tyson *et al.*, 2002a).

Detailed statistical analyses have provided convincing evidence for pronounced oscillations in precipitation within the summer rainfall region of South Africa (Tyson, 1971; Tyson *et al.*, 1975; Tyson and Dyer, 1975). Tyson *et al.* (1975) analysed rainfall values from 318 meteorological stations over the summer rainfall region for the meteorological record 1910 to 1972 in search of trend, serial correlation and spectral characteristics. The authors concluded that there were clear indications of oscillations which vary geographically. Tyson and Dyer (1975) examined such fluctuations within the summer rainfall region and concluded that the approximately 18 year cycle was the most strongly developed. Except for small areas along the border of the Transvaal (now Gauteng) and Orange Free State (now Free State), and in the Transkei (now Eastern Cape), the whole summer rainfall region exhibits this oscillation.

Subsequently, the signal has been observed in Vaal River (Abbott and Dyer, 1976) and Umfolozi River (Garden, 2005) flow data, and in tree-ring series from Karkloof, Tzaneen, Cedarberg and Knysna (Tyson *et al.*, 2002a). Variability in the range of 16 – 20 years is evident in studies of the El Niño-Southern Oscillation (such as Allan, 2000) and in the Southern Oscillation Index (Tyson *et al.*, 2002a). The cause of this cycle has been related to the projection of ENSO-like decadal modes with regional sea-surface temperature forcing and modulations of the southern hemisphere circulation (Mason and Jury, 1997). The ENSO proposal also explains similar interdecadal variability observed in Western Cape winter rainfall (Reason and Rouault, 2002).

#### 6.4.1.6 *The 45 Year Cycle*

Searches through ship logs and other historical documents dating back to 1700 have allowed identification of a climatic cycle approximately 40 years long (Davis, 1979). According to Davis (1979), the cycle is also evident in records of wind strength over the Pacific Ocean, in records of ocean temperature, in Nile River discharge data and in the extent of the Arctic ice pack. Studies on the increase in hurricane frequency in the United

States' mid-Atlantic region have indicated a possible cyclic pattern of 40 years (Lubick, 2005) linked to variation in sea-surface temperature of the Atlantic Ocean. This cycle, however, is not well documented and it is not possible to present an exact cause.

The results of a wavelet analysis of the calcification data were very similar to that of the length data, and the same cycles apply. The cycles are in phase with one another as would be expected since calcification is a product of length and density.

#### 6.4.2 The Makapansgat Stalagmite Record

A wavelet analysis of the Makapansgat  $\delta^{18}\text{O}$  record reveals major cycles with periods of 725 – 1000 years (the well documented quasi-1000 year cycle), approximately 1400 years (most likely to be a local manifestation of the well documented 1500 year cycle), and approximately 2250 years, as indicated in Figure 6.17.

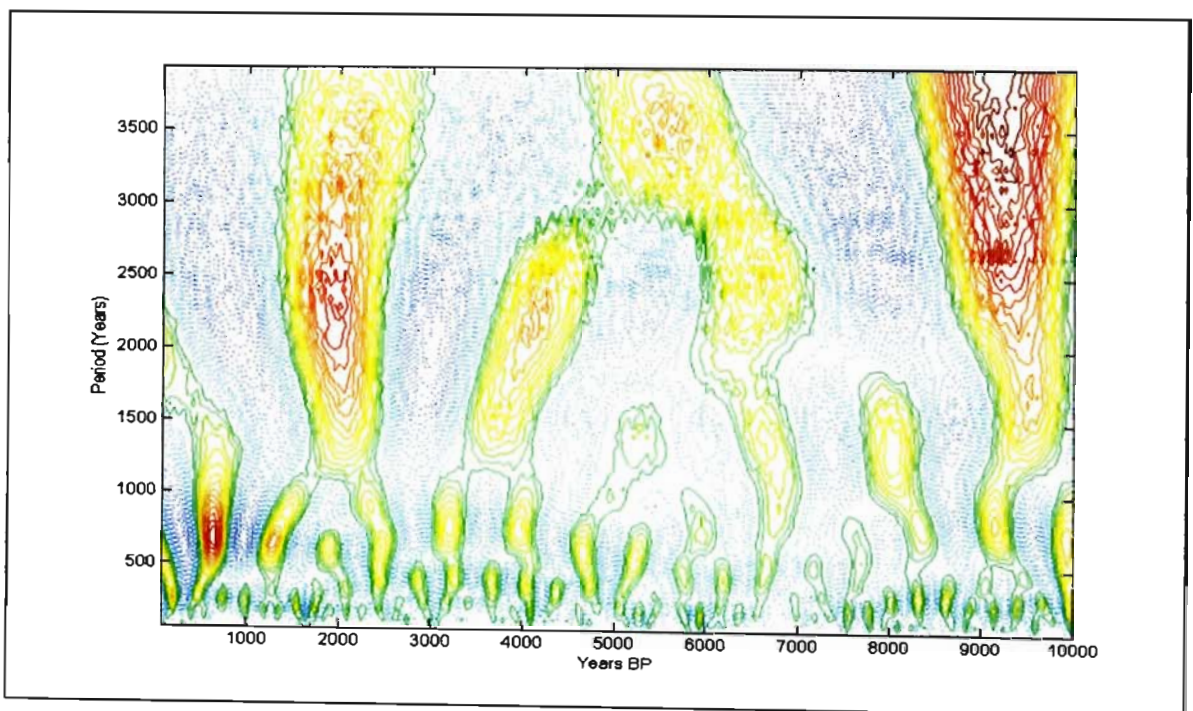


Figure 6.17 - Wavelet analysis of 10 000 year Makapansgat T8 stalagmite  $\delta^{18}\text{O}$  record using the Morlet wavelet, with positive values of the wavelet indicated by solid lines and negative values indicated by dotted lines.

There also appears to be a cycle of period 3000 - 3500 years, but since this is on the edge of the wavelet range, a wavelet analysis of a temporally extended dataset is necessary to

determine the validity of this cycle. However, the Fourier analysis (Figure, 6.18) does give some indication that this cycle exists.

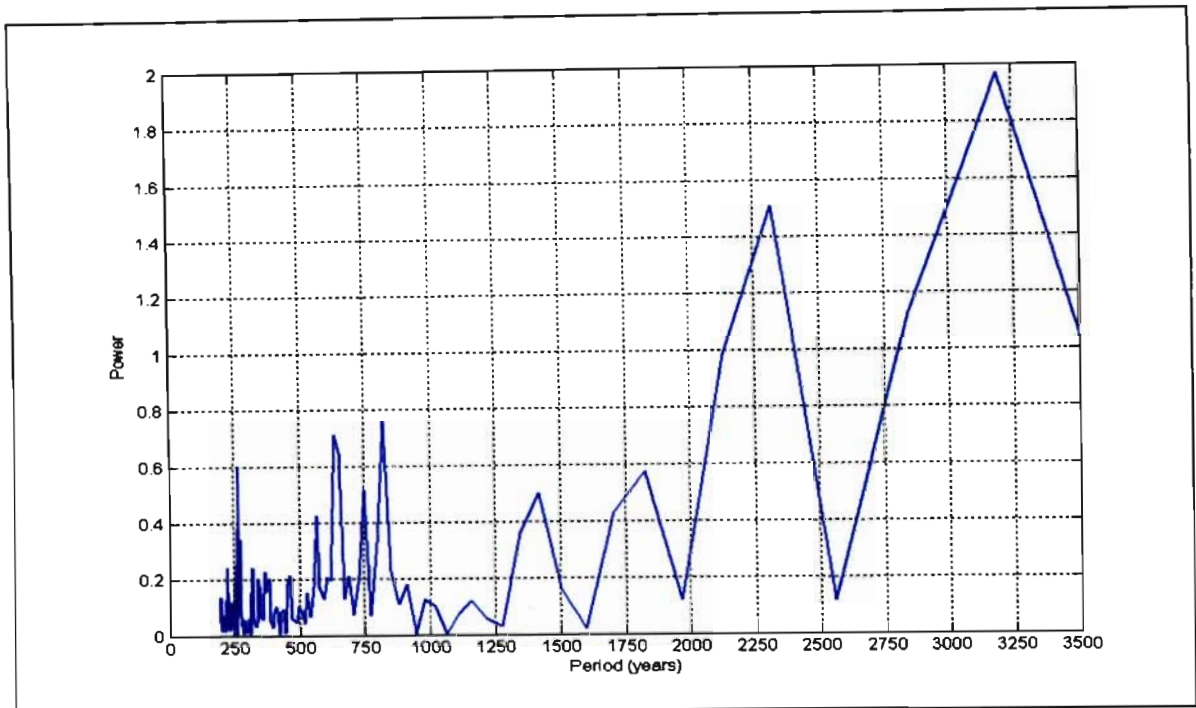


Figure 6.18 – Fourier analysis of 10 000 year Makapansgat T8 stalagmite  $\delta^{18}\text{O}$  record.

#### 6.4.2.1 The 3000 Year Cycle

Cyclicity in the 3000 year range has been detected in various datasets and named the Hallstatt cycle (Stuvier *et al.*, 1995). The cycle has been related to non-linear responses to the precession cycle (Pestiaux *et al.*, 1987) through stochastic resonance of Dansgaard-Oeschger events every 1500 years or multiples thereof (Ganopolski and Rahmstorf, 2002). Stochastic resonance occurs when a nonlinear system is subjected to a weak periodic signal that would be normally undetectable but becomes detectable due to resonance between the signal and stochastic (random) noise (Ganopolski and Rahmstorf, 2002).

In the extended 24 400 year Makapansgat T8 dataset, Holmgren *et al.* (2003) detected a 4500 year cycle which would also be linked to the stochastic resonance of Dansgaard-Oeschger events. Variability with a period of about 4700 years has been observed in marine cores from the Indian Ocean (Pestiaux *et al.*, 1988) and North Atlantic (Bond *et al.*, 1997).

#### 6.4.2.2 The 2000 - 2500 Year Cycle

Holmgren *et al.* (2003) detected periodicities in the range of 2000 years in their analysis of the Makapansgat data and suggested that frequency modulation of this oscillation appeared to have occurred regularly over the whole 20 000 period of their analysis. The wavelet analysis (Figure 6.17) clearly reveals the continuity of the oscillation despite small frequency changes over the 10 000 year record used here.

Moy *et al.* (2002) identified an approximately 2000 year cycle in a terrestrial record collected from Lake Pallcacocha in southern Ecuador, and ascribed it to a cycle of frequency and intensity in El Niño. A global 2500 year oscillation has been reported from glacier fluctuation (Denton and Karlén, 1973), ice core (Dansgaard *et al.*, 1973; O'Brien *et al.*, 1995) and marine core (Pestiaux *et al.*, 1988) studies and is evident in palaeoclimatological records from the tropical Pacific Ocean. The cycle has been ascribed to oceanic changes analogous to millennial scale ENSO-like shifts in sea-surface temperature distributions (Koutavas *et al.*, 2002).

#### 6.4.2.3 The 1500 Year Cycle

An approximately 1500 year oscillation was observed in the 4500 year time series derived from an ice core from Camp Century, Greenland (Dansgaard *et al.*, 1973). Ocean floor sediment cores collected south of Greenland suggest that a 1500 year cycle influences the variability of surface waters and the strength of North Atlantic deep water movements (Bond *et al.*, 1997; 1999; 2001), which in turn affects heat transfer across the globe and ultimately temperature and rainfall distribution. A decrease in North Atlantic deep water formation, for example, would cause a restriction of heat transfer from the western Indian Ocean into the eastern South Atlantic via the Agulhas current (Zonneveld *et al.*, 1997; Lutjeharms *et al.*, 2001) and, in turn, the process would lower sea-surface temperatures and amplify and prolong arid intervals over the western parts of southern Africa. Stochastic resonance of this cycle gives rise to the 3000 and 4500 year cycles (Ganopolski and Rahmstorf, 2002).

#### 6.4.2.4 The 1000 Year Cycle

A quasi-1000 year oscillation which has been shown to correspond to rainfall and vegetation changes in the southern African record (Tyson *et al.*, 2002a) and is apparent in both the Makapansgat  $\delta^{18}\text{O}$  and  $\delta^{13}\text{C}$  records (Figure 6.17 and 6.19). The cycle shows considerable frequency modulation with a shorter period of around 725 years and a longer period of up to 1100 years (Holmgren *et al.*, 2003). A similar cycle has been detected in the Greenland Camp Century series (Dansgaard *et al.*, 1973), in a Californian bristlecone pine tree-ring series (Sherratt, 1980), in a Chilean proxy rainfall record (Lamy *et al.*, 2001), and in Antarctic ice core data (Masson *et al.*, 2000). The oscillation is thought to be related to the production of North Atlantic deep water (NADW), evident in the deep-sea core records (Bond *et al.*, 1997; 1999; 2001; Bianchi and McCave, 1999; Chapman and Shackleton, 2000) and may be teleconnected to South Africa through the reversals in the thermohaline conveyor (Tyson *et al.*, 2002a). It has also been linked to vegetation-albedo positive feedbacks (DeMenocal *et al.*, 2000) and to variations in solar output (Stuvier *et al.*, 1995; Bond *et al.*, 2001).

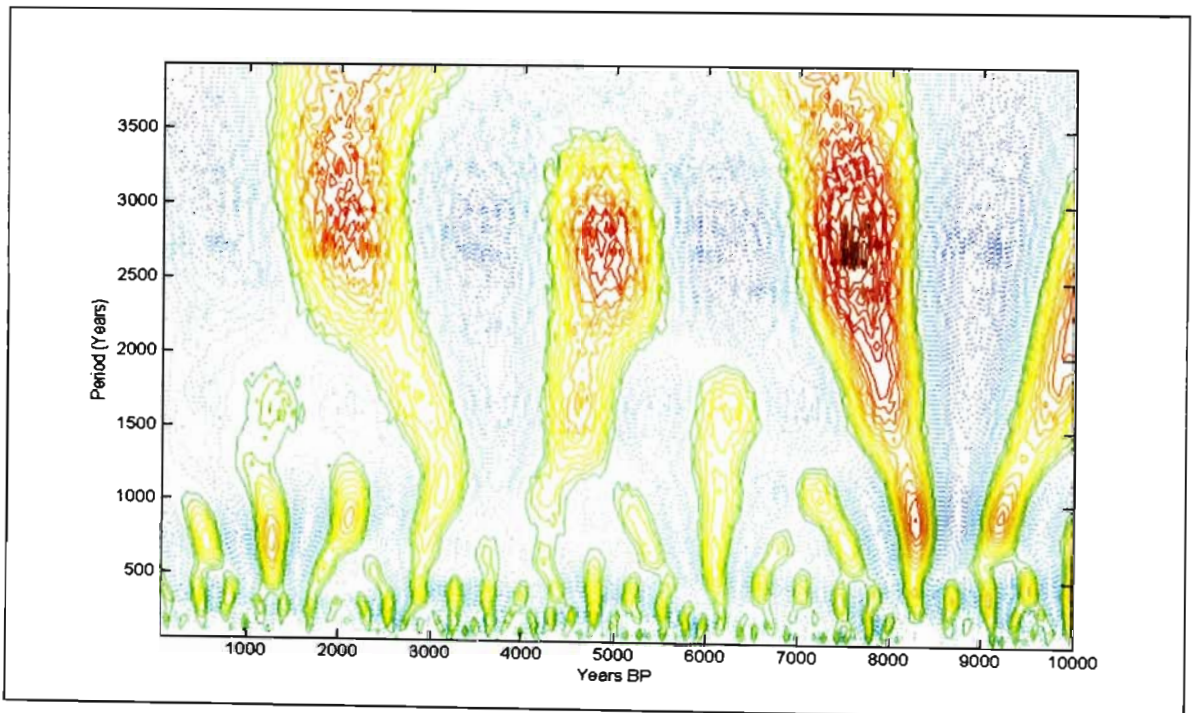


Figure 6.19 – Wavelet analysis of 10 000 year Makapansgat T8 stalagmite  $\delta^{13}\text{C}$  record using the Morlet wavelet, with positive values of the wavelet indicated by solid lines and negative values indicated by dotted lines.

A study of calcite from Lake Edward, an equatorial rift lake in central Africa showed a significant spectral power between 500 and 1000 years with a peak power at approximately 725 years (Russell *et al.*, 2003). Cycles of 750 – 775 year periods have also been detected in sea-surface salinity studies from the Arabian and South China Seas (Sarkar *et al.*, 2000; Von Rad *et al.*, 1999; Wang *et al.*, 1999). The African and Indian monsoons are intimately coupled and are influenced by land-sea contrasts, surface temperatures and inter-hemispheric heat gradients in the Indian Ocean (Schott and McCreary, 2001). Russell *et al.* (2003) suggested that the sub-millennial cycles evident in records of the African, Indian and East Asian monsoons share a common forcing mechanism.

Fluctuations in the Indian monsoon are believed to be related to iceberg surges of the North Atlantic during glacial times (Schulz *et al.*, 1998; Von Rad *et al.*, 1999; Wang *et al.*, 1999) and possibly during the late Holocene (Gupta *et al.*, 2003). However, a visual comparison of the magnesium record from the Lake Edward calcite and records of Late Holocene North Atlantic ice-rafted debris indicated no clear similarity, nor did a cross-spectral analysis present coherency at 750 year periods (Russell *et al.*, 2003). Millennial-scale North Atlantic cyclicity (Bond *et al.*, 2001) has been ascribed to periodic changes in solar output during the Holocene. However, 750 yr periods have not been observed in cosmogenic records of solar output (Russell *et al.*, 2003), indicating that this cycle is not driven directly by solar variability. Russell *et al.* (2003) could thus conclude that neither the temperature of the North Atlantic nor solar output exerted the dominant influence on millennial-scale climate variability of equatorial Africa during the late Holocene.

Russell *et al.* (2003) observed that the regional 725 year phasing resembled the rainfall anomalies associated with ENSO years, and suggested the existence of 725 year ENSO-like cycles. The 725 – 775 year cycles appear to result from long-term changes in tropical sea-surface temperatures and interactions with the tropical monsoons. Previously it was assumed that all major climate changes were initiated at the poles, with fluctuations in tropical processes being merely secondary responses. Recent studies (such as Clement *et al.*, 2001), however, show the importance of the tropical ocean-atmosphere as a source of abrupt climate change. According to the Makapansgat dataset shown here, the 725 year cycle may be a modulation of the 1000 year cycle, suggesting that the 1000 year globally-detected cycle may also have tropical origins. Further investigation of the relationship between these cycles and their origins is necessary.

At a higher resolution (Figure 6.20 and Figure 6.21), cycles with periods of approximately 450, 120 – 200, and 80 years become obvious.

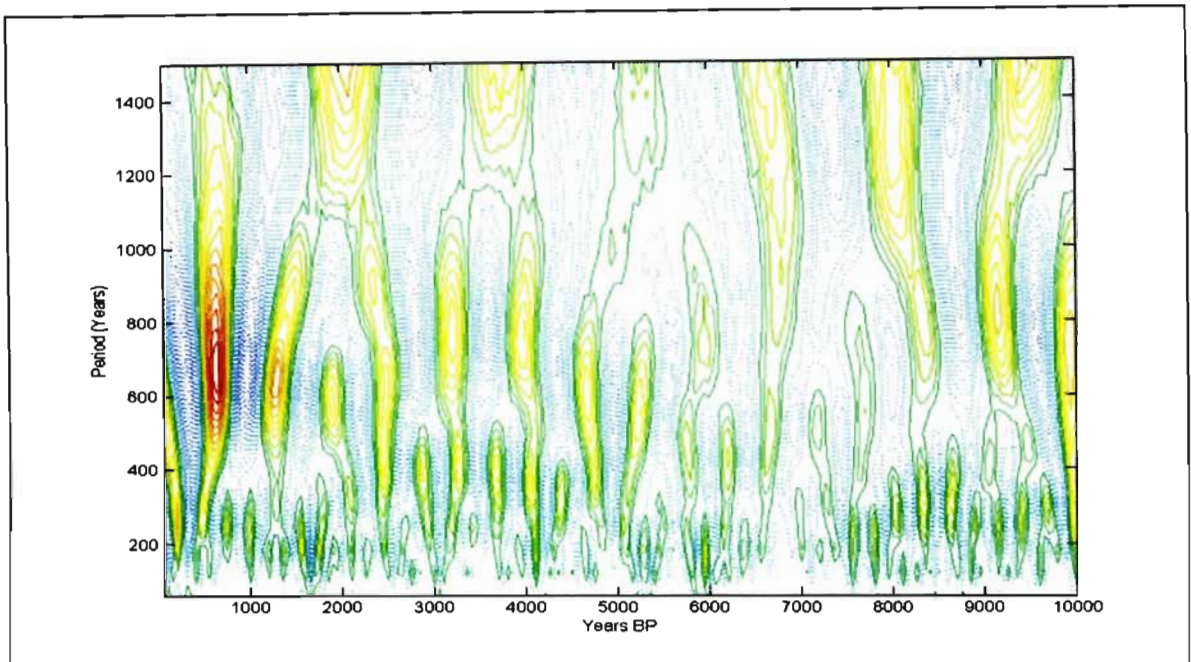


Figure 6.20 – Wavelet analysis of 10 000 year Makapansgat T8 stalagmite  $\delta^{18}\text{O}$  record using the Morlet wavelet showing higher frequency cycles, with positive values of the wavelet indicated by solid lines and negative values indicated by dotted lines.

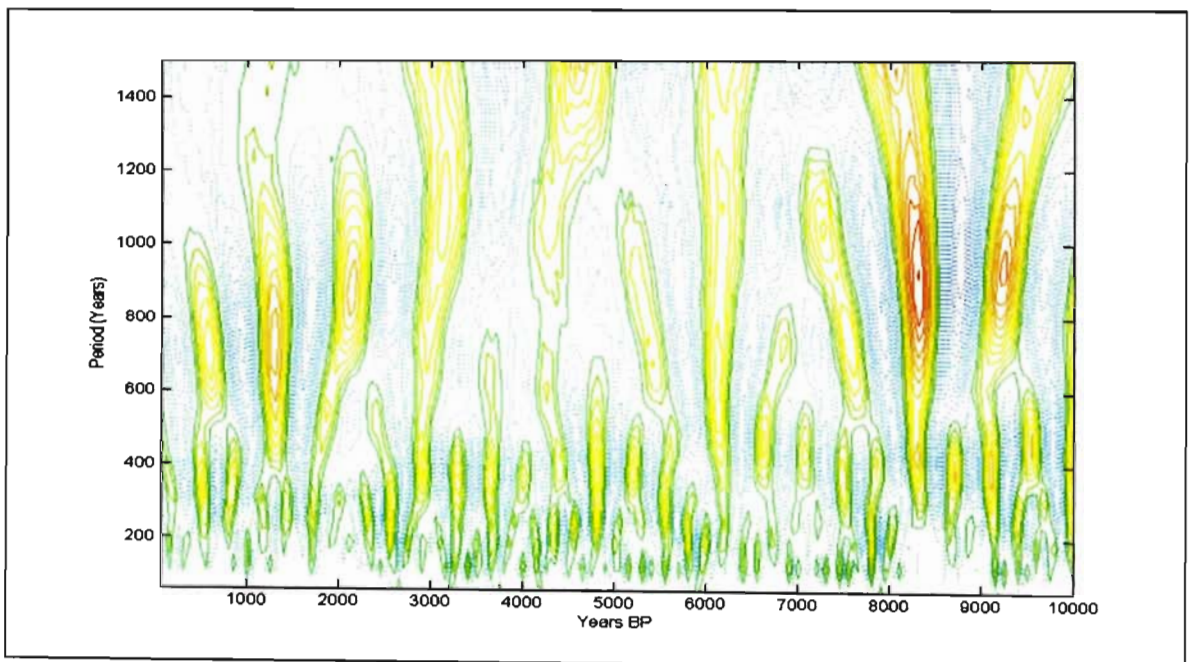


Figure 6.21 – Wavelet analysis of 10 000 year Makapansgat T8 stalagmite  $\delta^{13}\text{C}$  record using the Morlet wavelet showing higher frequency cycles, with positive values of the wavelet indicated by solid lines and negative values indicated by dotted lines.



#### 6.4.2.5 The 450 Year Cycle

Talma and Vogel (1992) suggest that on the basis of visual inspection of their Cango Cave data, fairly regular temperature changes have occurred in the area in a 300 – 400 year cycle. Burroughs (1992) concluded that there was clear evidence for a fundamental oscillatory mode of about 420 years in his dendroclimatological studies in California. Further scientific study is required before a cause can be assigned to this cycle.

#### 6.4.2.6 The 120 – 200 Year Cycle

Variability associated with a weak 120 - 200 year quasi-periodicity has been observed in records from Kenya (Johnson *et al.*, 1991), in records from the high latitudes in the northern hemisphere (Briffa *et al.*, 1992; Scuderi, 1993), in Californian dendroclimatology studies (Burroughs, 1992), in marine cores collected near the Antarctic Peninsula (Leventer *et al.*, 1996), from Tibetan ice cores (Thompson *et al.*, 1997) and from peat deposits in Scotland (Chambers *et al.*, 1997) and Denmark (Aaby, 1976). The 200 year cycle is thought to be caused by a solar cycle, named the Seuss Cycle (Seuss, 1980; Seuss and Linick, 1990; Stuvier and Braziunas, 1993), or lunar tidal effects (Burroughs, 1992).

#### 6.4.2.7 The 80 Year Cycle

The dominant variability in the Makapansgat record, with periods of less than 200 years, resides in a band extending from about 60 – 100 years. Naming it according to midpoint of the range, the 80 year variability is present throughout the record of the last 3500 years, but most significantly and persistently over the last two millennia in the  $\delta^{18}\text{O}$  record. The cycle can be discerned weakly and intermittently through the 24 400 year T8 record (Holmgren *et al.*, 2003). This cycle was discussed in Section 6.4.1.2.

### 6.4.3 The Wonderkrater Pollen Record

The PC1 of the Wonderkrater dataset offers a temperature record of the last 10 000 years. A wavelet analysis of PC1 indicates cyclicity with a period of 750 – 1200 years, suggesting frequency modulation of a quasi-1000 year cycle. Approximately 1500 and 2500 year cycles also are evident over parts of the record as shown in Figure 6.22.

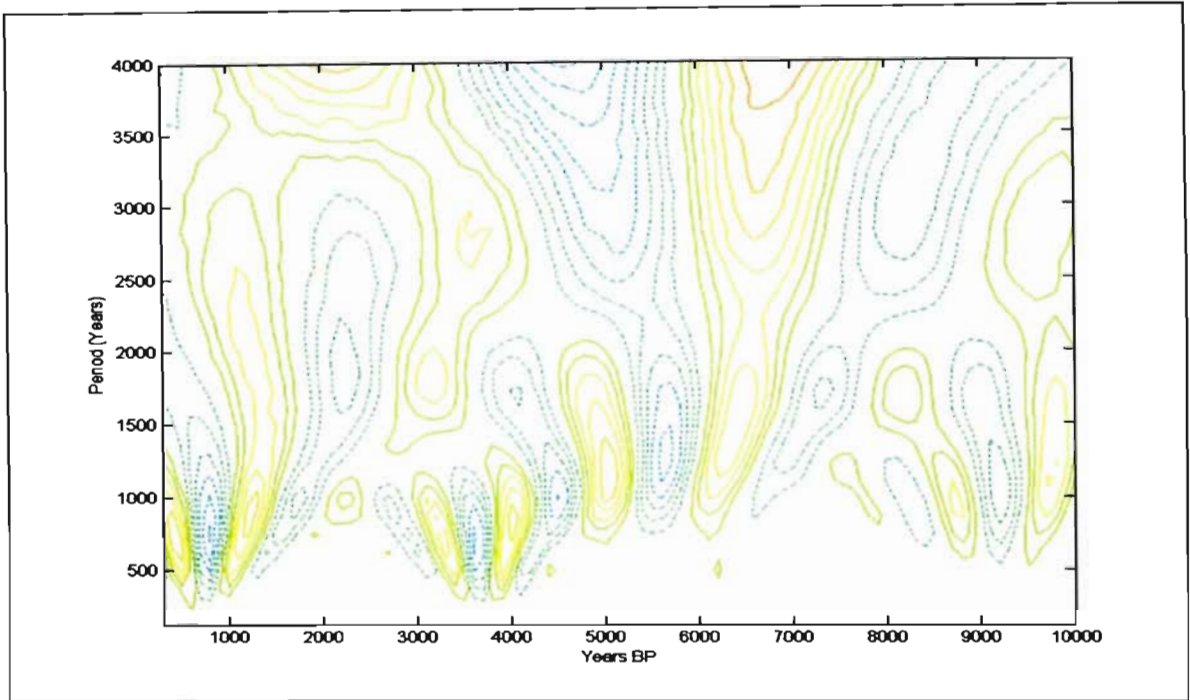


**Figure 6.22 – Wavelet analysis of PC1 of 10 000 year Wonderkrater pollen record using the Morlet wavelet, with positive values of the wavelet indicated by solid lines and negative values indicated by dotted lines.**

Fourier analysis (Figure 6.23) of PC1 clearly shows the approximately 1500 year and 2600 year cycles. The Fourier analysis indicates two distinct cycles with periods of approximately 900 and 1200 years, but according to the wavelet analysis, this is frequency modulation of the quasi-1000 year cycle.

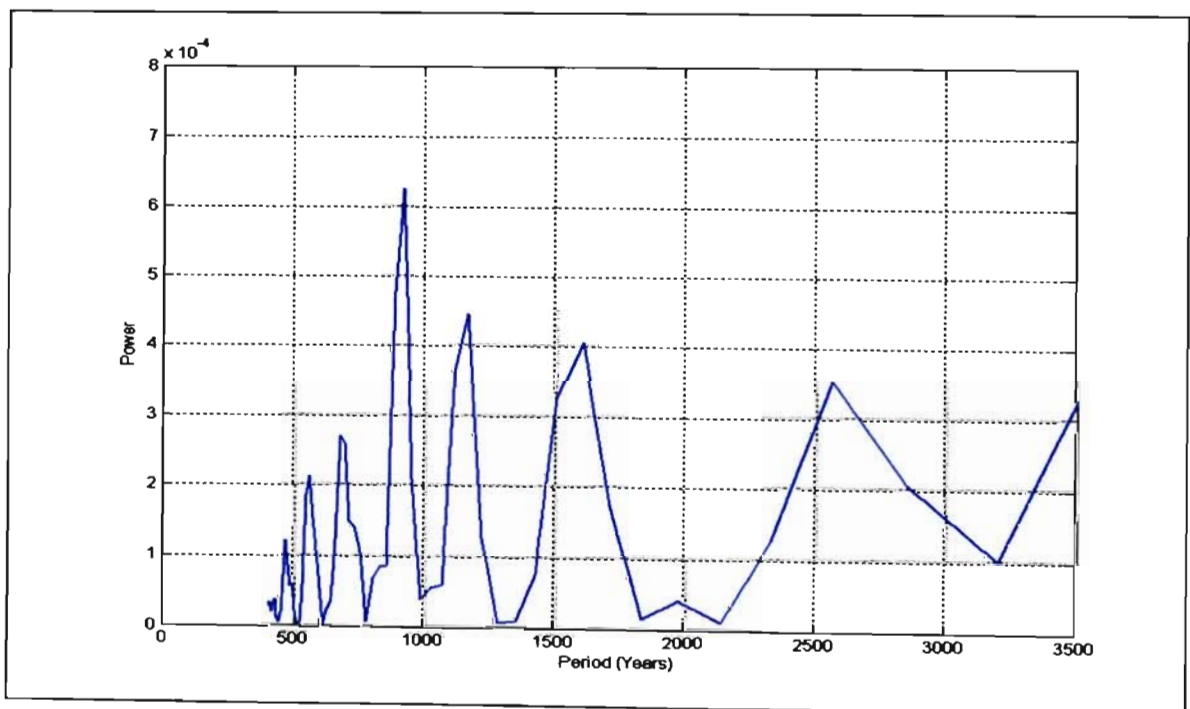


**Figure 6.23 – Fourier analysis of PC1 of 10 000 year Wonderkrater pollen record.**

The wavelet analysis of PC2 shows strong cyclicity with a period of around 2600 years, although the period increases progressively across the record to reach approximately 3000 years at the present (Figure 6.24). The prominence of the 2600 year cycle is indicated in the Fourier analysis of the PC2 data (Figure 6.25).

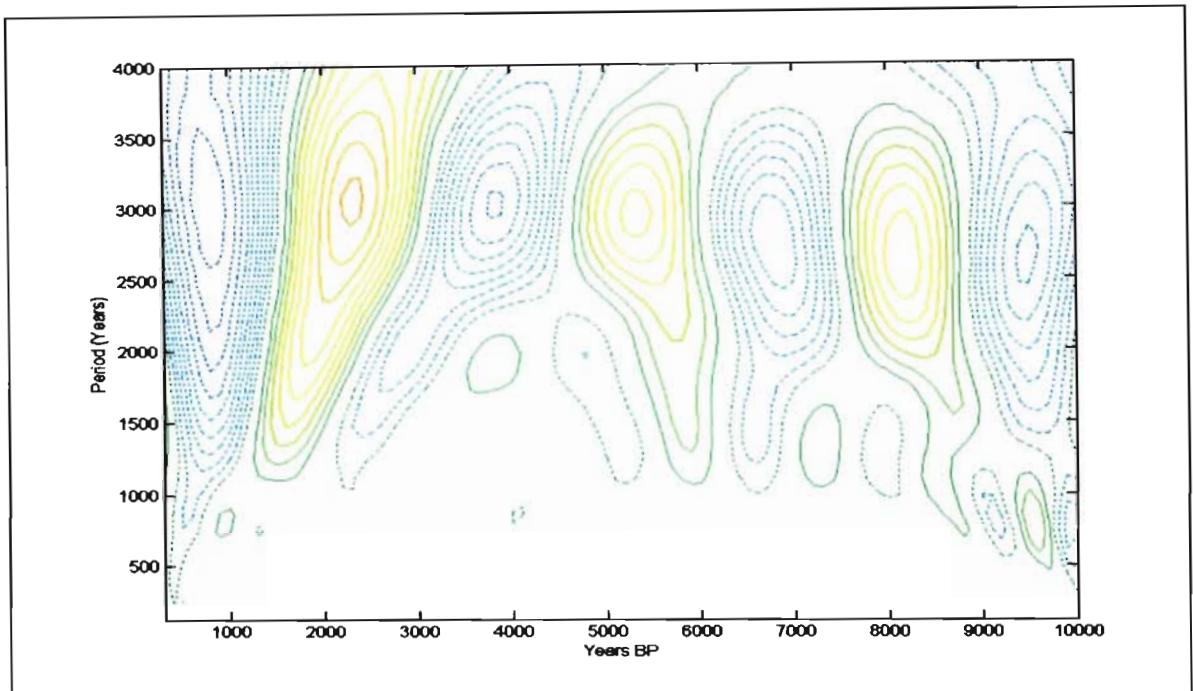


Figure 6.24 – Wavelet analysis of PC2 of 10 000 year Wonderkrater pollen record using the Morlet wavelet with positive values of the wavelet indicated by solid lines and negative values indicated by dotted lines.

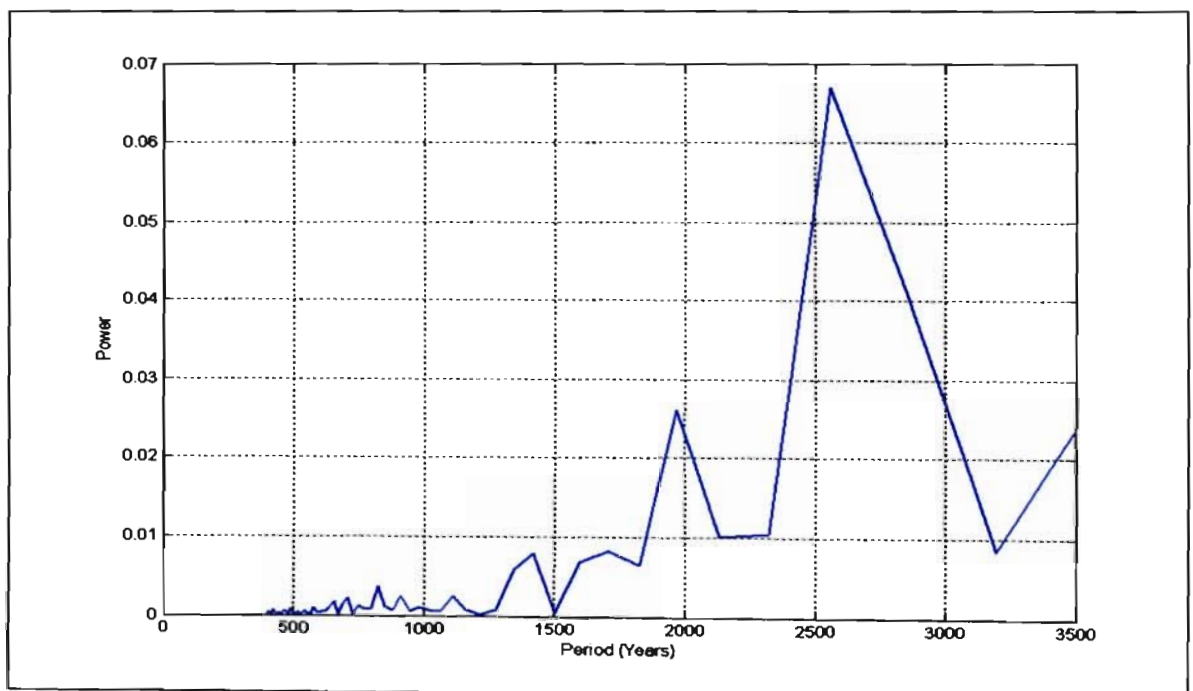


Figure 6.25 – Fourier analysis of PC2 of 10 000 year Wonderkrater pollen record.

A comparison of the Makapansgat and Wonderkrater wavelet analyses shows that the 1000 year cycle undergoes similar modulation, and that this cycle, the 1500 year cycle, and 2500 year cycle are in phase in both datasets. This would be expected due to the close proximity of the sites in the same climatic regime.

### 6.5 RECENT CLIMATE CHANGE DETECTION USING WAVELET ANALYSIS

In processing the climate data for the Sodwana Bay region, a wavelet analysis was performed on the Lake St Lucia (28° 01' S 32° 29' E) salinity record. The results indicated a prominent approximately 12 year cycle as shown in the Figure 6.26. The cycle period appears to be at 14 years at the start of the record in 1960, but reaches 11 years by 1995.

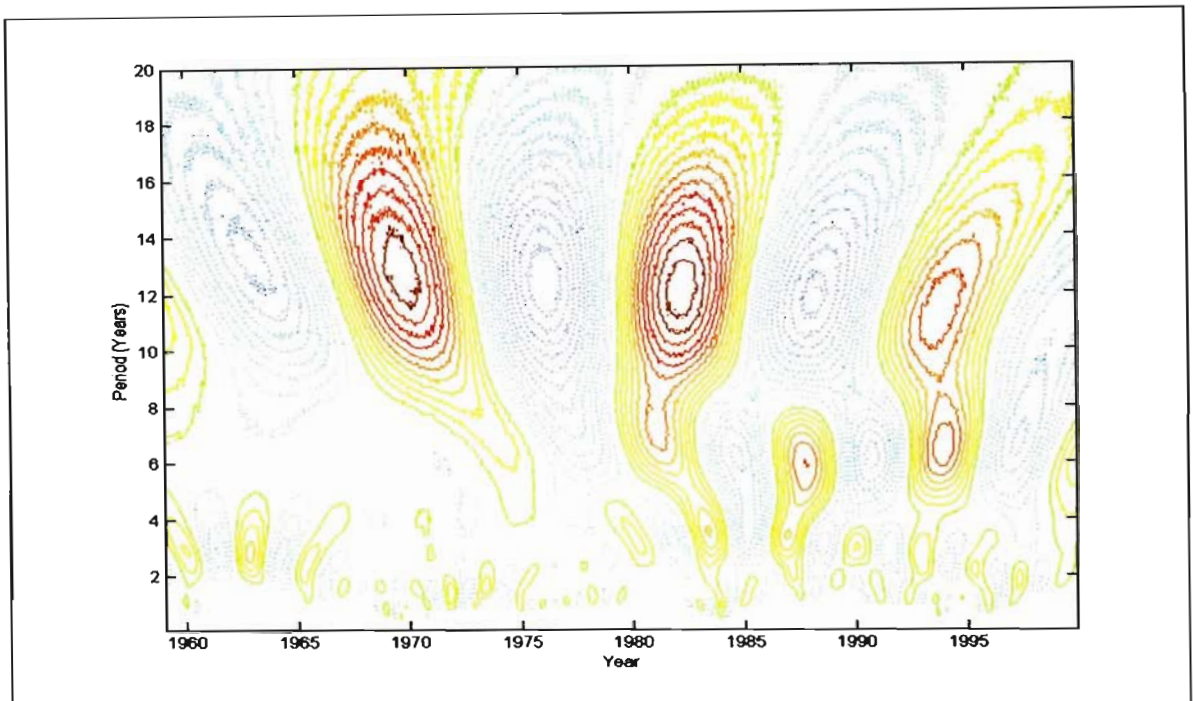
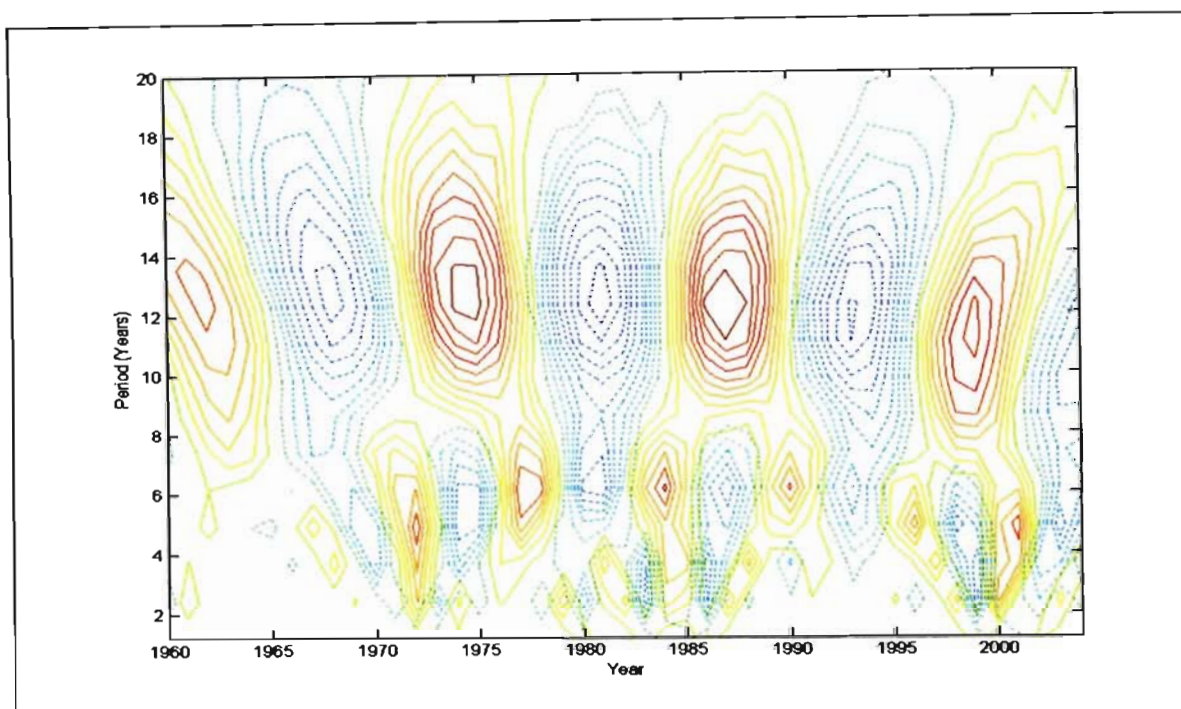


Figure 6.26 – Wavelet analysis of 50 year Lake St. Lucia salinity record using Morlet wavelet, with positive values of the wavelet indicated by solid lines and negative values indicated by dotted lines.

As mentioned before, Garric and Huber (2003) ascertain that many researchers attribute cyclicity with periods in the 7 – 15 year band to the 11 year sunspot cycle despite that the best-established sources of interannual variability are intrinsic. An initial response was to link this cycle to the 11 year solar cycle, but intrinsic causes were also investigated.

To determine whether rainfall follows a similar cycle, a wavelet analysis of the rainfall data for Cape St Lucia ( $28^{\circ} 30' S$   $32^{\circ} 24' E$ ) was performed. The results are shown in Figure 6.27. Once again an approximately 12 year cycle appears, modulated from a period of 13 years in 1960 to 11 years by 2000.



**Figure 6.27 – Wavelet analysis of 45 year Cape St Lucia rainfall record using Morlet wavelet, with positive values of the wavelet indicated by solid lines and negative values indicated by dotted lines.**

The main rainfall cycle documented for southern Africa is the approximately 18 year rainfall cycle apparent in the summer rainfall regions and first described by Tyson (1971). The period range described for this cycle was from 16 to 20 years and thus does not include the period of 12 years detected above. The strong presence of the twelve year cycle in Figure 6.27 and the absence of periodicity in the range of 16 – 20 years prompted further investigation.

A wavelet analysis was performed on the Vryheid rainfall dataset, which extends back to the 1920s. Vryheid ( $27^{\circ} 47' S$   $30^{\circ} 48' E$ ) lies on a similar line of latitude to Sodwana Bay, but further inland. Since the 12 year cycle was present in this dataset, it could be concluded that it was not exclusive to the coastal zone. The results of the wavelet analysis are shown in Figure 6.28.

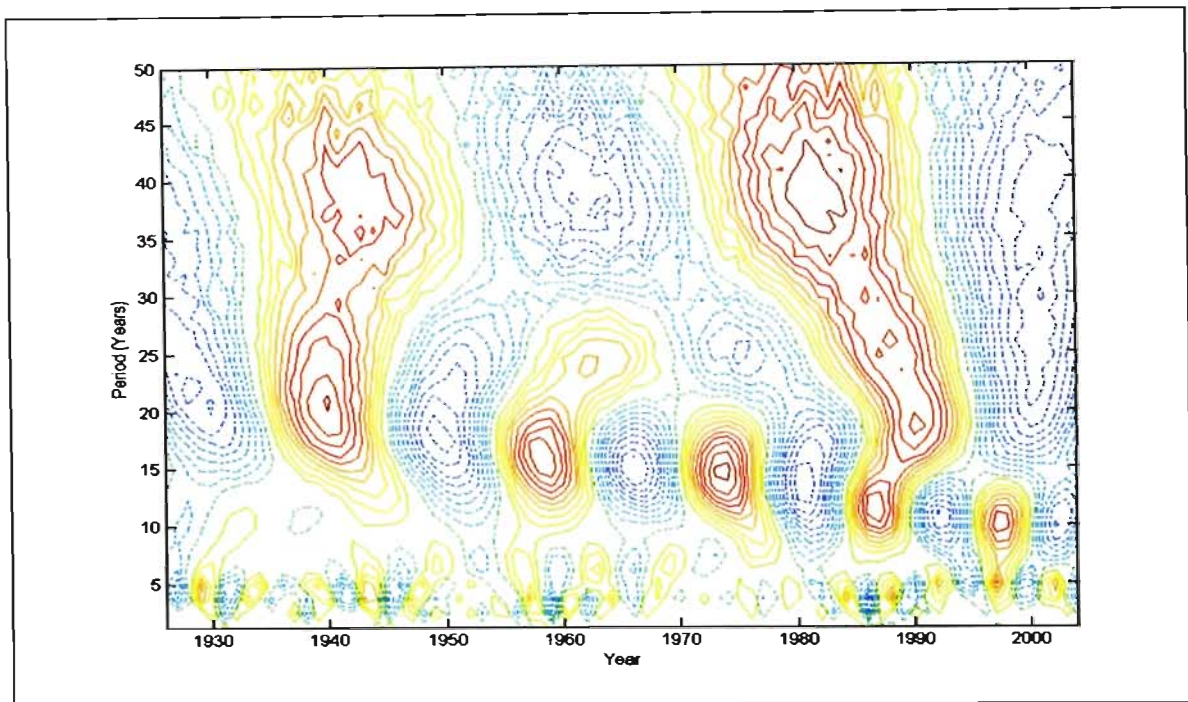


**Figure 6.28 – Wavelet analysis of 80 year Vryheid rainfall record using Morlet wavelet, with positive values of the wavelet indicated by solid lines and negative values indicated by dotted lines.**

Figure 6.28 shows a rainfall cycle extending back to the 1920s. This cycle initially had a period of around 20 years but experienced progressive modulation of the period over time. By the 1960s and 1970s, the period had reached around 15 years but continued to decrease until stabilising at around 11 years from 1990 to the present. This cycle is obviously not directly caused by the solar cycle as external forcing tends to reveal cycles of a regular period. It is more likely that the quasi-12 year cycle apparent in these records is the modulated 18 year cycle described by Tyson (1971).

The length data derived from the Sodwana Bay coral core was highly correlated with rainfall as shown in Chapter 4. A wavelet analysis of the length data was run to assess the presence of this cycle in the proxy rainfall record. The results indicate that the length data also exhibits this 18 year cycle with apparent modulation, as shown in Figure 6.29. The cycle has a period of approximately 20 years in the 1930s and 1940s, but this decreases to around 15 years by the 1960s. The cycle period doesn't appear to decrease beyond 15 years in this dataset.

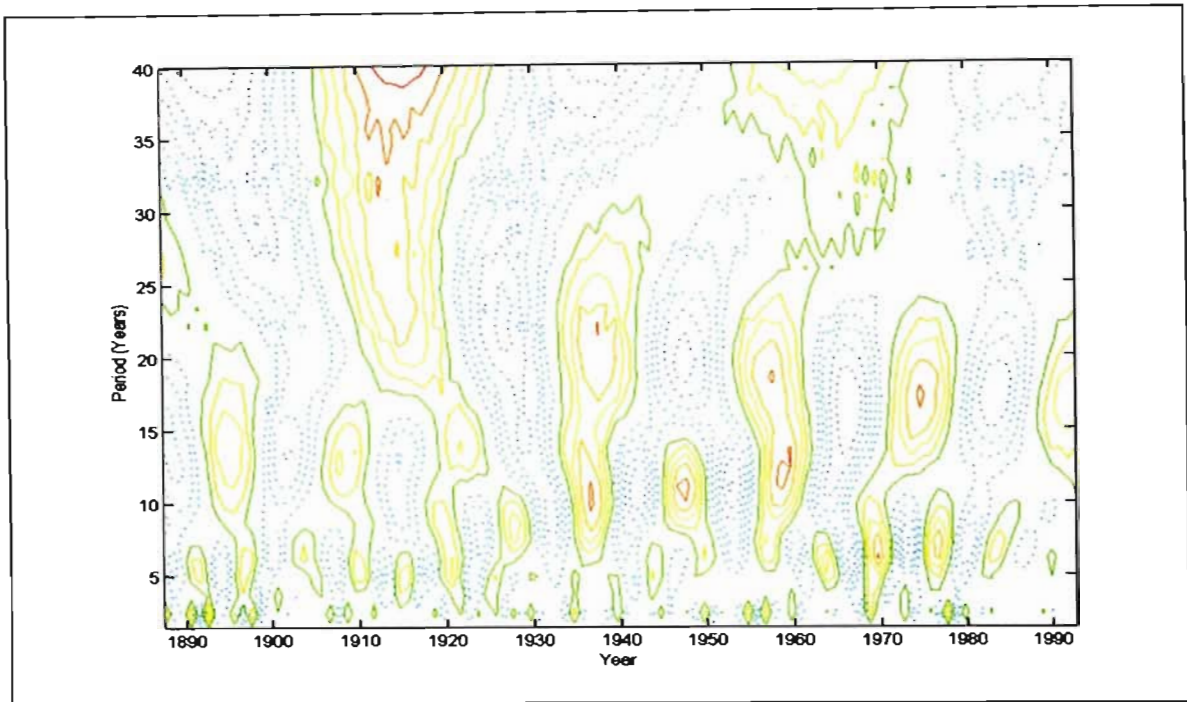


**Figure 6.29 – Wavelet analysis of 116 year coral length record from Sodwana Bay using Morlet wavelet, with positive values of the wavelet indicated by solid lines and negative values indicated by dotted lines.**

The results of these wavelet analyses indicate that either the 18 year cycle is not as stable as previously believed, or the cycle does not influence the entire summer rainfall region. The latitudinal position of the Vryheid, Sodwana Bay and Lake St Lucia sites in the zone of transition between tropical and temperate climate controls may be an important influence on the frequency modulation of this cycle. Future study will involve the wavelet analyses of rainfall data across southern Africa to ascertain the extent of the modulation of this cycle across the region. This will indicate whether such modulation is limited to this latitudinal position.

The shortening of the period of the 18 year cycle, evident in directly recorded and proxy climatic data, is not a singular example of an accelerating climatic cycle. Since the late 1970s, El Niño episodes have been unusually recurrent and this has been attributed to global warming due to an enhanced greenhouse effect (Timmerman *et al.*, 1999; Mason, 2001). The cause of the 18 year cycle has been related to the projection of ENSO-like decadal modes onto the region, with regional sea-surface temperature forcing and modulations of the southern hemisphere circulation (Mason and Jury, 1997; Tyson and Preston-Whyte, 2000). Thus the increase in El Niño frequency could imply an increase in the frequency of this rainfall cycle as well. This is supported by documented evidence that

suggests increased rainfall variability for various regions of southern Africa (such as Mason, 1996; McClelland, 1996). Between 1931 and 1990, the frequency and intensity of extreme rainfall events over South Africa increased substantially (Mason *et al.*, 1999; Poolman, 1999). The reasons for these changes need to be further investigated but are possibly related to anthropogenic climate change and its impact on natural cyclicity.

## 6.6 SUMMARY

Climatic variability is the result of a complex interaction between internal and external mechanisms. Cycles with regular periods tend to be externally controlled by the sun, the 'pacemaker' of the Earth, which has ultimate control over the amount of energy available to drive the geosphere-hydrosphere-cryosphere-atmosphere, and whose relation to the Earth is exhibited in the quasi-regular Milankovitch cycles. Once internal forces come into play, there are complex interactions and feedbacks, including stochastic resonance, which makes it difficult to isolate cycles and infer the driving forces behind variability.

However, wavelet analysis is a powerful tool which allowed for the detection of the climatic cycles that dominate southern African climatic variability on various timescales in a number of climatic and proxy climatic records. At sub-millennial timescales, dominant cycles include the 3 - 5 year Quasi-Biennial, 4 - 8 year El Niño, 11 year, 18 year, 22 year, 45 year, 80 year, and 450 year cycles. Millennial-scale cycles include the 1000 year cycle, 1500 year, 2000 - 2500 year cycle, 3000 year, and the 4500 year cycles. In extended datasets from marine and ice cores, the Milankovitch cycles with periods of approximately 23 000, 40 000, and 100 000 years become evident.

Wavelet analyses give an indication of frequency changes over time and are therefore useful for detecting climate changes. An analysis of proxy and recorded climatic data of rainfall in the Sodwana, Lake St Lucia and Vryheid regions over the last 100 years indicated a frequency modulation of the 18 year rainfall cycle. Although the exact causes of these frequency changes must still be investigated, it is a clear example of the usefulness of wavelet analysis in the assessment of climate change.



## 7. CONCLUSION

Compared to extensive study in the northern hemisphere, very little is known of southern African palaeoclimates. This study aimed to extend understanding of southern African palaeoclimates over the last 40 000 years. Due to the difficulty and expense in gathering palaeoclimatic data, experts in the field were approached to provide datasets for further analysis. Two extensive, high-resolution datasets for southern Africa were made available for this study – namely, the Makapansgat Cold Air Cave T8 stalagmite isotope data collected by Professor Karin Holmgren of Stockholm University, and the Wonderkrater pollen abundance data collected by Dr Louis Scott of Free State University. For an indication of short-term climatic fluctuations over the last century, this study also involved the development of an original coral record derived from a *Porites lutea* head from Sodwana Bay, covering the last 116 years. For comparison with these data, a number of recorded and modeled climatic datasets were utilised, but these generally did not extend beyond 1950.

From a study of the Makapansgat and Wonderkrater datasets, and an extensive literature review of southern African palaeoclimatic studies, a number of common rainfall and temperature fluctuations were detected across the region for the last 40 000 years. General models of rainfall and temperature fluctuations were developed for the summer rainfall region and these allowed for comparison with localised records. Similar fluctuations at distant sites made it clear that these were controlled by the interaction of the ocean and atmosphere on a regional scale. It was also apparent that an inverse correlation existed between rainfall fluctuations in the summer and winter rainfall regions, while the non-seasonal rainfall region along the south coast generally correlated positively with the summer rainfall region, but correlated positively with the winter rainfall region occasionally. An analysis of these relationships made the nature of regional teleconnections apparent, and these could be related to known atmospheric processes.

It was evident from the study of the Makapansgat and Wonderkrater records, and a review of various documented studies in the region, that warmer periods in the summer rainfall region over geological history have also been moister. At first this seemed counter-intuitive as present-day droughts, occurring on approximately monthly scales, are

associated with warm temperatures. On decadal, centennial and longer timescales, however, the major circulations changes that occur override these local effects and generally warmer conditions are associated with increased rainfall, while cooler conditions are associated with decreased rainfall.

The reasons for this trend are clear in an atmospheric model for southern Africa developed by Tyson (1986) and relate to latitudinal shifts of the westerly and easterly wind belts, *in situ* intensification of semi-permanent circulation cells, meridional shifts in the African cloud band and convergence zone, fluctuations in amplitude and position of the mid-tropospheric standing waves, and changes in sea-surface temperature (Tyson, 1999a). General circulation models have highlighted the importance of these mechanisms on the scale of decades to centuries (Tyson, 1999a). A poleward expansion of the tropical easterlies causes warmer and wetter conditions over the southern Africa summer rainfall region, while the winter rainfall region becomes warmer and drier. An equatorward expansion of the westerlies and associated frontal disturbances results in cooler, drier conditions in the summer rainfall region, while the winter rainfall region becomes cooler and wetter (Tyson, 1999a). Major adjustments of atmospheric circulation causing the association of warmer and wetter, and cooler and drier conditions in the summer rainfall region have been sustained for at least 200 000 years on multi-decadal and longer timescales (Tyson, 1999a).

These north-south shifts in mean circulation dominate climatic variability in the region. However, there are also regular disturbances to this mean, such as in the form of the El Nino–Southern Oscillation. The fluctuations seen in palaeoclimatic records are the result of a complex interaction between internal and external mechanisms of climate change. Since ultimately these mechanisms are externally controlled by the sun, through its influence on the amount of energy available to drive the Earth-atmosphere system, and whose relation to the Earth is influenced by the quasi-regular Milankovitch cycles, climate changes tend to have an inherent cyclicity. Long-term cycles with regular periods tend to be directly controlled by the sun, the ‘pacemaker’ of the Earth, but once internal forces come into play, there are complex feedbacks and interactions, including stochastic resonance, which makes it difficult to isolate the exact period of cycles and infer the driving forces.

Wavelet analysis is a powerful tool for detecting cyclicity and wavelet analyses of climatic and proxy-climatic datasets indicated the cycles which dominate southern African climatic variability on various timescales. At sub-millennial timescales, dominant cycles include the annual, Quasi-Biennial 3 – 5, El Nino 4 – 8, 11, 18, 22, 45, 80, and 450 year cycles. Millennial-scale cycles include the approximately 1000, 1500, 2000 – 2500, 3000, and 4500 year cycles. In extended datasets from marine and ice cores, the Milankovitch cycles with periods of approximately 23 000, 40 000, and 100 000 years become evident.

Wavelet analyses also give an indication of frequency changes over time and are therefore useful for detecting climate changes. Previously stable cycles with sudden frequency or amplitude changes in the last 100 years may be indicative of anthropogenic influences on climate. An analysis of proxy and recorded climatic data for southern African rainfall over the last 100 years indicated a frequency modulation of the 18 year rainfall cycle first described by Tyson (1971). Although exact causes of these frequency changes must still be investigated, it may be the impact of anthropogenic climate change and offers a clear example of how wavelet analysis can be used to distinguish natural cyclicity from anthropogenic influences.

Therefore it can be concluded that powerful tools are available for the assessment of climatic variability on various timescales. An understanding of natural cyclicity of various datasets from the southern African region will do much to put present climate changes in context and allow researchers developing climate models to distinguish anthropogenic influences from natural variability.

## **7.1 RECOMMENDATIONS**

There needs to be an increase in interest in climate change in the region, and this should become one of the focuses of environmental research. This is considered a critical issue across the globe but southern African is falling behind in climate change research. The number of continuous, high-resolution datasets for the region needs to be increased to allow for comparison and confirmation of various trends. Further sites need to be identified for palynological and stalagmite analyses. The number of dendrochronology studies must be increased, and these should rely on isotopic data methods instead of only on ring

counting. Additional marine core, coral, mollusc and diatom studies are necessary along the coasts to assess changes in sea-surface temperatures, sea-level and salinity in the region. As techniques for collection and analysis become more advanced, extensive study is necessary in the arid regions, particularly the Kalahari, due to a limited number of studies in these regions.

There is also a need for further understanding of short-term southern African climate variability on inter-annual timescales. While the El Niño cycle dominates southern African records, cycles of other periods may be detected associated with the Southern Annular Mode, the Atlantic ENSO, and Benguela warm and cold events. Very little is known of the influence of these cycles on southern African climate variability and this must be investigated.

It is important to increase the number of datasets involved in this particular study before conclusions can be made for the entire region. Wavelet analyses of the Congo II Cave and Tswaing Crater data would be hugely beneficial. It is important to access datasets for the Kalahari, and for the winter and non-seasonal rainfall regions. Once a sufficient number of datasets have been accessed it would be interesting to run the wavelet analyses as a quantitative study by indicating significance values and the cone of influence.

Further investigation of the apparent modulation of the 18 year cycle in the Sodwana Bay, Cape St. Lucia and Vryheid regions is necessary before the exact causes of this change can be ascertained. A comparison with rainfall data from further north, possibly Mozambique, and data from the rest of southern Africa will give some indication of whether this is the result of interaction between tropical and subtropical systems and thus limited to a particular latitudinal position. This topic would make for interesting and relevant doctoral research.

## REFERENCES

- Aaby, B. (1976): Cyclic climatic variations in climate over the past 5,500 yr reflected in raised bogs in *Science*, 263, 281 - 284.
- Abbott, M. and Dyer, T.G.J. (1976): The temporal variation of rainfall over the summer rainfall region of South Africa in *South African Journal of Science*, 72, 276 - 278.
- Acocks, J.P.H. (1953): *Veld types of South Africa*, Memoirs Botanical Survey of South Africa, 28, Government Printer, Pretoria.
- Allan, R. J. (2000): ENSO and climatic variability in the last 150 years, Chapter 1 in Diaz, H.F. and Markgraff, V. (eds.) *El Niño and the Southern Oscillation: Multiscale Variability, Global and Regional Impacts*, Cambridge University Press, Cambridge, UK, 3 - 56.
- Allan, R.J.; Lindsay, J.A. and Parker, D.E. (1996): *El Niño Southern Oscillation and Climate Variability*, CSIRO Publishing, Melbourne, 405 pp.
- Alley, R.B.; Mayewski, P.A.; Sowers, T.; Stuvier, M.; Taylor, K.C. and Clark, P.U. (1997) Holocene climatic instability: a prominent widespread event 8200 yr ago in *Geology*, 25 (6), 483 – 486.
- Argoul, F.; Arneodo, A.; Grasseau, G.; Gagne, Y. and Hopfinger, E. J. (1989): Wavelet analysis of turbulence reveals the multifractal nature of the Richardson Cascade in *Nature*, 338, 51 – 53.
- Avery, D.M. (1982a): Mircomammals as palaeoenvironmental indicators and an interpretation of the Late Quaternary in the southern Cape Province, South Africa in *Annals of the South African Museum*, 85, 183 – 374.
- Avery, D.M. (1982b): The micromammalian fauna from Border Cave, KwaZulu, South Africa in *Journal of Archaeological Science*, 9, 187 - 204.

Avery, D.M. (1988): The Holocene environment of central South Africa: micromammalian evidence in *Palaeoecology of Africa*, 19, 335 - 345.

Avery, D.M. (1991): Micromammals, owls and vegetation change in the Eastern Cape Midlands, South Africa during the last millennium in *Journal of Arid Environments*, 20, 357 - 369.

Avery, D.M. (2003): Early and middle Pleistocene environments and hominid biogeography: micromammalian evidence from Kabwer, Twin Rivers and Mumbwa Caves in central Zambia in *Palaeogeography, Palaeoclimatology, Palaeoecology*, 189, 55 - 69.

Bard, E.; Rostek, F. and Sonzogni, C. (1997): Interhemispheric synchrony of the last deglaciation inferred from palaeothermometry in *Nature*, 385, 707 - 710.

Bar-Matthews, M.; Ayalon, A. and Kaufman, A. (1997): Late Quaternary palaeoclimate in the eastern Mediterranean region from stable isotope analysis of speleothems at Soreq Cave, Israel in *Quaternary Research*, 47, 155 - 168.

Barnett, T.P. (1991): The interaction of multiple time scales in the tropical system in *Journal of Climatology*, 69, 285.

Barnett, T.P. and Latif, M. (1998): Decadal variability in the northern Pacific as simulated by a hybrid coupled model in *Journal of Climatology*, 11, 297 - 312.

Bartlein, P.J. and Whitlock, C. (1993): Palaeoclimatic interpretation of the Elk Lake pollen record in Branbury, J.P. and Dean, W.E. (eds.) *Elk Lake Minnesota: Evidence for Rapid Climate Change in the Northern United States*, Geology Society of America Special Paper 276, 275 - 293.

Baxter, A.J. (1997): *Late Quaternary palaeoclimate of the Sandveld, Western Cape Province, South Africa*, unpublished PhD thesis, University of Cape Town, South Africa.

Baxter, A.J. and Meadows, M.E. (1999): Evidence for Holocene sea level change at Verlorenvlei, Western Cape, South Africa in *Quaternary International*, 56, 65 - 79.

Bayer, M.B. (1984): The Cape flora and Karoo – a winter rainfall biome versus a fynbos biome in *Veld and Flora*, 70, 17 - 19.

Beaumont, P.B. (1986): Where did all the young men go during  $^{18}\text{O}$  Stage 2? in *Palaeoecology of Africa*, 17, 79 - 86.

Behera, S. K. and Yamagata, T. (2001): Subtropical SST dipole events in the southern Indian Ocean in *Geophysical Research Letters*, 28, 327 - 330.

Berger, A. (1988): Milankovitch theory and climate in *Review of Geophysics*, 26, 624 - 657.

Berger, A.L.; Imbrie, J.; Hays, J., Kukla, G., and Saltzman, B. (eds.) (1984): Milankovitch and Climate in *NATO Advanced Study Institute Series*, 127.

Berner, W.; Stauffer, B. and Oeschger, H. (1979): Past atmospheric composition and climate, gas parameters measured in ice-cores in *Nature*, 275, 53 - 55.

Bessat, F. and Buiges, D. (2001): Two centuries of variation in coral growth in a massive *Porites* colony from Moorea (French Polynesia): a response of ocean-atmosphere variability from south central Pacific in *Palaeogeography, Palaeoclimatology, Palaeoecology*, 175, 381 - 392.

Bianchi, G. and McCave, N. (1999): Holocene periodicity in North Atlantic climate and deep ocean flow south of Iceland in *Nature*, 397, 51 - 53.

Bjerknes, J. (1966): A possible response of the atmospheric Hadley circulation to equatorial anomalies of ocean temperature in *Tellus*, 18, 820 - 829.

Bjerknes, J. (1969): Atmospheric teleconnections from the equatorial in *Pacific Monthly Weather Review*, 97 (3) 163 - 172.

Blüniér, T.; Chappellaz, J.; Schwander, J.; Dällenbach, A.; Stauffer, B.; Stocker, T.F.; Raynaud, D.; Jouzel, K.; Clausen, H.B.; Hammer, C.U. and Johnsen, S.J. (1998): Asynchrony of Antarctic and Greenland climate change during the last glacial period in Nature, 394, 739 - 743.

Bolin, B. (1986): How much CO<sub>2</sub> will remain in the atmosphere? in Bolin, B.; Döös, B.R.; Jäger, J and Warrick, R.A. (eds.) The Greenhouse Effect, Climatic Change and Ecosystems, Wiley, Chichester.

Bolton, E.W.; Maasch, K.A. and Lilly, J.M. (1995): A wavelet analysis of Pleistocene climate indicators: a new view of periodicity evolution in Geophysical Research Letters, 24, 1351 - 1354.

Bond, G. (1996): New evidence: earth's natural cooling cycle in Columbia University Record, 21, 14.

Bond, G.; Heinrich, H.; Broecker, W.; Labeyrie, L.; McManus, J.; Andrews, J.; Huon, S.; Jantschik, B.; Clasen, S.; Simet, C.; Tedesco, K.; Klas, M.; Nonani, G.; and Ivy, S. (1992): Evidence for massive discharges of icebergs into the North Atlantic Ocean during the last glacial period in Nature, 360, 245 – 249.

Bond, G.; Kromer, B.; Beer, J.; Muscheler, R.; Evans, M.N.; Showers, W.; Hoffmann, S.; Lotti-Bond, R.; Hajdas, I. and Bonani, G. (2001): Persistent solar influence on North Atlantic climate during the Holocene in Science, 294, 2130 - 2136.

Bond, G.C. and Lotti, R. (1995): Iceberg discharges into the North Atlantic on millennial time scales during the last glaciation in Science, 267, 1005 - 1010.

Bond, G.; Showers, W.; Cheseby, M.; Lotti, R.; Almasi, P.; Demenocal, P.; Priore, P.; Cullen, H.; Hajdas, I. and Bonani, G. (1997): A pervasive millennial-scale cycle in North Atlantic Holocene and glacial climates in Science, 278, 1257 - 1266.

Bond, G.C.; Showers, W.; Elliot, M.; Evans, M.; Lotti, R. and Johnson, S. (1999): The North Atlantic's 1 – 2 kyr climate rhythm: relation to Heinrich Events,



Dansgaard/Oeschger Cycles and the Little Ice Age in Clark, P.U.; Webb, R.S. and Keigwin, L.D. (eds.) *Mechanisms of Global Climate Change at Millennial Time Scales*, Geophysical Monograph Series, American Geophysical Union, Washington, 112, 35 – 58.

Boninsegna, J.A. (1992): South American dendrochronological records in Bradley, R.S. and Jones, P.D. (eds.) *Climate Since AD 1500*, Routledge, London.

Bousman, C.B.; Partridge, T.C.; Scott, L.; Seaman, M.; Matcalfe, S.E.; Vogel, J.C. and Brink, J.S. (1988): Palaeoenvironmental implications of late Pleistocene and Holocene valley fills in Blydefontein Basin, Noupoort, C.P., South Africa in *Palaeoecology of Africa*, 19, 43 - 67.

Boyle, E. and Keigwin, L. (1982): Deep circulation of the North Atlantic over the last 200,000 years: geochemical evidence in *Science*, 218, 784 - 787.

Bradley, R.S. (1999): *Paleoclimatology: Reconstructing Climates of the Quaternary*, 2nd edition, Academic Press, London, 613 pp.

Bradshaw, G.A. (1991): *Hierarchical Analysis of Pattern and Process in Douglas-fir Forests Using the Wavelet Transform*, unpublished PhD thesis, Oregon State University, USA.

Bradshaw, G.A. and McIntosh, B.A. (1994): Detecting climate-induced patterns using wavelet analysis in *Environmental Pollution*, 83 (1-2), 135 – 142.

Bradshaw, G.A. and Spies, T.A. (1992): Characterising forest gap structure using the wavelet transform in *Journal of Ecology*, 80, 205 - 215.

Briffa, K.R.; Jones, P.D.; Bartholin, T.S.; Eckstein, D.; Schweingruber, F.H.; Karlen, W., Zetterberg, P. and Eronen, M. (1992): Fennoscandian summers from A.D. 500: temperature changes on short and long timescales in *Climate Dynamics*, 7, 111 - 119.

Broecker, W. (1979): A Revised Estimate for the Radiocarbon Age of North Atlantic Deep Water in *Journal of Geophysical Research*, 84 (C6), 3218 - 3226.

Broecker, W. (1981): Glacial to interglacial changes in ocean and atmosphere chemistry in Berger, A. (ed.) *Climate Variations and Variability: Facts and Theory*, Reidel, Dordrecht.

Broecker, W. (1982a): Glacial to interglacial changes in ocean chemistry in *Progress in Oceanography*, 11, 151 - 197.

Broecker, W. (1982b): Ocean chemistry in glacial time in *Geochimica et Cosmochimica Acta*, 46, 1689 - 1705.

Broecker, W.S.; Peteet, D.M. and Rind, D. (1985): Does the ocean-atmosphere system have more than one stable mode of operation? in *Nature*, 315, 21 - 25.

Broecker, W. and Takahashi, T. (1984): Is there a tie between Atmospheric CO<sub>2</sub> and Ocean Circulation in Hansen, J. and Takahashi, T. (eds.) *Climate Processes and Climate Sensitivity*, Geophysical Monograph, 29, 314 - 326.

Broecker, W. and Van Donk, J. (1970): Insolation changes, ice volume, and the O18 record in deep-sea cores in *Reviews of Geophysics and Space Physics*, 8, 169 - 198.

Brook, G.A.; Cowart, J.B.; Brandt, S.A. and Scott, L. (1997): Quaternary climatic change in southern and eastern Africa during the last 300 ka: the evidence from caves in Somalia and the Transvaal region of South Africa in *Zeitschrift für Geomorphologie*, NF Supplement, 108, 15 - 48.

Bryant, A.T. (1929): *Olden Times in Zululand and Natal*, Longman, Green and Company, London, 695 pp.

Burgess, R.L. and Jacobson, L. (1984): Archaeological sediments from a shell midden near Wortel Dam, Walvis Bay, Southern Africa in *Palaeoecology of Africa*, 16, 429 - 435.

Burney, D.A.; James, H.F.; Grady, F.V.; Rafamantanantsoa, J.G.; Ramilisonina, D.; Wright, H.T.; Cowart, J.B. (1997): Environmental change, extinction and human activity: evidence from caves in NW Madagascar in *Journal of Biogeography*, 24, 755 - 767.

Burroughs, W.J. (1992): *Weather Cycles: Real or Imaginary?* Cambridge University Press, Cambridge, 201 pp.

Butzer, K.W. (1983): *Summary Report for Workshop W1: Evidence for Late Quaternary Climatic Change in Southern Africa*, International Symposium on Late Cenozoic Palaeoclimates of the Southern Hemisphere, University of the Witwatersrand.

Butzer, K.W. (1984a): Late Quaternary environments in South Africa in Vogel, J.C. (ed.) *Late Cainozoic Palaeoclimates of the Southern Hemisphere*, Balkema, Rotterdam, 235 - 264.

Butzer, K.W. (1984b): The archaeology and Quaternary environments in the interior of southern Africa in Klein, R.G. (ed.) *South African Prehistory and Palaeoenvironments*, Balkema, Rotterdam, 1 - 64.

Butzer, K.W.; Beaumont, P.B. and Vogel, J.C. (1978a): Lithostratigraphy of Border Cave, KwaZulu, South Africa: Middle Stone Age sequence beginning c. 195 000 BP in *Journal of Archaeological Science*, 5, 317 - 341.

Butzer, K.W.; Fock, G.J.; Stuckenrath, R. and Zilch, A. (1973): Palaeohydrology of Late Pleistocene Lake Alexandersfontein, Kimberley, South Africa in *Nature*, 243, 328 - 330.

Butzer, K.W.; Stuckenrath, R.; Bruzewicz, A. and Helgren, D.M. (1978b): Late Cenozoic palaeoclimates of the Gaap Escarpment, Kalahari margin, South Africa in *Quaternary Research*, 10, 310 - 339.

Cane, M.A. (2005): The evolution of El Niño, past and future in *Earth and Planetary Science Letters*, 230, 227 - 240.

Celliers, L. and Schleyer, M.H. (2002): Coral bleaching on high-latitude marginal reefs at Sodwana Bay, South Africa in *Marine Pollution Bulletin*, 44, 1380 - 1387.

Chalker, B.; Barnes, D. and Isdale, P. (1985): Calibration of X-ray densitometry for the measurement of coral skeleton density in Coral Reefs, 4, 95 - 100.

Chambers, F.M.; Barber, K.E.; Maddy, D. and Brew, J. (1997): A 5500-year proxy-climate and vegetation record from blanket mire at Talla Moss, Borders, Scotland in The Holocene, 7 (4), 391 – 399.

Chang, P.; Wang, B.; Li, T. and Ji, L. (1994): Interactions between the seasonal cycle and the southern oscillation - frequency entrainment and chaos in a coupled ocean-atmosphere model in Geophysical Research Letters, 21, 817 – 820.

Chapman, M.R. and Shackleton, N.J. (2000): Evidence of 550-year and 1000-year cyclicities in North Atlantic circulation patterns during the Holocene in The Holocene, 10, 287 - 291.

Chappellaz, J. (1993): Synchronous changes in atmospheric CH<sub>4</sub> and Greenland climate between 40 kyr and 80 kyr BP in Nature, 366, 443 - 445.

Chatfield, C. (1989): *The Analysis of Time Series: An Introduction*, 4<sup>th</sup> edition, Chapman and Hall, London.

Cheddadi, R.; Yu, G.; Guiot, J.; Harrison, S.P.; Prentice, I.C. (1996): The climate 6000 years ago in Europe in Climate Dynamics, 13, 1 - 9.

Clapperton, C. (1993): *Quaternary Geology and Geomorphology of South America*, Elsevier, Amsterdam.

Clement, A.C.; Cane, M.A.; Seager, R. (2001): An orbitally driven tropical source for abrupt climate change in Journal of Climate, 14 (11), 2369 - 2375.

Cleveland, R.O.; Cohen, A. L.; Roy, R.A.; Singh, H. and Szabo, T. L. (2004): Imaging coral II: using ultrasound to image coral skeleton in Subsurface Sensing Technologies and Applications, 5 (1), 43 - 60.

CLIMAP (1981): *Seasonal reconstructions of the Earth's surface at the Last Glacial Maximum*, Geological Society of America Map and Chart Series, MC-36.

Cockcroft, M.J.; Wilkinson, M.J. and Tyson, P.D. (1987): The application of a present-day climatic model to the Late Quaternary in southern Africa in *Climate Change*, 10, 161 - 191.

Coetzee, J.A. (1967): Pollen analytical studies in East and Southern Africa in *Palaeoecology of Africa*, 3, 146.

Cohen, A. (2005): Woods Hole Oceanographic Institution, Cape Cod, personal communication by email, April 2005.

Cohen, A.L.; McCartney, M.S.; Smith, S.R. and van Etten, J. (2004): How brain corals record climate: an integration of skeletal structure, growth and chemistry in *Diploria labyrinthiformis* from Bermuda in *Marine Ecology Progress Series*, 271, 147 - 158.

Cohen A.L.; Parkington J.E.; Brundritt G.B.; and Van der Merwe N.J. (1992): A Holocene marine climate record in mollusc shells from the southwest African coast in *Journal of Quaternary Research*, 38, 379 - 385.

Cohen, A.L. and Tyson, P.D. (1995): Sea surface temperatures during the Holocene on the south coast of Africa: implications for terrestrial climate and rainfall in *Holocene*, 5, 304 - 312.

Cook, E.; Bird, T.; Peterson, M.; Barbetti, M.; Buckley, B., D' Arrigo, R.; Francey, R. and Tans, P. (1991): Climatic change in Tasmania inferred from a 1089-year tree-ring chronology of Huon Pine in *Science*, 253, 1266 - 1268.

Cook, K.H. (2001): A southern hemisphere wave response to ENSO with implications for southern Africa precipitation in *Journal of Atmospheric Science*, 58, 2146 - 2162.

Cooke, H.J. and Heine, K. (1983): *Summary Report for Workshop W1: Evidence for Late Quaternary Climatic Change in Southern Africa*, International Symposium on Late

Cenozoic Palaeoclimates of the Southern Hemisphere, University of the Witwatersrand, South Africa.

Cooke, H.J. and Verstappen, H.T. (1984): The landforms of the western Makgadigadi Basin in northern Botswana with a consideration of the chronology of the evolution of Lake Palaeo-Makgadigadi in *Zeitschrift für Geomorphologie*, 28, 1 - 19.

Cooper, G.R.J (2005): Department of Geophysics, University of the Witwatersrand, personal communication at the Student Geocongress in Durban, 5 July 2005.

Crossley, R.; Davison-Hirschmann, S.; Owen, R.B. and Shaw, P. (1983): Lake level fluctuations during the last 2000 years in Malawi in Vogel, J.C. (ed.): *Late Cainozoic Palaeoclimates of the Southern Hemisphere*, Balkema, Rotterdam, 391 - 404.

Dansgaard, W.; Johnsen, S.J.; Clausen, H.B.; and Langway, C.C. (1973): Climate record revealed by the Camp Century ice core in Turekian, K.K. (ed.): *The Late Cenozoic Ice Ages*, Yale University Press, New Haven, 43 - 44.

Daubechies, I. (1990): The wavelet transform time-frequency localization and signal analysis in *IEEE Transformation Theory*, 36, 961 - 1004.

Daubechies, I. (1992): *Ten Lectures in Wavelets*, Society for Industrial and Applied Mathematics, 357 pp.

Davis, T.N. (1979): On climate cycles in *Alaska Science Forum*, 314.

Dawson, A.G. (1992): *Ice Age Earth: Late Quaternary Geology and Climate*, Routledge, London.

Deacon, H.J.; Deacon, J.; Scholtz, A.; Thackeray, J.F. and Brink, J.S. (1984): Correlation of palaeoenvironmental data from the Late Pleistocene and Holocene deposits at Boomplaas cave, southern Cape in Vogel, J. (ed.) *Late Cainozoic Palaeoclimates of the Southern Hemisphere*, Balkema, Rotterdam, 339 - 351.

Deacon, J. and Lancaster, N. (1984): *A synthesis for the evidence for climate changes in southern Africa over the last 125 000 years*, Report to the National Programme for Weather, Climate and the Atmosphere, CSIR, Pretoria, 283 pp.

Deacon, H. and Lancaster, N. (1988): *Late Quaternary Palaeoenvironments of Southern Africa*, Clarendon Press, Oxford.

Deacon, J.; Lancaster, N. and Scott, L. (1983): Evidence for Late Quaternary climatic change in southern Africa in Vogel, J. (ed.) *Late Cainozoic Palaeoclimates of the Southern Hemisphere*, Balkema, Rotterdam, 391 - 404.

Dearing, J.L. and Foster, I.D.L. (1986): Lake sediments and palaeohydrological studies in Berglund, B.E. (ed.): *Handbook of Holocene Palaeoecology and Palaeohydrology*, Wiley-Interscience, Chichester, 67 - 90.

Delmas, R.; Ascencio, J.M. and Legrand, M. (1980): Polar ice evidence that atmospheric CO<sub>2</sub> 20,000 yr BP was 50% of present in *Nature*, 284, 155 - 157.

DeMenocal, P.; Ortiz, J.; Guilderson, T.; Sarnthein, M. (2000): Coherent high- and low-latitude climate variability during the Holocene warm period in *Science*, 288, 2198 – 2202.

Denton, G.H. and Karlen, W. (1973): Holocene climatic variations - their pattern and possible cause in *Quaternary Research*, 3, 155 - 205.

Dethloff, K.; Rinke, A.; Handorf, D.; Weisheimer, A. and Dorn, W. (2003): Nonlinear dynamics of the climate system in Fischer, H.; Kumke, T.; Lohmann, G.; Flöser, G.; Miller, H.; Von Storch, H. and Negendank, J.F.W. (eds.): *The Climate in Historical Times: Towards a Synthesis of Holocene Proxy Data and Climate Models*, Springer-Verlag, Berlin, 487 pp.

Dodge, R.E.; Szmant, A.M.; Garcia, R.; Swart, P.K.; Forester, A.; and Leder, J.J. (1992): Skeletal structural basis of density banding in the reef coral *Montastrea annularis* in *Proceedings of the 7th International Coral Reef Symposium, Guam*, 186–195.

Dorale, J.A.; González, L.A.; Reagan, M.K.; Pickett, D.A.; Murrel, M.T. and Baker, R.G. (1992): A high-resolution record of Holocene climate change in speleothem calcite from Cold Water Cave, Northeast Iowa in *Science*, 258, 1626 – 1630.

Douville, H.; Chauvin, F.; and Broqua, H. (2001): Influence of soil moisture on the Asian and African monsoons. Part I: Mean monsoon and daily precipitation in *Journal of Climate*, 14, 2381 - 2403.

Draschba, S.; Patzold, J.; and Wefer, G. (2000): North Atlantic climate variability since AD 1350 in  $\delta^{18}\text{O}$  and skeletal density of Bermuda coral in *International Journal of Earth Sciences*, 88, 733–741.

Dunbar, R.; Wellington, G.M.; Colgan, M.W. and Glynn, P.W. (1994): Eastern Pacific sea surface temperatures since 1600 AD in *Paleoceanography*, 9, 291 - 315.

Dunwiddie, P.W. and LaMarche, V. (1980): A climatologically-responsive tree-ring record from *Widdringtonia cedarbergensis*, Cape Province, South Africa in *Nature*, 286, 796 - 79.

Ellery, W.N. (1991): An initial approach to predicting the sensitivity of the grassland biome to climate change in *South African Journal of Science*, 87, 499 - 503.

Emiliani, C. (1955): Pleistocene temperatures in *Geology*, 63, 538 – 578.

Engle, D. (2005): *The Inter-Tropic Convergence Zone*, Hurricane Science Centre, National Science Digital Library, United States, accessed 2005 at [www.nsdlib.org](http://www.nsdlib.org).

Fairbanks, R.G.; Mortlock, R.A.; Chiu, T.-C.; Cao, L.; Kaplan, A.; Guilderson, T.P.; Fairbanks, T.W. and Bloom, A.L. (2005). Marine Radiocarbon Calibration Curve Spanning 10,000 to 50,000 Years B.P. Based on Paired  $^{230}\text{Th}/^{234}\text{U}/^{238}\text{U}$  and  $^{14}\text{C}$  Dates on Pristine Corals in *Quaternary Science Reviews*, 24, 1781 – 1796.

Farge, M. (1992): Wavelet transforms and their applications to turbulence in *Annual Review of Fluid Mechanics*, 24, 394 - 457.



Farrera, I.; Harrison, S.P.; Prentice, L.C.; Ramstein, G.; Guiot, J.; Bartlein, P.J.; Bonnefille, R.; Bush, M.; Cramer, W.; Von Grafenstein, U.; Holmgren, K.; Hooghiemstra, H.; Hope, G.; Jolly, D.; Lauritzen, S.-E.; Ono, Y.; Pinot, S.; Stute, M.; and Yu, H. (1999): Tropical climates at the Last Glacial Maximum: a new synthesis of terrestrial palaeoclimate data. I. Vegetation, lake-levels and geochemistry in *Climate Dynamics*, 15, 823 - 856.

Felis, T. and Pätzold, J. (2003): Corals as Climate Archive in Fischer, H.; Kumke, T.; Lohmann, G.; Flöser, G.; Miller, H.; Von Storch, H.; Negendank, J.F.W. (eds.): *The Climate in Historical Times: Towards a Synthesis of Holocene Proxy Data and Climate Models*, Springer-Verlag, Berlin, 487 pp.

Finch, A.A.; Shaw, P.A.; Holmgren, K.; and Lee-Thorp, J. (2003): Corroborated rainfall records from aragonitic stalagmites in *Earth and Planetary Science Letters*, 215.

Fischer, H.; Kumke, T.; Lohmann, G.; Flöser, G.; Miller, H.; Von Storch, H.; Negendank, J.F.W. (eds.) (2003): *The Climate in Historical Times: Towards a Synthesis of Holocene Proxy Data and Climate Models*, Springer-Verlag, Berlin, 487 pp.

Flueck, J.A. and Brown, T.J. (1993): Criteria and methods for performing and evaluating solar-weather studies in *Journal of Climate*, 6, 373 - 385.

Folland, C.K., Parker D.E., Colman A. and Washington, R. (1999): Large scale modes of ocean surface temperature since the late nineteenth century in Navarra, A. (ed.) *Beyond El Niño: Decadal and Interdecadal Climate Variability*, Springer-Verlag, Berlin, Chapter 4, 73 - 102.

Ford, D.C. and Williams, P. (1989): *Karst geomorphology and hydrology*, Unwin Hyman, London, page 370.

Frakes, L.A. (1979): Climate throughout Geological Time, Elsevier, Amsterdam.

Fritts, H.C. (1971): Dendroclimatology and dendroecology in *Quaternary Research*, 1(4), 419 - 450.

- Fyfe, J.C. (2003): Extratropical southern hemisphere cyclones: harbingers of climate change? in *Journal of Climate*, 16 (17), 2802 - 2805.
- Ganopolski, A. and Rahmstorf, S. (2002): Abrupt glacial climate changes due to stochastic resonance in *Physical Review Letters*, 88 (3).
- Garden, S.E. (2005): *Origin, Geomorphology and Dynamics of the Lower Umfolozi River Floodplain Wetlands*, uncompleted PhD thesis, University of KwaZulu-Natal, Durban.
- Garric, G. and Huber, M. (2003): in Quasi-decadal variability in paleoclimate records: Sunspot cycles or intrinsic oscillations? in *Paleoceanography*, 18 (3), 1068 - 1077.
- Garstang, M. and Tyson, P.D. (1997): Mesoscale convective activity in South Africa in storms in Pielke, R.A. (Snr.) and Pielke, R.A. (Jnr.) (eds.) *Natural Hazards and Disasters*, Routledge Press, London.
- Gascoyne, M. (1979): *Pleistocene climates determined from stable isotope and geochronologic studies of speleothem*, unpublished PhD thesis, McMaster University, Canada, 433 pp.
- Gascoyne, M. (1992): Palaeoclimate determination from cave calcite deposits in Quaternary Science Reviews, 11, 609 - 632.
- Gasse, F. (2000): Hydrological changes in the African tropics since the Last Glacial Maximum in *Quaternary Science Reviews*, 19, 189 - 211.
- Gasse, F. and Van Campo, E. (1998): A 40,000-yr pollen and diatom record from Lake Trutrivakely, Madagascar in the southern tropics in *Quaternary Research*, 49, 299 - 311.
- Gillooly, J. F. (1975): *A preliminary assessment of the potential offered by some indigenous tree species in the Rustenburg district for dendrochronology in South Africa*, unpublished BSc Honours seminar paper, University of the Witwatersrand, South Africa.

- Glynn, P.W. (1990): *Global Ecological Consequences of the 1982-83 El Niño-Southern Oscillation*, Elsevier Oceanography Series, 52, 563 pp.
- Goede, A., and Vogel, J.C. (1991): Trace element variations and dating of a Late Pleistocene Tasmanian spelethem in *Palaeogeography, Palaeoclimatology and Palaeoecology*, 88, 121 - 131.
- Grey, D.R.C. and Cooke, H.J. (1977): Some problems in the Quaternary evolution of landforms of northern Botswana in *Cantena*, 4, 123 - 133.
- Gribben, J. (1989): The end of the ice ages? in *New Scientist*, 17 June, 48 – 52.
- Grove, J. (1988): *The Little Ice Age*, Methuen, London.
- Gu, D. and Philander, S.G.H. (1995): Secular changes of annual and interannual variability in the tropics during the past century in *Journal of Climate*, 8, 864 - 876.
- Guiot, J. (1990): Methodology of palaeoclimatic reconstruction from pollen in France in *Palaeogeography, Palaeoclimatology and Palaeoecology*, 80, 49 - 69.
- Guiot, J. (1991): Structural characteristics of proxy data and methods for quantitative climate reconstruction in *Paläoklimatforschung*, 6, 271 – 284.
- Gupta, A.K.; Anderson, D.M. and Overpeck, J.T. (2003): Abrupt changes in the Asian southwest monsoon during the Holocene and their links to the north Atlantic Ocean in *Nature*, 421, 354 - 356.
- Hall, M.J. (1976): Dendroclimatology, rainfall and human adaptation in the later Iron Age of Natal and Zululand in *Annals of the Natal Museum*, 22, 693 – 703.
- Hameed, S. (1984): Fourier analysis of Nile flood levels in *Geophysical Research Letters*, 1, 843 - 845.

Handler, P. (1984): Possible association of stratospheric aerosols and El Niño type events in *Geophysical Research Letters*, 11, 1121 - 1124.

Handler, P. (1986): Possible association between the climatic effects of stratospheric aerosols and sea surface temperatures in the eastern tropical Pacific Ocean in *Journal of Climatology*, 6, 31 - 42.

Hanvey, P.M. and Marker, M.E. (1994): Sedimentary sequences in the Tlaeeng Pass area, Lesotho in *South African Geographical Journal*, 76, 63 - 67.

Hare, F.K. (1979): Climatic variation and variability: empirical evidence from meteorological and other sources in *Proceedings of the World Climate Conference*, World Meteorological Organisation.

Harrison, M.S.J. (1984): A generalized classification of South African summer rain-bearing synoptic systems in *Journal of Climatology*, 4, 547 - 560.

Harrison, S.P. and Digerfeldt, G. (1993): European lakes as palaeohydrological and palaeoclimatic indicators in *Quaternary Science Reviews*, 12, 233 - 248.

Hastenrath, S. (1972): A note on recent and Pleistocene altitudinal zonation in Southern Africa in *South African Journal of Science*, 68, 96 - 102.

Hastenrath, S. and Wilkinson, J. (1973): A contribution to the periglacial morphology of Lesotho, southern Africa in *Biuletyn Periglacjalny*, 22, 157 - 167.

Hays, J.D.; Imbrie, J. and Shackleton, N.J. (1976): Variations in the earth's orbit: pacemaker of the iceages in *Science*, 194, 1121 - 1132.

Heaton, T.H.E.; Talma, A.S. and Vogel, J.C. (1986): Dissolved gas palaeotemperatures and  $^{18}\text{O}$  variations derived from groundwater near Uitenhage in *Quaternary Research*, 25, 79 - 88.

Hecht, A.D. and Imbrie, J. (1979): Towards a comprehensive theory of climate change in Quaternary Research, 12, 2 - 5.

Heine, K. (1981): Aride und pluviale Bedingungen wahredn der letszer Kaltzeit in frt Sudwest-Kalahari (sudliches Afrika) in Zeitschrift fur Geomorphologie, 38, 1 - 37.

Heine, K. (1982): The main stages of the Late Quaternary evolution of the Kalahari Region, Southern Africa in Palaeoecology of Africa, 15, 53 - 76.

Heine, K. and Geyh, M.A. (1984): Radiocarbon dating of speleothems from the Rössing Cave, Namib Desert and palaeoclimatic implications in Vogel, J.C. (ed.) Late Cainozoic Palaeoclimates of the Southern Hemisphere, Balkema, Rotterdam, 465 - 470.

Heinrich, H. (1988): Origin and consequences of cyclic ice rafting in the northeast Atlantic Ocean during the past 130,000 years in Quaternary Research, 29, 142 - 152.

Helgren, D.M. (1984): Historical geomorphology and geoarchaeology in the southwestern Makgadigadi Basin, Botswana in Annals of the Association of American Geographers, 74, 298 - 307.

Helgren, D.M. and Brooks, A.S. (1983): Geoarchaeology at Gi, a Middle Stone Age and Later Stone Age site in the northwestern Kalahari in Journal of Archaeological Science, 10, 181 - 197.

Henderson-Sellers, B. (1984): *Engineering Limnology*, Pitman, London, 356 pp.

Henderson-Sellers, A. and McGuffie, K. (1987): *A Climate Modelling Primer*, Wiley, Chichester.

Hendersen-Sellers, A. and Robinson, P.J. (1986): *Contemporary Climatology*, Longman, New York.

Hendy, C.H. (1971): The isotopic geochemistry of speleothems I: the calculation of the effects of different modes of formation on the isotopic composition of speleothems and

their applicability as palaeoclimatic indicators in *Geochimica et Cosmochimica*, 35, 801 - 824.

Higuchi, K. A. Z.; Jianping, H. and Shabar, A. (1999): A wavelet characterisation of the North Atlantic oscillation variation and its relationship to North Atlantic sea surface temperature in *International Journal of Climatology*, 19, 1119 - 1129.

Hirst, A.C. and Hastenrath, S. (1983): Atmosphere-ocean mechanisms of climate anomalies in the Angola-Tropical Atlantic sector in *Journal of Physical Oceanography*, 13, 1146 – 1157.

Hodell, D.A.; Kanfoush, S.L.; Shemesh, A.; Crosta, X.; Charles, C.D. and Guilderson, T.C. (2001) Abrupt cooling of Antarctic surface waters and sea ice expansion in the South Atlantic sector of the Southern Ocean at 5000 cal yr BP in *Quaternary Research*, 25, 79 - 88.

Holmgren, K. (1996): *The potential of speleothems in the reconstruction of southern African palaeoclimates – an example from Lobatse II Cave, Botswana*, Speech presented at the International Geological Correlation Program (IGCP) Meeting, Bergen.

Holmgren, K.; Karlén, W., Lauritzen, S.E.; Lee-Thorp, J.A.; Partridge, T.C.; Piketh, S.; Repinski, P.; Stevenson, C.; Svanered, O. and Tyson, P.D. (1999): A 3000-year high-resolution stalagmite-based record of palaeoclimate for north-eastern South Africa in Holocene, 9, 295 - 309.

Holmgren, K.; Karlén, W. and Shaw, P.A. (1995): Palaeoclimatic significance of variations in the stable isotopic composition and petrology of a Late Pleistocene Stalagmite from Botswana in *Quaternary Research*, 43, 320 - 328.

Holmgren, K.; Lee-Thorp, J.A.; Gordon, R.J.; Cooper, G.R.J.; Lundblad, K.; Partridge T.C.; Scott, L.; Sithaldeen, R.; Talma, A.S. and Tyson, P.D. (2003): Persistent millennial-scale climatic variability over the past 25,000 years in Southern Africa in *Quaternary Science Reviews*, 22, 2311 - 2326.

Holmgren, K. and Shaw, P. (1999): Palaeoenvironmental interpretation of cores from large stalagmites: an example from Lobatse II Cave, Botswana in *Theoretical and Applied Karstology*, 11 – 12; 1998 – 1999, 23 - 34.

Holmgren, K.; Tyson, P.D.; Moberg, A. and Svanered, O. (2001): A preliminary 3000-year regional temperature reconstruction for South Africa in *South African Journal of Science*, 97, 49 - 51.

Howard, W.R. (1985): Late Quaternary southern Indian Ocean circulation in *South African Journal of Science*, 81, 253 - 254.

Hoyt, D.V. and Schatten, K.H. (1997): *The Role of the Sun in Climate Change*, Oxford University Press, New York, 279 pp.

Huffman, T.N. (1996): Archaeological evidence for climatic change during the last 2000 years in southern Africa in *Quaternary International*, 33, 55 - 60.

Imbrie, J. (1985): A theoretical framework for the Pleistocene ice ages in *Journal of the Geological Society of London*, 142, 417 - 432.

Imbrie, J.; Hays, J.D.; Martinson, D.G.; McIntyre, A.; Mix, A.C.; Morley, J.J.; Pisias, N.G.; Prell, W.L. and Shackleton, N.J. (1984): The orbital theory of Pleistocene climate: Support from a revised chronology of the marine  $\delta^{18}\text{O}$  record in Berger, A.; Imbrie, J.; Hays, J.; Kukla, G. and Saltzman, B. (eds.) *Milankovitch and Climate I*, Reidel, Dordrecht, 269 - 305.

Imbrie, J. and Imbrie, J.Z. (1980): Modelling the climatic response to orbital variations in *Science*, 207, 943 - 953.

Jackson, S.T.; Overpeck, J.T.; Webb, T. III; Keatch, S.E. and Anderson, K.H. (1997): Mapped plant-macrofossil and pollen records of Late Quaternary vegetation changes in eastern North America in *Quaternary Science Reviews*, 16, 1 - 70.

Jerardino, A. (1995): Late Holocene neoglacial episodes in southern South America and southern Africa: a comparison in *The Holocene*, 5, 361 - 368.

Johnson, R.F. (1988): A history of climate and marine productivity from sediment off the west coast of southern Africa in *Final Report of the National Programme on Weather, Climate and Atmospheric Research*, Pretoria.

Johnson, T.C.; Brown, E.T.; McManus, J.; Barry, S.; Barker, P. and Gasse, F. (2002) A high-resolution palaeoclimate record spanning the past 25,000 years in southern east Africa in *Science*, 296, 113 - 132.

Johnson, T.C.; Halfman, J.D.; and Showers, W.J. (1991): Paleoclimate of the past 4000 years at Lake Turkana, Kenya, based on the isotopic composition of authigenic calcite in *Palaeogeography, Palaeoclimatology, Palaeoecology*, 85, 189 - 198.

Jolly, D.; Prentice, I.C.; Bonnefille, R.; Ballouche, A.; Bengo, M.; Brenac, P.; Buchet, G.; Burney, D.; Cazet, J.P.; Cheddadi, R.; Ector, T.; Elenga, H.; Elmoutaki, S.; Guiot, J.; Laarif, F.; Lamb, H.; Lezine, A.M.; Maley, J.; Mbenza, M.; Peyron, O.; Reille, M.; Reynaud-Farrera, I.; Riollet, G.; Ritchie, J.C.; Roche, E.; Scott, L.; Ssemmanda, I.; Straka, H.; Umer, M.; Van Campo, E.; Vilimumbalo, S.; Vincens, A. and Waller, M. (1998): Biome reconstruction from pollen and plant macrofossil data for Africa and Arabian peninsular at 0 and 6000 years in *Journal of Biogeography*, 1007 - 1027.

Jones, M.Q.W.; Tyson, P.D. and Cooper, G.R.J. (1999): Modelling climate change in South Africa from perturbed temperature profiles in *Quaternary International*, 57 - 58, 185 - 192.

Jouzel, J. (1998): Palaeoclimate record of climate: polar ice cores in *Clivar Exchanges*, 3, 6 - 8.

Jouzel, J., Lorius C., Petit, J.R., Gebthon, C., Barkow, N.I., Kotlyakov, V., and Petrov, V.M. (1987): Vostok ice core: a continuous isotope and temperature record over the last climatic cycle (160000 years) in *Nature*, 329, 403 - 407.



Jury, M.; Pathack, B and Sohn, B.J. (1992): Spatial structures of interannual variability of summer convection over southern Africa and the SW Indian Ocean in *South African Journal of Science*, 88, 275 - 280.

Karlén, W.; Fastook, J.K.; Holmgren, K.; Malmström, M.; Matthews, J.A.; Odada, E.; Risberg, J.; Rosqvist, G.; Sandgren, P.; Shemesh, A.; and Westerberg, L.-O. (1999): Glacier fluctuations on Mount Kenya since 6000 Cal. Years BP: implications for Holocene climatic change in Africa in *Ambio*, 28, 409 - 418.

Kent, L.E. and Gribnitz, K.-H. (1985): Freshwater shell deposits in the northwestern Cape Province: further evidence for a widespread wet phase during the Late Pleistocene in southern Africa in *South African Journal of Science*, 81, 361 - 370.

Klein, R.G. (1980): Environmental and ecological implications of large mammals from upper Pleistocene and Holocene sites in southern Africa in *Annals of the South African Museum*, 81, 223 - 283.

Knox, F. and McElroy, M. (1984): Change in atmospheric CO<sub>2</sub>: Influence of the marine biota at high latitude in *Journal of Geophysical Research*, 89, 4629 - 4637.

Koutavas, A.; Lynch-Stieglitz, J.; Marchitto, T.M. and Sachs, J.P. (2002): El Niño-like pattern in ice age tropical Pacific sea surface temperature in *Science*, 297, 226 - 230.

KwaZulu-Natal (KZN) Wildlife (2005): *Lake St Lucia salinity data*, provided by Ricky Taylor.

Labitzke, K. and van Loon, H. (1987): Associations between the 11-year solar cycle, the QBO, and the atmosphere: Part I: the troposphere and stratosphere of the Northern Hemisphere in winter in *Journal of Atmospheric and Terrestrial Physics*, 50, 197 - 206.

Labitzke, K. and van Loon, H. (1989): Associations between the 11-year solar cycle, the QBO, and the atmosphere: Part III: aspects of the association in *Journal of Climate*, 2, 554 - 565.

Lamb, H.H. (1982): *Climate, History and the Modern World*, Methuen, London.

Lamy, F.; Hebbeln, D.; Röhl, U. and Wefer, G. (2001): Holocene rainfall variability in southern Chile: a marine record of latitudinal shifts of the Southern Westerlies in *Earth and Planetary Science Letters*, 185, 369 - 382.

Lancaster, N. (1979): *Quaternary Environments in the Arid Zone of Southern Africa*, Occasional Paper No. 22, Department of Geography and Environmental Studies, University of the Witwatersrand, South Africa, 77 pp.

Lancaster, N. (1983): Palaeoenvironments in the Tsondab Valley, Central Namib Desert in *Palaeoecology of Africa*, 16, 411 - 419.

Lancaster, N. (2000): Eolian deposits in Partridge, T.C. and Maud, R.R. (eds.) *The Cenozoic of Southern Africa*, Oxford University Press, New York, 371 - 387.

Lau, K.M. and Weng, H.-Y. (1995): Climate signal detection using wavelet transform: how to make a time series sing in *Bulletin of the American Meteorological Society*, 76, 2391 - 2402.

Lauritzen, S.E. (1995): A high-resolution palaeotemperature proxy record during the last interglaciation in Norway from speleothems in *Quaternary Research*, 43, 133 - 146.

Lee-Thorp, J.A.; Holmgren, K.; Lauritzen, S.-E.; Linge, H.; Moberg, A.; Partridge, T.C.; Stevenson, C. and Tyson, P.D. (2001): Rapid climate shifts in the southern African interior throughout the mid to late Holocene in *Geophysical Research Letters*, 28 (23), 4507 - 4510.

Leventer, A.; Domack, E. W.; Ishman, S.E.; Brachfield, S.; McClennen, C.E.; and Manley, P. (1996): Productivity cycles of 200 - 300 years in the Antarctic Peninsula region: understanding linkages among the sun, atmosphere, oceans, sea-ice and biota in *Geological Society of America Bulletin*, 108, 1626 - 1644.

- Lewis, C.A. and Dardis, G.F. (1985): Periglacial ice-wedge casts and head deposits at Dynevor Park, Barkly Pass area, north-eastern Cape Province in *South African Journal of Science*, 81, 673 - 677.
- Li, W.-X.; Lundberg, J.; Dickin, A.P.; Ford, D.C.; Schwarcz, H.P.; McNutt, R. and Williams, D. (1989): High-precision mass-spectrometric uranium-series dating of cave deposits and the implications for palaeoclimate studies in *Nature*, 339, 534 – 536.
- Liebig, J. (1840). *Chemistry and its application to agriculture and physiology*, Taylor and Walton, London.
- Lilly, M.A. (1977): *An assessment of the dendrochronological potential of indigenous species of trees in South Africa*, Occasional Paper No. 18, Department of Geographical and Environmental Studies, University of Witwatersrand, South Africa.
- Lindesay J.A. (1988): South African rainfall, the Southern Oscillation and a southern hemisphere semi-annual cycle in *Journal of Climatology*, 8, 17 - 30.
- Lindesay, J.A. (1990): Mechanisms of climate change: a review in *South African Journal of Science*, 89, 340 - 349.
- Lindesay, J., Harrison, M.S.J. and Haffner, M.P. (1986): The Southern Oscillation and South African rainfall in *South African Journal of Science*, 82, 196 - 198.
- Lindesay, J.A. and Vogel, C.H. (1990): Historical evidence for Southern Oscillation – Southern African relationships in *International Journal of Climatology*, 10, 679 – 689.
- Linton, D.L. (1969): Evidences of Pleistocene cryonival phenomena in South Africa in *Palaeoecology of Africa and Surrounding Islands*, 5, 71 - 89.
- Liu, Z., 2002: A simple model study of the forced response of ENSO to an external periodic forcing in *Journal Climatology*, 15, 1088 – 1098.

Lough, J. and Barnes, D.J. (1997): Several centuries of variation in skeleton extension, density and calcification in massive *Porites* colonies from the Great Barrier Reef: a proxy for seawater temperature and a background of variability against which to identify unnatural change in *Journal of Explorative Marine Biology and Ecology*, 211, 29 - 67.

Lough, J.; and Barnes, D.J. (2000): Environmental controls on growth of massive coral *Porites* in *Journal of Explorative Marine Biology and Ecology*, 245, 225 - 243.

Low, A.B. and Rebelo, A.G. (1996): *Vegetation of South Africa, Lesotho and Swaziland: a companion to the Vegetation Map of South Africa, Lesotho and Swaziland*, Department of Environmental Affairs and Tourism, Pretoria, 85 pp.

Lowell, T.V.; Heusser, C.J.; Andersen, B.G.; Moreno, P.I., Hauser, A.; Heusser, L.E.; Schlucter, C.; Marchant, D.R. and Denton, G.H. (1995): Interhemispheric correlation of late Pleistocene glacial events in *Science*, 269, 1541 -1549.

Lubick, N. (2005): Extreme storms as climate warms in *Geotimes*, 1.

Lutjeharms, J.R.E.; Monteiro, P.M.S.; Tyson, P.D. and Obura, D. (2001): The oceans around southern Africa and regional effects of global change in *South African Journal of Science*, 97, 119 - 130.

Mann, M.E.; Bradley, R.S. and Hughes, M.K. (1998). Global-scale temperature patterns and climate forcing over the past six centuries in *Nature*, 392, 779 – 787.

Mann, M.E. and Park, J. (1994): Global-scale modes of surface temperature variability on interannual to century timescale in *Journal of Geophysical Research*, 99 (D12), 25819 - 25833.

Mann, M.E. and Park, J. (1996): Joint spatiotemporal modes of surface temperature and sea level pressure variability in the Northern Hemisphere during last century in *Journal of Climate*, 9, 2137 - 2162.

Marker, M. (1974): Dating Quaternary climatic fluctuations using cave and tufa deposits in *Goodwin Series*, 2, 13 - 19.

Marker, M.E. (1998): Cenozoic climate change in southern Africa: the evidence from geomorphology, 1967 – 1996, a personal view in *South African Geographical Journal*, 80, 1- 8.

Mason, S.J. (1995): Sea-surface temperature south African rainfall associations, 1910 – 1989 in *International Journal of Climatology*, 15, 119 - 135.

Mason, S.J. (1996): Rainfall trends over the Lowveld of South Africa in *Climate Change* 32, 35 - 54.

Mason, S.J. (2001): El Niño, climate change and southern African climate in *Environmetrics*, 12, 327 - 345.

Mason, I.M.; Guzkowska, M.A.J.; Rapley, C.G. and Street-Perrott, F.A. (1994): The response of lake levels and areas to climatic change in *Climate Change*, 27, 161 - 197.

Mason, S. J. and Jury, M.R. (1997): Climatic change and inter-annual variability over southern Africa: a reflection on underlying processes in *Progress in Physical Geography*, 21, 23 - 50.

Mason, S.J. and Lindesay, J.A. (1993): A note on the modulation of Southern Oscillation – Southern African rainfall associations with the Quasi-Biennial Oscillation in *Journal of Geophysical Research*, 98, 8847 - 8850.

Mason, S.J.; Waylen, P.R.; Mimmack, G.M.; Rajaratnam, B. and Harrison, M.J. (1999): Seasonal flooding in the Okavango Delta – recent history and prospects in *South African Journal of Science*, 96, 25 - 33.

Mass, C.F. and Portman, D.A. (1989): Major volcanic eruptions and climate: a critical evaluation in *Journal of Climate*, 2, 566 - 593.

Masson, V.; Vimeux, F.; Jouzel, J.; Morgan, V.; Delmotte, M.; Ciais, P.; Hammer, C.; Johnsen, S.; Lipenkov, V.Y.; Mosley-Thompson, E.; Petit, J.R.; Steig, E.J.; Stievenard, M. and Vaikmae, R. (2000): Holocene climate variability in Antarctica based on 11 ice-core isotopic records in *Quaternary Research*, 54, 348 - 359.

Matrix Laboratory (MATLAB) (2004): Statistics Toolbox: Principal Components Analysis in *MATLAB Help Documentation*, The Mathworks.

Mayewski, P.A.; Meeker, L.D.; Whitlow, S.; Twickler, M.S.; Morrison, M.C.; Bloomfield, P.; Bond, G.C.; Alley, R.B.; Gow, A.J.; Grootes, P.M.; Meese, D.A.; Ram, M.; Taylor, K.C.; and Wumkes, W. (1994) Changes in atmospheric circulation and ocean ice cover over the North Atlantic during the last 41,000 years in *Science*, 263, 1747 - 1751.

McCarthy, J.J.; Brewer, P.G. and Feldman, G. (1986): Global ocean flux in *Oceanus*, 29 (4), 16 - 26.

McCarthy, T.S.; Cooper, G.R.J.; Tyson, P.D. and Ellery, W.N. (2000): Seasonal flooding in the Okavango delta, Botswana – recent history and future prospects in *South African Journal of Science*, 96, 25 - 34.

McClelland, L. (1996): *Climate variability and outlooks for maize production in South Africa*, unpublished MSc thesis, University of the Witwatersrand, South Africa, 78 pp.

Meadows, M.E. (1988): Landforms and Quaternary climatic change in Moon, B.P. and Dardis, G.F. (eds.) *The Geomorphology of Southern Africa*, Southern Books, Johannesburg, pp 296 - 315.

Meadows, M.E. (2001): The role of quaternary environmental change in the evolution of landscapes: case studies from southern Africa in *Cantena*, 42, 39 - 57.

Meadows, M.E. and Baxter, A.J. (1999): Late Quaternary palaeoenvironment of the southwestern Cape, South Africa: a regional synthesis in *Quaternary International*, 57 - 58, 193 - 206.

Miller, D.E.; Yates, R.J.; Jerardino, A. and Parkington, J.E. (1993): Late Holocene coastal change in the southwestern Cape, South Africa in *South African Journal of Science*, 89, 35 - 44.

Mix, A.C.; Morey, A.; Pisias, N.G. and Hostetler, S. (1999): Foraminiferal faunal estimates of paleotemperature: Circumventing the no-analog problem yields cool ice age tropics in *Paleoceanography*, 14, 350 - 359.

Moore, B. and Bolin, B. (1986): The oceans, carbon dioxide and climate change in *Oceanus*, 29 (4), 9 - 15.

Moy, C.M.; Seltzer, G.O.; Rodbell, D.Y. and Andersen, D.M. (2002): Variability of the El Niño/ Southern Oscillation at millennial time scales during the Holocene epoch in *Nature*, 420, 162 -165.

Mulenga, H.M., Rouault, M. and Reason, C.J.C. (2003): Dry summers over NE South Africa and associated circulation anomalies in *Climate Research*, 25, 29 - 41.

Muller, M.J. and Tyson, P.D. (1988): Winter rainfall over the interior of South Africa during extreme dry years in *South African Geographical Journal*, 70, 20 - 30.

Natal Sharks Board (2005): *Richard's Bay sea surface temperature*, provided by Pushpa Soobraya, March 2005.

National Aeronautics and Space Administration (NASA), Massachusetts Institute of Technology (MIT), United Kingdom Meteorological Office (UKMO) and Physical Oceanography Distributed Active Archive Centre (PODAAC) (1995): *Global Ocean Surface Temperature Atlas Plus (GOSTAplus)*.

National Centre for Atmospheric Research (NCAR) (2005): *Southern Oscillation Index data*, accessed at <http://www.cgd.ucar.edu/cas/catalog/climind/soi.html>.

National Oceanic Atmospheric Administration (NOAA) (2005): *Tropical Atmosphere Ocean (TAO) Project*, United States, accessed 2005 at <http://www.pmel.noaa.gov/tao/elNiño/el-Niño-story.html>.

National Oceanic Atmospheric Administration and Cooperative Institute for Research in Environmental Sciences (NOAA-CIRES) Climate Diagnostic Centre (2000): *NOAA Extended Reconstructed SST data*.

Neftel, A.; Oeschger, H.; Schwander, J.; Stauffer, B. and Zumbunn, R. (1982): Ice core measurements give atmospheric CO<sub>2</sub> content during the past 40,000 yr in *Nature*, 295, 220 - 233.

Negendank, J.F.W (2003): The Holocene: considerations with regard to its climate and climate archives in Fischer, H.; Kumke, T.; Lohmann, G.; Flöser, G.; Miller, H.; Von Storch, H.; and Negendank, J.F.W. (eds.): *The Climate in Historical Times: Towards a Synthesis of Holocene Proxy Data and Climate Models*, Springer-Verlag, Berlin, 487 pp.

Newell, R.E.; Gould-Stewart, S. and Chung, J.C. (1981): A possible interpretation of Palaeoclimatic reconstructions for 18000 BP for the region of 60°N to 60°S, 60°W to 100°E in *Palaeoecology of Africa*, 13, 1 - 19.

Newell, N.E.; Newell, R.E.; Hsiung, J. and Zhongxiang, W. (1989): Global marine temperature variation and the solar magnetic cycle in *Geophysical Research Letters*, 16, 311 - 314.

Ngara, T.; McNaughton, D.L. and Lineham, S. (1983): Seasonal rainfall fluctuations in Zimbabwe in *Zimbabwe Agricultural Journal*, 80, 149 - 150.

Nicholls, N. (2000): The insignificance of significance testing in *Bulletin of the American Meteorological Society*, 81, 981 - 986.

Nicholson, S. E. and Entekhabi, D. (1986): The quasi-periodic behavior of rainfall variability in Africa and its relationship to the Southern Oscillation in *Archives for Meteorology, Geophysics and Bioclimatology*, Series A, 34, 311 - 348.



Nicholson, S.E. and Flohn, H. (1980): African environmental and climatic changes and the general atmospheric circulation in Late Pleistocene and Holocene in *Climatic Change*, 2, 313 - 348.

Nicholson, S. E. and Kim, J. (1997): The Relationship of the El-Niño Southern Oscillation to African rainfall in *The International Journal of Climatology*, 17, 117 - 135.

O'Brien, S.R.; Mayewski, P.A.; Meeker, L.D.; Meese, D.A.; Twickler, M.S. and Whitlow, S.I. (1995): Complexity of Holocene climate as reconstructed from a Greenland ice core in *Science*, 270, 1962 - 1964.

O'Connor, P.W. and Thomas, D.S.G. (1999): The timing and environmental significance of Late Quaternary linear dune development in western Zambia in *Quaternary Research*, 52, 44 - 55.

Oeschger, H.; Beer, J., Siegenthaler, U., Stauffer, B., Dansgaard, W., and Langway, C.C. (1984): Late glacial climate history from ice cores in Hansen, J.E. and Takahashi, T. (eds.) *Climate Processes and Climate Sensitivity*, Monograph 29 (Maurice Ewing Series), American Geophysical Union, 299 - 306.

Ogallo, L. J.; Janowiak, J.E. and Halpert, M.S. (1988): Teleconnection between seasonal rainfall over East Africa and global sea surface temperature anomalies in *Journal of the Meteorological Society of Japan*, 66, 807 - 821.

Oliver, J.E. and Hidore, J.J. (1984): *Climatology: An Introduction*, Charles E. Merrill, Columbus.

Otto-Bleisner, B.L.; Brady, E.C.; Shin, S.I.; Liu, Z. and Shields, C. (2003): Modeling El Niño and its tropical teleconnections during the last glacial–interglacial cycle in *Geophysical Research Letters*, 30, 2198.

Partridge, T.C. (1985): The palaeoclimatic significance of Cainozoic terrestrial stratigraphic and tectonic evidence from southern Africa: a review in *Southern African Journal of Science*, 81, 245 - 247.

Partridge, T.C. (1993): Warming phases in southern Africa during the last 150 000 years: an overview in *Paleogeography, Paleoclimatology, Paleoecology*, 101, 237 - 244.

Partridge, T.C. (1997): Cainozoic environmental change in southern Africa during the last 150,000 years: an overview in *Progress in Physical Geography*, 21, 3 - 22.

Partridge, T.C. (ed.) (1999): *Investigations into the origin, age and palaeoenvironments of the Pretoria Saltpan*, Memoir No. 85, Council for Geoscience, Pretoria.

Partridge, T.C.; Avery, D.M.; Botha, G.A.; Brink, J.S.; Deacon, J.; Herbert, R.S.; Maud, R.R.; Scott, L.; Talma, A.S. and Vogel, J.C. (1990): Late Pleistocene and Holocene climatic change in southern Africa in *South African Journal of Science*, 86, 302 – 306.

Partridge, T.C.; deMenocal, P.B.; Lorentz, S.A.; Paiker, M.J. and Vogel, J.C. (1997): Orbital forcing of tropical northerly airflow over South Africa: a 200,000-year rainfall record from the Pretoria Saltpan in *Quaternary Science Reviews*, 16, 1125 - 1133.

Partridge, T.C.; Kerr, S.J.; Metcalf, S.E.; Scott, L.; Talma, A.S. and Vogel, J.C. (1993): The Pretoria Saltpan: a 200,000 year South African lacustrine sequence in *Palaeogeography, Palaeoclimatology, Palaeoecology*, 101, 317 - 337.

Pearman, G.I. (ed.) (1988): *Greenhouse: Planning for Climate Change*, CSIRO, Melbourne.

Pestiaux, P.; Duplessy, J.C. and Berger, A. (1987): Palaeoclimate variability at frequencies ranging from 10<sup>-4</sup> cycle to per year 10<sup>-3</sup> cycle per year – evidence for nonlinear behaviour of the climate system in Rampino, M.R.; Sanders, J.E.; Newman, W.S. and Konigsson, L.K. (eds.) *Climate: History, Periodicity and Predictability*, Van Nostrand Reinhold, New York.

Pestiaux, P.; Van der Mersch, I.; and Berger, A. (1988): Paleoclimatic variability at frequencies ranging from 1 cycle per 10000 years to 1 cycle per 1000 years: Evidence for nonlinear behaviour of the climate system in *Climatic Change*, 12, 9 - 37.

Philander, S.G.H. (1990): *El Niño, La Niña and the Southern Oscillation*, Academic Press, San Diego, 289 pp.

Phillips, J. (1973): *The agricultural and related development of the Tugela Basin and its influent surrounds*, Natal Town and Regional Planning Report 19, Pietermaritzburg, 299 pp.

Pisias, N.G. and Imbrie, J. (1986): Orbital geometry, CO<sub>2</sub>, and Pleistocene climate in Oceans, 29 (4), 43 - 49.

Pisias, N.G. and Shackleton, N.J. (1984): Modelling the global climate response to orbital forcing and atmospheric carbon dioxide changes: a frequency domain approach in *Nature*, 310, 757 - 759.

Pittock, A.B. (1973): Global meridional interactions in stratosphere and troposphere in *Quarterly Journal of the Royal Meteorological Society*, 99, 424 - 437.

Poolman, E. (1999): Heavy rain events over South Africa in *Proceedings of the 15<sup>th</sup> Annual Conference for the South African Society of Atmospheric Sciences*, Richards Bay.

Porter, S.C. (2000): Onset of neoglaciation in the Southern Hemisphere in *Journal of Quaternary Science*, 15, 395 - 408.

Prentice, I.C. (1998): Records of vegetation in time and space: the principles of pollen analysis in Huntley, B. and Webb, T. III (eds.) *Vegetation History*, Kluwer Academic Publishers, Dordrecht, 17 - 42.

Prentice, I.C.; Guiot J. and Harrison, S.P. (1992): Mediterranean vegetation, lake levels and palaeoclimate at the Last Glacial Maximum in *Nature*, 360, 658 - 670.

Prentice, I.C.; Guiot, J.; Huntley, B.; Jolly, D. and Cheddadi, R. (1996): Reconstructing biomes from palaeoecological data: a general method and its application to European pollen data at 0 and 6 ka in *Climate Dynamics*, 12, 185 - 194.

Price-Williams, D.; Watson, A.; and Goudie, A.S. (1982): Quaternary colluvial stratigraphy, archaeological sequences and palaeoenvironments in Swaziland, southern Africa in *The Geographical Journal*, 148, 50 - 67.

Priess, K. (1997): *La croissance de Porites sp. du groupe lobatalutea-solida dans le lagon de Mayotte (Canal du Mozambique)*, unpublished PhD thesis, University Mediterranee, France.

Priestly, M.B. (1981): *Spectral Analysis and Time Series*, Volume 1 and 2, Academic Press, London.

Rahmstorf, S. (2003): Timing of abrupt climate change: A precise clock in *Geophysical Research Letters*, 30 (10), 1510.

Railsback, L.B.; Brook, G.A.; Chen, J.; Kalin, R.; and Fleisher, C.J. (1994): Environmental controls on the petrology of a late Holocene speleothem from Botswana with annual layers of aragonite and calcite in *Journal of Sedimentary Research A*, 64, 147 - 155.

Ramanathan, V.; Barkstrom, B.R. and Harrison, E.F. (1989): Climate and the earth's radiation budget in *Physics Today*, 42, 22 - 32.

Ramsay, P.J. (1990): Use of computer graphics software to produce a three-dimensional morphological and bathymetric model of a Zululand coral reef in *South African Journal of Science*, 86, 130 - 131.

Ramsay, P.J. (1994): Marine Geology of the Sodwana Bay shelf, southeast Africa in *Marine Geology*, 120, 225 - 247.

Ramsay, P.J. and Mason, T. R. (1990): Development of a type zoning model for Zululand coral reefs, Sodwana Bay, South Africa in *South African Journal of Coastal Research*, 6, 829 - 852.

Reason, C.J.C. (1999): International warm and cool events in the subtropical/midlatitude south Indian Ocean region in *Geophysical Research Letters*, 26, 215 - 218.

Reason, C.J.C. (2000): Multidecadal climate variability in the Southern Hemisphere oceans in *Tellus*, 52 A, 203 - 223.

Reason, C.J.C. (2002): Sensitivity of the southern African circulation to dipole SST patterns in the South Indian Ocean in *International Journal of Climatology*, 22, 377 - 393.

Reason, C.J.C.; Allan, R.J.; Lindsay, J.A. and Ansell, T.J. (2000): ENSO and climatic signals across the Indian Ocean basin in the global context: Part I - Interannual composite patterns in *International Journal of Climatology*, 20, 1285 - 1327.

Reason, C.J.C., Jagadheesha, D. and Tadross, M. (2003): A model investigation of interannual winter rainfall variability over southwestern South Africa and associated ocean-atmosphere interaction in *South African Journal of Science*, 99, 75 - 80.

Reason, C.J.C.; Landman, W.; Tadross, M.; Tennant, W. and Kgatuke, M.-J. (2004): *Seasonal to Decadal Predictability and Prediction of Southern African Climate*, White Paper presented to the CLIVAR Workshop on Atlantic Predictability, University of Reading, UK.

Reason, C.J.C. and Mulenga, H.M. (1999): Relationships between South African rainfall and SST anomalies in the South West Indian Ocean in *International Journal of Climatology*, 19, 1651 - 1673.

Reason, C.J.C. and Rouault, M. (2002): ENSO-like decadal variability and South African rainfall in *Geophysical Research Letters*, 29 (13), 1638.

Reddy, R.S., Nerall, V.R. and Godson, W.L. (1989): The solar cycle and Indian rainfall in Theoretical and Applied Climatology, 39, 194 – 198.

Riegl, B. (1996): Hermatypic coral fauna of subtropical south east Africa: a checklist in Pac Science, 50, 404 - 414.

Riegl, B. (2001): Inhibition of reef framework by frequent disturbance: Examples from the Arabian Gulf, South Africa, and the Cayman Islands in Palaeogeography, Palaeoclimatology, Palaeoecology, 175, 79 - 101.

Riegl, B. and Riegl, A. (1996): The effect of episodic coral breakage on community structure: a case study from South Africa in Marine Ecology, 17, 399 - 410.

Riegl, B.; Schleyer, M.H.; Cook, P.J. and Branch, G.M. (1995): The structure of Africa's southernmost coral communities in Bulletin of Marine Science, 56, 678 - 691.

Rind, D. and Overpeck, J. (1993): Hypothesized causes of decadal-to-century-scale climate variability: Climate model results in Quaternary Science Review, 12, 357 - 374.

Ropelewski, G.F. and Jones, P.D. (1987): An extension o the Tahiti-Darwin southern oscillation index in Monthly Weather Reviews, 115, 2161 - 2165.

Rouault, M., Florenchie, P.; Fauchereau, N. and Reason, C.J.C. (2003): South East Atlantic warm events and southern African rainfall in Geophysical Research Letters, 30, 9-1 - 9-4.

Russell, J.M.; Johnson, T.C. and Talbot, M.R. (2003): A 725 yr cycle in the climate of central Africa during the late Holocene in Geology, 31 (8), 677 - 680.

Rutherford, M.C. (1997): Categorisation of biomes in Cowling, R.M.; Richardson, D.M. and Pierce, S.M. (eds.) Vegetation of Southern Africa, Cambridge University Press, Cambridge, 91 - 98.

Salinger, M.J. (1984): New Zealand climate: The last 5 million years in Vogel, J.C. (ed.) *Late Cainozoic Palaeoclimates of the Southern Hemisphere*, Balkema, Rotterdam, 131 – 150.

Sarkar, A.; Ramesh, R.; Somayajulu, B.L.K.; Agnihorti, R.; Jull, A.J.T. and Burr, G.S. (2000): High resolution Holocene monsoon record from the eastern Arabian Sea: High resolution Holocene monsoon record from the eastern Arabian Sea in *Earth and Planetary Science Letters*, 177, 209 - 218.

Sarmiento, J. and Toggweiler, R. (1984): New model for the role of the oceans in determining atmospheric pCO<sub>2</sub> in *Nature*, 308, 621 - 624.

Scholes, R.J. (1997): Savanna in Cowling, R.M.; Richardson, D.M. and Pierce, S.M. (eds.) *Vegetation of Southern Africa*, Cambridge University Press, Cambridge, 258 - 277.

Scholtz, A. (1986): *Palynological and Palaeobotanical Studies in the Southern Cape*, unpublished MA thesis, University of Stellenbosch, South Africa.

Schott F. and McCreary J. (2001): The monsoon circulation of the Indian Ocean in *Progress in Oceanography*, 51, 1 - 123.

Schulz, H.; Von Rad, U. and Erlenkeuser, H. (1998): Correlation between Arabian Sea and Greenland climate oscillations of the past 110 000 years in *Nature*, 393, 54 - 57.

Schuermans, C.J.E. (1981): Climate of the last 1000 years in Berger, A. (ed.) *Climatic Variations and Variability: Fact and Theories*, Reidel, Dordrecht.

Schwarcz, H.P. (1986): Geochronology and isotopic geochemistry of speleothems in Fritz, P. and Fontes, J. (eds.): *Handbook of Environmental Isotope Geochemistry 2*, Elsevier, Amsterdam, 271 - 303.

Scott, L. (1982a): A late Quaternary pollen record from the Transvaal bushveld, South Africa in *Quaternary Research*, 17, 339 - 370.

Scott, L. (1982b): Late Quaternary fossil pollen grains from the Transvaal, South Africa in *Reviews in Palaeobotany and Palynology*, 36, 241 - 278.

Scott, L. (1988a): Holocene environmental change at western Orange Free State pans, South Africa, inferred from pollen analysis in *Palaeoecology of Africa*, 19, 109 - 118.

Scott, L. (1988b): The Pretoria Salt Pan: a unique source of Quaternary palaeoenvironmental information in *South African Journal of Science*, 84, 560 - 562.

Scott, L. (1989): Late Quaternary vegetation history and climate change in the eastern OFS, South Africa in *South African Journal of Botany*, 55, 107 - 116.

Scott, L. (1991): *Past Vegetation Changes in Mountainous Areas of South Africa as Revealed by Pollen Analysis of Hyrax Middens*, Speech presented at the Association for the Taxonomic Study of the Flora of Tropical Africa (AETFAT) Congress, Malawi.

Scott, L. (1993): Palynological evidence for late Quaternary warming episodes in southern Africa in *Palaeogeography, Palaeoclimatology, Palaeoecology*, 101, 229 - 236.

Scott, L. (1996): Palynology of hyrax middens: 2000 years of palaeoenvironmental history in Namibia in *Quaternary International*, 33, 73 - 79.

Scott, L. (1999): The vegetation history and climate in the Savanna biome, South Africa, since 190 000 ka: a comparison of pollen data from the Tswaing Crater (the Pretoria Saltpan) and Wonderkrater in *Quaternary International*, 57 - 58, 215 - 223.

Scott, L. and Brink, J.S. (1991): Quaternary palaeoenvironments of pans in central South Africa: palynological and palaeontological evidence in *South African Journal of Geography*, 19, 22 - 34.

Scott, L.; Holmgren, K., Talma, A. S.; Woodborne, S. and Vogel, J.C. (2003): Age interpretation of the Wonderkrater spring sediments and vegetation change in the Savanna Biome, Limpopo province, South Africa in *South African Journal of Science*, 99, 484 - 488.



Scott K. and Nyakale, M. (2002): Pollen indications of Holocene palaeo-environments at Florisbad in the central Free State, South Africa in *The Holocene*, 12 (4), 497 - 503.

Scott, L. and Thackeray, J.F. (1987): Multivariate analysis of Late Pleistocene and Holocene pollen spectra from Wonderkrater, Transvaal, South Africa in *South African Journal of Science*, 83, 93 - 98.

Scott, L. and Vogel, J.C. (1983): Late Quaternary pollen profile from the Transvaal highveld, South Africa in *South African Journal of Science*, 79, 266 - 272.

Scuderi, L.A. (1993): A 2000-year tree ring record of annual temperatures in the Sierra Nevada mountains in *Science*, 259, 1433 - 1436.

Seuss, H.E. (1980): The radiocarbon record in tree-rings of the last 8000 years in *Radiocarbon*, 22(2), 200 - 209.

Seuss, H.E. and Linick, T.W. (1990): The  $^{14}\text{C}$  record in bristlecone pine wood of the past 8000 years based on the dendrochronology of the late C. W. Ferguson in *Philosophical Transactions of the Royal Society of London, Series A*, 330, 403 - 412.

Shannon, I.V. (1985): The Benguela ecosystem: Part I: Evolution of the Benguela, physical features and processes in *Oceanography and Marine Biology: An Annual Review*, 23, 105 - 182.

Shaw, P.A. and Cooke, H.J. (1986): Geomorphic evidence for the late Quaternary palaeoclimates of the Middle Kalahari of northern Botswana in *Cantena*, 13, 349 - 359.

Shaw, P.A. and Thomas, D.S.G. (1996): The Quaternary paleoenvironmental history of the Kalahari, southern Africa in *Journal of Arid Environments*, 32, 9 - 22.

Sherratt, A. (1980): *Cambridge Encyclopedia of Archaeology*, Cambridge University Press, Cambridge.

Siegenthaler, U. and Wenk, T. (1984): Rapid atmospheric CO<sub>2</sub> variations and ocean circulation in *Nature*, 308, 624 - 626.

Sigman, D.M. and Boyle, E.A. (2000): Glacial/interglacial variations in atmospheric carbon dioxide in *Nature* 407, 859 – 869.

Simmonds, I., Keay, K., and Lim, E.-P. (2002): Synoptic activity in the seas around Antarctica in *Monthly Weather Reviews*, 131, 272 - 288.

Sinclair, S.A.; Lane, S.B. and Grindley, J.R. (1986): Verlorenvlei in Heydorn, A.E.F. and Morant, P.D. (eds.) *Estuaries of the Cape*, Part 2, Council for Scientific and Industrial Research, Pretoria.

South African Weather Service (SAWS) (2005): *Rainfall and temperature data for selected towns*, provided by Glenda Swart, info1@weathersa.co.za.

Stager, J.C.; Mayewski, P.A. and Meeker, L.D. (2002): Cooling cycles, Heinrich event 1 and the desiccation of Lake Victoria in *Palaeogeography, Palaeoclimatology, Palaeoecology*, 183, 167 - 178.

Steig, E.J.; Morse, D.L.; Waddington, E.D.; Stuiver, M.; Grootes, P.M.; Mayewski, P.A.; Twickler, M.S. and Whitlow, S.I. (2000): Wisconsinian and Holocene climate history from an ice core at Taylor Dome, Western Ross Embayment, Antarctica in *Geografiska Annaler*, 82 A, 2 - 3, 213 - 235.

Storry, J.G.S. (1975): Preliminary dendrochronology study in Rhodesia in *South African Journal of Science*, 71, 248.

Street-Perrott, F.A. and Harrison, S.P. (1985): Lake levels and climate reconstruction in Hecht, A.D. (ed.): *Palaeoclimate Analysis and Modeling*, John Wiley, New York, 291 – 340.

Stute, M. and Talma, S. (1998): Glacial temperatures and moisture transport regimes reconstructed from noble gases and  $\delta^{18}\text{O}$ , Stampriet aquifer, Namibia in *Proceedings of the*

*Symposium of Isotope Techniques in Studying Past and Current Environmental Changes in the Hydrosphere and the Atmosphere*, IAEA, Vienna, 307.

Stuut, J.-B.W. and Lamy, F. (2004): Climate variability at southern boundaries of the Namib (southwestern Africa) and Atacama (northern Chile) coastal deserts during the last 120 000 yr in *Quaternary Research*, 62, 301 - 309.

Stuvier, M. and Braziunas, T.F. (1993): Sun, ocean, climate and atmospheric  $^{14}\text{CO}_2$ : An evaluation of causal and spectral relationships in *The Holocene*, 3, 289 - 305.

Stuvier, M.; Grootes, P.M. and Braziunas, T. F. (1995): The GISP2  $\delta^{18}\text{O}$  climate record of the past 16,500 years and the role of the sun, ocean, and volcanoes in *Quaternary Research*, 44, 341 - 354.

Sugden, J.M. and Meadows, M.E. (1989): The use of multiple discriminant analysis in reconstructing recent vegetation changes on the Nuweveldberg, South Africa in *Reviews of Palaeobotany and Palynology*, 60, 131 - 147.

Svanared, (1998): *Growth Layer Analysis of a Stalagmite from South Africa*, unpublished report, Stockholm University, Sweden, 28 pp.

Szestay, K. (1974): Water balance and water level fluctuations of lakes in *Hydrological Science Bulletin*, 19, 73 - 84.

Takahashi, T. (1986): *The climatic feedbacks for carbon dioxide in the world ocean*, Report of the Lamont-Doherty Geological Observatory, Columbia University, New York.

Talma, A.S. and Vogel, J.C. (1988): *Isotopic Investigation of Climate Change during the Late Quaternary of Southern Africa*, Report CIEMA 8826, CSIR, Pretoria, 28 pp.

Talma, A.S. and Vogel, J.C. (1992): Late Quaternary palaeotemperatures derived from a speleothem from Cango Caves, Cape province, South Africa in *Quaternary Research*, 37, 203 -213.

- Talma, A.S.; Vogel, J.C. and Heaton, T.H.E. (1984): The geochemistry of the Uitenhage artesian aquifer in *Isotope Hydrology*, 1983, 481 - 497.
- Talma, A.S.; Vogel, J.C.; and Partridge, T.C. (1974): Isotopic contents of some Transvaal speleothems and their palaeoclimatic significance in *South African Journal of Science*, 70, 135 - 140.
- Tankard, A.J. (1976): The stratigraphy of a coastal cave and its palaeoclimatic significance in *Palaeoecology of Africa*, 9, 151 - 159.
- Thackeray, J.F. (1987): Late Quaternary environmental changes inferred from small mammalian fauna, southern Africa in *Climate Change*, 10, 285 - 305.
- Thackeray, J.F. (1996): Ring width variation in a specimen of South African *Podocarpus*, circa 1350 – 1937 AD in *Palaeoecology of Africa*, 24, 233 – 240.
- Thackeray, J. F. and Avery, D. M. (1990). A comparison between temperature indices for late Pleistocene sequences at Klasies River mouth and Border Cave in *Palaeoecology of Africa*, 21, 311 - 316.
- Thackeray, J.F. and Potze, S. (2000): A sectioned yellowwood tree trunk housed at the Transvaal Museum, Pretoria in *Annals of the Transvaal Museum*, 37, 131 - 137.
- Thackeray, I.A.; Thackeray, J.F. and Beaumont, P. B. (1983): Excavations at the Blinkklipkop specularite mine near Posmasburg, northern Cape in *South African Archaeological Bulletin*, 38, 17 - 35.
- Thomas, D.S.G.; O'Connor, P.W.; Bateman, M.D.; Shaw, P.A.; Stokes, S. and Nash, D.J. (2000) Dune activity as a record of Late Quaternary aridity in the Northern Kalahari: new evidence from northern Namibia interpreted in the context of regional and humid chronologies in *Palaeogeography, Palaeoclimatology and Palaeoecology*, 156, 243 - 259.

Thomas, D.S.G., Stokes, S. and Shaw, P.A. (1997): Holocene Aeolian activity in the southwestern Kalahari desert, southern Africa: significance and relationships to late-Pleistocene dune-building events in *The Holocene*, 7, 273 - 281.

Thompson, L. G. (1992): Ice core evidence from Peru and China in Bradley, R.S. and Jones, P.D. (eds.) *Climate Since AD 1500*; Routledge, London, 571 - 648.

Thompson, L.G.; Mosley-Thompson, E.; Bolzan, J.F. and Koci, B.R. (1985): A 1500 year record of tropical precipitation in ice cores of the Quelccaya Ice Cap, Peru in *Science*, 229, 971 - 973.

Thompson, L.G.; Mosley-Thompson, E.; Davis, M.E.; Henderson, K.A.; Brecher, H.H.; Zagorodnov, V.S.; Mashiotta, T.A.; Mikhalenko, V.N.; Hardy, D.R.; and Beer, J. (2002) Kilimanjaro ice core records: evidence of Holocene climate change in tropical Africa in *Science*, 298, 589 - 593.

Thompson, L.G.; Mosley-Thompson, E.; Davis, M.E.; Lin, P.-N.; Henderson, K.A.; Cole-Dai, J.; Bolzan, J.F. and Liu, K.-B. (1995): Late glacial stage and Holocene tropical ice core records from Huascaran, Peru in *Science*, 269, 46 - 50.

Thompson, L.G.; Yao, T.; Davis, M.E.; Henderson, K.A.; Mosley-Thompson, E.; Lin, P.N.; Beer, J.; Synal H. A.; Cole - Dai, J.; and Bolzan, J.F. (1997): Tropical climate instability: the last glacial cycle from a Qinghai-Tibetan ice core in *Science*, 276, 1821-1827.

Thompson, R.D. (1989): Short-term climatic change: evidence, causes and environmental consequences and strategies for action in *Progress in Physical Geography*, 13, 315 - 347.

Timmerman, A.; Oberhuber, J.; Bacher, A.; Esch, M.; Latif, M. and Roeckner, E. (1999): Increased El Niño frequency in a climate forced by future greenhouse gas warming in *Nature*, 398, 694 - 696.

Timmerman, A.; Lorenz, S.; An S.-I.; Clement, A. and Xie, S.-P. (2006): Generation of precessional cycles in tropical climates, submitted.

- Tinsley, B.A. (1988): Latitude variations of storm tracks in the North Atlantic: the solar cycle and QBO influences in *Geophysical Research Letters*, 15, 409 - 412.
- Torrence, C. and Compo, G.P. (1998): A practical guide to wavelet analysis in *Bulletin of the American Meteorological Society*, 79, 61 - 78.
- Torrence, C. and Webster, P.J. (1999): Interdecadal changes in the ENSO-monsoon system in *Journal of Climate*, 12, 2679 - 2690.
- Trenberth, K.E. (1975): A quasi-biennial standing wave in the southern hemisphere and interrelations with the sea surface temperature in *Quarterly Journal of the Royal Meteorological Society*, 101, 55 - 74.
- Tudhope, A.W.; Cillcott, C.P.; McCulloch, M.T.; Cook, E.R.; Chappell, J.; Ellam, R.M.; Lea, D.W.; Lough, J.M. and Shimmield, G.B. (2001): Variability in the El Niño–Southern Oscillation through a glacial–interglacial cycle in *Science*, 291, 1511 - 1517.
- Tyson, P.D. (1971): Spatial variation of rainfall spectra in South Africa in *Annals of the Association of American Geographers*, 61, 711 - 720.
- Tyson, P.D. (1986): Climatic Change and Variability in Southern Africa, Oxford University Press, Cape Town.
- Tyson, P.D. (1990): Modelling climatic change in southern Africa: a review of available methods in *South African Journal of Science*, 86, 318 - 330.
- Tyson, P.D. (1991): Climatic change in southern Africa: past and present conditions and possible future scenarios in *Climatic Change*, 18, 241 - 258.
- Tyson, P.D. (1993): Recent developments in modelling climatic change in southern Africa in *South African Journal of Science*, 95, 194 - 200.

- Tyson, P.D. (1999a): Atmospheric circulation changes and palaeoclimates of southern Africa in *South African Journal of Science*, 95, 194 - 200.
- Tyson, P.D. (1999b): Late Quaternary and Holocene palaeoclimates of southern Africa: a synthesis in *South African Journal of Geology*, 102, 335 - 349.
- Tyson, P.D. and Dyer, T.G.J. (1975): Mean annual fluctuations of precipitation in the summer rainfall region of South Africa in *Annals of the Association of American Geographers*, 61, 711 - 720.
- Tyson, P.D.; Cooper, G. R. J. and McCarthy, T.S. (2002a): Millennial to multi-decadal variability in the climate of Southern Africa in *International Journal of Climatology*, 22, 1105 - 1117.
- Tyson, P.D., Dyer, T.G.J. and Mametse, M.N. (1975): Secular changes in South African rainfall: 1880 – 1972 in *Quarterly Journal of the Royal Meteorological Society*, 101, 817 - 833.
- Tyson, P.D.; Karlén, W.; Holmgren, K. and Heiss, G. (2000): The Little Ice Age and Medieval Warming in South Africa in *South African Journal of Science*, 96, 121 - 126.
- Tyson, P.D.; Lee-Thorp, J.; Holmgren, K. and Thackeray, J.F. (2002b): Changing gradients of climate change in southern Africa during the past millennium: implications for population movements in *Climate Change*, 52, 129 - 135.
- Tyson, P.D. and Lindsay, J. A. (1992): The climate of the last 2000 years in southern Africa in *Holocene*, 2, 271 - 278.
- Tyson, P.D.; Mason, S.J.; Jones, M.Q.W. and Cooper, G.R.J. (1998): Global warming in southern Africa: evidence from geothermal profiles in *Geophysical Research Letters*, 25, 2711 - 2713.
- Tyson, P.D.; Odada, E.O. and Partridge, T.C. (2001): Late Quaternary environmental change in southern Africa in *South African Journal of Science*, 97, 139 - 150.

Tyson, P.D. and Partridge, T.C. (2000): The evolution of Cenozoic climates in Partridge, T.C. and Maud, R.R. (eds.) *The Cenozoic of Southern Africa*, Oxford University Press, New York, 406 pp.

Tyson, P.D. and Preston-Whyte, R.A. (2000): *Weather and Climate of Southern Africa*, Oxford University Press, Cape Town, 396 pp.

Van Deventer, T.R.; Thompson, R.S. and Betancourt, J.L. (1987): Vegetation history of the deserts of southwestern North America: The nature and timing of the Late Wisconsin-Holocene transition in Ruddiman, W.F. and Wright, H.E. Jr. (eds.) *North America and Adjacent Oceans during the Last Deglaciation*, K3, 323 - 352.

Van Loon, H. and Labitzke, K. (1988): Associations between the 11-year solar cycle, the QBO, and the atmosphere: Part II: surface and 700 mb in the Northern Hemisphere in winter in *Journal of Climate*, 1, 905 - 920.

Van Zinderen Bakker, E.M. (1967): Upper Pleistocene stratigraphy and Holocene ecology on the basis of vegetation changes in Sub-Saharan Africa in Bishop, W.W. and Clark, J.D. (eds.) *Background to Evolution in Africa*, University of Chicago Press, Chicago, 125 – 147.

Van Zinderen Bakker, E.M. (1976): The evolution of late Quaternary palaeoenvironments of southern Africa in *Palaecology of Africa*, 9, 160 – 202.

Van Zinderen Bakker, E.M. (1978): Quaternary vegetation changes in southern Africa in Werger, M.J.A. (ed.) *Biogeography and Ecology of Southern Africa*, W. Junk, The Hague, 131- 143.

Van Zinderen Bakker, E.M. (1982): Pollen analytical studies of the Wonderwerk Cave, South Africa in *Pollen and Spores*, 24, 235 - 250.



- Venegas, S.A.; Mysak, L.A. and Straub, D.N. (1996): Evidence for interannual and interdecadal climate variability in the South Atlantic in *Geophysical Research Letters*, 23 (19), 2673 - 2676.
- Verschuren, D.; Laird, K.R. and Cumming, B.F. (2000): Rainfall and drought in equatorial east Africa during the past 1,100 years in *Nature*, 403, 410 - 414.
- Vogel, J.C. (1983a)  $^{14}\text{C}$  variations during the upper Pleistocene in *Radiocarbon*, 25, 213 - 218.
- Vogel, J.C. (1983b): Isotopic evidence for past climates and vegetation of South Africa in Bothalia, 14, 391 - 394.
- Vogel, J.C. (1989): A document-derived climate chronology for southern Africa, 1820 – 1900 in *Climate Change*, 14, 291 - 306.
- Vogel, J.C.; Fuls, A. and Ellis, R.P. (1978): The geographical distribution of kranz grasses in South Africa in *South African Journal of Science*, 74, 209 - 215.
- Vogel, J.C. and Rust, U. (1990): Ein in der Kleinen Eiszeit begrabener Walk in der nördlichen Namib in *Berliner Geographical Studies*, 30, 15 - 34.
- Von Rad, U.; Schaaf, M.; Michels, K.H.; Schulz, H.; Berger, W.H. and Sirocko, F. (1999): A 5000-yr record of climate changes in varved sediments from the oxygen minimum zone off Pakistan, northeastern Arabian Sea in *Quaternary Research*, 52, 39 - 53.
- Von Storch, H. and Zwiers, F.W. (1999): *Statistical Analysis in Climate Research*, Cambridge University Press, Cambridge, 484 pp.
- Walker, G.T. (1924): Correlation in seasonal variations of weather IX: A further study of world weather in *Memoirs of the Indian Meteorological Department*, 24 (9) 275 - 332.
- Walker, G.T. and Bliss, E.W. (1932): World Weather V in *Memoirs of the Royal Meteorological Society*, 4, (36), 53 – 84.

Walker, N.D. (1990): Links between South African summer rainfall and temperature variability of the Agulhas and Benguela currents systems in *Journal of Geophysical Research*, 95, 3297 -3319.

Wang, Y.J.; Cheng, H. and Edwards, R.L. (2001): A high-resolution absolute-dated Late Pleistocene monsoon record from Hulu Cave, China in *Science*, 294, 2345 – 2348.

Wang, L.; Sarnthein, M.; Erlenkeuser, H.; Grimalt, J.; Grootes, P.; Heilig, S.; Ivanova, E.; Kienast, M.; Pelejero, C. and Pflaumann, U. (1999): East Asian monsoon climate during the Late Pleistocene: High-resolution sediment records from the South China Sea in *Marine Geology*, 156, 245 - 284.

Wang, B. and Wang, Y. (1996): Temporal structure of the southern oscillation as revealed by waveform and wavelet analysis in *Journal of Climate*, 9, 1586 - 1598.

Ward, J.D.; Seely, M.K.; and Lancaster, N. (1983): On the antiquity of the Namib in *South African Journal of Science*, 79, 175 - 183.

Webb, C. de B. and Wright, J.B. (1976): *The James Stuart Archive of Recorded Oral Evidence Relating to the History of Zulu and Neighbouring Peoples*, Volume 1, University of Natal Press and the Killie Campbell Africana Library, Pietermaritzburg.

Wellington, G.M. and Glynn, P.W. (1983): Environmental influences on skeletal banding in eastern Pacific (Panama) corals in *Coral Reefs*, 1 (4), 215 – 222.

Weng, H. and Lau, K.-M. (1994): Wavelets, period doubling and time frequency localization with application to organization of convection over the tropical western Pacific in *Journal of the Atmospheric Sciences*, 51, 2523 - 2541.

Willet, H.C. (1987): Climatic responses to variable solar activity – past, present, and predicted in Rampino, M.R., Sanders, J.E.; Newman, W.S. and Konigsson, L.K. (eds.) *Climate: History, Periodicity and Predictability*, Van Nostrand Reinhold, New York.

Wilson, A.T.; Hendy, C.H. and Reynolds, C.P. (1979): Short-term climate change and New Zealand temperatures during the last millennium in *Nature*, 279, 315 - 317.

Woodward, F.I. (1987): *Climate and Plant Distribution*, Cambridge University Press, Cambridge.

Xiong, L. (1995): *A Dendroclimatic study of Libocedrus bidwillii Hook F (Kaikakawa)*, unpublished PhD thesis, Lincoln University, New Zealand.

Yu, G.; Prentice, I.C.; Harrison, S.P. and Sun, X. (1998): Biome reconstructions for China at 0 and 6 ka in *Journal of Biogeography*, 25, 1055 - 1069.

Zawada, P.; Hattingh, J. and Van Bladeren, D. (1996): *Palaeoflood Hydrological Analysis of Selected South African Rivers*, Water Research Commission, Pretoria, 209 pp.

Zebiak, S.E. (1993): Air-sea interaction in the equatorial Atlantic region in *Journal of Climate*, 6 (8), 1567 – 1586.

Zebiak, S.E. and Cane, M.A. (1987): A model of El Niño/ Southern Oscillation in *Monthly Weather Reviews*, 115, 2262 - 2278.

Zheng, X. and Eltahir, E.A.B. (1998): The role of vegetation in the dynamics of west African monsoons in *Journal of Climate*, 11, 2078 - 2096.

Zhu, J.H. and Wang, S.W. (2001): 80a-oscillation of summer rainfall over the east part of China and east-Asian summer monsoon in *Advanced Atmospheric Science*, 18 (5), 1043 - 1051.

Zonneveld, K. A. F.; Ganssen, G.; Troelstra, S.; Versteegh, G.J.M and Visscher, H. (1997): Mechanisms forcing abrupt fluctuations of the Indian Ocean summer monsoon during the last deglaciation in *Quaternary Science Reviews*, 16, 187 - 201.

## APPENDIX 1 – MATLAB SCRIPT FOR MEASURING PIXAL DISTANCE

```
function imdist
[x,y] = getline;

x1 = x(1);
x2 = x(2);
y1 = y(1);
y2 = y(2);

coords = [x(1),y(1);x(2),y(2)]

distance=sqrt((x(2)-x(1))^2 + (y(2)-y(1))^2)
```

## APPENDIX 2 – MATLAB SCRIPTS FOR WAVELET ANALYSIS

### a) Function for padding the dataset with zeroes

```
function x = padZeroes(data)
    data = data - mean(data);
    log2Length = ceil(log2(length(data)));
    % Find the next largest power of 2
    newSize = 2 .^ (log2Length + 1);
    numZeroes = newSize - length(data);

    x = [zeros(1, floor(numZeroes / 2)) data zeros(1, ceil(numZeroes /
2))];
```

### b) Function for removing the padded zeroes after the wavelet analysis

```
function x = stripZeroes(coefs, noCols)
    noZeroes = size(coefs, 2) - noCols;
    leftCol = (floor(noZeroes / 2) + 1);
    x = coefs(:, leftCol:(leftCol + noCols - 1));
```

### c) Function for plotting the wavelet diagram, with time on the x-axis and periods on the y-axis

```
% lisaContour(X, Z, noLines)
% X contains the labels for the X axis
% Z contains the coefficients
% noLines specifies the total number of contour lines
function f = lisaContour(X, Z, noLines)
    delta = X(2) - X(1);

    posZ = (Z > 0) .* Z;
    negZ = (Z <= 0) .* Z;

    contour(X, 1 ./ scal2frq(1:size(Z, 1), 'morl', delta), posZ,
noLines);
    hold on;
    contour(X, 1 ./ scal2frq(1:size(Z, 1), 'morl', delta), negZ, noLines,
':');
```

```
hold off;
```

**d) Functions for calculating variance across each period and plotting a wave spectrum diagram**

```
function x = variance(data)
    noRows = size(data, 1);
    noCols = size(data, 2);
    meanVals = mean(data);
    x = [];
```

```
    for i = 1:noRows,
        data(i, :) = data(i, :) - meanVals(i);
        x = [x; sum(abs(data(i, :)))/noCols];
    end
```

```
function f = plotWaveSpectrum(specData, delta)
    plot(1 ./ scal2frq(1:1:length(specData), 'morl', delta), specData)
```

**e) Function for running the Fast Fourier transform and plotting the spectral diagram**

```
function [x, y] = getFFT(data, delta)
    paddedData = padZeroes(data);
    paddedLen = length(paddedData);

    sampFreq = 1 / delta;

    F = fft(paddedData);
    powerF = (F .* conj(F)) / length(paddedData);

    x = sampFreq * (1:(paddedLen / 4)) / paddedLen;
    y = powerF(1:(paddedLen / 4));
```

**APPENDIX 3 - CORAL DATA**

Year	Months	Density HU*	Length cm	Calcification HU.cm	Year	Months	Density HU*	Length cm	Calcification HU.cm
1888	February - March	1156.26	23.50	27172.20	1904	February - March	926.28	40.50	37514.28
	April - January	995.11	2.50	2487.77		April - January	750.77	9.00	6756.94
1889	February - March	1274.11	29.00	38949.16	1905	February - March	1192.88	19.00	22664.88
	April - January	829.30	9.50	7878.38		April - January	907.56	11.00	9983.11
1890	February - March	1002.91	36.50	36606.18	1906	February - March	1168.17	28.00	32708.82
	April - January	1013.83	1.00	1013.83		April - January	971.81	7.00	6802.86
1891	February - March	978.37	34.50	33753.92	1907	February - March	1004.16	32.00	32133.15
	April - January	639.43	3.00	1918.29		April - January	873.86	5.50	4806.21
1892	February - March	950.12	32.50	30878.92	1908	February - March	987.62	25.00	24690.44
	April - January	704.95	10.50	7401.96		April - January	871.29	9.50	8277.24
1893	February - March	851.17	38.50	32769.94	1909	February - March	991.64	29.50	29253.49
	April - January	679.99	4.50	3059.95		April - January	832.29	5.00	4161.47
1894	February - March	931.46	25.50	23752.26	1910	February - March	922.78	27.50	25376.53
	April - January	896.83	4.50	4035.73		April - January	842.40	2.00	1684.81
1895	February - March	1015.31	39.00	39596.97	1911	February - March	1017.64	31.50	32056.68
	April - January	807.91	2.00	1615.82		April - January	876.10	9.00	7884.92
1896	February - March	969.65	26.50	25695.72	1912	February - March	1068.01	21.50	22962.27
	April - January	689.35	11.00	7582.84		April - January	872.06	13.00	11336.76
1897	February - March	948.89	33.50	31787.95	1913	February - March	1095.82	24.50	26847.67
	April - January	742.39	6.00	4454.33		April - January	832.29	8.00	6658.35
1898	February - March	990.28	32.00	31688.90	1914	February - March	1137.61	33.50	38109.96
	April - January	751.75	2.50	1879.37		April - January	823.53	8.00	6588.25
1899	February - March	1014.13	32.50	32959.26	1915	February - March	1078.46	44.00	47452.08
	April - January	737.71	3.50	2581.98		April - January	950.24	3.00	2850.72
1900	February - March	1273.83	40.00	50953.16	1916	February - March	1011.99	32.00	32383.61
	April - January	972.82	2.50	2432.05		April - January	873.86	8.00	6990.85
1901	February - March	1102.64	18.00	19845.67	1917	February - March	980.04	21.50	21070.84
	April - January	797.10	5.00	3985.49		April - January	808.70	20.00	16174.07
1902	February - March	1048.44	18.00	18871.84	1918	February - March	1050.94	20.50	21544.34
	April - January	812.72	11.50	9346.26		April - January	835.66	6.50	5431.81
1903	February - March	925.30	18.00	16655.33	1919	February - March	1011.26	21.00	21236.36
	April - January	910.52	5.50	5007.86		April - January	942.15	5.50	5181.85

**APPENDIX 3 - CORAL DATA**

Year	Months	Density HU*	Length cm	Calcification HU.cm	Year	Months	Density HU*	Length cm	Calcification HU.cm
1920	February - March	1031.83	38.50	39725.45	1936	February - March	1216.19	38.50	50472.05
	April - January	772.31	6.00	4633.85		April - January	790.73	7.00	5237.44
1921	February - March	1029.01	33.00	33957.47	1937	February - March	1100.71	29.13	33495.47
	April - January	932.91	8.00	7463.28		April - January	985.23	4.50	4378.73
1922	February - March	975.81	29.50	28786.30	1938	February - March	1062.03	31.13	33078.03
	April - January	1004.16	3.50	3514.56		April - January	1005.31	1.50	1507.96
1923	February - March	1101.45	24.50	26985.52	1939	February - March	1080.18	21.00	22683.88
	April - January	1085.04	3.00	3255.12		April - January	973.15	3.00	2919.44
1924	February - March	1174.34	25.00	29358.58	1940	February - March	1052.66	27.00	28421.74
	April - January	1044.60	7.00	7312.20		April - January	1026.74	5.00	5133.71
1925	February - March	1260.28	8.50	10712.35	1941	February - March	1097.18	42.00	46081.64
	April - January	1017.64	3.00	3052.92		April - January	935.74	8.50	7953.80
1926	February - March	1299.22	10.50	13641.80	1942	February - March	1018.11	34.50	35124.87
	April - January	1118.74	5.00	5593.70		April - January	904.24	4.50	4069.08
1927	February - March	1231.90	21.50	26485.82	1943	February - March	1024.60	31.50	32274.87
	April - January	1134.47	4.00	4537.86		April - January	917.10	11.00	10088.14
1928	February - March	1221.52	10.00	12215.23	1944	February - March	992.23	28.00	27782.45
	April - January	1031.12	4.50	4640.04		April - January	885.87	6.00	5315.19
1929	February - March	1165.17	19.50	22720.81	1945	February - March	957.15	30.00	28714.47
	April - January	1064.82	3.00	3194.46		April - January	927.21	3.00	2781.63
1930	February - March	1127.73	13.00	14660.43	1946	February - March	980.80	40.00	39232.18
	April - January	916.54	3.00	2749.63		April - January	885.87	3.50	3100.53
1931	February - March	1023.03	6.00	6138.20	1947	February - March	1061.33	43.50	46167.75
	April - January	874.42	9.50	8306.97		April - January	956.30	4.00	3825.22
1932	February - March	926.80	25.50	23633.36	1948	February - March	983.25	30.50	29989.26
	April - January	586.29	10.50	6156.01		April - January	913.43	1.00	913.43
1933	February - March	980.20	21.00	20564.13	1949	February - March	966.43	14.00	13530.08
	April - January	775.00	6.50	5037.53		April - January	879.74	5.00	4398.70
1934	February - March	1089.14	27.00	29406.84	1950	February - March	989.99	14.50	14354.89
	April - January	748.04	6.00	4488.27		April - January	899.65	4.00	3598.59
1935	February - March	1117.29	30.00	33518.85	1951	February - March	1022.21	27.00	27599.68
	April - January	1053.59	5.00	5267.93		April - January	862.90	4.50	3883.03



APPENDIX 3 - CORAL DATA

Year	Months	Density HU*	Length cm	Calcification HU.cm	Year	Months	Density HU*	Length cm	Calcification HU.cm
1952	February - March	999.04	24.00	23976.98	1968	February - March	935.01	21.50	20102.82
	April - January	849.11	3.00	2547.34		April - January	685.07	5.00	3425.33
1953	February - March	951.66	33.00	31404.81	1969	February - March	822.47	30.00	24674.00
	April - January	873.61	7.50	6552.11		April - January	579.35	4.50	2607.08
1954	February - March	1049.97	37.50	39373.78	1970	February - March	855.13	24.50	20950.65
	April - January	913.43	2.50	2283.57		April - January	736.84	20.00	14732.78
1955	February - March	1017.00	12.00	12203.98	1971	February - March	851.00	26.50	21551.89
	April - January	881.27	3.50	3084.45		April - January	665.89	4.50	2996.51
1956	February - March	994.28	22.00	21874.16	1972	February - March	857.40	20.00	17148.09
	April - January	833.80	6.50	5419.71		April - January	612.67	5.00	3063.33
1957	February - March	1009.90	21.50	21712.83	1973	February - March	831.62	29.50	24532.80
	April - January	886.63	14.00	12412.83		April - January	485.75	5.00	2428.75
1958	February - March	980.37	9.00	8823.30	1974	February - March	729.84	24.50	17881.00
	April - January	853.71	4.00	3414.83		April - January	559.44	5.50	3076.94
1959	February - March	954.77	12.00	11457.27	1975	February - March	783.39	23.50	18409.70
	April - January	849.11	5.00	4245.57		April - January	598.34	8.00	4786.70
1960	February - March	962.63	32.00	30804.06	1976	February - March	742.17	24.00	17812.09
	April - January	858.30	5.00	4291.51		April - January	399.77	7.00	2798.41
1961	February - March	1098.14	33.50	36787.74	1977	February - March	738.36	26.50	19566.44
	April - January	829.41	4.50	3732.33		April - January	461.18	7.00	3228.29
1962	February - March	987.71	25.50	25186.71	1978	February - March	656.83	23.50	15435.60
	April - January	841.60	7.00	5891.23		April - January	499.40	7.00	3485.77
1963	February - March	978.27	29.50	28858.85	1979	February - March	727.54	22.50	16369.72
	April - January	908.69	4.00	3634.77		April - January	474.83	10.50	4985.73
1964	February - March	932.28	31.50	29366.68	1980	February - March	788.71	22.00	17351.71
	April - January	792.81	5.50	4360.47		April - January	553.30	12.00	6639.62
1965	February - March	907.10	24.50	22224.00	1981	February - March	744.76	25.50	18991.28
	April - January	823.31	4.00	3293.23		April - January	350.64	7.00	2454.50
1966	February - March	984.93	22.50	22160.92	1982	February - March	784.62	23.50	18438.57
	April - January	791.59	7.50	5936.95		April - January	426.79	9.00	3841.14
1967	February - March	873.32	22.50	19649.88	1983	February - March	697.13	29.50	20565.25
	April - January	636.27	5.00	3181.37		April - January	612.67	5.00	3063.33

**APPENDIX 3 - CORAL DATA**

Year	Months	Density HU*	Length cm	Calcification HU.cm	Year	Months	Density HU*	Length cm	Calcification HU.cm
1984	February - March	878.39	23.50	20642.28	1989	February - March	616.16	30.00	18484.90
	April - January	664.25	7.00	4649.77		April - January	349.54	6.50	2272.04
1985	February - March	759.41	20.00	15188.18	1990	February - March	639.07	28.50	18213.45
	April - January	624.60	7.00	4372.23		April - January	376.45	9.00	3388.03
1986	February - March	684.97	24.00	16439.22	1991	February - March	638.78	21.50	13733.40
	April - January	584.95	6.50	3802.20		April - January	480.70	6.00	2884.21
1987	February - March	629.08	28.50	17928.70	1992	February - March	601.23	34.50	20742.34
	April - January	376.45	5.50	2070.48		April - January	322.64	5.00	1613.20
1988	February - March	701.91	23.50	16494.94	1993	February - March	687.19	23.00	15805.37
	April - January	436.98	6.00	2621.89		April - May	593.03	6.50	3854.67

\* HU = Hounsfield units

**APPENDIX 4 - STALAGMITE DATA**

AGE (Yr)	RAW DATA		CORRECTION ARAGONITE		AGE (Yr)	RAW DATA		CORRECTION ARAGONITE		AGE (Yr)	RAW DATA		CORRECTION ARAGONITE	
	T8 13C	T8 18O	T8 13C	T8 18O		T8 13C	T8 18O	T8 13C	T8 18O		T8 13C	T8 18O	T8 13C	T8 18O
2.00	-4.63	-2.88	-6.33	-3.48	259.37	-4.64	-4.22	-6.34	-4.82	452.54	-3.42	-2.65	-5.12	-3.25
8.53	-5.09	-2.98	-6.79	-3.58	267.07	-3.94	-3.99	-5.64	-4.59	458.29	-3.41	-3.60	-5.11	-4.20
15.06	-4.21	-2.88	-5.91	-3.48	274.78	-3.77	-3.30	-5.47	-3.90	464.05	-3.63	-3.38	-5.33	-3.98
21.59	-4.67	-3.31	-6.37	-3.91	282.48	-4.83	-5.70	-6.53	-6.30	469.80	-3.52	-4.50	-5.22	-5.10
28.12	-4.54	-3.54	-6.24	-4.14	290.19	-4.73	-5.35	-6.43	-5.95	481.32	-3.32	-3.29	-5.02	-3.89
34.65	-4.54	-3.91	-6.24	-4.51	297.89	-3.76	-5.61	-5.46	-6.21	487.07	-3.40	-2.83	-5.10	-3.43
41.18	-4.59	-3.95	-6.29	-4.55	305.59	-4.56	-5.28	-6.26	-5.88	492.83	-3.18	-3.17	-4.88	-3.77
47.71	-4.37	-4.02	-6.07	-4.62	313.30	-4.33	-4.48	-6.03	-5.08	498.59	-2.74	-2.41	-4.44	-3.01
54.24	-4.40	-4.27	-6.10	-4.87	321.00	-5.12	-4.45	-6.82	-5.05	504.34	-3.73	-4.28	-5.43	-4.88
67.29	-3.90	-3.67	-5.60	-4.27	325.85	-4.18	-3.85	-5.88	-4.45	510.10	-3.74	-4.07	-5.44	-4.67
80.35	-4.19	-3.45	-5.89	-4.05	330.70	-3.99	-3.27	-5.69	-3.87	515.85	-3.44	-4.38	-5.14	-4.98
86.88	-3.80	-2.57	-5.50	-3.17	340.40	-4.20	-3.73	-5.90	-4.33	521.61	-3.38	-3.67	-5.08	-4.27
93.41	-3.79	-4.43	-5.49	-5.03	345.25	-4.13	-3.85	-5.83	-4.45	527.37	-3.86	-3.03	-5.56	-3.63
106.47	-3.80	-3.49	-5.50	-4.09	350.10	-4.43	-4.27	-6.13	-4.87	533.12	-4.21	-2.94	-5.91	-3.54
113.00	-3.91	-3.50	-5.61	-4.10	354.95	-3.98	-3.95	-5.68	-4.55	538.88	-3.75	-3.28	-5.45	-3.88
120.70	-3.70	-3.24	-5.40	-3.84	359.80	-3.28	-3.77	-4.98	-4.37	544.63	-3.73	-3.08	-5.43	-3.68
128.41	-4.07	-3.48	-5.77	-4.08	364.65	-3.36	-3.55	-5.06	-4.15	550.39	-3.66	-3.03	-5.36	-3.63
136.11	-4.25	-3.23	-5.95	-3.83	369.50	-2.75	-3.52	-4.45	-4.12	556.15	-3.82	-3.37	-5.52	-3.97
143.81	-4.09	-3.11	-5.79	-3.71	374.35	-3.38	-3.74	-5.08	-4.34	561.90	-2.89	-2.84	-4.59	-3.44
151.52	-3.81	-2.83	-5.51	-3.43	379.20	-3.88	-3.66	-5.58	-4.26	567.66	-4.11	-3.13	-5.81	-3.73
159.22	-3.88	-3.44	-5.58	-4.04	384.05	-3.27	-2.62	-4.97	-3.22	573.41	-4.45	-2.81	-6.15	-3.41
166.93	-3.40	-3.90	-5.10	-4.50	388.90	-4.44	-3.78	-6.14	-4.38	579.17	-4.39	-3.50	-6.09	-4.10
174.63	-3.61	-3.72	-5.31	-4.32	393.75	-3.94	-3.57	-5.64	-4.17	584.93	-3.96	-3.01	-5.66	-3.61
182.33	-3.82	-3.76	-5.52	-4.36	398.60	-4.32	-4.06	-6.02	-4.66	590.68	-4.11	-3.11	-5.81	-3.71
190.04	-4.18	-3.30	-5.88	-3.90	403.45	-2.49	-3.95	-4.19	-4.55	596.44	-4.16	-2.91	-5.86	-3.51
205.44	-4.47	-3.91	-6.17	-4.51	408.30	-4.68	-3.66	-6.38	-4.26	602.20	-4.18	-3.94	-5.88	-4.54
213.15	-4.34	-3.98	-6.04	-4.58	413.15	-4.30	-3.37	-6.00	-3.97	607.95	-4.50	-4.12	-6.20	-4.72
220.85	-3.90	-3.90	-5.60	-4.50	418.00	-4.12	-4.05	-5.82	-4.65	613.71	-4.05	-3.73	-5.75	-4.33
228.56	-4.42	-4.81	-6.12	-5.41	423.76	-3.32	-3.57	-5.02	-4.17	619.46	-3.86	-3.83	-5.56	-4.43
236.26	-4.34	-4.82	-6.04	-5.42	429.51	-3.12	-3.32	-4.82	-3.92	625.22	-4.12	-3.62	-5.82	-4.22
243.96	-4.31	-4.74	-6.01	-5.34	441.02	-3.60	-4.14	-5.30	-4.74	630.98	-4.03	-2.57	-5.73	-3.17
251.67	-4.52	-4.53	-6.22	-5.13	446.78	-3.98	-4.27	-5.68	-4.87	636.73	-3.85	-2.67	-5.55	-3.27

**APPENDIX 4 - STALAGMITE DATA**

AGE (Yr)	RAW DATA		CORRECTION ARAGONITE		AGE (Yr)	RAW DATA		CORRECTION ARAGONITE		AGE (Yr)	RAW DATA		CORRECTION ARAGONITE	
	T8 13C	T8 18O	T8 13C	T8 18O		T8 13C	T8 18O	T8 13C	T8 18O		T8 13C	T8 18O	T8 13C	T8 18O
642.49	-4.01	-2.97	-5.71	-3.57	1010.80	-3.90	-4.12	-5.60	-4.72	1411.00	-3.20	-3.39	-4.90	-3.99
648.24	-4.18	-2.97	-5.88	-3.57	1022.93	-3.38	-4.56	-5.08	-5.16	1417.66	-2.97	-3.35	-4.67	-3.95
654.00	-4.12	-2.78	-5.82	-3.38	1035.05	-3.93	-4.62	-5.63	-5.22	1424.31	-3.23	-3.71	-4.93	-4.31
664.00	-3.98	-2.77	-5.68	-3.37	1047.18	-4.16	-4.71	-5.86	-5.31	1430.97	-3.30	-3.35	-5.00	-3.95
669.00	-4.13	-3.17	-5.83	-3.77	1059.31	-3.47	-4.28	-5.17	-4.88	1437.63	-3.62	-3.86	-5.32	-4.46
674.00	-4.27	-3.11	-5.97	-3.71	1071.44	-3.34	-4.15	-5.04	-4.75	1444.29	-3.18	-3.17	-4.88	-3.77
679.00	-4.31	-2.83	-6.01	-3.43	1083.56	-3.48	-4.27	-5.18	-4.87	1450.94	-3.17	-4.00	-4.87	-4.60
684.00	-4.22	-3.17	-5.92	-3.77	1095.69	-3.03	-4.51	-4.73	-5.11	1457.60	-3.11	-3.70	-4.81	-4.30
689.00	-4.20	-3.55	-5.90	-4.15	1107.82	-3.25	-4.18	-4.95	-4.78	1464.26	-2.99	-4.16	-4.69	-4.76
709.00	-3.88	-3.10	-5.58	-3.70	1119.95	-2.77	-3.82	-4.47	-4.42	1470.91	-2.97	-4.19	-4.67	-4.79
714.00	-3.79	-3.32	-5.49	-3.92	1132.07	-2.65	-3.87	-4.35	-4.47	1477.57	-2.78	-3.43	-4.48	-4.03
719.00	-3.15	-2.85	-4.85	-3.45	1144.20	-2.92	-3.96	-4.62	-4.56	1484.23	-3.72	-3.62	-5.42	-4.22
724.00	-3.51	-3.27	-5.21	-3.87	1156.33	-2.89	-3.54	-4.59	-4.14	1490.89	-3.75	-3.68	-5.45	-4.28
729.00	-3.36	-3.12	-5.06	-3.72	1168.45	-2.83	-3.92	-4.53	-4.52	1497.54	-3.88	-3.67	-5.58	-4.27
744.00	-3.57	-3.34	-5.27	-3.94	1192.71	-3.01	-3.67	-4.71	-4.27	1504.20	-3.86	-3.47	-5.56	-4.07
756.13	-3.52	-3.17	-5.22	-3.77	1204.84	-2.67	-3.31	-4.37	-3.91	1510.86	-3.79	-3.22	-5.49	-3.82
768.25	-3.73	-3.20	-5.43	-3.80	1216.96	-2.20	-3.18	-3.90	-3.78	1517.51	-3.84	-3.60	-5.54	-4.20
780.38	-3.88	-4.36	-5.58	-4.96	1229.09	-2.13	-2.91	-3.83	-3.51	1524.17	-3.91	-3.28	-5.61	-3.88
792.51	-3.70	-4.47	-5.40	-5.07	1241.22	-2.29	-3.47	-3.99	-4.07	1530.83	-3.75	-3.43	-5.45	-4.03
816.76	-3.26	-4.28	-4.96	-4.88	1253.35	-3.08	-3.85	-4.78	-4.45	1537.49	-3.76	-3.36	-5.46	-3.96
828.89	-3.24	-3.79	-4.94	-4.39	1265.47	-3.39	-3.79	-5.09	-4.39	1550.80	-3.74	-2.90	-5.44	-3.50
865.27	-3.99	-4.83	-5.69	-5.43	1277.60	-2.91	-3.18	-4.61	-3.78	1557.46	-3.66	-3.14	-5.36	-3.74
877.40	-4.24	-5.14	-5.94	-5.74	1289.73	-2.89	-2.98	-4.59	-3.58	1564.11	-3.53	-3.13	-5.23	-3.73
889.53	-4.18	-4.91	-5.88	-5.51	1301.85	-3.25	-3.27	-4.95	-3.87	1584.09	-3.25	-4.70	-4.95	-5.30
901.65	-4.61	-4.85	-6.31	-5.45	1313.98	-3.22	-3.90	-4.92	-4.50	1590.74	-3.17	-3.64	-4.87	-4.24
925.91	-3.48	-4.49	-5.18	-5.09	1326.11	-2.66	-4.73	-4.36	-5.33	1597.40	-3.97	-3.62	-5.67	-4.22
938.04	-3.23	-4.95	-4.93	-5.55	1338.24	-2.86	-3.79	-4.56	-4.39	1604.06	-4.64	-4.99	-6.34	-5.59
950.16	-3.69	-3.91	-5.39	-4.51	1350.36	-2.33	-3.26	-4.03	-3.86	1610.71	-4.19	-3.51	-5.89	-4.11
962.29	-3.75	-4.35	-5.45	-4.95	1362.49	-3.30	-3.86	-5.00	-4.46	1617.37	-4.09	-3.67	-5.79	-4.27
974.42	-3.55	-4.56	-5.25	-5.16	1374.62	-2.85	-3.59	-4.55	-4.19	1624.03	-4.39	-3.50	-6.09	-4.10
986.55	-3.56	-5.04	-5.26	-5.64	1386.75	-2.57	-3.44	-4.27	-4.04	1630.69	-4.36	-3.07	-6.06	-3.67
998.67	-4.16	-4.44	-5.86	-5.04	1398.87	-2.98	-3.92	-4.68	-4.52	1637.34	-4.10	-3.05	-5.80	-3.65

**APPENDIX 4 - STALAGMITE DATA**

AGE (Yr)	RAW DATA		CORRECTION ARAGONITE		AGE (Yr)	RAW DATA		CORRECTION ARAGONITE		AGE (Yr)	RAW DATA		CORRECTION ARAGONITE	
	T8 13C	T8 18O	T8 13C	T8 18O		T8 13C	T8 18O	T8 13C	T8 18O		T8 13C	T8 18O	T8 13C	T8 18O
1644.00	-2.57	-2.73	-4.27	-3.33	1827.78	-3.28	-3.82	-4.98	-4.42	2039.91	-2.61	-3.20	-4.31	-3.80
1650.38	-2.99	-4.41	-4.69	-5.01	1831.93	-2.97	-3.96	-4.67	-4.56	2045.83	-3.11	-3.48	-4.81	-4.06
1656.76	-3.82	-3.33	-5.52	-3.93	1836.07	-3.03	-3.61	-4.73	-4.21	2051.74	-2.84	-2.48	-4.54	-3.06
1663.14	-3.64	-3.71	-5.34	-4.31	1840.22	-3.31	-3.53	-5.01	-4.13	2057.65	-2.75	-3.08	-4.45	-3.68
1669.52	-3.51	-3.63	-5.21	-4.23	1844.37	-3.33	-3.58	-5.03	-4.18	2063.57	-3.10	-3.05	-4.80	-3.65
1675.90	-3.10	-3.79	-4.80	-4.39	1848.52	-3.08	-3.19	-4.78	-3.79	2069.48	-3.04	-3.08	-4.74	-3.68
1682.29	-3.34	-3.63	-5.04	-4.23	1852.67	-3.08	-3.10	-4.78	-3.70	2075.39	-2.51	-3.58	-4.21	-4.18
1688.67	-3.22	-2.78	-4.92	-3.38	1856.81	-3.21	-3.35	-4.91	-3.95	2081.30	-2.07	-2.99	-3.77	-3.59
1695.05	-3.11	-2.44	-4.81	-3.04	1860.96	-3.14	-3.46	-4.84	-4.06	2087.22	-2.13	-2.76	-3.83	-3.36
1701.43	-3.06	-2.61	-4.76	-3.21	1865.11	-3.16	-3.69	-4.86	-4.29	2093.13	-2.34	-3.02	-4.04	-3.62
1707.81	-2.73	-2.42	-4.43	-3.02	1869.26	-2.97	-3.19	-4.67	-3.79	2099.04	-2.43	-3.07	-4.13	-3.67
1714.19	-3.18	-3.20	-4.88	-3.80	1873.41	-2.78	-2.95	-4.48	-3.55	2104.96	-2.39	-3.36	-4.09	-3.96
1720.57	-3.79	-3.73	-5.49	-4.33	1877.56	-3.20	-3.50	-4.90	-4.10	2110.87	-2.59	-3.29	-4.29	-3.89
1726.95	-3.66	-3.53	-5.36	-4.13	1881.70	-2.97	-3.40	-4.67	-4.00	2116.78	-2.75	-3.90	-4.45	-4.50
1733.33	-3.57	-3.25	-5.27	-3.85	1885.85	-3.17	-3.17	-4.87	-3.77	2122.70	-2.87	-2.67	-4.57	-3.27
1739.71	-3.39	-3.12	-5.09	-3.72	1890.00	-2.89	-2.89	-4.59	-3.49	2128.61	-3.10	-2.68	-4.80	-3.28
1746.10	-3.27	-2.96	-4.97	-3.56	1899.00	-2.55	-3.00	-4.25	-3.60	2134.52	-2.94	-3.34	-4.64	-3.94
1752.48	-3.13	-3.47	-4.83	-4.07	1908.00	-3.07	-3.53	-4.77	-4.13	2140.43	-2.85	-3.55	-4.55	-4.15
1758.86	-3.21	-4.28	-4.91	-4.88	1917.00	-3.00	-3.64	-4.70	-4.24	2146.35	-2.56	-3.19	-4.26	-3.79
1765.24	-3.24	-5.05	-4.94	-5.65	1926.00	-2.69	-4.13	-4.39	-4.73	2152.26	-3.45	-4.07	-5.15	-4.67
1771.62	-3.16	-4.14	-4.86	-4.74	1935.00	-2.77	-4.03	-4.47	-4.63	2158.17	-2.94	-2.83	-4.64	-3.43
1778.00	-3.43	-4.22	-5.13	-4.82	1944.00	-2.54	-3.97	-4.24	-4.57	2164.09	-3.08	-3.12	-4.78	-3.72
1782.15	-3.23	-4.32	-4.93	-4.92	1953.00	-2.81	-2.73	-4.51	-3.33	2170.00	-3.86	-3.02	-5.56	-3.62
1786.30	-3.35	-3.88	-5.05	-4.48	1962.00	-1.86	-2.93	-3.56	-3.53	2179.00	-3.66	-3.40	-5.36	-4.00
1794.59	-3.31	-3.38	-5.01	-3.98	1971.00	-2.68	-3.00	-4.38	-3.60	2188.00	-3.45	-3.52	-5.15	-4.12
1798.74	-3.24	-3.14	-4.94	-3.74	1980.00	-2.79	-3.09	-4.49	-3.69	2197.00	-2.91	-3.61	-4.61	-4.21
1802.89	-3.17	-3.56	-4.87	-4.16	1989.00	-2.85	-3.47	-4.55	-4.07	2206.00	-2.45	-3.70	-4.15	-4.30
1807.04	-3.12	-3.40	-4.82	-4.00	1998.00	-2.56	-3.29	-4.26	-3.89	2215.00	-1.99	-3.17	-3.69	-3.77
1811.19	-2.88	-3.59	-4.58	-4.19	2007.00	-2.81	-3.45	-4.51	-4.05	2224.00	-2.08	-3.23	-3.78	-3.83
1815.33	-3.33	-3.72	-5.03	-4.32	2016.00	-2.68	-3.43	-4.38	-4.03	2233.00	-2.55	-3.84	-4.25	-4.44
1819.48	-3.45	-3.63	-5.15	-4.23	2025.00	-2.04	-3.37	-3.74	-3.97	2242.00	-2.59	-3.62	-4.29	-4.22
1823.63	-3.63	-3.69	-5.33	-4.29	2034.00	-2.26	-3.27	-3.96	-3.87	2251.00	-2.59	-3.32	-4.29	-3.92

**APPENDIX 4 - STALAGMITE DATA**

RAW DATA		CORRECTION ARAGONITE			RAW DATA		CORRECTION ARAGONITE			RAW DATA		CORRECTION ARAGONITE		
AGE (Yr)	T8 13C	T8 18O	T8 13C	T8 18O	AGE (Yr)	T8 13C	T8 18O	T8 13C	T8 18O	AGE (Yr)	T8 13C	T8 18O	T8 13C	T8 18O
2260.00	-1.91	-3.07	-3.61	-3.67	2548.00	-1.82	-4.14	-3.52	-4.74	2836.00	-1.35	-2.96	-3.05	-3.56
2269.00	-2.44	-3.05	-4.14	-3.65	2557.00	-2.96	-3.46	-4.66	-4.06	2840.00	-2.19	-2.82	-3.89	-3.42
2278.00	-2.07	-2.98	-3.77	-3.58	2566.00	-3.26	-3.07	-4.96	-3.67	2845.00	-1.85	-2.47	-3.55	-3.07
2287.00	-2.02	-3.26	-3.72	-3.86	2575.00	-3.25	-3.07	-4.95	-3.67	2850.72	-2.64	-3.82	-4.34	-4.42
2296.00	-2.30	-3.51	-4.00	-4.11	2584.00	-4.00	-3.66	-5.70	-4.26	2856.45	-2.49	-3.84	-4.19	-4.44
2305.00	-2.70	-3.68	-4.40	-4.28	2593.00	-3.84	-3.25	-5.54	-3.85	2862.17	-2.05	-4.11	-3.75	-4.71
2314.00	-2.71	-4.08	-4.41	-4.68	2602.00	-3.95	-3.94	-5.65	-4.54	2867.89	-2.33	-4.10	-4.03	-4.70
2323.00	-2.64	-3.22	-4.34	-3.82	2611.00	-4.07	-4.01	-5.77	-4.61	2873.62	-2.89	-4.61	-4.59	-5.21
2332.00	-3.04	-2.98	-4.74	-3.58	2620.00	-3.71	-3.88	-5.41	-4.48	2879.34	-2.49	-4.09	-4.19	-4.69
2341.00	-3.15	-3.01	-4.85	-3.61	2629.00	-3.76	-4.24	-5.46	-4.84	2885.07	-2.84	-4.73	-4.54	-5.33
2350.00	-2.90	-3.10	-4.60	-3.70	2638.00	-3.87	-4.06	-5.57	-4.66	2890.79	-2.30	-4.40	-4.00	-5.00
2359.00	-3.14	-3.43	-4.84	-4.03	2647.00	-3.98	-4.00	-5.68	-4.60	2896.51	-2.35	-4.66	-4.05	-5.26
2368.00	-3.19	-2.87	-4.89	-3.47	2656.00	-3.95	-4.66	-5.65	-5.26	2907.96	-2.65	-3.65	-4.35	-4.25
2377.00	-3.31	-2.93	-5.01	-3.53	2665.00	-4.02	-5.31	-5.72	-5.91	2913.88	-2.65	-4.46	-4.35	-5.06
2386.00	-3.25	-3.09	-4.95	-3.69	2674.00	-3.92	-3.92	-5.62	-4.52	2925.13	-2.66	-4.88	-4.36	-5.48
2395.00	-3.59	-2.88	-5.29	-3.48	2683.00	-4.03	-4.07	-5.73	-4.67	2930.85	-2.55	-4.35	-4.25	-4.95
2404.00	-3.74	-3.16	-5.44	-3.76	2692.00	-3.55	-4.22	-5.25	-4.82	2936.58	-2.66	-4.65	-4.36	-5.25
2413.00	-3.66	-3.34	-5.36	-3.94	2701.00	-3.37	-4.53	-5.07	-5.13	2942.30	-2.60	-3.80	-4.30	-4.40
2422.00	-3.86	-3.95	-5.56	-4.55	2710.00	-3.30	-4.38	-5.00	-4.98	2948.02	-3.29	-3.30	-4.99	-3.90
2431.00	-3.67	-3.87	-5.37	-4.47	2719.00	-2.39	-4.06	-4.09	-4.66	2953.75	-2.29	-4.04	-3.99	-4.64
2440.00	-3.48	-3.03	-5.18	-3.63	2728.00	-2.70	-4.72	-4.40	-5.32	2959.47	-2.46	-3.92	-4.16	-4.52
2449.00	-3.19	-2.58	-4.89	-3.18	2737.00	-2.60	-3.28	-4.30	-3.88	2965.20	-2.46	-4.09	-4.16	-4.69
2458.00	-3.06	-2.74	-4.76	-3.34	2746.00	-2.66	-3.76	-4.36	-4.36	2970.92	-2.67	-4.20	-4.37	-4.80
2467.00	-3.01	-2.93	-4.71	-3.53	2755.00	-3.06	-4.44	-4.76	-5.04	2982.37	-2.11	-4.27	-3.81	-4.87
2476.00	-3.21	-3.35	-4.91	-3.95	2764.00	-4.38	-5.59	-6.08	-6.19	2988.09	-2.41	-4.14	-4.11	-4.74
2485.00	-3.05	-3.56	-4.75	-4.16	2773.00	-4.26	-3.99	-5.96	-4.59	2993.81	-2.78	-5.12	-4.48	-5.72
2494.00	-3.19	-3.63	-4.89	-4.23	2782.00	-3.88	-4.60	-5.58	-5.20	2999.54	-3.06	-4.75	-4.76	-5.35
2503.00	-3.04	-3.70	-4.74	-4.30	2791.00	-3.35	-4.96	-5.05	-5.56	3005.26	-3.00	-4.29	-4.70	-4.89
2512.00	-2.96	-3.63	-4.66	-4.23	2800.00	-3.14	-4.63	-4.84	-5.23	3010.98	-2.90	-4.27	-4.60	-4.87
2521.00	-2.66	-2.87	-4.36	-3.47	2809.00	-3.08	-3.68	-4.78	-4.28	3016.71	-3.04	-3.88	-4.74	-4.48
2530.00	-2.68	-2.87	-4.38	-3.47	2818.00	-2.08	-3.39	-3.78	-3.99	3022.43	-3.06	-3.78	-4.76	-4.38
2539.00	-2.20	-3.47	-3.90	-4.07	2827.00	-1.58	-3.05	-3.28	-3.65	3028.15	-3.06	-3.95	-4.76	-4.55

**APPENDIX 4 - STALAGMITE DATA**

		RAW DATA		CORRECTION ARAGONITE				RAW DATA		CORRECTION ARAGONITE				RAW DATA		CORRECTION ARAGONITE	
AGE (Yr)	T8 13C	T8 18O	T8 13C	T8 18O	AGE (Yr)	T8 13C	T8 18O	T8 13C	T8 18O	AGE (Yr)	T8 13C	T8 18O	T8 13C	T8 18O	AGE (Yr)	T8 13C	T8 18O
3033.88	-3.04	-4.25	-4.74	-4.85	3217.03	-3.34	-4.53	-5.04	-5.13	3400.19	-4.26	-4.14	-5.96	-4.74			
3039.60	-3.10	-4.11	-4.80	-4.71	3222.76	-3.33	-4.13	-5.03	-4.73	3405.91	-4.09	-3.55	-5.79	-4.15			
3045.33	-3.23	-4.41	-4.93	-5.01	3228.48	-3.01	-3.97	-4.71	-4.57	3411.63	-4.19	-3.67	-5.89	-4.27			
3051.05	-3.28	-4.47	-4.98	-5.07	3234.20	-2.44	-4.32	-4.14	-4.92	3417.36	-4.06	-3.96	-5.76	-4.56			
3056.77	-3.56	-5.00	-5.26	-5.60	3239.93	-1.18	-4.09	-2.88	-4.69	3423.08	-4.48	-3.90	-6.18	-4.50			
3062.50	-3.31	-3.61	-5.01	-4.21	3245.65	-2.01	-3.42	-3.71	-4.02	3428.80	-4.02	-3.32	-5.72	-3.92			
3068.22	-3.49	-4.82	-5.19	-5.42	3251.37	-2.13	-3.82	-3.83	-4.42	3434.53	-4.13	-4.01	-5.83	-4.61			
3073.94	-3.51	-4.58	-5.21	-5.18	3257.10	-3.41	-3.80	-5.11	-4.40	3440.25	-3.63	-3.80	-5.33	-4.40			
3079.67	-3.55	-4.20	-5.25	-4.80	3262.82	-3.70	-3.57	-5.40	-4.17	3445.98	-4.39	-4.16	-6.09	-4.76			
3085.39	-3.38	-4.40	-5.08	-5.00	3268.54	-3.69	-3.23	-5.39	-3.83	3451.70	-4.14	-3.98	-5.84	-4.58			
3091.11	-2.55	-3.21	-4.25	-3.81	3274.27	-3.42	-3.11	-5.12	-3.71	3457.42	-4.42	-4.11	-6.12	-4.71			
3096.84	-3.17	-3.45	-4.87	-4.05	3279.99	-3.61	-2.93	-5.31	-3.53	3463.15	-3.53	-3.92	-5.23	-4.52			
3102.56	-3.34	-4.20	-5.04	-4.80	3285.72	-3.68	-3.18	-5.38	-3.78	3468.87	-3.12	-3.47	-4.82	-4.07			
3108.28	-3.39	-3.57	-5.09	-4.17	3291.44	-3.86	-3.46	-5.56	-4.06	3474.59	-3.47	-3.73	-5.17	-4.33			
3114.01	-3.55	-3.68	-5.25	-4.28	3297.16	-3.95	-3.55	-5.65	-4.15	3480.32	-4.34	-3.94	-6.04	-4.54			
3119.73	-3.29	-3.18	-4.99	-3.78	3302.89	-4.01	-4.04	-5.71	-4.64	3486.04	-4.53	-4.32	-6.23	-4.92			
3125.46	-3.28	-3.58	-4.98	-4.18	3308.61	-3.73	-4.09	-5.43	-4.69	3491.76	-4.15	-4.29	-5.85	-4.89			
3131.18	-2.84	-2.85	-4.54	-3.45	3314.33	-3.12	-3.28	-4.82	-3.88	3497.49	-3.08	-4.46	-4.78	-5.06			
3136.90	-2.97	-3.13	-4.67	-3.73	3320.06	-3.53	-3.61	-5.23	-4.21	3503.21	-4.14	-4.69	-5.84	-5.29			
3142.63	-3.54	-3.63	-5.24	-4.23	3325.78	-3.59	-3.98	-5.29	-4.58	3508.93	-4.35	-4.27	-6.05	-4.87			
3148.35	-3.58	-3.55	-5.28	-4.15	3331.50	-3.61	-3.77	-5.31	-4.37	3514.66	-4.59	-3.83	-6.29	-4.43			
3154.07	-3.81	-3.37	-5.51	-3.97	3337.23	-3.40	-3.84	-5.10	-4.44	3531.83	-4.14	-4.03	-5.84	-4.63			
3159.80	-3.23	-2.85	-4.93	-3.45	3342.95	-3.10	-3.85	-4.80	-4.45	3537.55	-4.53	-4.61	-6.23	-5.21			
3165.52	-3.14	-2.83	-4.84	-3.43	3348.67	-3.44	-3.72	-5.14	-4.32	3543.28	-3.56	-3.91	-5.26	-4.51			
3171.24	-2.62	-2.82	-4.32	-3.42	3354.40	-3.62	-3.75	-5.32	-4.35	3549.00	-4.29	-3.95	-5.99	-4.55			
3176.97	-3.24	-2.94	-4.94	-3.54	3360.12	-4.03	-4.60	-5.73	-5.20	3563.87	-4.52	-4.02	-6.22	-4.62			
3182.69	-3.17	-3.43	-4.87	-4.03	3365.85	-3.38	-3.97	-5.08	-4.57	3578.75	-4.32	-4.16	-6.02	-4.76			
3188.41	-3.65	-3.21	-5.35	-3.81	3371.57	-2.95	-3.42	-4.65	-4.02	3593.62	-4.24	-4.24	-5.94	-4.84			
3194.14	-4.02	-2.83	-5.72	-3.43	3377.29	-3.28	-3.28	-4.98	-3.88	3608.49	-2.82	-3.51	-4.52	-4.11			
3199.86	-3.57	-3.38	-5.27	-3.98	3383.02	-3.14	-3.92	-4.84	-4.52	3623.37	-2.92	-3.99	-4.62	-4.59			
3205.59	-3.33	-3.73	-5.03	-4.33	3388.74	-3.43	-3.89	-5.13	-4.49	3638.24	-2.15	-3.58	-3.85	-4.18			
3211.31	-3.23	-3.99	-4.93	-4.59	3394.46	-4.01	-4.05	-5.71	-4.65	3653.11	-3.14	-3.09	-4.84	-3.69			

**APPENDIX 4 - STALAGMITE DATA**

		RAW DATA		CORRECTION ARAGONITE				RAW DATA		CORRECTION ARAGONITE				RAW DATA		CORRECTION ARAGONITE	
AGE (Yr)	T8 13C	T8 18O	T8 13C	T8 18O	AGE (Yr)	T8 13C	T8 18O	T8 13C	T8 18O	AGE (Yr)	T8 13C	T8 18O	T8 13C	T8 18O	AGE (Yr)	T8 13C	T8 18O
3667.99	-3.73	-3.93	-5.43	-4.53	4143.94	-4.06	-4.29	-5.76	-4.89	4634.76	-3.43	-3.55	-5.13	-4.15			
3682.86	-3.77	-3.75	-5.47	-4.35	4158.81	-4.11	-4.59	-5.81	-5.19	4649.63	-4.16	-3.62	-5.86	-4.22			
3697.73	-4.23	-3.37	-5.93	-3.97	4173.68	-3.56	-4.46	-5.26	-5.06	4664.51	-3.89	-3.81	-5.59	-4.41			
3712.61	-4.53	-4.71	-6.23	-5.31	4188.56	-4.08	-3.64	-5.78	-4.24	4694.25	-3.51	-3.31	-5.21	-3.91			
3727.48	-4.71	-4.41	-6.41	-5.01	4203.43	-4.04	-3.95	-5.74	-4.55	4709.13	-4.08	-3.66	-5.78	-4.26			
3742.35	-4.77	-3.80	-6.47	-4.40	4218.30	-4.29	-4.13	-5.99	-4.73	4724.00	-4.07	-3.49	-5.77	-4.09			
3757.23	-4.58	-3.80	-6.28	-4.40	4233.18	-4.57	-4.39	-6.27	-4.99	4731.23	-3.29	-3.52	-4.99	-4.12			
3772.10	-4.18	-3.93	-5.88	-4.53	4248.05	-3.47	-4.10	-5.17	-4.70	4738.46	-2.98	-3.61	-4.68	-4.21			
3786.97	-4.52	-4.06	-6.22	-4.66	4262.92	-4.00	-4.73	-5.70	-5.33	4745.69	-2.77	-3.15	-4.47	-3.75			
3801.85	-4.08	-3.74	-5.78	-4.34	4277.80	-3.92	-4.09	-5.62	-4.69	4752.92	-2.42	-3.32	-4.12	-3.92			
3816.72	-4.58	-4.13	-6.28	-4.73	4292.67	-3.45	-3.73	-5.15	-4.33	4760.15	-3.49	-3.42	-5.19	-4.02			
3831.59	-4.27	-3.69	-5.97	-4.29	4307.54	-2.26	-3.31	-3.96	-3.91	4767.38	-2.87	-3.36	-4.57	-3.96			
3846.47	-4.66	-4.30	-6.36	-4.90	4322.42	-3.91	-4.38	-5.61	-4.98	4774.62	-3.36	-3.78	-5.06	-4.38			
3861.34	-2.40	-2.78	-4.10	-3.38	4337.29	-3.53	-4.50	-5.23	-5.10	4781.85	-3.46	-4.43	-5.16	-5.03			
3876.22	-2.80	-2.87	-4.50	-3.47	4352.16	-3.04	-3.75	-4.74	-4.35	4789.08	-3.63	-4.33	-5.33	-4.93			
3891.09	-3.40	-2.96	-5.10	-3.56	4367.04	-4.25	-3.56	-5.95	-4.16	4796.31	-3.15	-3.93	-4.85	-4.53			
3905.96	-4.39	-3.52	-6.09	-4.12	4381.91	-3.47	-3.57	-5.17	-4.17	4803.54	-3.09	-3.45	-4.79	-4.05			
3920.84	-3.93	-3.29	-5.63	-3.89	4396.78	-3.74	-3.87	-5.44	-4.47	4810.77	-3.16	-2.96	-4.86	-3.56			
3935.71	-4.12	-3.31	-5.82	-3.91	4411.66	-4.33	-3.42	-6.03	-4.02	4818.00	-3.64	-3.58	-5.34	-4.18			
3950.58	-3.99	-3.44	-5.69	-4.04	4426.53	-3.83	-3.56	-5.53	-4.16	4832.46	-3.98	-3.97	-5.68	-4.57			
3965.46	-4.12	-3.75	-5.82	-4.35	4441.41	-3.49	-3.49	-5.19	-4.09	4839.69	-3.39	-3.31	-5.09	-3.91			
3980.33	-4.46	-3.40	-6.16	-4.00	4456.28	-4.06	-4.33	-5.76	-4.93	4846.92	-3.42	-3.94	-5.12	-4.54			
3995.20	-3.24	-3.21	-4.94	-3.81	4466.03	-4.02	-4.89	-5.72	-5.49	4854.15	-3.36	-3.66	-5.06	-4.26			
4010.08	-4.19	-3.71	-5.89	-4.31	4500.90	-3.02	-3.92	-4.72	-4.52	4861.38	-3.93	-3.72	-5.63	-4.32			
4024.95	-3.98	-3.65	-5.68	-4.25	4515.77	-3.89	-3.56	-5.59	-4.16	4868.62	-3.74	-3.33	-5.44	-3.93			
4039.82	-4.23	-3.20	-5.93	-3.80	4530.65	-3.68	-4.10	-5.38	-4.70	4875.85	-3.57	-3.29	-5.27	-3.89			
4054.70	-4.55	-2.74	-6.25	-3.34	4545.52	-3.86	-4.24	-5.56	-4.84	4883.08	-3.47	-3.58	-5.17	-4.18			
4069.57	-4.48	-2.64	-6.18	-3.24	4560.39	-3.89	-4.00	-5.59	-4.60	4890.31	-3.46	-3.77	-5.16	-4.37			
4084.44	-3.38	-2.76	-5.08	-3.36	4575.27	-3.33	-3.35	-5.03	-3.95	4897.54	-4.49	-4.47	-6.19	-5.07			
4099.32	-2.87	-2.78	-4.57	-3.36	4590.14	-3.58	-3.00	-5.28	-3.60	4904.77	-4.24	-4.04	-5.94	-4.64			
4114.19	-3.82	-3.36	-5.52	-3.96	4605.01	-3.79	-3.25	-5.49	-3.85	4912.00	-3.76	-4.16	-5.46	-4.76			
4129.06	-4.86	-4.09	-6.56	-4.69	4619.89	-2.80	-3.22	-4.50	-3.82	4919.23	-4.12	-4.42	-5.82	-5.02			



**APPENDIX 4 - STALAGMITE DATA**

AGE (Yr)	RAW DATA		CORRECTION ARAGONITE		AGE (Yr)	RAW DATA		CORRECTION ARAGONITE		AGE (Yr)	RAW DATA		CORRECTION ARAGONITE	
	T8 13C	T8 18O	T8 13C	T8 18O		T8 13C	T8 18O	T8 13C	T8 18O		T8 13C	T8 18O	T8 13C	T8 18O
4926.46	-3.68	-4.03	-5.38	-4.63	5217.71	-4.14	-4.35	-5.84	-4.95	5594.40	-5.04	-3.92	-6.74	-4.52
4933.69	-3.68	-4.37	-5.38	-4.97	5229.49	-3.66	-3.43	-5.36	-4.03	5606.17	-4.51	-3.13	-6.21	-3.73
4940.92	-3.68	-4.26	-5.38	-4.86	5241.26	-3.72	-3.08	-5.42	-3.68	5617.94	-5.00	-4.11	-6.70	-4.71
4948.15	-4.49	-4.47	-6.19	-5.07	5253.03	-3.18	-2.47	-4.88	-3.07	5629.71	-4.75	-4.27	-6.45	-4.87
4955.38	-3.34	-3.97	-5.04	-4.57	5264.80	-3.08	-3.13	-4.78	-3.73	5641.49	-4.61	-3.78	-6.31	-4.38
4962.62	-3.79	-3.72	-5.49	-4.32	5276.57	-3.98	-3.29	-5.68	-3.89	5653.26	-4.50	-3.86	-6.20	-4.46
4969.85	-3.75	-3.54	-5.45	-4.14	5288.34	-3.90	-3.31	-5.60	-3.91	5665.03	-4.65	-3.47	-6.35	-4.07
4977.08	-3.74	-3.36	-5.44	-3.96	5300.11	-4.16	-3.95	-5.86	-4.55	5676.80	-4.45	-3.41	-6.15	-4.01
4991.54	-3.81	-3.73	-5.51	-4.33	5311.89	-3.77	-3.61	-5.47	-4.21	5688.57	-5.41	-3.76	-7.11	-4.36
4998.77	-3.77	-3.85	-5.47	-4.45	5323.66	-4.20	-3.45	-5.90	-4.05	5700.34	-5.17	-3.33	-6.87	-3.93
5006.00	-3.25	-3.72	-4.95	-4.32	5335.43	-5.33	-5.09	-7.03	-5.89	5712.11	-4.68	-3.49	-6.38	-4.09
5013.23	-3.33	-2.86	-5.03	-3.46	5347.20	-4.72	-3.60	-6.42	-4.20	5723.89	-4.65	-3.24	-6.35	-3.84
5020.46	-3.96	-3.43	-5.66	-4.03	5358.97	-4.30	-4.34	-6.00	-4.94	5735.66	-4.60	-3.18	-6.30	-3.78
5027.69	-4.56	-4.18	-6.26	-4.78	5370.74	-3.95	-4.05	-5.65	-4.65	5747.43	-4.25	-3.13	-5.95	-3.73
5034.92	-4.08	-3.77	-5.78	-4.37	5382.51	-4.35	-4.45	-6.05	-5.05	5759.20	-4.18	-3.18	-5.88	-3.78
5042.15	-4.48	-4.12	-6.18	-4.72	5394.29	-4.29	-3.76	-5.99	-4.36	5770.97	-4.77	-3.18	-6.47	-3.78
5049.38	-4.06	-3.35	-5.76	-3.95	5406.06	-3.93	-3.33	-5.63	-3.93	5782.74	-4.07	-3.26	-5.77	-3.86
5056.62	-4.28	-3.17	-5.98	-3.77	5417.83	-4.50	-3.33	-6.20	-3.93	5794.51	-4.30	-3.33	-6.00	-3.93
5063.85	-4.04	-3.12	-5.74	-3.72	5429.60	-3.86	-3.13	-5.56	-3.73	5806.29	-3.55	-2.87	-5.25	-3.47
5071.08	-4.37	-3.08	-6.07	-3.68	5441.37	-4.01	-3.31	-5.71	-3.91	5818.06	-5.25	-3.96	-6.95	-4.56
5078.31	-4.90	-3.11	-6.60	-3.71	5453.14	-4.82	-3.74	-6.52	-4.34	5830.83	-5.04	-4.34	-6.74	-4.94
5085.54	-4.48	-3.68	-6.18	-4.28	5464.91	-4.45	-3.78	-6.15	-4.38	5843.60	-4.92	-4.14	-6.62	-4.74
5092.77	-4.11	-3.68	-5.81	-4.28	5476.69	-4.48	-3.14	-6.18	-3.74	5856.37	-4.05	-3.65	-5.75	-4.25
5100.00	-4.09	-3.43	-5.79	-4.03	5488.46	-4.40	-3.85	-6.10	-4.45	5869.14	-3.75	-3.27	-5.45	-3.87
5111.77	-3.67	-3.12	-5.37	-3.72	5500.23	-3.77	-3.74	-5.47	-4.34	5881.91	-4.90	-2.72	-6.60	-3.32
5123.54	-4.01	-3.49	-5.71	-4.09	5512.00	-3.75	-3.56	-5.45	-4.16	5894.68	-5.13	-3.51	-6.83	-4.11
5135.31	-4.44	-3.60	-6.14	-4.20	5523.77	-3.90	-4.24	-5.60	-4.84	5907.45	-4.41	-3.15	-6.11	-3.75
5147.09	-3.13	-3.43	-4.83	-4.03	5535.54	-4.11	-4.29	-5.81	-4.89	5920.22	-4.76	-3.46	-6.46	-4.06
5158.86	-3.64	-4.12	-5.34	-4.72	5547.31	-3.51	-3.91	-5.21	-4.51	5932.99	-3.12	-3.47	-4.82	-4.07
5170.63	-2.39	-3.36	-4.09	-3.96	5559.09	-3.81	-4.55	-5.51	-5.15	5945.76	-3.96	-2.99	-5.66	-3.59
5182.40	-3.70	-3.78	-5.40	-4.38	5570.86	-4.22	-3.29	-5.92	-3.89	5958.53	-4.25	-3.64	-5.95	-4.24
5205.94	-4.30	-3.94	-6.00	-4.54	5582.63	-4.73	-3.30	-6.43	-3.90	5971.30	-4.13	-3.80	-5.83	-4.40

**APPENDIX 4 - STALAGMITE DATA**

		CORRECTION				CORRECTION				RAW DATA		CORRECTION			
RAW DATA		ARAGONITE		RAW DATA		ARAGONITE		RAW DATA		ARAGONITE		RAW DATA		ARAGONITE	
AGE (Yr)	T8 13C	T8 18O	T8 13C	T8 18O	AGE (Yr)	T8 13C	T8 18O	T8 13C	T8 18O	AGE (Yr)	T8 13C	T8 18O	T8 13C	T8 18O	
5994.63	-4.31	-4.34	-6.01	-4.94	6371.31	-4.39	-3.74	-6.09	-4.34	6761.97	-3.25	-2.82	-4.95	-3.42	
6006.40	-4.37	-4.16	-6.07	-4.76	6383.09	-4.56	-3.21	-6.26	-3.81	6775.93	-4.62	-3.08	-6.32	-3.68	
6018.17	-3.95	-3.54	-5.65	-4.14	6394.86	-4.78	-3.58	-6.48	-4.18	6789.90	-4.65	-2.84	-6.35	-3.44	
6029.94	-3.95	-3.33	-5.65	-3.93	6406.63	-4.15	-4.01	-5.85	-4.61	6803.86	-5.39	-3.17	-7.09	-3.77	
6041.71	-3.58	-2.51	-5.28	-3.11	6418.40	-4.22	-3.63	-5.92	-4.23	6817.83	-4.19	-2.57	-5.89	-3.17	
6053.49	-4.21	-3.35	-5.91	-3.95	6430.17	-4.37	-2.92	-6.07	-3.52	6831.79	-4.45	-3.02	-6.15	-3.62	
6065.26	-3.29	-2.80	-4.99	-3.40	6441.94	-4.32	-3.35	-6.02	-3.95	6845.76	-3.74	-3.34	-5.44	-3.94	
6077.03	-3.38	-3.17	-5.08	-3.77	6453.71	-5.09	-3.62	-6.79	-4.22	6859.72	-4.86	-3.31	-6.56	-3.91	
6088.80	-3.82	-3.77	-5.52	-4.37	6465.49	-4.82	-3.37	-6.52	-3.97	6873.69	-5.09	-3.48	-6.79	-4.08	
6100.57	-3.77	-3.43	-5.47	-4.03	6477.26	-4.91	-3.73	-6.61	-4.33	6887.66	-4.26	-3.13	-5.96	-3.73	
6112.34	-3.29	-3.40	-4.99	-4.00	6489.03	-4.37	-3.31	-6.07	-3.91	6901.62	-4.37	-3.21	-6.07	-3.81	
6124.11	-4.06	-3.84	-5.76	-4.24	6500.80	-4.28	-3.19	-5.98	-3.79	6915.59	-4.10	-3.23	-5.80	-3.83	
6135.89	-4.05	-3.70	-5.75	-4.30	6512.57	-4.00	-3.42	-5.70	-4.02	6929.55	-3.29	-1.82	-4.99	-2.42	
6147.66	-3.17	-2.98	-4.87	-3.58	6524.34	-4.36	-3.43	-6.06	-4.03	6943.52	-4.28	-3.21	-5.98	-3.81	
6159.43	-3.16	-2.72	-4.86	-3.32	6536.11	-4.90	-3.26	-6.60	-3.86	6957.48	-4.15	-3.14	-5.85	-3.74	
6171.20	-4.72	-4.02	-6.42	-4.62	6547.89	-4.00	-2.66	-5.70	-3.26	6971.45	-3.03	-2.66	-4.73	-3.26	
6182.97	-4.76	-3.82	-6.46	-4.42	6559.66	-3.93	-3.21	-5.63	-3.81	6985.41	-4.41	-3.49	-6.11	-4.09	
6194.74	-4.15	-2.99	-5.85	-3.59	6571.43	-4.54	-3.12	-6.24	-3.72	6999.38	-3.65	-2.98	-5.35	-3.58	
6206.51	-3.96	-3.46	-5.66	-4.06	6583.20	-4.49	-3.02	-6.19	-3.62	7013.34	-3.31	-3.12	-5.01	-3.72	
6218.29	-4.21	-3.90	-5.91	-4.50	6594.97	-4.60	-2.73	-6.30	-3.33	7027.31	-3.67	-3.11	-5.37	-3.71	
6230.06	-4.38	-4.15	-6.08	-4.75	6606.74	-4.84	-3.19	-6.54	-3.79	7041.28	-3.46	-2.75	-5.16	-3.35	
6241.83	-4.42	-3.97	-6.12	-4.57	6618.51	-4.63	-3.03	-6.33	-3.63	7055.24	-4.72	-3.92	-6.42	-4.52	
6253.60	-3.79	-3.47	-5.49	-4.07	6630.29	-4.80	-3.74	-6.50	-4.34	7069.21	-3.94	-3.18	-5.64	-3.78	
6265.37	-4.08	-3.83	-5.78	-4.43	6642.06	-3.31	-2.87	-5.01	-3.47	7083.17	-3.90	-3.53	-5.60	-4.13	
6277.14	-3.69	-3.63	-5.39	-4.23	6653.83	-4.19	-3.05	-5.89	-3.65	7097.14	-3.92	-3.51	-5.62	-4.11	
6288.91	-4.47	-3.35	-6.17	-3.95	6665.60	-4.72	-3.80	-6.42	-4.40	7111.10	-4.18	-3.46	-5.88	-4.06	
6300.69	-5.20	-3.68	-6.90	-4.28	6677.37	-4.74	-3.29	-6.44	-3.89	7125.07	-3.84	-2.47	-5.54	-3.07	
6312.46	-3.71	-3.83	-5.41	-4.43	6689.14	-4.73	-3.15	-6.43	-3.75	7139.03	-4.04	-2.75	-5.74	-3.35	
6324.23	-3.93	-3.76	-5.63	-4.36	6700.91	-4.17	-2.84	-5.87	-3.44	7153.00	-3.81	-3.09	-5.51	-3.69	
6336.00	-3.77	-3.59	-5.47	-4.19	6712.69	-4.77	-2.89	-6.47	-3.49	7166.97	-3.87	-3.73	-5.57	-4.33	
6347.77	-4.42	-3.06	-6.12	-3.66	6724.46	-4.72	-3.53	-6.42	-4.13	7180.93	-3.52	-3.60	-5.22	-4.20	
6359.54	-3.89	-2.91	-5.59	-3.51	6736.23	-5.26	-3.30	-6.96	-3.90	7194.90	-3.94	-3.34	-5.64	-3.94	

**APPENDIX 4 - STALAGMITE DATA**

AGE (Yr)	RAW DATA		CORRECTION ARAGONITE		AGE (Yr)	RAW DATA		CORRECTION ARAGONITE		AGE (Yr)	RAW DATA		CORRECTION ARAGONITE	
	T8 13C	T8 18O	T8 13C	T8 18O		T8 13C	T8 18O	T8 13C	T8 18O		T8 13C	T8 18O	T8 13C	T8 18O
7208.86	-4.06	-3.33	-5.78	-3.93	7673.71	-3.65	-2.83	-5.35	-3.43	8136.55	-3.50	-3.06	-5.20	-3.66
7222.83	-3.90	-3.00	-5.60	-3.60	7688.17	-3.83	-2.81	-5.53	-3.41	8151.01	-3.82	-3.20	-5.52	-3.80
7236.79	-3.32	-3.07	-5.02	-3.67	7702.64	-4.76	-3.24	-6.46	-3.84	8165.48	-3.65	-2.89	-5.35	-3.49
7250.76	-4.51	-3.32	-6.21	-3.92	7717.10	-4.23	-2.92	-5.93	-3.52	8179.94	-3.78	-2.81	-5.48	-3.41
7264.72	-3.50	-3.09	-5.20	-3.69	7731.57	-4.08	-2.17	-5.78	-2.77	8194.41	-3.38	-2.52	-5.08	-3.12
7278.69	-3.93	-3.49	-5.63	-4.09	7746.03	-3.07	-2.37	-4.77	-2.97	8208.87	-2.05	-1.80	-3.75	-2.40
7292.66	-3.45	-3.20	-5.15	-3.80	7760.49	-3.37	-2.40	-5.07	-3.00	8237.80	-3.26	-2.76	-4.96	-3.36
7306.62	-3.69	-3.22	-5.39	-3.82	7774.96	-3.39	-3.01	-5.09	-3.61	8252.26	-3.21	-2.26	-4.91	-2.86
7320.59	-3.35	-2.83	-5.05	-3.43	7789.42	-3.28	-2.84	-4.98	-3.44	8266.72	-3.67	-2.50	-5.37	-3.10
7334.55	-3.95	-2.90	-5.65	-3.50	7803.88	-2.99	-2.53	-4.69	-3.13	8281.19	-3.52	-2.75	-5.22	-3.35
7348.52	-4.79	-3.36	-6.49	-3.96	7818.35	-3.65	-2.87	-5.35	-3.47	8295.65	-2.88	-1.70	-4.58	-2.30
7362.48	-4.30	-3.44	-6.00	-4.04	7832.81	-3.86	-3.21	-5.56	-3.81	8310.12	-3.43	-2.52	-5.13	-3.12
7376.45	-2.95	-2.96	-4.65	-3.56	7847.28	-4.59	-3.43	-6.29	-4.03	8324.58	-3.25	-2.27	-4.95	-2.87
7390.41	-2.81	-3.05	-4.51	-3.65	7861.74	-4.74	-3.06	-6.44	-3.66	8339.04	-3.53	-2.17	-5.23	-2.77
7404.38	-2.89	-3.73	-4.59	-4.33	7876.20	-4.72	-3.00	-6.42	-3.60	8353.51	-3.54	-1.95	-5.24	-2.55
7418.34	-2.91	-2.75	-4.61	-3.35	7890.67	-4.32	-3.24	-6.02	-3.84	8367.97	-3.54	-2.85	-5.24	-3.45
7432.31	-3.82	-3.60	-5.52	-4.20	7905.13	-4.26	-2.79	-5.96	-3.39	8382.43	-3.84	-3.17	-5.54	-3.77
7446.28	-3.70	-3.79	-5.40	-4.39	7919.59	-4.39	-2.93	-6.09	-3.53	8396.90	-3.94	-2.63	-5.64	-3.23
7460.24	-3.23	-3.59	-4.93	-4.19	7934.06	-4.09	-2.76	-5.79	-3.36	8411.36	-4.54	-2.92	-6.24	-3.52
7474.21	-3.53	-2.79	-5.23	-3.39	7948.52	-3.62	-2.51	-5.32	-3.11	8425.83	-4.81	-3.00	-6.51	-3.60
7488.17	-3.74	-2.99	-5.44	-3.59	7962.99	-3.71	-1.93	-5.41	-2.53	8440.29	-5.01	-2.74	-6.71	-3.34
7502.14	-3.37	-3.09	-5.07	-3.69	7977.45	-3.72	-2.05	-5.42	-2.65	8454.75	-4.99	-3.40	-6.69	-4.00
7516.10	-3.44	-2.67	-5.14	-3.27	7991.91	-3.66	-2.25	-5.36	-2.85	8469.22	-4.85	-2.54	-6.55	-3.14
7544.03	-3.43	-2.77	-5.13	-3.37	8006.38	-4.24	-2.88	-5.94	-3.48	8483.68	-4.50	-2.28	-6.20	-2.88
7558.00	-3.00	-2.14	-4.70	-2.74	8020.84	-4.15	-2.50	-5.85	-3.10	8498.14	-5.00	-2.37	-6.70	-2.97
7572.46	-3.67	-3.02	-5.37	-3.62	8035.30	-4.19	-3.02	-5.89	-3.62	8512.61	-4.59	-2.78	-6.29	-3.38
7586.93	-3.57	-3.30	-5.27	-3.90	8049.77	-4.02	-2.45	-5.72	-3.05	8527.07	-5.39	-3.81	-7.09	-4.41
7601.39	-4.24	-3.29	-5.94	-3.89	8064.23	-4.21	-3.10	-5.91	-3.70	8541.54	-5.67	-3.24	-7.37	-3.84
7615.86	-3.25	-2.89	-4.95	-3.49	8078.70	-4.07	-4.01	-5.77	-4.61	8556.00	-5.10	-2.34	-6.80	-2.94
7630.32	-2.84	-3.51	-4.54	-4.11	8093.16	-3.93	-2.42	-5.63	-3.02	8570.95	-4.66	-1.95	-6.36	-2.55
7644.78	-3.80	-2.95	-5.50	-3.55	8107.62	-3.63	-2.45	-5.33	-3.05	8585.89	-5.67	-3.36	-7.37	-3.96
7659.25	-3.67	-2.66	-5.37	-3.26	8122.09	-3.91	-3.37	-5.61	-3.97	8600.84	-4.93	-2.15	-6.63	-2.75

**APPENDIX 4 - STALAGMITE DATA**

AGE (Yr)	RAW DATA		CORRECTION ARAGONITE		AGE (Yr)	RAW DATA		CORRECTION ARAGONITE		AGE (Yr)	RAW DATA		CORRECTION ARAGONITE	
	T8 13C	T8 18O	T8 13C	T8 18O		T8 13C	T8 18O	T8 13C	T8 18O		T8 13C	T8 18O	T8 13C	T8 18O
8615.78	-5.02	-1.87	-6.72	-2.47	9094.04	-4.25	-1.53	-5.95	-2.13	9500.46	-4.21	-2.93	-5.91	-3.53
8630.73	-4.79	-1.97	-6.49	-2.57	9108.98	-2.36	-0.93	-4.06	-1.53	9509.88	-4.69	-2.89	-6.39	-3.49
8645.67	-4.51	-1.93	-6.21	-2.53	9123.93	-3.61	-1.33	-5.31	-1.93	9519.30	-3.08	-2.10	-4.78	-2.70
8660.62	-5.12	-2.78	-6.82	-3.38	9138.87	-3.89	-1.61	-5.59	-2.21	9528.72	-3.87	-1.64	-5.57	-2.24
8675.56	-5.30	-2.97	-7.00	-3.57	9153.82	-4.15	-1.21	-5.85	-1.81	9538.14	-3.60	-1.60	-5.30	-2.20
8690.51	-4.71	-2.34	-6.41	-2.94	9168.76	-3.79	-0.92	-5.49	-1.52	9547.56	-4.16	-1.88	-5.86	-2.48
8705.45	-5.47	-2.73	-7.17	-3.33	9183.71	-4.75	-1.69	-6.45	-2.29	9556.98	-3.75	-2.10	-5.45	-2.70
8720.40	-5.20	-3.39	-6.90	-3.99	9198.65	-5.03	-2.02	-6.73	-2.62	9566.40	-4.25	-2.01	-5.95	-2.61
8735.35	-5.56	-2.99	-7.26	-3.59	9213.60	-4.81	-1.48	-6.51	-2.08	9575.81	-5.28	-2.94	-6.98	-3.54
8750.29	-5.76	-3.34	-7.46	-3.94	9228.55	-4.61	-2.14	-6.31	-2.74	9585.23	-4.57	-2.69	-6.27	-3.29
8765.24	-5.21	-2.44	-6.91	-3.04	9243.49	-4.45	-1.67	-6.15	-2.27	9594.65	-4.64	-1.98	-6.34	-2.58
8780.18	-4.83	-1.74	-6.53	-2.34	9258.44	-4.81	-1.98	-6.51	-2.58	9604.07	-3.12	-2.50	-4.82	-3.10
8795.13	-5.21	-2.05	-6.91	-2.65	9273.38	-4.40	-1.90	-6.10	-2.50	9613.49	-4.82	-2.64	-6.52	-3.24
8810.07	-5.64	-2.65	-7.34	-3.25	9288.33	-5.09	-2.32	-6.79	-2.92	9622.91	-4.54	-2.32	-6.24	-2.92
8825.02	-4.99	-1.82	-6.69	-2.42	9303.27	-5.10	-2.03	-6.80	-2.63	9632.33	-5.24	-2.90	-6.94	-3.50
8839.96	-5.74	-1.92	-7.44	-2.52	9318.22	-3.43	-1.88	-5.13	-2.48	9641.75	-4.70	-2.61	-6.40	-3.21
8854.91	-5.61	-2.55	-7.31	-3.15	9333.16	-4.31	-1.13	-6.01	-1.73	9651.17	-4.53	-2.18	-6.23	-2.78
8869.85	-5.77	-3.15	-7.47	-3.75	9348.11	-3.40	-0.96	-5.10	-1.56	9660.59	-3.68	-1.91	-5.38	-2.51
8884.80	-5.28	-2.16	-6.98	-2.76	9363.05	-4.32	-1.76	-6.02	-2.36	9670.01	-4.15	-2.28	-5.85	-2.88
8899.75	-5.28	-2.13	-6.98	-2.73	9378.00	-4.20	-1.80	-5.90	-2.40	9679.43	-4.76	-1.85	-6.46	-2.45
8914.69	-5.48	-2.69	-7.18	-3.29	9387.42	-3.99	-1.57	-5.69	-2.17	9688.85	-4.48	-2.50	-6.18	-3.10
8929.64	-4.66	-2.38	-6.36	-2.98	9396.84	-4.02	-1.92	-5.72	-2.52	9698.27	-4.58	-2.21	-6.28	-2.81
8944.58	-5.46	-1.72	-7.16	-2.32	9406.26	-4.13	-2.01	-5.83	-2.61	9707.69	-4.08	-2.74	-5.78	-3.34
8959.53	-5.74	-2.10	-7.44	-2.70	9415.68	-2.99	-1.23	-4.69	-1.83	9717.11	-4.12	-1.90	-5.82	-2.50
8974.47	-4.96	-2.14	-6.66	-2.74	9425.10	-3.34	-0.78	-5.04	-1.38	9726.53	-3.42	-1.87	-5.12	-2.47
8989.42	-4.52	-2.55	-6.22	-3.15	9434.52	-3.07	-0.97	-4.77	-1.57	9735.95	-4.13	-1.57	-5.83	-2.17
9004.36	-4.32	-1.91	-6.02	-2.51	9443.94	-3.82	-1.42	-5.52	-2.02	9745.37	-4.15	-2.16	-5.85	-2.76
9019.31	-3.96	-2.24	-5.66	-2.84	9453.36	-4.24	-1.61	-5.94	-2.21	9754.79	-4.30	-2.11	-6.00	-2.71
9034.25	-4.07	-2.25	-5.77	-2.85	9462.78	-4.59	-2.05	-6.29	-2.65	9764.21	-4.44	-1.81	-6.14	-2.41
9049.20	-4.54	-1.77	-6.24	-2.37	9472.20	-4.34	-2.07	-6.04	-2.67	9773.63	-4.36	-2.57	-6.06	-3.17
9064.15	-4.44	-2.17	-6.14	-2.77	9481.62	-4.04	-2.44	-5.74	-3.04	9783.05	-3.16	-3.30	-4.86	-3.90
9079.09	-4.16	-2.04	-5.86	-2.64	9491.04	-4.96	-2.50	-6.66	-3.10	9792.47	-4.56	-2.75	-6.26	-3.35

**APPENDIX 4 - STALAGMITE DATA**

AGE (Yr)	RAW DATA		CORRECTION ARAGONITE		AGE (Yr)	RAW DATA		CORRECTION ARAGONITE		AGE (Yr)	RAW DATA		CORRECTION ARAGONITE	
	T8 13C	T8 18O	T8 13C	T8 18O		T8 13C	T8 18O	T8 13C	T8 18O		T8 13C	T8 18O	T8 13C	T8 18O
9801.89	-4.85	-2.47	-6.55	-3.07	10122.16	-2.08	-1.62	-3.78	-2.22	13208.16	-6.37	-3.45	-6.37	-3.45
9811.31	-4.56	-2.32	-6.26	-2.92	10131.58	-3.60	-1.99	-5.30	-2.59	13244.76	-5.24	-2.98	-5.24	-2.96
9820.73	-3.49	-1.87	-5.19	-2.47	10141.00	-1.91	-1.85	-3.61	-2.45	13281.36	-5.28	-3.72	-5.28	-3.72
9830.15	-3.21	-1.32	-4.91	-1.92	10150.00	-2.45	-2.35	-4.15	-2.95	13317.95	-5.21	-3.58	-5.21	-3.58
9839.57	-4.59	-2.05	-6.29	-2.65	10160.00	-1.74	-1.70	-3.44	-2.30	13354.55	-5.47	-3.32	-5.47	-3.32
9848.99	-4.44	-2.34	-6.14	-2.94	12640.00	-1.64	-1.98	-3.34	-2.58	13397.00	-5.56	-3.30	-5.56	-3.30
9858.41	-4.20	-2.41	-5.90	-3.01	12658.00	-1.66	-1.79	-3.36	-2.39	13439.44	-5.83	-3.72	-5.83	-3.72
9886.67	-2.96	-1.53	-4.66	-2.13	12670.00	-2.10	-2.19	-3.80	-2.79	13481.88	-5.62	-4.26	-5.62	-4.26
9896.09	-3.94	-1.77	-5.64	-2.37	12687.00	-1.81	-2.64	-3.51	-3.24	13524.32	-5.50	-3.75	-5.50	-3.75
9905.51	-3.64	-2.51	-5.34	-3.11	12704.80	-2.29	-2.84	-3.99	-3.44	13566.76	-5.72	-3.61	-5.72	-3.61
9914.93	-3.97	-1.86	-5.67	-2.46	12722.60	-1.21	-1.86	-2.91	-2.46	13609.20	-5.71	-3.52	-5.71	-3.52
9924.35	-4.34	-1.89	-6.04	-2.49	12740.39	-4.12	-2.87	-4.12	-2.87	13651.64	-5.64	-4.24	-5.64	-4.24
9933.77	-2.99	-1.84	-4.69	-2.44	12758.19	-4.67	-3.36	-4.67	-3.36	13694.08	-4.80	-3.31	-4.80	-3.31
9943.19	-3.20	-1.66	-4.90	-2.26	12775.99	-5.18	-3.40	-5.18	-3.40	13736.52	-4.52	-3.37	-4.52	-3.37
9952.60	-2.39	-0.99	-4.09	-1.59	12793.79	-4.53	-2.81	-4.53	-2.81	13778.97	-4.38	-3.48	-4.38	-3.48
9962.02	-2.54	-1.94	-4.24	-2.54	12811.59	-4.92	-3.12	-4.92	-3.12	13821.41	-4.74	-3.53	-4.74	-3.53
9971.44	-2.93	-1.30	-4.63	-1.90	12829.38	-5.55	-3.61	-5.55	-3.61	13863.85	-5.08	-3.51	-5.08	-3.51
9980.86	-1.74	-1.31	-3.44	-1.91	12847.18	-4.51	-2.66	-4.51	-2.66	13906.29	-5.65	-3.72	-5.65	-3.72
9990.28	-2.64	-1.20	-4.34	-1.80	12864.98	-5.47	-3.12	-5.47	-3.12	13948.73	-5.14	-3.22	-5.14	-3.22
9999.70	-2.86	-1.50	-4.56	-2.10	12882.78	-5.40	-3.56	-5.40	-3.56	13991.17	-5.93	-3.34	-5.93	-3.34
10009.12	-3.28	-2.15	-4.98	-2.75	12900.57	-4.43	-3.70	-4.43	-3.70	14076.05	-5.38	-3.27	-5.38	-3.27
10018.54	-3.27	-2.04	-4.97	-2.64	12918.37	-5.24	-3.86	-5.24	-3.86	14118.49	-5.23	-3.24	-5.23	-3.24
10027.96	-2.23	-1.07	-3.93	-1.67	12936.17	-5.34	-3.33	-5.34	-3.33	14160.94	-4.95	-3.77	-4.95	-3.77
10037.38	-2.30	-1.29	-4.00	-1.89	12953.97	-5.43	-2.77	-5.43	-2.77	14203.38	-4.65	-3.39	-4.65	-3.39
10046.80	-1.44	-1.01	-3.14	-1.61	12971.77	-4.98	-2.75	-4.98	-2.75	14328.66	-4.56	-3.52	-4.56	-3.52
10056.22	-1.53	-1.88	-3.23	-2.48	12989.56	-4.88	-3.36	-4.88	-3.36	14453.94	-4.66	-3.20	-4.66	-3.20
10065.64	-1.48	-1.64	-3.18	-2.24	13007.36	-5.12	-2.80	-5.12	-2.80	14579.22	-5.62	-3.56	-5.62	-3.56
10075.06	-2.67	-1.25	-4.37	-1.85	13025.16	-5.03	-2.68	-5.03	-2.68	14704.51	-5.37	-3.98	-5.37	-3.98
10084.48	-2.90	-1.62	-4.60	-2.22	13061.76	-4.63	-2.97	-4.63	-2.97	14829.79	-5.20	-3.71	-5.20	-3.71
10093.90	-2.46	-1.17	-4.16	-1.77	13098.36	-4.92	-2.98	-4.92	-2.98	14955.07	-4.56	-3.45	-4.56	-3.45
10103.32	-2.97	-2.46	-4.67	-3.06	13134.96	-5.54	-3.93	-5.54	-3.93	15205.64	-4.59	-3.44	-4.59	-3.44
10112.74	-2.46	-2.29	-4.16	-2.89	13171.56	-5.79	-3.19	-5.79	-3.19	15330.92	-5.01	-3.34	-5.01	-3.34

**APPENDIX 4 - STALAGMITE DATA**

AGE (Yr)	RAW DATA		CORRECTION ARAGONITE		AGE (Yr)	RAW DATA		CORRECTION ARAGONITE		AGE (Yr)	RAW DATA		CORRECTION ARAGONITE	
	T8 13C	T8 18O	T8 13C	T8 18O		T8 13C	T8 18O	T8 13C	T8 18O		T8 13C	T8 18O	T8 13C	T8 18O
15368.93	-5.37	-4.38	-5.37	-4.38	16989.41	-3.65	-2.72	-3.65	-2.72	18758.46	-5.88	-2.39	-5.88	-2.39
15406.93	-4.14	-3.03	-4.14	-3.03	17044.69	-4.76	-2.42	-4.76	-2.42	18813.74	-5.44	-3.68	-5.44	-3.68
15444.94	-4.06	-3.07	-4.06	-3.07	17099.97	-4.67	-2.55	-4.67	-2.55	18869.02	-5.80	-3.01	-5.80	-3.01
15482.95	-3.88	-2.90	-3.88	-2.90	17155.25	-5.05	-2.84	-5.05	-2.84	18924.31	-5.20	-3.08	-5.20	-3.08
15520.95	-3.83	-3.70	-3.83	-3.70	17210.54	-4.69	-3.14	-4.69	-3.14	18979.59	-5.16	-3.47	-5.16	-3.47
15558.96	-3.77	-3.40	-3.77	-3.40	17265.82	-4.48	-3.00	-4.48	-3.00	19034.87	-5.57	-3.07	-5.57	-3.07
15596.97	-4.35	-3.20	-4.35	-3.20	17321.10	-5.09	-3.40	-5.09	-3.40	19090.16	-6.08	-3.20	-6.08	-3.20
15634.97	-3.90	-3.31	-3.90	-3.31	17376.39	-5.13	-3.14	-5.13	-3.14	19145.44	-5.81	-2.79	-5.81	-2.79
15672.98	-4.44	-3.53	-4.44	-3.53	17431.67	-3.67	-3.04	-3.67	-3.04	19200.72	-4.96	-2.85	-4.96	-2.85
15749.00	-3.45	-3.29	-3.45	-3.29	17486.95	-4.59	-3.65	-4.59	-3.65	19256.00	-5.26	-3.20	-5.26	-3.20
15787.00	-3.66	-3.69	-3.66	-3.69	17542.23	-5.47	-3.60	-5.47	-3.60	19311.29	-5.21	-2.92	-5.21	-2.92
15825.01	-3.90	-3.11	-3.90	-3.11	17597.52	-5.96	-4.41	-5.96	-4.41	19366.57	-5.55	-3.79	-5.55	-3.79
15863.02	-3.34	-2.73	-3.34	-2.73	17652.80	-5.83	-3.89	-5.83	-3.89	19421.85	-5.78	-2.84	-5.78	-2.84
15901.02	-3.40	-2.50	-3.40	-2.50	17708.08	-5.09	-3.49	-5.09	-3.49	19477.14	-5.57	-2.78	-5.57	-2.78
15939.03	-4.80	-3.17	-4.80	-3.17	17763.37	-6.22	-3.39	-6.22	-3.39	19532.42	-5.52	-2.97	-5.52	-2.97
15994.31	-4.29	-3.15	-4.29	-3.15	17818.65	-5.18	-3.27	-5.18	-3.27	19587.70	-4.73	-3.40	-4.73	-3.40
16049.60	-3.68	-3.61	-3.68	-3.61	17873.93	-5.72	-2.74	-5.72	-2.74	19641.83	-5.06	-2.21	-5.06	-2.21
16104.88	-3.95	-3.07	-3.95	-3.07	17929.21	-5.37	-3.12	-5.37	-3.12	19695.96	-4.73	-3.40	-4.73	-3.40
16215.44	-4.38	-3.06	-4.38	-3.06	17984.50	-5.17	-2.75	-5.17	-2.75	19750.10	-5.06	-2.21	-5.06	-2.21
16270.73	-3.94	-3.84	-3.94	-3.84	18039.78	-5.25	-2.99	-5.25	-2.99	19804.23	-4.03	-2.95	-4.03	-2.95
16326.01	-3.78	-2.85	-3.78	-2.85	18095.06	-5.55	-3.40	-5.55	-3.40	19858.36	-3.64	-2.64	-3.64	-2.64
16381.29	-3.81	-2.49	-3.81	-2.49	18150.35	-4.97	-2.92	-4.97	-2.92	19912.49	-5.11	-2.86	-5.11	-2.86
16436.58	-3.59	-2.60	-3.59	-2.60	18205.63	-5.69	-3.51	-5.69	-3.51	19966.62	-4.67	-3.01	-4.67	-3.01
16491.86	-4.05	-3.68	-4.05	-3.68	18260.91	-5.83	-2.90	-5.83	-2.90	20020.75	-5.44	-3.65	-5.44	-3.65
16547.14	-3.90	-2.87	-3.90	-2.87	18316.20	-5.96	-3.07	-5.96	-3.07	20074.88	-4.40	-2.42	-4.40	-2.42
16602.42	-4.24	-2.89	-4.24	-2.89	18371.48	-5.36	-3.27	-5.36	-3.27	20129.01	-4.30	-2.81	-4.30	-2.81
16657.71	-3.94	-2.54	-3.94	-2.54	18426.76	-5.79	-3.99	-5.79	-3.99	20183.14	-4.86	-2.98	-4.86	-2.98
16712.99	-4.38	-3.47	-4.38	-3.47	18482.04	-5.76	-3.20	-5.76	-3.20	20237.28	-5.02	-2.29	-5.02	-2.29
16768.27	-4.25	-2.82	-4.25	-2.82	18537.33	-6.06	-3.70	-6.06	-3.70	20291.41	-4.75	-3.07	-4.75	-3.07
16823.56	-3.47	-3.26	-3.47	-3.26	18592.61	-5.75	-4.12	-5.75	-4.12	20345.54	-4.80	-2.66	-4.80	-2.66
16878.84	-3.95	-2.95	-3.95	-2.95	18647.89	-5.21	-3.63	-5.21	-3.63	20399.67	-4.57	-3.16	-4.57	-3.16
16934.12	-3.58	-2.57	-3.58	-2.57	18703.18	-5.96	-3.41	-5.96	-3.41	20453.80	-5.20	-2.84	-5.20	-2.84

**APPENDIX 4 - STALAGMITE DATA**

AGE (Yr)	RAW DATA		CORRECTION ARAGONITE		AGE (Yr)	RAW DATA		CORRECTION ARAGONITE		AGE (Yr)	RAW DATA		CORRECTION ARAGONITE	
	T8 13C	T8 18O	T8 13C	T8 18O		T8 13C	T8 18O	T8 13C	T8 18O		T8 13C	T8 18O	T8 13C	T8 18O
20582.06	-5.10	-2.76	-5.10	-2.76	22348.39	-5.83	-2.81	-5.83	-2.81	23871.62	-4.20	-2.89	-4.20	-2.89
20616.19	-5.34	-3.50	-5.34	-3.50	22402.52	-5.99	-3.25	-5.99	-3.25	23914.43	-4.83	-3.32	-4.83	-3.32
20670.33	-5.10	-2.65	-5.10	-2.65	22456.65	-6.19	-3.37	-6.19	-3.37	23957.24	-4.23	-2.63	-4.23	-2.63
20724.46	-5.20	-2.95	-5.20	-2.95	22510.79	-6.49	-3.33	-6.49	-3.33	24000.06	-5.06	-3.04	-5.06	-3.04
20778.59	-5.47	-2.90	-5.47	-2.90	22564.92	-6.56	-3.96	-6.56	-3.96	24042.87	-4.89	-2.89	-4.89	-2.89
20832.72	-5.21	-2.99	-5.21	-2.99	22619.05	-5.57	-3.37	-5.57	-3.37	24085.68	-4.36	-2.77	-4.36	-2.77
20886.85	-3.61	-3.15	-3.61	-3.15	22673.18	-6.25	-3.74	-6.25	-3.74	24128.49	-4.22	-2.98	-4.22	-2.98
20940.98	-5.27	-3.68	-5.27	-3.68	22727.31	-6.64	-3.05	-6.64	-3.05	24171.31	-5.04	-2.87	-5.04	-2.87
20995.11	-5.03	-2.96	-5.03	-2.96	22781.44	-5.58	-3.00	-5.58	-3.00	24214.12	-5.25	-2.93	-5.25	-2.93
21049.24	-4.67	-3.20	-4.67	-3.20	22835.57	-5.90	-3.19	-5.90	-3.19	24256.93	-4.71	-3.06	-4.71	-3.06
21103.38	-5.42	-3.12	-5.42	-3.12	22889.70	-6.52	-3.45	-6.52	-3.45	24299.74	-4.73	-3.25	-4.73	-3.25
21157.51	-4.46	-3.12	-4.46	-3.12	22943.84	-5.49	-3.82	-5.49	-3.82	24342.56	-3.46	-2.61	-3.46	-2.61
21211.64	-5.65	-3.33	-5.65	-3.33	22997.97	-5.85	-3.26	-5.85	-3.26	24385.37	-4.01	-2.76	-4.01	-2.76
21265.77	-5.58	-3.32	-5.58	-3.32	23052.10	-4.19	-3.23	-4.19	-3.23	24428.18	-4.31	-2.77	-4.31	-2.77
21319.90	-5.21	-4.15	-5.21	-4.15	23106.23	-3.23	-3.12	-3.23	-3.12					
21374.03	-5.51	-3.37	-5.51	-3.37	23160.36	-5.19	-3.53	-5.19	-3.53					
21428.16	-5.57	-3.00	-5.57	-3.00	23186.62	-5.39	-3.35	-5.39	-3.35					
21482.29	-5.24	-2.92	-5.24	-2.92	23229.43	-3.95	-3.57	-3.95	-3.57					
21536.42	-5.60	-3.16	-5.60	-3.16	23272.24	-4.22	-3.21	-4.22	-3.21					
21590.56	-4.73	-3.21	-4.73	-3.21	23315.06	-5.52	-3.41	-5.52	-3.41					
21644.69	-5.23	-3.57	-5.23	-3.57	23357.87	-5.22	-3.40	-5.22	-3.40					
21698.82	-5.88	-3.08	-5.88	-3.08	23400.68	-4.38	-3.58	-4.38	-3.58					
21752.95	-6.10	-3.76	-6.10	-3.76	23443.49	-4.01	-3.15	-4.01	-3.15					
21807.08	-6.69	-3.31	-6.69	-3.31	23486.31	-4.70	-2.94	-4.70	-2.94					
21861.21	-6.46	-3.69	-6.46	-3.69	23529.12	-5.16	-3.46	-5.16	-3.46					
21915.34	-6.31	-3.85	-6.31	-3.85	23571.93	-5.37	-2.70	-5.37	-2.70					
21969.47	-6.14	-3.34	-6.14	-3.34	23614.74	-5.23	-3.23	-5.23	-3.23					
22023.61	-5.66	-3.25	-5.66	-3.25	23657.56	-4.98	-2.37	-4.98	-2.37					
22131.87	-4.34	-3.41	-4.34	-3.41	23700.37	-4.41	-2.42	-4.41	-2.42					
22186.00	-6.27	-3.30	-6.27	-3.30	23743.18	-4.63	-2.93	-4.63	-2.93					
22240.13	-5.03	-2.70	-5.03	-2.70	23785.99	-4.36	-3.17	-4.36	-3.17					
22294.26	-4.87	-2.63	-4.87	-2.63	23828.81	-4.46	-2.93	-4.46	-2.93					

**APPENDIX 5 - POLLEN DATA**

<b>CODE</b>	<b>NAME</b>	<b>CODE</b>	<b>NAME</b>	<b>CODE</b>	<b>NAME</b>	<b>CODE</b>	<b>NAME</b>
TRE	<i>TREMA</i>	RHA	RHAMNACEAE TYPE	ACL	<i>ACALYPHA</i>	HAL	HALORAGIDACEAE
PSO	<i>PSORALEA</i>	EUC	<i>EUCLEA</i>	COP	COMPOSITAE	NYM	<i>NYMPHAEA</i>
MYR	MYRTACEAE	DIO	<i>DIOSPYROS</i> TYPE	LAC	LACTUCOIDEAE	POT	POTAMOGETONACEAE
ALC	<i>ALCHORNEA</i>	SPI	<i>SPIROSTACHYS</i>	ART	<i>ARTEMISIA</i>	ERO	<i>ERIOCAULON</i>
KIG	<i>KIGGELARIA</i>	PAL	PALMAE	STO	<i>STOEBE</i> TYPE	ANH	<i>ANTHOCEROS</i> TYPE
MYI	MYRICACEAE	SCL	<i>SCLEROCARYA</i>	RUS	<i>RUSCHIA</i> TYPE	RIC	<i>RICCIA</i>
CLU	<i>CLUTIA</i> TYPE	ACA	<i>ACACIA</i>	TUL	<i>TULBAGHIA</i> TYPE	MON	MONOLETE SPORES
MYS	<i>MYRSINE</i> TYPE	MIO	MIMOSOIDEAE	ANT	<i>ANTHOSPERMUM</i>	TRI	TRILETE SPORES
POD	<i>PODOCARPUS</i>	PEL	<i>PELTOPHORUM</i>	THY	THYMELAEACEAE	LYO	<i>LYCOPODIUM</i>
CEL	<i>CELTIS</i>	COI	<i>COMMIPHORA</i>	MOH	<i>MOHRIA</i>	POY	POLYPODIACEAE
KIR	<i>KIRKIA</i>	TAR	TARCHONANTHEAE	CLI	<i>CLIFFORTIA</i>	PTE	<i>PTERIS</i>
BRA	<i>BRACHYSTEGLIA</i>	CAP	CAPPARACEAE	RES	RESTIONACEAE	CYP	CYPERACEAE
MIM	<i>MIMUSOPS</i>	OXY	<i>OXYGONUM</i>	PAS	<i>PASSERINA</i>	ASC	<i>ASCOLEPSIS</i>
BUR	<i>BURKEA</i>	ASP	<i>ASPARAGUS</i> TYPE	ERI	ERICACEAE	GEN	GENTIANACEAE
CAN	<i>CANTHIUM</i>	ALO	<i>ALOE</i> TYPE	AIZ	AIZOACEAE TYPE	PLA	<i>PLANTAGO</i>
CRO	<i>CROTON</i>	LAN	<i>LANNEA</i>	CHE	CHENOPODIACEAE TYPE	SOL	<i>SOLANAUM</i>
ENC	<i>ENCEPHALARTOS</i>	MAL	MALVACEAE	AMA	AMARANTHACEAE TYPE	LIL	LILIACEAE
BEQ	<i>BEQUAERTIODENDRON</i>	ACN	ACANTHACEAE	TRB	<i>TRIBULUS</i>	CEP	<i>CEPHALARIA</i>
PRO	PROTEACEAE	VAN	<i>VANGUERIA</i> TYPE	MYO	<i>MYROTHAMNUS</i>	SCA	<i>SCABIOSA</i>
OLE	OLEACEAE	SEL	SELAGINELLACEAE	MAR	<i>MARSILEA</i>	LAB	LABIATAE
EUP	<i>EUPHORBIA</i>	RUB	RUBIACEAE TYPE	TYP	<i>TYPHA</i>	CRA	<i>CRASSULA</i>
DOM	<i>DOMBEYA</i>	OPH	<i>OPHIOGLOSSUM</i>	POG	<i>POLYGONUM</i>	UMB	UMBELLIFERAE TYPE
COM	COMBRETACEAE TYPE	PEA	<i>PELLAEA</i> TYPE	HYD	<i>HYDROCOTYLE</i>	CAM	CAMPANULACEAE
RHU	<i>RHUS</i>	CON	CONVOLVULACEAE	RAN	RANUNCULACEAE	HET	<i>HETEROMORPHA</i> TYPE
GRE	<i>GREWIA</i>	POL	POLYGALACEAE	LUD	<i>LUDWIGIA</i>	POA	POACEAE
LYC	<i>LYCIUM</i>	SEA	<i>SELAGO</i> TYPE	GUN	<i>GUNNERA</i>	UNI	UNIDENTIFIED
CEE	CELASTRACEAE	CMM	COMMELINACEAE	LEN	LENTIBULARIACEAE		



APPENDIX 5 - POLLEN DATA

Age (cal yr)	TRE	PSO	MYR	ALC	KIG	MYI	CLU	MYS	POD	CEL	Age (cal yr)	TRE	PSO	MYR	ALC	KIG	MYI	CLU	MYS	POD	CEL	
0.00	0.00	0.00	0.00	0.00	0.00	0.00	0.00	0.00	0.04	0.00	7460.18	0.00	0.00	0.00	0.00	0.00	0.00	0.00	0.00	0.00	0.33	0.00
221.69	0.00	0.00	0.15	0.00	0.00	0.00	0.00	0.00	0.15	0.00	7882.53	0.00	0.00	0.00	0.00	0.00	0.00	0.00	0.00	0.00	0.00	0.00
443.38	0.00	0.00	0.00	0.02	0.04	0.00	0.00	0.00	0.02	0.00	8304.88	0.00	0.00	0.00	0.00	0.00	0.00	0.00	0.00	0.00	0.00	0.00
554.22	0.03	0.00	0.03	0.00	0.00	0.00	0.00	0.00	0.00	0.00	8727.24	0.00	0.00	0.00	0.00	0.00	0.00	0.00	0.00	0.00	0.05	0.00
611.11	0.00	0.00	0.02	0.00	0.00	0.00	0.00	0.00	0.09	0.00	9149.59	0.00	0.00	0.00	0.00	0.00	0.00	0.00	0.00	0.00	0.06	0.00
724.89	0.00	0.00	0.00	0.00	0.23	0.00	0.00	0.00	0.06	0.00	9551.53	0.02	0.00	0.00	0.00	0.00	0.00	0.00	0.02	0.00	0.00	0.00
838.67	0.00	0.00	0.00	0.00	0.00	0.06	0.00	0.00	0.32	0.00	9922.86	0.00	0.00	0.00	0.00	0.00	0.00	0.00	0.00	0.00	0.03	0.08
972.43	0.00	0.00	0.30	0.10	0.00	0.00	0.00	0.00	0.00	0.00	10294.18	0.00	0.00	0.00	0.00	0.03	0.03	0.00	0.00	0.00	0.14	0.00
1069.29	0.00	0.00	0.00	0.00	0.21	0.00	0.00	0.07	0.14	0.00	10665.51	0.00	0.00	0.00	0.00	0.00	0.07	0.00	0.00	0.00	0.27	0.00
1166.14	0.00	0.00	0.00	0.00	0.00	0.00	0.40	0.00	0.40	0.00	11085.35	0.00	0.00	0.00	0.00	0.00	0.01	0.00	0.00	0.00	0.15	0.00
1650.56	0.00	0.00	0.00	0.09	0.00	0.00	0.00	0.00	0.09	0.09	11368.04	0.00	0.00	0.00	0.00	0.00	0.10	0.00	0.00	0.00	0.19	0.00
2926.95	0.00	0.00	0.00	0.00	0.00	0.00	0.00	0.00	0.14	0.00	11650.73	0.00	0.00	0.00	0.00	0.00	0.12	0.00	0.00	0.00	0.24	0.00
3360.00	0.00	0.00	0.00	0.00	0.00	0.00	0.07	0.00	0.21	0.00	12216.11	0.00	0.00	0.00	0.00	0.05	0.05	0.00	0.00	0.00	0.20	0.00
3600.19	0.00	0.00	0.00	0.00	0.04	0.00	0.00	0.00	0.05	0.00	12724.95	0.00	0.00	0.00	0.00	0.00	0.12	0.00	0.00	0.00	0.33	0.00
3840.38	0.00	0.00	0.05	0.00	0.29	0.00	0.00	0.00	0.19	0.00	13064.18	0.00	0.00	0.00	0.00	0.03	0.00	0.03	0.00	0.00	0.03	0.00
4080.57	0.02	0.00	0.00	0.00	0.02	0.00	0.00	0.00	0.08	0.00	13346.87	0.00	0.00	0.00	0.00	0.00	0.07	0.00	0.00	0.00	0.09	0.00
4453.00	0.00	0.00	0.03	0.00	0.07	0.00	0.00	0.00	0.29	0.03	13912.25	0.00	0.00	0.00	0.00	0.00	0.36	0.00	0.05	0.00	0.77	0.00
4957.67	0.00	0.00	0.00	0.00	0.03	0.00	0.00	0.00	0.06	0.00	14477.64	0.00	0.00	0.00	0.00	0.06	4.44	0.00	0.00	0.00	0.71	0.00
5462.33	0.00	0.00	0.00	0.00	0.00	0.00	0.00	0.00	0.13	0.00	15043.02	0.00	0.00	0.00	0.00	0.00	0.85	0.00	0.00	0.00	1.16	0.00
5967.00	0.00	0.00	0.00	0.00	0.00	0.00	0.00	0.00	0.00	0.00	15608.40	0.00	0.00	0.03	0.00	0.00	0.49	0.00	0.00	0.00	0.43	0.00
6045.29	0.00	0.00	0.00	0.00	0.00	0.00	0.00	0.00	0.19	0.00	16173.78	0.00	0.00	0.00	0.00	0.00	0.68	0.00	0.00	0.00	0.64	0.00
6123.58	0.00	0.00	0.00	0.00	0.00	0.00	0.00	0.00	0.00	0.00	16739.16	0.00	0.00	0.00	0.00	0.00	0.41	0.00	0.00	0.00	0.85	0.00
6280.17	0.00	0.00	0.00	0.00	0.00	0.00	0.00	0.00	0.09	0.00	17304.55	0.00	0.00	0.00	0.00	0.00	0.64	0.00	0.00	0.00	1.41	0.00
6436.75	0.00	0.00	0.00	0.00	0.00	0.00	0.00	0.00	0.19	0.00	17587.24	0.00	0.00	0.00	0.00	0.00	0.11	0.00	0.00	0.00	0.34	0.00
6515.04	0.00	0.00	0.00	0.00	0.00	0.00	0.00	0.00	0.56	0.00	18435.31	0.00	0.00	0.00	0.00	0.00	0.09	0.00	0.04	0.00	0.52	0.00
6593.33	0.00	0.00	0.00	0.00	0.00	0.00	0.00	0.00	0.31	0.00	19000.69	0.00	0.00	0.00	0.00	0.00	0.09	0.00	0.00	0.00	0.58	0.00
6855.60	0.00	0.00	0.00	0.00	0.00	0.00	0.00	0.00	0.21	0.00	19600.00	0.00	0.03	0.00	0.00	0.00	0.23	0.00	0.00	0.00	0.38	0.00
7117.87	0.00	0.00	0.00	0.00	0.00	0.00	0.00	0.00	0.08	0.00	19750.00	0.00	0.00	0.03	0.00	0.03	0.20	0.00	0.00	0.00	0.47	0.03

### APPENDIX 5 - POLLEN DATA

Age (cal yr)	KIR	BRA	MIM	BUR	CAN	CRO	ENC	BEQ	PRO	OLE	Age (cal yr)	KIR	BRA	MIM	BUR	CAN	CRO	CEC	BEQ	PRO	OLE
0.00	0.00	0.00	0.00	0.37	0.00	0.00	0.00	0.00	0.04	0.00	7460.18	0.00	0.00	0.00	0.27	0.00	0.00	0.00	0.07	0.07	0.07
221.69	0.00	0.00	0.00	0.45	0.00	0.00	0.00	0.00	0.30	0.15	7882.53	0.04	0.00	0.00	0.26	0.00	0.00	0.00	0.00	0.00	0.00
443.38	0.00	0.00	0.00	0.65	0.00	0.00	0.00	0.02	0.09	0.02	8304.88	0.00	0.00	0.00	0.59	0.00	0.00	0.00	0.00	0.00	0.00
554.22	0.03	0.00	0.00	1.15	0.00	0.03	0.00	0.00	0.09	0.12	8727.24	0.00	0.00	0.00	0.44	0.00	0.00	0.00	0.00	0.00	0.05
611.11	0.00	0.02	0.00	0.37	0.00	0.00	0.00	0.05	0.02	0.00	9149.59	0.00	0.00	0.00	0.10	0.00	0.00	0.00	0.00	0.00	0.11
724.89	0.00	0.00	0.00	0.57	0.00	0.00	0.00	0.06	0.23	0.06	9551.53	0.00	0.00	0.00	0.12	0.00	0.00	0.00	0.00	0.00	0.00
838.67	0.06	0.00	0.00	0.13	0.00	0.00	0.00	0.00	0.19	0.06	9922.86	0.00	0.00	0.00	0.14	0.00	0.00	0.00	0.00	0.03	0.03
972.43	0.00	0.00	0.00	0.30	0.00	0.00	0.00	0.00	2.37	0.49	10294.18	0.00	0.00	0.00	0.41	0.00	0.00	0.00	0.00	0.03	0.17
1069.29	0.00	0.00	0.00	0.42	0.00	0.00	0.00	0.00	1.56	0.14	10665.51	0.00	0.00	0.00	0.27	0.00	0.00	0.00	0.00	0.07	0.20
1166.14	0.00	0.00	0.10	0.50	0.00	0.00	0.00	0.00	1.60	0.10	11085.35	0.00	0.00	0.00	0.01	0.00	0.00	0.00	0.00	0.03	0.03
1650.56	0.00	0.00	0.00	0.35	0.00	0.00	0.00	0.00	1.42	0.18	11368.04	0.00	0.00	0.00	0.10	0.00	0.00	0.00	0.05	0.05	0.29
2926.95	0.00	0.00	0.00	0.14	0.00	0.00	0.00	0.00	0.09	0.00	11650.73	0.00	0.00	0.00	0.18	0.00	0.00	0.00	0.00	0.06	0.30
3360.00	0.00	0.00	0.00	0.76	0.00	0.00	0.00	0.00	0.07	0.07	12216.11	0.00	0.00	0.00	0.30	0.00	0.00	0.00	0.00	0.30	0.35
3600.19	0.00	0.00	0.00	0.05	0.00	0.00	0.00	0.00	0.01	0.01	12724.95	0.00	0.00	0.00	0.12	0.00	0.00	0.00	0.00	0.12	0.24
3840.38	0.00	0.00	0.00	0.29	0.00	0.00	0.00	0.00	0.19	0.00	13064.18	0.00	0.00	0.00	0.00	0.00	0.00	0.00	0.06	0.03	0.23
4080.57	0.00	0.02	0.00	0.15	0.00	0.00	0.00	0.00	0.03	0.00	13346.87	0.00	0.00	0.00	0.07	0.00	0.00	0.00	0.00	0.02	0.11
4453.00	0.00	0.00	0.00	0.07	0.00	0.00	0.00	0.00	0.03	0.10	13912.25	0.00	0.00	0.00	0.00	0.00	0.00	0.00	0.05	0.10	0.51
4957.67	0.00	0.00	0.00	0.36	0.00	0.00	0.00	0.00	0.06	0.15	14477.64	0.00	0.00	0.00	0.39	0.00	0.00	0.00	0.06	0.00	0.19
5462.33	0.00	0.00	0.00	0.13	0.00	0.00	0.00	0.03	0.05	0.05	15043.02	0.00	0.00	0.00	0.08	0.00	0.00	0.04	0.00	0.04	0.04
5967.00	0.04	0.00	0.00	0.62	0.00	0.00	0.00	0.00	0.04	0.04	15608.40	0.00	0.00	0.00	0.03	0.00	0.00	0.00	0.00	0.03	0.06
6045.29	0.00	0.00	0.00	0.56	0.00	0.00	0.00	0.00	0.19	0.37	16173.78	0.00	0.00	0.00	0.04	0.00	0.00	0.00	0.00	0.00	0.21
6123.58	0.00	0.00	0.00	0.32	0.00	0.05	0.00	0.09	0.32	0.18	16739.16	0.00	0.00	0.00	0.00	0.00	0.00	0.00	0.00	0.00	0.04
6280.17	0.00	0.00	0.00	0.28	0.00	0.00	0.00	0.00	0.28	0.65	17304.55	0.00	0.00	0.00	0.00	0.00	0.00	0.00	0.00	0.14	0.18
6436.75	0.00	0.00	0.00	0.09	0.00	0.00	0.00	0.00	0.19	0.09	17587.24	0.00	0.00	0.00	0.03	0.00	0.00	0.00	0.00	0.00	0.03
6515.04	0.00	0.00	0.00	0.47	0.00	0.00	0.00	0.00	0.00	0.84	18435.31	0.00	0.00	0.00	0.00	0.00	0.00	0.00	0.00	0.04	0.04
6593.33	0.00	0.00	0.00	0.54	0.00	0.00	0.00	0.00	0.23	0.54	19000.69	0.00	0.00	0.00	0.04	0.00	0.00	0.00	0.00	0.00	0.00
6855.60	0.00	0.00	0.00	0.05	0.00	0.00	0.00	0.00	0.11	0.05	19600.00	0.00	0.00	0.00	0.00	0.00	0.00	0.00	0.00	0.03	0.08
7117.87	0.00	0.00	0.00	0.33	0.00	0.00	0.00	0.00	0.00	0.00	19750.00	0.00	0.00	0.00	0.03	0.00	0.00	0.00	0.00	0.03	0.10

**APPENDIX 5 - POLLEN DATA**

Age (cal yr)	EUP	DOM	COM	RHU	GRE	LYC	CEE	RHA	EUC	DIO	Age (cal yr)	EUP	DOM	COM	RHU	GRE	LYC	CEE	RHA	EUC	DIO
0.00	0.00	0.00	0.33	0.07	0.00	0.00	0.00	0.00	0.37	0.00	7460.18	0.00	0.00	1.66	0.00	0.13	0.00	0.00	0.00	0.07	0.00
221.69	0.00	0.00	0.83	0.45	0.08	0.00	0.00	0.00	0.38	0.00	7882.53	0.00	0.00	0.49	0.00	0.00	0.00	0.08	0.00	0.00	0.00
443.38	0.00	0.00	0.25	0.02	0.00	0.00	0.02	0.00	0.20	0.00	8304.88	0.00	0.00	0.48	0.27	0.00	0.00	0.00	0.00	0.05	0.00
554.22	0.00	0.00	0.32	0.06	0.00	0.00	0.00	0.00	0.15	0.00	8727.24	0.00	0.00	0.83	0.00	0.00	0.00	0.00	0.00	0.00	0.00
611.11	0.00	0.00	0.18	0.07	0.00	0.00	0.00	0.00	0.07	0.00	9149.59	0.00	0.02	0.13	0.02	0.00	0.00	0.02	0.00	0.00	0.00
724.89	0.00	0.00	0.51	0.06	0.00	0.06	0.06	0.00	0.06	0.00	9551.53	0.00	0.00	0.12	0.07	0.00	0.00	0.00	0.00	0.07	0.00
838.67	0.00	0.13	0.44	0.06	0.00	0.00	0.00	0.00	0.00	0.00	9922.86	0.00	0.00	0.14	0.11	0.00	0.00	0.00	0.00	0.00	0.00
972.43	0.00	0.00	4.05	0.20	0.00	0.00	0.00	0.00	0.10	0.00	10294.18	0.00	0.00	0.17	0.03	0.00	0.00	0.00	0.00	0.03	0.00
1069.29	0.00	0.00	0.50	0.14	0.07	0.00	0.00	0.00	0.00	0.00	10665.51	0.00	0.00	0.53	0.00	0.00	0.00	0.00	0.00	0.07	0.00
1166.14	0.00	0.00	1.90	0.40	0.00	0.00	0.00	0.00	0.40	0.00	11085.35	0.00	0.00	0.04	0.03	0.01	0.00	0.01	0.00	0.02	0.00
1650.56	0.00	0.09	0.44	0.53	0.00	0.00	0.18	0.00	0.27	0.00	11368.04	0.00	0.00	0.10	0.10	0.00	0.00	0.00	0.00	0.00	0.00
2926.95	0.00	0.00	0.38	0.05	0.05	0.00	0.00	0.00	0.05	0.00	11650.73	0.00	0.00	0.06	0.06	0.00	0.00	0.24	0.00	0.06	0.00
3360.00	0.00	0.00	0.69	0.21	0.00	0.00	0.00	0.00	0.00	0.00	12216.11	0.00	0.00	0.44	0.10	0.00	0.00	0.00	0.00	0.00	0.00
3600.19	0.00	0.00	0.07	0.00	0.00	0.00	0.00	0.00	0.00	0.00	12724.95	0.00	0.00	0.41	0.08	0.00	0.00	0.08	0.00	0.04	0.00
3840.38	0.00	0.05	0.29	0.00	0.00	0.00	0.00	0.00	0.10	0.00	13064.18	0.00	0.00	0.10	0.06	0.00	0.00	0.00	0.00	0.00	0.00
4080.57	0.00	0.00	0.18	0.00	0.00	0.00	0.00	0.00	0.00	0.00	13346.87	0.00	0.00	0.06	0.08	0.00	0.00	0.01	0.00	0.03	0.00
4453.00	0.00	0.00	0.72	0.10	0.03	0.00	0.00	0.00	0.03	0.00	13912.25	0.00	0.00	0.05	0.00	0.00	0.00	0.05	0.00	0.10	0.00
4957.67	0.00	0.00	0.24	0.15	0.00	0.00	0.03	0.00	0.00	0.00	14477.64	0.00	0.00	0.13	0.26	0.00	0.00	0.00	0.13	0.06	0.00
5462.33	0.00	0.00	0.15	0.00	0.00	0.00	0.00	0.00	0.10	0.00	15043.02	0.00	0.00	0.00	0.04	0.00	0.00	0.00	0.00	0.00	0.00
5967.00	0.00	0.00	0.25	0.16	0.00	0.00	0.00	0.00	0.08	0.00	15608.40	0.00	0.00	0.18	0.22	0.00	0.00	0.00	0.00	0.06	0.00
6045.29	0.00	0.00	2.22	0.28	0.00	0.00	0.00	0.09	0.19	0.00	16173.78	0.00	0.00	0.00	0.00	0.00	0.00	0.00	0.00	0.00	0.00
6123.58	0.00	0.00	1.15	0.00	0.00	0.00	0.00	0.00	0.05	0.00	16739.16	0.00	0.00	0.04	0.12	0.00	0.00	0.00	0.00	0.04	0.00
6280.17	0.00	0.00	4.28	0.00	0.00	0.00	0.00	0.00	0.00	0.00	17304.55	0.00	0.00	0.00	0.09	0.00	0.00	0.00	0.00	0.05	0.00
6436.75	0.00	0.00	3.12	0.28	0.09	0.00	0.00	0.00	0.00	0.00	17587.24	0.00	0.00	0.17	0.03	0.00	0.00	0.00	0.00	0.00	0.00
6515.04	0.00	0.00	3.17	0.00	0.09	0.00	0.00	0.00	0.28	0.00	18435.31	0.00	0.00	0.09	0.00	0.00	0.00	0.04	0.00	0.00	0.00
6593.33	0.00	0.08	3.73	0.16	0.00	0.00	0.00	0.00	0.00	0.00	19000.69	0.00	0.00	0.00	0.00	0.00	0.00	0.00	0.00	0.00	0.00
6855.60	0.00	0.05	0.75	0.11	0.05	0.00	0.00	0.00	0.05	0.00	19600.00	0.00	0.00	0.13	0.10	0.00	0.00	0.00	0.00	0.03	0.00
7117.87	0.00	0.00	2.72	0.00	0.08	0.00	0.00	0.00	0.00	0.00	19750.00	0.00	0.00	0.07	0.10	0.00	0.00	0.00	0.03	0.00	0.00

**APPENDIX 5 - POLLEN DATA**

Age (cal yr)	SPI	PAL	SCL	ACA	MIO	PEL	COI	TAR	CAP	OXY	Age (cal yr)	SPI	PAL	SCL	ACA	MIO	PEL	COI	TAR	CAP	OXY
0.00	0.00	0.00	0.04	0.11	0.00	0.73	0.00	0.29	0.22	0.00	7460.18	0.00	0.00	0.00	0.20	0.13	0.20	0.00	2.65	3.84	0.00
221.69	0.08	0.00	0.08	0.00	0.00	0.00	0.00	0.08	0.30	0.00	7882.53	0.04	0.00	0.00	0.00	0.00	0.08	0.00	0.49	1.62	0.00
443.38	0.09	0.00	0.00	0.00	0.00	0.02	0.00	0.04	0.02	0.00	8304.88	0.00	0.00	0.05	0.16	0.00	0.05	0.00	2.13	2.45	0.00
554.22	0.24	0.00	0.06	0.06	0.00	0.09	0.00	0.03	0.15	0.00	8727.24	0.00	0.00	0.00	0.29	0.00	0.00	0.00	1.95	1.70	0.00
611.11	0.05	0.00	0.04	0.00	0.00	0.00	0.02	0.04	0.02	0.00	9149.59	0.00	0.00	0.00	0.02	0.00	0.00	0.06	0.67	0.32	0.00
724.89	0.34	0.00	0.00	0.06	0.00	0.06	0.00	0.17	0.00	0.00	9551.53	0.05	0.00	0.00	0.02	0.00	0.00	0.02	0.60	0.60	0.00
838.67	0.19	0.00	0.06	0.06	0.00	0.00	0.00	0.06	0.00	0.00	9922.86	0.00	0.00	0.00	0.00	0.00	0.00	0.00	0.42	0.42	0.00
972.43	0.00	0.00	0.00	0.59	0.00	0.00	0.00	0.10	0.10	0.00	10294.18	0.00	0.00	0.00	0.07	0.00	0.00	0.00	0.47	0.44	0.00
1069.29	0.00	0.00	0.14	0.00	0.00	0.00	0.00	0.00	0.07	0.00	10665.51	0.00	0.00	0.07	0.07	0.00	0.00	0.00	0.27	0.47	0.00
1166.14	0.00	0.00	0.10	0.00	0.00	0.20	0.00	0.20	0.10	0.00	11085.35	0.00	0.00	0.00	0.00	0.00	0.00	0.00	0.03	0.04	0.00
1650.56	0.18	0.00	0.00	0.09	0.00	0.00	0.00	0.09	0.18	0.00	11368.04	0.00	0.00	0.05	0.05	0.00	0.00	0.00	0.14	0.19	0.00
2926.95	0.00	0.00	0.00	0.00	0.00	0.05	0.00	0.05	0.14	0.00	11650.73	0.00	0.00	0.00	0.00	0.00	0.00	0.00	0.06	0.24	0.00
3360.00	0.07	0.00	0.00	0.00	0.00	0.00	0.00	0.07	0.69	0.00	12216.11	0.00	0.00	0.00	0.00	0.00	0.00	0.00	0.59	0.84	0.00
3600.19	0.00	0.00	0.00	0.01	0.00	0.01	0.00	0.00	0.01	0.00	12724.95	0.04	0.00	0.00	0.12	0.00	0.00	0.00	1.10	0.98	0.00
3840.38	0.00	0.00	0.00	0.10	0.00	0.00	0.00	0.05	0.05	0.00	13064.18	0.00	0.00	0.00	0.00	0.00	0.00	0.00	0.23	0.32	0.00
4080.57	0.00	0.00	0.00	0.02	0.00	0.12	0.00	0.00	0.03	0.00	13346.87	0.00	0.00	0.00	0.00	0.00	0.00	0.00	0.01	0.02	0.00
4453.00	0.00	0.00	0.00	0.07	0.00	0.03	0.00	0.23	0.46	0.00	13912.25	0.00	0.00	0.00	0.00	0.00	0.00	0.00	0.46	0.46	0.00
4957.67	0.03	0.00	0.00	0.06	0.00	0.00	0.00	0.15	0.06	0.00	14477.64	0.00	0.00	0.00	0.13	0.00	0.00	0.00	0.13	0.32	0.00
5462.33	0.08	0.00	0.00	0.00	0.00	0.00	0.00	0.00	0.13	0.00	15043.02	0.00	0.00	0.00	0.00	0.00	0.00	0.00	0.00	0.04	0.00
5967.00	0.04	0.00	0.00	0.00	0.00	0.00	0.00	0.08	0.37	0.00	15608.40	0.00	0.00	0.00	0.06	0.00	0.00	0.00	0.03	0.15	0.00
6045.29	0.00	0.00	0.00	0.00	0.00	0.00	0.00	0.56	2.59	0.00	16173.78	0.00	0.00	0.00	0.00	0.00	0.00	0.00	0.00	0.00	0.00
6123.58	0.00	0.00	0.00	0.09	0.00	0.00	0.00	0.14	0.64	0.00	16739.16	0.00	0.00	0.00	0.00	0.00	0.00	0.00	0.04	0.12	0.00
6280.17	0.00	0.00	0.00	0.09	0.00	0.00	0.00	0.56	3.91	0.00	17304.55	0.00	0.00	0.00	0.00	0.00	0.00	0.00	0.05	0.05	0.00
6436.75	0.00	0.00	0.09	0.09	0.00	0.19	0.00	1.70	3.97	0.00	17587.24	0.00	0.00	0.00	0.00	0.00	0.00	0.00	0.03	0.03	0.00
6515.04	0.00	0.00	0.09	0.09	0.00	0.00	0.00	0.93	1.96	0.00	18435.31	0.00	0.00	0.00	0.00	0.00	0.00	0.00	0.04	0.04	0.00
6593.33	0.00	0.00	0.08	0.00	0.00	0.08	0.00	0.70	1.48	0.00	19000.69	0.00	0.00	0.00	0.00	0.00	0.00	0.00	0.13	0.00	0.00
6855.60	0.11	0.00	0.00	0.00	0.00	0.05	0.00	1.39	2.29	0.00	19600.00	0.00	0.00	0.00	0.03	0.00	0.00	0.00	0.05	0.05	0.00
7117.87	0.00	0.00	0.00	0.08	0.08	0.16	0.00	2.22	1.32	0.00	19750.00	0.00	0.00	0.00	0.00	0.00	0.00	0.03	0.27	0.17	0.00

**APPENDIX 5 - POLLEN DATA**

Age (cal yr)	ASP	ALO	LAN	MAL	CAN	VAN	SEL	RUB	OPH	PEA	Age (cal yr)	ASP	ALO	LAN	MAL	CAN	VAN	SEL	RUB	OPH	PEA
0.00	0.00	0.04	0.00	0.00	0.22	0.00	0.00	0.00	0.00	0.00	7460.18	0.00	4.00	0.00	0.00	0.13	0.07	0.00	0.00	0.07	0.00
221.69	0.00	1.00	0.00	0.00	0.08	0.00	0.00	0.00	0.00	0.00	7882.53	0.04	3.00	0.00	0.00	0.04	0.00	0.00	0.00	0.00	0.00
443.38	0.02	0.50	0.00	0.00	0.11	0.00	0.00	0.00	0.00	0.00	8304.88	1.00	4.00	0.00	0.00	0.05	0.00	0.00	0.00	0.00	0.00
554.22	0.03	0.00	0.00	0.00	0.03	0.00	0.00	0.00	0.00	0.00	8727.24	0.05	4.00	0.00	0.00	0.00	0.00	0.00	0.00	0.00	0.00
611.11	0.00	0.02	0.00	0.00	0.04	0.00	0.00	0.00	0.00	0.00	9149.59	0.00	0.50	0.00	0.00	0.02	0.00	0.00	0.00	0.00	0.00
724.89	0.00	0.00	0.00	0.00	0.11	0.00	0.00	0.00	0.00	0.00	9551.53	0.00	0.00	0.00	0.00	0.07	0.00	0.00	0.00	0.02	0.00
838.67	0.00	0.06	0.00	0.00	0.13	0.00	0.00	0.00	0.00	0.00	9922.86	0.00	0.50	0.00	0.00	0.00	0.00	0.00	0.00	0.00	0.50
972.43	0.40	0.50	0.00	0.00	0.20	0.00	0.00	0.00	0.00	0.00	10294.18	0.00	1.50	0.00	0.00	0.07	0.10	0.00	0.00	0.00	0.00
1069.29	0.50	0.50	0.00	0.00	0.07	0.00	0.00	0.00	0.00	0.00	10665.51	0.00	2.50	0.00	0.00	0.13	0.00	0.00	0.00	0.00	0.00
1166.14	0.00	0.00	0.00	0.00	0.50	0.00	0.00	0.00	0.00	0.00	11085.35	0.00	1.51	0.00	0.00	0.00	0.01	0.00	0.01	0.00	0.00
1650.56	0.00	0.00	0.00	0.00	0.44	0.00	0.00	0.09	0.09	0.00	11368.04	0.05	0.24	0.00	0.00	0.14	0.00	0.00	0.00	0.00	0.00
2926.95	0.00	0.00	0.00	0.00	0.05	0.00	0.00	0.00	0.00	0.00	11650.73	0.00	0.00	0.00	0.00	0.00	0.00	0.00	0.00	0.00	0.00
3360.00	0.00	0.00	0.00	0.00	0.07	0.00	0.00	0.00	0.00	0.00	12216.11	0.00	0.00	0.00	0.00	0.20	0.00	0.00	0.00	0.05	0.00
3600.19	0.00	0.00	0.00	0.00	0.00	0.00	0.00	0.00	0.00	0.00	12724.95	0.00	0.50	0.00	0.00	0.08	0.04	0.00	0.00	0.00	0.00
3840.38	0.00	0.80	0.00	0.00	0.00	0.00	0.00	0.00	0.00	0.00	13064.18	0.50	1.00	0.00	0.00	0.06	0.00	0.00	0.00	0.00	0.00
4080.57	0.00	0.00	0.00	0.00	0.00	0.00	0.00	0.00	0.00	0.00	13346.87	0.00	1.00	0.00	0.00	0.01	0.00	0.00	0.00	0.00	0.00
4453.00	0.00	2.00	0.00	0.00	0.07	0.00	0.00	0.00	0.00	0.00	13912.25	0.00	0.50	0.00	0.05	0.10	0.00	0.00	0.00	0.00	0.00
4957.67	0.00	1.00	0.00	0.00	0.00	0.00	0.00	0.00	0.00	0.00	14477.64	0.00	0.00	0.00	0.00	0.06	0.00	0.00	0.00	0.00	0.00
5462.33	0.00	0.03	0.00	0.00	0.05	0.00	0.00	0.00	0.00	0.00	15043.02	0.04	0.50	0.00	0.00	0.04	0.00	0.00	0.00	0.00	0.04
5967.00	0.04	0.50	0.00	0.00	0.00	0.00	0.00	0.00	0.00	0.00	15608.40	0.00	1.20	0.00	0.00	0.00	0.00	0.00	0.00	0.00	0.00
6045.29	0.00	0.09	0.00	0.00	0.00	0.00	0.00	0.00	0.00	0.09	16173.78	0.00	0.00	0.00	0.00	0.04	0.00	0.00	0.00	0.04	0.04
6123.58	0.00	1.50	0.00	0.00	0.09	0.00	0.00	0.00	0.00	0.00	16739.16	0.00	0.00	0.00	0.00	0.08	0.00	0.00	0.00	0.00	0.00
6280.17	0.09	0.00	0.00	0.00	0.00	0.00	0.00	0.09	0.00	0.00	17304.55	0.00	1.00	0.00	0.00	0.09	0.00	0.00	0.00	0.05	0.00
6436.75	0.00	3.50	0.00	0.00	0.19	0.00	0.00	0.09	0.00	0.00	17587.24	0.00	0.03	0.00	0.00	0.03	0.00	0.00	0.00	0.00	0.00
6515.04	0.00	0.00	0.00	0.00	0.00	0.00	0.00	0.00	0.00	0.19	18435.31	0.00	0.00	0.00	0.00	0.04	0.00	0.00	0.00	0.00	0.00
6593.33	0.08	5.36	0.00	0.00	0.00	0.00	0.00	0.00	0.00	0.00	19000.69	0.50	0.00	0.00	0.00	0.00	0.00	0.00	0.00	0.00	0.00
6855.60	0.50	4.00	0.00	0.00	0.11	0.00	0.00	0.00	0.00	0.00	19600.00	0.40	0.40	0.00	0.00	0.00	0.00	0.00	0.00	0.00	0.00
7117.87	0.08	2.01	0.00	0.00	0.25	0.00	0.00	0.00	0.08	0.00	19750.00	0.00	7.00	0.00	0.00	0.13	0.00	0.00	0.00	0.00	0.07

**APPENDIX 5 - POLLEN DATA**

Age (cal yr)	CON	POL	SEA	CMM	ACL	COP	LAC	ART	STO	RUS	Age (cal yr)	CON	POL	SEA	CMM	ACL	COP	LAC	ART	STO	RUS
0.00	0.00	0.00	0.00	0.00	0.00	2.90	0.15	0.00	0.00	0.00	7460.18	0.00	0.00	0.00	0.00	0.00	2.05	1.33	0.00	0.00	0.00
221.69	0.00	0.00	0.00	0.08	0.00	5.36	0.08	0.08	0.00	0.00	7882.53	0.00	0.00	0.00	0.00	0.00	2.45	0.00	0.00	0.00	0.00
443.38	0.00	0.00	0.00	0.00	0.00	1.50	0.00	0.02	0.02	0.00	8304.88	0.00	0.00	0.00	0.00	0.05	2.99	0.32	0.32	0.05	0.00
554.22	0.00	0.00	0.00	0.00	0.00	1.88	0.03	0.00	0.00	0.00	8727.24	0.00	0.00	0.00	0.10	0.05	3.36	0.19	0.10	0.10	0.00
611.11	0.00	0.00	0.00	0.00	0.00	1.77	0.14	0.02	0.04	0.00	9149.59	0.00	0.00	0.00	0.00	0.00	1.71	0.11	0.10	0.04	0.00
724.89	0.00	0.00	0.00	0.00	0.00	7.98	0.00	0.06	0.00	0.00	9551.53	0.00	0.00	0.00	0.00	0.00	1.42	0.35	0.02	0.12	0.00
838.67	0.00	0.00	0.00	0.00	0.00	3.11	0.00	0.06	0.00	0.00	9922.86	0.00	0.00	0.00	0.00	0.00	2.66	0.17	0.25	0.06	0.00
972.43	0.00	0.00	0.00	0.00	0.10	8.50	0.00	0.10	0.00	0.00	10294.18	0.00	0.00	0.00	0.00	0.03	2.67	0.51	0.57	0.30	0.00
1069.29	0.00	0.00	0.00	0.00	0.00	6.87	0.07	0.07	0.00	0.00	10665.51	0.00	0.00	0.00	0.00	0.00	5.12	0.60	0.27	0.27	0.00
1166.14	0.00	0.00	0.00	0.00	0.00	10.00	0.50	0.10	0.00	0.00	11085.35	0.00	0.00	0.00	0.00	0.00	0.50	0.10	0.12	0.03	0.00
1650.56	0.00	0.00	0.00	0.09	0.18	14.46	0.00	0.00	0.00	0.00	11368.04	0.00	0.00	0.00	0.00	0.00	3.53	0.34	0.68	0.14	0.00
2926.95	0.00	0.00	0.00	0.00	0.00	9.00	0.00	0.00	0.00	0.00	11650.73	0.00	0.00	0.00	0.50	0.06	4.91	0.36	1.70	0.24	0.00
3360.00	0.00	0.00	0.00	0.00	0.00	10.67	0.00	0.07	0.00	0.00	12216.11	0.00	0.00	0.00	0.00	0.00	3.80	1.04	0.59	0.05	0.00
3600.19	0.00	0.00	0.00	0.00	0.01	0.51	0.00	0.00	0.00	0.00	12724.95	0.00	0.00	0.00	0.04	0.00	2.89	0.69	0.12	0.12	0.00
3840.38	0.00	0.00	0.00	0.00	0.05	6.53	0.00	0.05	0.00	0.00	13064.18	0.00	0.00	0.00	0.00	0.00	2.05	0.13	0.19	0.06	0.00
4080.57	0.00	0.00	0.00	0.00	0.00	2.43	0.00	0.00	0.00	0.00	13346.87	0.00	0.00	0.00	0.01	0.00	0.56	0.11	0.24	0.10	0.00
4453.00	0.00	0.00	0.00	0.00	0.00	2.96	0.07	0.03	0.00	0.00	13912.25	0.00	0.00	0.00	0.00	0.05	2.62	0.51	0.46	1.64	0.00
4957.67	0.00	0.00	0.00	0.00	0.00	4.07	0.03	0.00	0.00	0.00	14477.64	0.00	0.00	0.00	0.00	0.00	2.90	0.45	0.97	0.77	0.00
5462.33	0.00	0.00	0.00	0.03	0.03	0.77	0.00	0.03	0.00	0.03	15043.02	0.00	0.00	0.00	0.00	0.08	1.09	0.08	0.12	2.13	0.00
5967.00	0.00	0.00	0.00	0.00	0.00	6.37	0.08	0.12	0.00	0.00	15608.40	0.00	0.00	0.00	0.00	0.03	1.69	0.15	0.34	0.86	0.00
6045.29	0.00	0.00	0.00	0.09	0.00	9.16	0.00	0.00	0.00	0.00	16173.78	0.00	0.00	0.00	0.00	0.17	2.51	0.30	0.60	1.66	0.04
6123.58	0.00	0.00	0.00	0.05	0.00	5.64	0.09	0.05	0.05	0.00	16739.16	0.00	0.04	0.00	0.00	0.00	2.64	0.20	0.61	1.38	0.00
6280.17	0.00	0.00	0.00	0.00	0.00	8.94	0.93	0.00	0.00	0.00	17304.55	0.00	0.00	0.00	0.00	0.05	1.05	0.36	0.32	1.91	0.00
6436.75	0.00	0.00	0.00	0.00	0.00	9.45	0.95	0.09	0.00	0.00	17587.24	0.00	0.03	0.00	0.00	0.00	1.44	0.06	0.37	1.38	0.06
6515.04	0.00	0.00	0.00	0.00	0.09	7.37	0.93	0.09	0.00	0.00	18435.31	0.00	0.00	0.00	0.00	0.04	3.89	0.04	0.39	1.68	0.00
6593.33	0.00	0.00	0.00	0.08	0.00	8.85	0.70	0.08	0.00	0.00	19000.69	0.00	0.00	0.00	0.00	0.00	3.63	0.35	0.62	1.64	0.09
6855.60	0.00	0.00	0.00	0.00	0.00	4.16	0.32	0.11	0.00	0.00	19600.00	0.00	0.03	0.00	0.00	0.00	1.54	0.13	0.25	0.63	0.03
7117.87	0.00	0.00	0.00	0.00	0.00	6.76	2.22	0.08	0.00	0.00	19750.00	0.00	0.00	0.00	0.00	0.03	2.54	0.13	0.30	0.64	0.00

### APPENDIX 5 - POLLEN DATA

Age (cal yr)	TUL	ANT	THY	MOH	CLI	RES	PAS	ERI	AIZ	CHE	Age (cal yr)	TUL	ANT	THY	MOH	CLI	RES	PAS	ERI	AIZ	CHE
0.00	0.00	0.00	0.00	0.00	0.00	0.00	0.00	0.00	0.37	1.03	7460.18	0.00	0.00	0.00	0.00	0.00	0.00	0.00	0.00	0.00	0.33
221.69	0.00	0.00	0.08	0.00	0.00	0.00	0.00	0.00	0.15	4.76	7882.53	1.00	0.04	0.00	0.00	0.00	0.00	0.00	0.00	0.08	0.15
443.38	0.00	0.13	0.00	0.00	0.00	0.00	0.00	0.00	0.04	0.74	8304.88	0.00	0.05	0.00	0.00	0.00	0.00	0.00	0.00	0.11	0.21
554.22	0.00	0.21	0.00	0.00	0.00	0.00	0.00	0.00	0.00	0.35	8727.24	0.00	0.05	0.00	0.00	0.00	0.00	0.00	0.05	0.00	0.39
611.11	0.00	0.12	0.00	0.00	0.00	0.00	0.00	0.00	0.02	0.12	9149.59	0.00	0.06	0.00	0.00	0.00	0.00	0.00	0.00	0.02	0.15
724.89	0.00	0.06	0.00	0.00	0.00	0.00	0.00	0.00	0.06	0.57	9551.53	0.00	0.05	0.00	0.00	0.00	0.00	0.00	0.02	0.02	0.05
838.67	0.00	0.06	0.00	0.00	0.00	0.00	0.00	0.00	0.00	0.44	9922.86	0.00	0.00	0.00	0.00	0.00	0.00	0.00	0.00	0.79	0.39
972.43	0.00	0.00	0.00	0.00	0.00	0.00	0.00	0.00	0.00	1.68	10294.18	0.50	0.20	0.03	0.00	0.00	0.00	0.00	0.03	0.03	0.34
1069.29	0.00	0.00	0.00	0.00	0.00	0.00	0.00	0.00	0.14	2.41	10665.51	0.20	0.47	0.00	0.00	0.07	0.00	0.07	0.07	0.27	4.06
1166.14	0.00	0.00	0.00	0.00	0.00	0.00	0.00	0.00	0.30	3.80	11085.35	0.50	0.11	0.00	0.00	0.00	0.00	0.01	0.03	0.02	0.24
1650.56	0.00	0.00	0.00	0.00	0.00	0.00	0.00	0.00	0.18	0.35	11368.04	0.14	0.24	0.00	0.00	0.14	0.00	0.05	0.19	0.05	0.97
2926.95	0.00	0.00	0.00	0.00	0.00	0.00	0.00	0.00	0.00	0.00	11650.73	2.01	0.30	0.00	0.00	0.00	0.00	0.00	0.06	0.18	3.82
3360.00	0.00	0.14	0.00	0.00	0.00	0.00	0.00	0.00	0.00	0.14	12216.11	0.05	0.05	0.00	0.00	0.00	0.00	0.05	0.05	0.00	0.74
3600.19	0.00	0.00	0.00	0.00	0.00	0.00	0.00	0.00	0.00	0.01	12724.95	0.00	0.20	0.00	0.00	0.00	0.00	0.00	0.00	0.04	0.20
3840.38	0.00	0.00	0.00	0.00	0.00	0.00	0.00	0.00	0.05	0.24	13064.18	0.50	0.23	0.00	0.00	0.00	0.00	0.00	0.00	0.13	0.26
4080.57	0.00	0.00	0.00	0.00	0.00	0.00	0.00	0.00	0.00	0.08	13346.87	2.00	0.19	0.00	0.00	0.03	0.00	0.00	0.06	0.08	0.17
4453.00	0.00	0.13	0.00	0.00	0.00	0.00	0.00	0.00	0.07	0.10	13912.25	1.00	0.46	0.05	0.00	0.21	0.00	0.26	0.10	0.15	0.67
4957.67	0.00	0.09	0.00	0.00	0.00	0.03	0.00	0.00	0.03	0.06	14477.64	1.50	0.39	0.00	0.00	0.00	0.00	0.13	0.13	0.13	0.58
5462.33	0.00	0.05	0.00	0.00	0.00	0.00	0.00	0.00	0.00	0.00	15043.02	2.00	0.74	0.12	0.50	0.12	0.04	0.08	0.54	0.04	0.27
5967.00	0.00	0.00	0.00	0.00	0.00	0.00	0.00	0.00	0.04	0.08	15608.40	6.00	0.40	0.00	0.00	0.06	0.00	0.09	0.06	0.00	0.34
6045.29	0.00	0.00	0.00	0.00	0.00	0.00	0.00	0.00	0.00	0.19	16173.78	3.50	0.30	0.00	0.00	0.09	0.00	0.60	0.34	0.09	0.38
6123.58	0.00	0.05	0.00	0.00	0.00	0.00	0.05	0.00	0.05	0.28	16739.16	2.50	0.08	0.00	0.04	0.04	0.00	0.24	0.16	0.08	0.45
6280.17	0.00	0.00	0.00	0.00	0.00	0.00	0.00	0.00	0.00	0.28	17304.55	3.50	0.82	0.05	0.00	0.50	0.09	0.64	0.82	0.05	0.41
6436.75	0.00	0.00	0.00	0.00	0.00	0.00	0.00	0.00	0.09	0.57	17587.24	2.00	0.11	0.06	0.06	0.09	0.00	0.23	0.11	0.06	0.37
6515.04	0.00	0.00	0.09	0.00	0.00	0.00	0.00	0.00	0.09	0.37	18435.31	1.51	0.52	0.00	0.00	0.09	0.00	0.60	0.22	0.00	0.43
6593.33	0.00	0.08	0.00	0.00	0.00	0.00	0.00	0.00	0.16	0.31	19000.69	1.50	0.13	0.04	0.04	0.13	0.00	0.49	0.27	0.09	0.44
6855.60	0.00	0.00	0.00	0.00	0.00	0.00	0.00	0.00	0.16	0.91	19600.00	0.80	0.18	0.03	0.00	0.13	0.00	0.15	0.03	0.13	0.28
7117.87	0.00	0.08	0.00	0.00	0.00	0.00	0.00	0.00	0.00	0.00	19750.00	2.00	0.20	0.03	0.00	0.13	0.00	0.03	0.13	0.03	0.57

**APPENDIX 5 - POLLEN DATA**

Age (cal yr)	AMA	TRB	MYO	MAR	TYP	POG	HYD	RAN	LUD	GUN	Age (cal yr)	AMA	TRB	MYO	MAR	TYP	POG	HYD	RAN	LUD	GUN
0.00	0.00	0.00	0.00	0.00	7.00	0.11	0.04	0.00	0.04	0.00	7460.18	0.00	0.00	0.00	0.00	1.50	1.00	0.00	0.00	0.00	0.00
221.69	0.00	0.00	0.00	0.00	2.00	0.45	0.00	0.00	0.00	0.00	7882.53	0.04	0.00	0.00	0.00	2.00	0.08	0.00	0.00	1.00	0.00
443.38	0.00	0.00	0.00	0.00	0.50	0.02	0.00	0.02	0.00	0.00	8304.88	0.00	0.00	0.00	0.00	1.50	0.05	0.05	0.00	0.00	0.00
554.22	0.00	0.00	0.00	0.00	2.00	0.00	0.00	0.00	0.00	0.00	8727.24	0.00	0.00	0.00	0.00	1.00	0.00	0.00	0.00	0.05	0.00
611.11	0.00	0.00	0.00	0.00	1.36	0.00	0.02	0.00	0.00	0.00	9149.59	0.00	0.04	0.00	0.00	0.50	0.02	0.02	0.00	0.02	0.00
724.89	0.00	0.00	0.00	0.00	44.50	0.06	0.50	0.00	0.00	0.00	9551.53	0.02	0.00	0.00	0.00	1.00	0.02	0.00	0.00	0.00	0.00
838.67	0.00	0.00	0.00	0.00	3.00	0.06	0.00	0.06	0.06	0.00	9922.86	0.00	0.00	0.00	0.00	4.50	0.03	0.00	0.00	0.50	0.00
972.43	0.00	0.00	0.00	0.00	4.00	0.50	0.10	0.00	0.00	0.00	10294.18	0.00	0.00	0.00	0.00	6.50	0.50	0.03	0.00	0.03	0.00
1069.29	0.00	0.00	0.00	0.00	6.00	2.00	0.07	0.14	0.00	0.00	10665.51	0.00	0.00	0.00	0.00	5.50	0.07	0.00	0.07	0.07	0.00
1166.14	0.00	0.10	0.00	0.00	3.00	1.50	0.50	0.10	0.50	0.00	11085.35	0.00	0.00	0.00	0.00	2.51	0.02	0.02	0.00	0.01	0.00
1650.56	0.00	0.00	0.00	0.00	1.00	0.09	0.00	0.18	0.00	0.00	11368.04	0.05	0.05	0.00	0.00	5.00	1.00	0.00	0.00	0.10	0.00
2926.95	0.00	0.00	0.00	0.00	0.50	0.00	0.00	0.00	0.50	0.00	11650.73	0.00	0.00	0.00	0.00	11.56	0.06	0.00	0.00	0.06	0.06
3360.00	0.00	0.00	0.00	0.00	2.00	0.00	0.07	0.00	0.00	0.00	12216.11	0.05	0.05	0.00	0.00	5.00	0.00	0.00	0.20	0.05	0.00
3600.19	0.00	0.00	0.00	0.00	2.00	0.00	0.03	0.01	0.00	0.00	12724.95	0.00	0.00	0.00	0.00	3.50	0.04	0.00	0.00	0.04	0.00
3840.38	0.00	0.00	0.00	0.00	1.60	0.05	0.05	0.05	0.00	0.00	13064.18	0.03	0.03	0.00	0.00	5.50	0.00	0.03	0.00	0.50	0.00
4080.57	0.00	0.00	0.00	0.00	2.50	0.02	0.12	0.00	0.00	0.00	13346.87	0.00	0.01	0.01	0.00	4.00	0.00	0.01	0.01	0.00	0.00
4453.00	0.00	0.03	0.00	0.00	1.00	0.03	0.00	0.03	0.00	0.00	13912.25	0.00	0.00	0.00	0.00	8.50	0.05	0.00	0.05	0.05	0.00
4957.67	0.00	0.00	0.00	0.00	1.50	0.00	0.03	0.03	0.03	0.00	14477.64	0.00	0.06	0.00	0.00	7.00	0.06	0.00	0.00	0.06	0.00
5462.33	0.00	0.00	0.00	0.00	0.03	0.03	0.03	0.13	0.03	0.00	15043.02	0.00	0.00	0.00	0.00	3.50	0.00	0.00	0.00	0.00	0.00
5967.00	0.00	0.00	0.00	0.00	0.50	0.00	0.00	0.08	0.00	0.00	15608.40	0.00	0.00	0.00	0.00	8.40	0.00	0.00	0.03	0.00	0.00
6045.29	0.00	0.00	0.00	0.00	6.00	0.09	0.09	1.39	0.00	0.00	16173.78	0.00	0.00	0.00	0.00	0.04	0.00	0.00	0.00	0.00	0.00
6123.58	0.00	0.00	0.00	0.00	3.50	0.05	0.05	0.23	0.00	0.00	16739.16	0.00	0.00	0.00	0.00	7.00	0.00	0.00	0.00	0.00	0.00
6280.17	0.00	0.00	0.00	0.00	1.00	0.00	0.00	0.28	0.00	0.00	17304.55	0.00	0.00	0.00	0.00	5.00	0.05	0.00	0.05	0.00	0.00
6436.75	0.00	0.00	0.00	0.00	3.00	0.00	0.00	1.89	0.00	0.00	17587.24	0.00	0.00	0.00	0.00	4.00	0.00	0.00	0.00	0.00	0.00
6515.04	0.00	0.00	0.00	0.00	3.00	0.00	0.00	1.12	0.00	0.00	18435.31	0.00	0.00	0.00	0.00	8.04	0.00	0.00	0.50	0.00	0.00
6593.33	0.00	0.00	0.00	0.00	1.34	0.89	0.00	1.79	0.45	0.00	19000.69	0.00	0.00	0.00	0.00	4.50	0.00	0.00	0.04	0.00	0.00
6855.60	0.00	0.00	0.00	0.00	1.50	0.50	0.00	0.00	0.00	0.00	19600.00	0.00	0.03	0.00	0.00	5.60	0.00	0.00	0.00	0.00	0.00
7117.87	0.00	0.00	0.00	0.00	3.02	0.25	0.00	0.25	0.00	0.00	19750.00	0.00	0.03	0.00	0.00	5.50	0.50	0.03	0.13	0.00	0.00



APPENDIX 5 - POLLEN DATA

Age (cal yr)	LEN	HAL	NYM	POT	ERO	ANH	RIC	MON	TRI	LYO	Age (cal yr)	LEN	HAL	NYM	POT	ERO	ANH	RIC	MON	TRI	LYO
0.00	0.00	0.00	0.00	0.00	0.00	0.00	0.00	6.00	0.00	0.00	7460.18	0.00	0.00	0.00	0.00	0.00	0.00	0.00	3.00	0.00	0.00
221.69	0.00	2.00	0.00	0.00	0.00	0.00	0.00	5.00	0.00	0.00	7882.53	0.00	0.00	0.00	0.00	0.00	0.00	0.00	0.08	0.00	0.00
443.38	0.00	0.09	0.00	0.00	2.00	0.00	0.00	0.00	0.02	0.00	8304.88	0.00	0.00	0.00	0.00	0.00	0.00	0.00	0.00	0.00	0.00
554.22	0.00	6.00	0.00	0.00	4.00	0.00	0.00	0.00	0.00	0.00	8727.24	0.00	0.00	0.00	0.50	0.00	0.00	0.00	1.00	0.00	0.00
611.11	0.00	5.45	0.00	0.00	1.36	0.00	0.00	0.00	0.91	0.00	9149.59	0.00	0.00	0.00	0.00	0.00	0.00	0.00	1.50	0.00	0.00
724.89	0.00	0.00	0.00	0.00	0.00	0.00	0.00	0.00	0.00	0.00	9551.53	0.00	0.00	0.00	0.00	0.00	0.00	0.00	0.00	0.00	0.00
838.67	0.00	0.00	0.00	0.00	0.00	0.00	0.00	0.00	0.00	0.00	9922.86	0.00	0.00	0.00	0.00	0.00	0.00	0.00	0.00	0.00	0.00
972.43	0.00	0.00	0.00	0.00	0.00	0.00	0.10	0.50	0.00	0.00	10294.18	0.00	0.00	0.00	0.00	0.50	0.00	0.00	4.00	0.00	0.00
1069.29	0.00	0.00	0.00	0.00	0.00	0.00	0.00	2.00	0.00	0.00	10665.51	0.00	0.00	0.00	0.00	0.00	0.00	0.00	1.50	0.00	0.00
1166.14	0.00	0.00	0.00	0.00	0.00	0.00	0.00	8.00	0.00	0.00	11085.35	0.00	0.00	0.00	0.00	0.00	0.00	0.00	7.54	0.50	0.00
1650.56	0.00	0.00	0.00	0.00	0.00	0.00	0.00	32.50	0.00	0.00	11368.04	0.00	0.00	0.00	0.00	0.00	0.00	0.00	1.00	0.00	0.00
2926.95	0.00	0.00	0.00	0.00	0.00	0.00	0.00	49.50	0.05	0.00	11650.73	0.00	0.00	0.00	0.00	0.00	0.00	0.00	1.01	0.00	0.00
3360.00	0.00	0.00	0.00	0.00	0.00	0.00	0.07	40.00	0.00	0.00	12216.11	0.00	0.00	0.00	0.00	0.50	0.00	0.00	1.00	0.50	0.00
3600.19	0.00	0.00	0.00	0.00	0.00	0.00	0.00	81.50	0.00	0.00	12724.95	0.00	0.00	0.00	0.00	0.04	0.00	0.00	5.50	0.00	0.00
3840.38	0.00	0.10	0.00	0.00	0.00	0.00	0.00	42.00	0.00	0.05	13064.18	0.00	0.00	0.00	0.00	0.03	0.00	0.00	11.00	0.00	0.00
4080.57	0.00	0.02	0.00	0.00	0.00	0.00	0.00	66.00	0.00	0.00	13346.87	0.00	0.00	0.00	0.00	0.50	0.00	0.00	0.00	0.00	0.00
4453.00	0.00	0.00	0.00	0.00	0.00	0.00	0.00	70.00	0.00	0.00	13912.25	0.00	0.00	0.00	0.00	0.50	0.00	0.05	0.50	0.05	0.00
4957.67	0.00	0.00	0.03	0.00	0.00	0.00	0.00	53.00	0.00	0.00	14477.64	0.00	0.00	0.00	0.00	2.00	0.06	0.00	1.50	0.00	0.00
5462.33	0.00	0.00	0.00	0.00	0.00	0.00	0.00	69.50	0.00	0.00	15043.02	0.04	0.00	0.00	0.00	0.04	0.00	0.12	6.00	0.04	0.00
5967.00	0.00	0.00	0.00	0.00	0.00	0.00	0.04	47.00	0.00	0.00	15608.40	0.03	0.00	0.00	0.00	0.03	0.00	0.03	1.20	0.00	0.00
6045.29	0.00	0.00	0.00	0.00	1.00	0.00	0.00	28.00	0.00	0.00	16173.78	0.00	0.00	0.00	0.00	2.00	0.00	0.50	0.00	0.00	0.00
6123.58	0.00	0.00	0.00	0.00	0.00	0.00	0.00	29.50	0.00	0.00	16739.16	0.00	0.00	0.00	0.00	0.04	0.00	0.04	10.00	0.04	0.00
6280.17	0.00	0.00	0.00	0.00	0.00	0.00	0.00	16.50	0.00	0.00	17304.55	0.00	0.00	0.00	0.00	0.50	0.09	0.05	14.50	0.05	0.00
6436.75	0.00	0.00	0.00	0.00	0.00	0.00	0.00	4.50	0.00	0.00	17587.24	0.00	0.00	0.00	0.00	0.03	0.00	0.00	8.00	0.00	0.00
6515.04	0.00	0.00	0.00	0.00	0.00	0.00	0.00	5.00	0.09	0.00	18435.31	0.00	0.00	0.00	0.00	0.50	0.00	0.04	11.56	0.00	0.00
6593.33	0.00	0.00	0.00	0.00	0.00	0.00	0.00	2.68	0.00	0.00	19000.69	0.00	0.00	0.00	0.00	1.00	0.00	0.13	0.50	0.50	0.00
6855.60	0.00	0.00	0.00	0.00	0.00	0.00	0.00	0.50	0.00	0.00	19600.00	0.00	0.00	0.00	0.00	0.03	0.03	0.40	16.80	0.00	0.00
7117.87	0.00	0.00	0.00	0.50	0.08	0.00	0.00	2.01	0.00	0.00	19750.00	0.03	0.00	0.00	0.00	1.00	0.00	0.00	7.50	0.00	0.00

**APPENDIX 5 - POLLEN DATA**

Age (cal yr)	POY	PTE	CYP	ASC	GEN	PLA	SOL	LIL	CEP	SCA	Age (cal yr)	POY	PTE	CYP	ASC	GEN	PLA	SOL	LIL	CEP	SCA
0.00	0.00	0.00	32.00	0.00	0.15	0.00	0.07	0.00	0.00	0.00	7460.18	0.00	0.00	13.00	0.00	0.00	0.00	0.53	0.00	0.00	0.00
221.69	0.00	0.00	43.00	0.00	1.00	0.00	0.08	0.00	0.00	0.00	7882.53	0.00	0.00	20.00	0.00	0.00	0.00	0.19	0.00	0.00	0.00
443.38	0.00	0.00	51.50	0.00	0.09	0.00	0.00	0.02	0.00	0.02	8304.88	0.00	0.00	11.00	0.00	0.00	0.00	0.21	0.00	0.00	0.00
554.22	0.00	0.00	37.00	0.00	4.00	0.00	0.00	0.00	0.00	0.00	8727.24	0.00	0.00	21.50	0.00	0.00	0.00	0.54	0.00	0.00	0.00
611.11	0.00	0.00	66.36	0.00	3.64	0.00	0.02	0.00	0.00	0.02	9149.59	0.00	0.00	70.50	0.00	0.00	0.00	0.02	0.00	0.00	0.00
724.89	0.00	0.00	32.50	0.00	0.00	0.00	0.17	0.06	0.00	0.00	9551.53	0.00	0.00	33.50	0.00	0.02	0.00	0.12	0.00	0.00	0.00
838.67	0.00	0.00	65.50	0.00	0.00	0.00	0.00	0.00	0.00	0.00	9922.86	0.00	0.00	57.50	0.00	0.00	0.00	0.00	0.06	0.00	0.00
972.43	0.00	0.00	25.00	0.10	0.00	0.00	2.08	0.00	0.00	0.00	10294.18	0.00	0.00	36.50	0.00	0.03	0.00	0.14	0.00	0.00	0.00
1069.29	0.00	0.00	28.50	0.00	0.07	0.00	0.14	0.00	0.00	0.00	10665.51	0.00	0.00	37.00	0.00	0.07	0.00	0.00	1.00	0.00	0.00
1166.14	0.00	0.00	30.00	0.00	0.00	0.00	1.20	0.00	0.00	0.00	11085.35	0.00	0.00	64.82	0.00	0.01	0.00	0.03	0.00	0.00	0.00
1650.56	0.00	0.00	4.50	0.00	0.00	0.00	0.18	0.00	0.00	0.00	11368.04	0.00	0.00	39.00	0.00	0.00	0.00	0.24	0.00	0.00	0.00
2926.95	0.00	0.00	6.50	0.00	0.00	0.00	0.05	0.00	0.00	0.00	11650.73	0.00	0.00	30.15	0.00	0.00	0.00	0.06	0.00	0.00	0.00
3360.00	0.00	0.00	4.40	0.00	1.65	0.00	0.00	0.00	0.00	0.00	12216.11	0.00	0.00	48.00	0.00	0.00	0.00	0.20	0.00	0.00	0.00
3600.19	0.00	0.00	3.50	0.00	0.01	0.00	0.02	0.00	0.00	0.00	12724.95	0.00	0.00	39.50	0.00	0.04	0.00	0.24	0.00	0.00	0.00
3840.38	0.00	0.00	8.00	0.00	0.05	0.00	1.56	0.05	0.00	0.00	13064.18	0.00	0.00	51.00	0.00	0.06	0.00	0.03	0.00	0.00	0.00
4080.57	0.00	0.00	14.00	0.00	0.00	0.00	0.00	0.00	0.00	0.00	13346.87	0.00	0.00	53.50	0.00	0.01	0.00	0.00	0.00	0.00	0.01
4453.00	0.00	0.03	4.50	0.00	0.03	0.00	0.03	0.00	0.00	0.00	13912.25	0.00	0.00	26.00	0.00	0.26	0.00	0.10	0.00	0.00	0.05
4957.67	0.00	0.00	6.50	0.00	0.00	0.00	0.09	0.00	0.00	0.00	14477.64	0.00	0.00	36.00	0.00	0.50	0.00	0.00	2.50	0.00	0.00
5462.33	0.00	0.00	8.00	0.00	0.00	0.00	0.03	0.00	0.00	0.00	15043.02	0.04	0.00	24.50	0.04	0.08	0.00	0.00	0.50	0.04	0.04
5967.00	0.00	0.00	10.50	0.00	0.00	0.00	0.00	0.00	0.00	0.04	15608.40	0.00	0.00	35.60	0.00	0.18	0.00	0.03	0.00	0.00	0.00
6045.29	0.00	0.00	10.00	0.00	0.00	0.00	0.37	0.00	0.00	0.00	16173.78	0.00	0.00	35.00	0.00	0.04	0.00	0.00	0.00	0.00	0.00
6123.58	0.00	0.00	13.00	0.00	0.05	0.00	0.09	0.00	0.00	0.00	16739.16	0.00	0.00	19.00	0.00	0.04	0.00	0.00	0.00	0.00	0.00
6280.17	0.00	0.00	4.00	0.00	0.09	0.00	0.56	8.00	0.00	0.00	17304.55	0.00	0.00	21.50	0.00	0.23	0.00	0.00	0.50	0.00	0.05
6436.75	0.00	0.00	6.50	0.00	0.00	0.00	0.28	0.00	0.00	0.00	17587.24	0.00	0.00	32.00	0.00	0.00	0.00	0.03	0.03	0.00	0.00
6515.04	0.00	0.00	11.00	0.00	0.00	0.00	0.37	1.00	0.00	0.00	18435.31	0.00	0.00	29.15	0.00	0.04	0.09	0.00	1.01	0.04	0.00
6593.33	0.00	0.00	10.71	0.00	0.08	0.00	0.23	0.00	0.00	0.00	19000.69	0.00	0.00	36.00	0.00	0.09	0.00	0.00	0.50	0.00	0.00
6855.60	0.00	0.00	12.00	0.00	0.00	0.00	0.37	0.00	0.00	0.00	19600.00	0.00	0.00	30.40	0.00	0.20	0.00	0.00	0.00	0.00	0.00
7117.87	0.00	0.00	11.06	0.00	0.00	0.00	0.99	0.00	0.00	0.00	19750.00	0.00	0.00	27.50	0.00	0.17	0.00	0.07	0.00	0.00	0.07

**APPENDIX 5 - POLLEN DATA**

Age (cal yr)	LAB	CRA	UMB	CAM	HET	POA	UNI				Age (cal yr)	LAB	CRA	UMB	CAM	HET	POA	UNI			
0.00	0.00	0.00	0.00	0.00	0.18	44.00	1.39				7460.18	0.00	0.00	0.00	0.00	1.86	60.00	1.46			
221.69	0.00	0.00	0.00	0.00	1.36	29.00	0.76				7882.53	0.00	0.08	0.00	0.00	0.98	65.00	0.68			
443.38	0.00	0.00	0.00	0.00	0.02	40.50	0.38				8304.88	0.00	0.05	0.00	0.00	0.69	70.50	0.53			
554.22	0.00	0.00	0.00	0.03	0.18	41.00	0.47				8727.24	0.00	0.05	0.00	0.00	2.00	59.00	0.63			
611.11	0.00	0.02	0.00	0.04	0.39	16.82	0.25				9149.59	0.00	0.00	0.00	0.00	2.50	20.50	0.15			
724.89	0.00	0.06	0.00	0.17	0.40	9.50	0.51				9551.53	0.00	0.00	0.00	0.00	0.30	60.50	0.65			
838.67	0.00	0.00	0.00	0.00	0.83	24.00	0.70				9922.86	0.00	0.00	0.00	0.00	0.00	30.50	0.20			
972.43	0.00	0.30	0.00	0.10	1.58	43.50	1.98				10294.18	0.00	0.07	0.00	0.00	0.64	42.00	0.14			
1069.29	0.00	0.00	0.00	0.00	2.83	43.50	0.14				10665.51	0.00	0.00	0.00	0.00	0.53	37.00	0.80			
1166.14	0.00	0.30	0.00	0.00	0.50	31.00	1.70				11085.35	0.01	0.01	0.00	0.00	0.19	20.60	0.15			
1650.56	0.00	0.00	0.00	0.00	0.09	40.00	0.80				11368.04	0.00	0.10	0.10	0.00	0.29	44.00	0.77			
2926.95	0.00	0.00	0.00	0.00	0.14	32.50	0.09				11650.73	0.00	0.00	0.00	0.00	0.36	40.70	0.18			
3360.00	0.00	0.00	0.00	0.07	0.21	36.80	0.62				12216.11	0.05	0.00	0.00	0.00	1.24	32.50	0.79			
3600.19	0.00	0.00	0.00	0.00	0.00	12.00	0.10				12724.95	0.08	0.00	0.00	0.00	0.49	41.00	0.81			
3840.38	0.00	0.05	0.00	0.00	0.10	36.00	0.73				13064.18	0.00	0.00	0.00	0.00	0.36	25.00	0.16			
4080.57	0.00	0.00	0.00	0.00	0.08	14.00	0.07				13346.87	0.00	0.00	0.00	0.00	0.14	36.50	0.14			
4453.00	0.00	0.03	0.00	0.00	0.42	15.50	0.55				13912.25	0.05	0.00	0.00	0.00	0.98	50.00	0.98			
4957.67	0.00	0.00	0.00	0.00	0.03	31.50	0.51				14477.64	0.06	0.19	0.00	0.00	0.19	34.00	0.77			
5462.33	0.00	0.00	0.00	0.00	0.15	20.00	0.18				15043.02	0.12	0.04	0.00	0.04	0.74	53.00	0.27			
5967.00	0.00	0.00	0.00	0.00	0.37	32.00	0.33				15608.40	0.00	0.00	0.03	0.03	0.25	40.80	0.34			
6045.29	0.00	0.09	0.00	0.00	0.46	34.00	1.48				16173.78	0.00	0.00	0.00	0.00	0.30	49.50	0.34			
6123.58	0.00	0.00	0.00	0.00	0.50	41.50	0.46				16739.16	0.08	0.00	0.00	0.00	0.57	52.50	0.49			
6280.17	0.00	0.00	0.00	0.00	1.12	47.50	0.37				17304.55	0.09	0.00	0.00	0.00	0.77	42.00	0.32			
6436.75	0.00	0.00	0.00	0.09	0.76	56.00	1.23				17587.24	0.03	0.03	0.00	0.00	0.37	48.00	0.23			
6515.04	0.00	0.00	0.00	0.00	0.56	59.00	0.93				18435.31	0.00	0.00	0.00	0.00	0.04	38.19	0.39			
6593.33	0.00	0.00	0.00	0.00	0.08	57.14	0.78				19000.69	0.00	0.00	0.04	0.00	0.44	45.00	0.44			
6855.60	0.00	0.00	0.00	0.05	0.32	69.00	0.21				19600.00	0.00	0.03	0.00	0.05	0.10	39.60	0.53			
7117.87	0.00	0.00	0.00	0.00	1.24	61.31	0.66				19750.00	0.03	0.03	0.00	0.07	0.44	41.00	0.30			